

Melt Spinning of the Fine PEEK Filaments

(Schmelzspinnen von feinen PEEK Filamenten)

Der

Fakultät Maschinenwesen

der

Technischen Universität Dresden

zur

Erlangung des akademischen Grades

Doktoringenieur (Dr.-Ing.)

vorgelegte Dissertation

MSc Mohammad Golzar

geboren am 24 April 1968 in Najaf

Tag der Einreichung: 21.06.2004

Tag der Verteidigung: 15.11.2004

Vorwort

Die vorliegende Arbeit entstand während meiner Tätigkeit als wissenschaftlicher Mitarbeiter der Abteilung Mechanik und Fadenbildung des Instituts für Polymerforschung Dresden e.V. von August 2000 bis Februar 2004 im Rahmen des von der Deutschen Forschungsgemeinschaft geförderten Projektes „Schmelzspinnen von PEEK-Garnen mit feintitrigen Filamenten“.

Dem Leiter des Teilinstitutes Polymerwerkstoffe des Instituts für Polymerforschung Dresden Herrn Prof. Dr. rer. nat. habil. G. Heinrich möchte ich für die Übernahme der Betreuung und die Unterstützung dieser Arbeit danken. Herrn Prof. Dr.-Ing. habil. R. Beyreuther, dem ehemaligen Leiter der Abteilung Fadenbildung, danke ich ganz herzlich für die stete Förderung und die Begutachtung der Arbeit. Mein besonderer Dank gilt Herrn Dr. rer. nat. H. Brünig für die interessante Aufgabenstellung, viele Gelegenheiten zur Diskussion, fachliche Betreuung und Durchsicht der Arbeit. Dem Senior Vice President Barmag GmbH, Herrn Dr.-Ing. K. Schäfer danke ich für das Interesse an der Arbeit und die Übernahme eines Korreferates. Herrn Prof. Dr.-Ing. habil. W. Hufenbach und Herrn Prof. Dr.-Ing. habil. Dr. h. c. P. Offerman danke ich für die Mitgestaltung des kooperativen Promotionsverfahrens.

Ich danke allen Kolleginnen und Kollegen der ehemaligen Abteilung Fadenbildung für die gute Zusammenarbeit. Herrn Dipl.-Ing. B. Tändler danke ich für die Versuchsdurchführung und die ständige Hilfsbereitschaft. Herrn Dr.-Ing. R. Vogel danke ich für die sehr gute Zusammenarbeit bei den rheologischen Untersuchungen. Für die Unterstützung bei der Versuchsdurchführung und den Charakterisierungsarbeiten danke ich Frau S. Körtel, Frau Dipl.-Chem. L. Häußler, Herrn H. J. Wiesner, Herrn F. Eberth und vor allem Frau G. Kottwitz, die sehr engagiert an den Doppelbrechungs- und DSC-Messungen mitgearbeitet hat.

Zum Schluß gilt mein herzlicher Dank meiner Frau für ihre große Unterstützung, und ihr und unseren Kindern für die Geduld und das Verständnis für meine Arbeit.

Mohammad Golzar

Dresden, im Juni 2004

Zusammenfassung

Das Schmelzspinnen von feinen Polyetheretherketon- (PEEK) Filamenten wurde in der vorliegenden Dissertation erstmals umfassend untersucht. Feine PEEK-Filamente sind für innovative Anwendungen aufgrund ihrer mechanischen und thermischen Eigenschaften (hohe Dauergebrauchstemperatur) sowie ihrer chemischen Beständigkeit sehr gut geeignet, z.B. als textil-verstärkte leichte Hochleistungsrotoren. Ziel dieser Arbeit bestand darin, feine PEEK-Filamente (Durchmesser zwischen 10 μm und 15 μm) erstmals zu erspinnen und dafür die Spinnbedingung des Schmelzspinnens mit Hilfe der experimentellen und theoretischen Untersuchungen zu optimieren. Zum Vergleich wurde das Verhalten von feinen Polypropylen- (PP) Filamenten beim Schmelzspinnen mit herangezogen. Innerhalb der Fadenbildungszone wurden online-Messungen der Filamentgeschwindigkeit (Laser-Doppler-Anemometrie) und der Filamenttemperatur (Infrarot-Thermographie) simultan durchgeführt. Der Verlauf der Filamentgeschwindigkeit in Abhängigkeit vom Abstand zur Spinndüse wird beeinflusst durch die technologischen Spinnparameter, insbesondere aber durch die sich ausprägende innere Struktur der PEEK-Filamente. Für die Bestimmung der Filamenttemperatur wurden zwei verschiedene Methoden der Emissivitätskorrektur in Abhängigkeit vom Filamentdurchmesser entwickelt und angewendet. Dabei wurde auch eine neuartige Methode zur Bestimmung des Filamentdurchmessers simultan zur Temperaturbestimmung mittels der Infrarot-Thermographie entwickelt. Die Genauigkeit der Durchmesserbestimmung ist hierbei von der Auflösung der verwendeten Kamera abhängig.

Die rheologischen Messungen bestätigten die thermische Stabilität der PEEK-Schmelze bei 400°C für mehr als 30 min, es war keine thermische Degradation erkennbar und die untersuchte (komplexe) Scherviskosität blieb über diesen Zeitraum unveränderlich. Bei hohen Schergeschwindigkeiten ($d\gamma/dt > 10 \text{ s}^{-1}$) im dynamischen Schwingungsversuch zeigte die (komplexe) Scherviskosität ein mit der Schwingungsfrequenz abnehmendes Verhalten, das nicht mit dem bekannten Potenzgesetz, sondern besser durch das Bueche (Cross) Modell beschrieben werden kann. Eine Masterkurve wurde berechnet und die Temperaturabhängigkeit der Viskosität nach Arrhenius bestimmt. Entlang der Spinnstrecke wurde innerhalb der Fadenbildungszone mit Hilfe der gemessenen Filamentgeschwindigkeiten die (scheinbare) Dehnviskosität bei hohen Dehnraten (Gradient der Filamentgeschwindigkeit $> 10 \text{ s}^{-1}$) abgeschätzt. Es sind in der Literatur keine Angaben für die Dehnviskosität von PEEK in diesem Bereich verfügbar. Die ermittelte (scheinbare) Dehnviskosität konnte über die Temperaturabhängigkeit nach Arrhenius reduziert

werden. Das üblich angewendete Maxwell-Modell und das Upper-convected Maxwell Modell stellen dabei keine geeignete Anpassung an die Messwerte dar, eine eigene Anpassung für den abfallenden Verlauf der Dehnviskosität in Abhängigkeit von der Dehnrates konnte dieses Verhalten von PEEK-Material interpretieren und wurde deshalb verwendet.

Die Orientierung der PEEK-Spinnfilamente, ausgedrückt durch die Doppelbrechung, nimmt mit wachsender Abzugsgeschwindigkeit (untersuchter Bereich: 1000 bis 2000 m/min) zu. Mit wachsendem Durchsatz (Bereich 0.17 bis 3.5 g/min) nimmt dagegen die Doppelbrechung ab. Dieses Verhalten entspricht dem üblicher thermoplastischer Spinnpolymere, es besteht eine Relation zwischen Orientierung und Spinnverzug bzw. Spinnspannung. Feine PEEK-Filamente weisen eine hohe Orientierung auf. DSC-Messungen an den ersponnenen PEEK-Filamenten zeigten, dass der Kristallisationsgrad der Spinnfilamente von ihrer Abzugsgeschwindigkeit und dem verwendeten Durchsatz abhängig ist und mit der Orientierung der Polymerketten korreliert. Die durchgeführten Untersuchungen weisen einen hohen Kristallisationsgrad für feine PEEK-Filamente nach. Für die berechneten und gemessenen Filamentfeinheiten und –durchmesser ergaben sich im Rahmen der Spinnversuche gute Übereinstimmungen. Dieses Ergebnis deutet auf ein homogen und stabil realisiertes Spinnverfahren für feine PEEK-Filamente hin. Mit wachsender Spinnspannung, insbesondere bei hoher mechanischer Spannung im Verfestigungspunkt, erhöht sich die Orientierung der Polymerketten und in Folge davon verringert sich die Reißdehnung der ersponnenen Filamente. Ein hoher Spinnverzug, d. h. eine hohe Dehnung innerhalb der Fadenbildungszone, wirkt ebenfalls in gleicher Weise auf die innere Strukturausprägung. Im Ergebnis dessen liegen hochorientierte feine PEEK-Filamente vor, deren bereits gestreckte Molekülketten keine wesentlichen Dehnungen mehr ermöglichen, die aber ohne weitere Prozessschritte bereits über ausreichende Festigkeiten (bis 4 cN/dTex) verfügen.

Das Fadenbildungsmodell (angewendet in IPF für andere Polymere) wurde in der Form eines entsprechend modifizierten Satzes eindimensionaler gekoppelter Differenzialgleichungen für das Material PEEK angepasst und numerisch für die Fadenbildungszone des PEEK-Spinnprozesses gelöst. Beim Vergleich der berechneten und gemessenen Filamenttemperaturen und –geschwindigkeiten wurde nachgewiesen, dass im Modell die Abhängigkeit der Dehnviskosität von Temperatur *und* Dehnrates (im Bereich von $V'=10...1000\text{ s}^{-1}$) berücksichtigt werden muss, um den Fadenbildungsverlauf, die Strukturbildung und die Wärmeübertragung zu erfassen. Die Wärmeübertragung bei der Abkühlung wurde auch mit Hilfe geeigneter Temperaturmessungen innerhalb der Fadenbildungszone untersucht und die Übertragungskoeffizienten (Nusselt-Zahlen) bestimmt. Die so abgeschätzten Nusselt-Zahlen zeigten dabei im Gegensatz zum häufig verwendeten Modellansatz von Kase und Matsuo einen leicht abnehmenden Verlauf in der

Fadenbildungszone. Es konnte gezeigt werden, dass die Ursachen dafür in dem für PEEK nicht zu vernachlässigenden Anteil von freier Konvektion und Wärmestrahlung am Gesamtwärmeübergang liegen. Beispielsweise beträgt in der Nähe der Spinndüse der Strahlungsanteil etwa 12% des Gesamtbetrags des Wärmeübergangs. Die im Fadenbildungsmodell verschiedenen verwendeten konstitutiven Gleichungen (differenziell viskoelastisch bzw. nichtlinear viskoelastisch) zeigten bei der Lösung der Differenzialgleichungen keine großen Unterschiede bezüglich des viskosen Verhaltens im Fadenbildungsverlauf. Das liegt daran, dass bei starker Verstreckung das PEEK-Material sich viskos (und weniger elastisch) beschreiben lässt, obwohl die PEEK-Schmelze direkt nach der Düse auch viskoelastisches Verhalten zeigt.

Mit dem vorliegenden Modell kann die Strangaufweitung nicht erfasst werden, eine Kompensation kann ggf. durch eine Verschiebung des Anfangspunktes der numerischen Lösung erreicht werden. Eine weitere Korrektur kann erforderlich sein, wenn auch die in der Düsennähe erhöhte Lufttemperatur im Modell mit einbezogen werden soll. So lassen sich berechnete und gemessene Filamenttemperaturen und –geschwindigkeiten auch in größerem Abstand von der Düse sinnvoll vergleichen. Bei den Spinnversuchen mit zunehmender Abzugsgeschwindigkeit, aber konstanten Spinnbedingungen, insbesondere konstantem Durchsatz, zeigten die gemessenen Geschwindigkeitsprofile in Düsennähe einen nahezu identischen Verlauf, die Differenzierung der Profile fand hauptsächlich erst nach der viskosen Deformation statt. Am Ende der Fadenbildungszone, im Bereich der Verfestigung, unterschieden sich die Spinnfilamente dann wesentlich bezüglich ihrer durchlaufenen Dehnungen und der damit verknüpften Strukturausprägung (Orientierung und Kristallisation). Die innere Fadenkraft, d. h. die Fadenspannung, wird bestimmt durch die Spinnbedingungen und die Abkühlung entlang der Spinnstrecke. Es besteht eine Korrelation, wie bei anderen Thermoplastics, zwischen der Spannung (berechnet von o.g. PEEK Modell) am Verfestigungspunkt und der Orientierung (gemessene Doppelbrechung) der Spinnfilamente. Die berechnete Fadenspannung ist zusätzlich noch von den im Modell verwendeten Beziehungen für die Nusselt-Zahl und für die Dehnviskosität abhängig. Die Korrelation zwischen der berechneten Spannung im Verfestigungspunkt und der Orientierung, dargestellt durch die gemessene Doppelbrechung, konnte für PEEK nachgewiesen werden.

Die Spinnbarkeitsgrenzen von PEEK bezüglich Abzugsgeschwindigkeit und Durchsatz wurden untersucht. Dabei wurden solche Spinnbedingungen bestimmt, die ein stabiles Schmelzspinnverfahren ermöglichen: Für Durchsätze (pro Düsenbohrung) >0.5 g/min und Abzugsgeschwindigkeiten <7000 m/min konnten so PEEK-Filamente mit minimalem

Durchmesser bis etwa 13 μm hergestellt werden. Ebenfalls konnte PEEK auch noch mit einem Durchsatz von 0.1 g/min versponnen werden, wobei die Abzugsgeschwindigkeiten hier jedoch deutlich bis ca. 1000 m/min begrenzt blieben. Im Vergleich dazu konnte Polypropylen bei höheren Abzugsgeschwindigkeiten versponnen werden, so dass hier feinere PP-Filamente als PEEK-Filamente möglich wurden. Mit Hilfe des PEEK-Fadenbildungsmodells wurden die Einflüsse von erhöhter Schmelztemperatur und verkürztem Spinnweg (Abstand zwischen Düse und Wickler) untersucht. Beide Effekte bewirken eine Verringerung der Spinnspannung und der Dehnrate (infolge der vergrößerten Fadenbildungszone), was günstig für die Erspinnung von feinen Filamenten ist und experimentell auch bestätigt wurde. Es wurden auf diese Weise sehr feine PEEK-Filamente mit Durchmessern $< 6 \mu\text{m}$ hergestellt. Bei diesen Spinnversuchen war jedoch die Realisierung des erforderlichen geringen Durchsatzes problematisch, da sowohl der Schmelzdruck in der Kapillare sehr niedrig war als auch die lange Verweilzeit sich ungünstig auf die Stabilität des Spinnprozesses auswirkte.

Im Ergebnis dieser Dissertation lassen sich Empfehlungen für weiterführende Arbeiten auf dem Gebiet des Schmelzspinnens von feinen Filamenten ableiten. Insbesondere besteht weiterer Forschungsbedarf in den Bereichen der spannungsinduzierten Kristallisation, der zweidimensionalen Behandlung der Strangaufweitung nach der Spindüse, der erzwungenen (zusätzlichen) Wärmeübertragung durch die laterale Bewegung des Spinnfilaments und zur zeitbezogenen Spinnstabilität. Die vorliegende Arbeit stellt eine Konzeption für das Schmelzspinnen feiner PEEK-Filamente dar, die vom Prinzip auch auf das Schmelzspinnen von anderen thermoplastischen Materialien angewendet werden kann. Diese Konzeption beinhaltet die systematischen Untersuchungen zu Granulat und Filament, insbesondere die Untersuchungen zur Korrelation zwischen innerer Strukturausprägung und mechanischen Eigenschaften der feinen Filamente. Mit dem grundlegenden Verständnis der Zusammenhänge können so die Spinnbedingungen im Schmelzspinnprozess für feine Filamente optimiert werden. Das verbesserte Fadenbildungsmodell und die Erkenntnisse zu den Spinnbarkeitsgrenzen bei der Herstellung von feinen Filamenten können für relevante Anwendungen in der Industrie genutzt werden.

Abstract

The production of fine filaments using the melt spinning process needs considerable effort. A thermoplastic melt is stretched from the spinneret under a constant take-up speed. The high performance thermoplastic PEEK is solidified in the melt spinning process in a small distance and short time. Therefore, the fine PEEK filaments in the fibre formation zone underwent a high deformation and cooling rate. To make the melt spinning process stable and to produce the fine PEEK filaments, material properties and material behaviour are examined using on-line and off-line measurements. The fibre speed measured using Laser Doppler Anemometry and simultaneous temperature measured using infrared thermography enable both the strain rate and consequently the apparent extensional viscosity to be estimated. This provides the apparent extensional viscosity over the spinning line, which can itself show the structural development of PEEK fibres in the fibre formation zone, i.e. necking and solidification phenomena.

The one-dimensional fibre formation model must include both procedural and material parameters. The heat transfer coefficient was estimated using the filament temperature measurement and showed a relatively high contribution of radiation and free convection in comparison to forced convection near the spinneret. The improved model of PEEK fibre formation gave a good agreement to both temperature and speed measurements, and also confirmed the high deformation rate effect on the extensional viscosity, which could be simulated with a properly generalised Newtonian constitutive equation.

The end properties of the fibres, such as as-spun filament fineness, orientation (expressed using total birefringence) and total crystallisation (examined using DSC) are investigated in relation to different spinning conditions, i.e. take-up speed, throughput and the draw down ratio. The tensile test diagram results, measuring phenomena such as the elongation at break, tenacity, and the Young modulus of elasticity are also analysed in order to complete the correlation of the above-mentioned spinning conditions to the structural properties of as-spun fine PEEK filaments.

The melt spinning of fine PEEK fibres under different spinning conditions is examined with the purpose of finding the optimum take-up speed and throughputs. Other spinning conditions, such as the temperature of melt processing, and the arrangement and diameter of the spinneret holes, are changed in order to make the process more stable. The recommendations for further study can be used to further examine some aspects of this work; however, this work presents a new concept for fine PEEK melt spinning supported by spinnability examinations under different spinning conditions and the improved model of fibre formation, which is also relevant for typical industrial processing applications.

Contents

Abstract

List of Symbols and Abbreviations

1 Introduction

1.1	Melt spinning of fine thermoplastics.....	1
1.2	Specific application of fine PEEK fibres for hybrid yarn.....	3
1.3	Goals of the work.....	5
1.4	Outline of the thesis	6

2 Experiments and measurements

2.1	Melt spinning equipment.....	7
2.2	On-line measurements (along the spinning line).....	9
2.2.1	Fibre speed measurements.....	9
2.2.2	Temperature thermography and emission correction.....	9
2.2.3	Diameter estimation via infrared temperature measurements.....	14
2.3	Off-line measurements (as-spun fibre characterisation methods).....	17
2.3.1	Fineness and diameter measurements.....	17
2.3.2	Tensile test.....	18
2.3.3	Crystallinity and birefringence measurements.....	19
2.4	Material properties of original granules.....	20
2.4.1	Rheometry.....	20
2.4.2	General material properties of PEEK (PP as comparison).....	21

3 Rheological studies in the melt spinning as extensional flow

3.1	Rheological characterization and material function from shear flow.....	26
3.1.1	Shear viscosity and spinnability using the small amplitude oscillatory test..	26
3.1.2	Temperature dependence of viscosity.....	30
3.1.3	Strain rate und molecular weight dependence of shear viscosity.....	32
3.2	Extensional viscosity in the melt spinning process.....	35
3.2.1	Estimation of extensional viscosity along spinning line.....	36
3.2.2	Strain rate dependence of extensional viscosity.....	39
3.2.3	Conclusion	46

4 Structural, mechanical and geometrical properties of as-spun fibres

4.1	Structural properties of as-spun fine PEEK fibres.....	48
4.1.1	Orientation investigations.....	48
4.1.2	Crystallinity of the as-spun PEEK fibre.....	52
4.2	Mechanical and geometrical properties of as-spun fine fibres.....	58
4.2.1	Fineness and Tenacity (PEEK and PP).....	58
4.2.2	Elasticity modulus and stress-strain diagram (PEEK).....	64

5	Applying the model of fibre formation to PEEK	
5.1	Fundamental equations steady state melt spinning.....	69
5.1.1	One-dimensional model for fibre formation.....	71
5.1.2	Constitutive equations.....	72
5.2	Heat transfer and fibre temperature along spinning line.....	75
5.2.1	Fibre temperature and Nusselt number for PEEK fibres.....	78
5.2.2	Temperature comparison: model and on-line measurement.....	84
5.2.3	Crystallisation investigation by on-line temperature measurement.....	86
5.3	Speed of PEEK fibre along spinning line.....	88
5.3.1	Fibre speed comparison: model and on-line measurement.....	88
5.3.2	Solidification point.....	96
5.4	Tension in the spinning line (force-stress estimation).....	98
6	Stability and fineness limitations of PEEK melt spinning	
6.1	Failure theory in the melt spinning.....	104
6.2	Fineness limitations.....	105
6.2.1	Throughput, take-up speed and draw down ratio.....	105
6.2.2	Temperature of melt and viscosity.....	109
6.2.3	Take-up point.....	111
6.3	Optimisation of spinning conditions for fine filaments.....	113
6.4	Ultra-fine PEEK filaments ($D_L < 9 \mu\text{m}$).....	114
7	Conclusion and recommendations	
7.1	Summary and Conclusion.....	116
7.2	Recommendations.....	121

References

Appendix

List of Symbols

a, b	coefficient constant	-
A	cross sectional area of fibre	m ²
A _i	initial cross section of fibre in tensile test	m ²
B	distance from winder to spinneret	cm
C _{p,a} , C _{p,p}	heat capacity of air, heat capacity of polymer	J/kg.°C
C1,C2	constant of WLF equation	-
D(z)	diameter of fibre	mm
De(z)	Deborah number.	-
D _L	end diameter of fibre	µm
em, em _f , em _d , em _p	emisivity factor, -of fibre, -of drum, -of reference point	-
E	elasticity Young's modulus	Pa
E _a	activation energy	kJ/mol
E _{am} , E _{cr}	amorphous, crystalline (elasticity module)	Pa
f _{am} , f _{cr}	amorphous, crystalline (orientation function)	-
F(z)	spin-line tension force	mN
F' (z)	force gradient	mN/cm
F ₀	initial force	mN
F _i , F _g , F _s	inertial force, gravitational force, skin drag force	mN
g _i	relaxation strenght	Pa
G	shear strenght	Pa
G _E , G _V	elastic modulus, viscous modulus	Pa
Gr	Grasshof number	-
h	heat convection coefficient	W/m ² K
K, k	constant	-
l	length of an uniaxially stretched fibre sample	cm
l ₀	length of capillary channel	cm
L _e	extruder screw length	cm
L	solidification length	cm
m	Power constant of Beuche equation	-
M, M _w , M _c	molecular weight, -average, -critical	-
n	power constant of power law	-
n _p	number of pixel	-
Nu	Nusselt number Nu=hD/v	-
Nu _n , Nu _f	Nusselt number due to natural, force convection	-
P	pressure	Pa
Pr	Prandtl number	-
Q, Q _h , Q _t	mass throughput, throughput per hole, total throughput	g/min
r	radial direction in polar coordinate	cm
r ₀	radius of capillary	mm
re, re _f	reflection factor, - of fibre	-
R	molar gas constant	kJ/mol.K
R _{GPa}	tensile strength	Pa
R _u	ultimate tenacity	Pa
Ra	Rayleigh number	-
Rad	apparent radiation coefficient	-

Re	Reynolds number	-
t	time	s
tr, tr _f	transmission factor of fibre	-
t _s	solidification time	s
T(z)	temperature	°C
T'(z)	temperature gradient (dT/dz)	°C/cm
T ₀	initial temperature	°C
T _a , T _f	air temperature, fibre temperature	°C
T _g , T _m	glass temperature, melt temperature of polymer	°C
T _r	arbitrary reference temperature point	°C
T _∞	ambient temperature	°C
Tr	Trouton ratio	-
Tt	fineness or Titer	g/km
V(z)	velocity of fibre	m/min
V'(z)	velocity gradient	1/s
V' _{max}	maximum of velocity gradient	1/s
V ₀	initial or outlet velocity	m/min
V _L	end or take-up velocity	m/min
W	total energy received by camera	J.s
W _f , W _h	energy of Fibre, energy of heated area	J.s
W _e , W _r , W _t	emitted energy, reflected energy, transmitted energy	J.s
X	relative cristallinity of polymer	%
X _{cr}	critical cristallinity for crosslinking	%
z	distance from spinneret along spinning line	cm
Z	dimensionless fibre diameter (z/L)	-

Greece Symbols

α	coefficient of expansion	-
η	viscosity	Pa. s
η ₀	zero shear viscosity	Pa. s
η _{app}	apparent extensional viscosity	Pa. s
η _e	extensional viscosity	Pa. s
η _r	shear viscosity	Pa. s
η _∞	zero shear viscosity at reference temperature	Pa. s
σ	stress - normal stress in fibre-	Pa
σ'	stress gradient dσ/dz	Pa/cm
σ̇	stress rate dσ/dt	Pa/s
γ̇	shear strain rate	1/s
λ	relaxation time constant	s
λ _a	air heat conductivity	W/m/K
ω	rotational frequency	rad/s
ΔH	enthalpy of fully crystalline polymer	J/g
Δn	birefringence	-
Δn _{am} , Δn _{cr}	total amorphous, total crystalline birefringence	-
ΔP	pressure loss in capillary	Pa
Θ	dimensionless temperature	-

β	thermal expansion coefficient of air	1/K
δ	deformation, elongation	%
δ_u	ultimate elongation	%
ε	Hencky's strain	-
ε'	strain gradient ($d\varepsilon/dz$)	1/cm
$\dot{\varepsilon}$	strain rate or deformation rate ($d\varepsilon/dt$)	1/s
ε_m	emissivity correction factor	-
ε_m	emissivity coefficient	-
γ, γ_0	shear strain, shear amplitude	-
ν_a	kinematic viscosity of air	m^2/s
θ	angular direction in polar coordinate	-
ρ_0	initial density of polymer	g/cm^3
ρ_a, ρ_p	density of air, density of polymer	g/cm^3
ρ_{am}, ρ_{cr}	density of amorphous, density of crystalline of polymer	g/bm^3
σ_{SB}	Stefan-Boltzman constant	W/m^2K^4
τ, τ_0	shear stress, shear stress amplitude	Pa
ξ	retardation time constant	s
ζ	dimensionless distance to spinneret	-

Abbreviations

CF	carbon fibre	
DSC	differential scanning calorimetry	
ddr	draw down ratio (V_L/V_0)	-
FRC	fibre reinforced composites	
GF	glass fibre	
IR	infrared	
IRBIS [®]	software of infrared camera	
MFI	melting flow index	
NADIA	software for <u>n</u> ew <u>a</u> pproach of <u>d</u> iameter measurement	
RTC	reinforced thermoplastics composites	

1 Introduction

This thesis focuses on the theoretical and experimental investigations of the melt spinning process, which is used to produce fine thermoplastic filaments of poly (ether ether ketone) PEEK. The following chapter provides an overview and explains the goals of this work.

1.1 Fine thermoplastic filaments: an overview

Fine thermoplastic fibres have been produced since 1950 and can be used in a wide range of applications [Okatomo 1994]. The many different characteristics of fine filaments, such as softness, flexibility and smoothness, make the fine fibres also suitable for potential new applications. The motive of this work is the usage of fine filaments as matrix for a reinforced composite. In this connection, the thermoplastic material is melted and processed to produce the fine thermoplastic fibres, these fibres are then mixed with the reinforcement fibres; which are normally fine fibres as well. Finally the fine thermoplastic is melted to make a special fibre reinforced composite (this is dealt with in greater detail in section 1.2).

Various methods and processes have been developed to produce the fine fibres in continuous or random forms. While the direct conventionally melt spinning process is an approved technique for producing continuous fine fibres, it can also raise some difficulties. Nevertheless, the direct melt spinning method is an optimised method of producing the fine fibre properly [Fourné 1995].

This thesis concerns the melt spinning of fine PEEK filaments and brings together the required theoretical and practical understandings. At present, the as-spun PEEK yarn is commercially available [Zyex, Hoechst], but not in fine fibres requested here. The first melt spinning of PEEK was reported by Shimizu et al. [1985] and was also dealt with widely by Ohkoshi [1990-2000], but no more reports on fine PEEK fibres have appeared since this time. Results by Beyreuther et al. [2001] and Brünig et al. [2002] have however been published on research and experiments conducted on fine as-spun PEEK fibres.

The fine fibres can normally be extruded by reducing the polymer throughput and increasing the draw down ratio, but this reduction of mass throughput is observed to have its limits. Other problems in the process of direct melt spinning must also be fully explored. Fourné [1995] developed the melt spinning equipment of fine PET filaments, but a new improved technology in the equipment is still in process by other developer [Schäfer 2002] and [Stibal 2002]. To produce

fine filaments Fourné suggested the necessary conditions for production of fine PET fibres: very pure and homogenous polymer (usage of good filtration), increase the melt temperature higher than normal spinning, a wide holes distance for multifilament spinneret, a short blowing way and lower air velocity, fibre lubrication, double sided preparation after the blowing way and small fibre way (distance between spinneret and winder). More steps to modify the fine spinning process of PET in more detail are listed in [Fourné 1995]. In order to overcome the melt spinning problems for fine PEEK filaments, the same solutions have been suggested: to optimise the viscosity (using high temperature to reduce viscosity), special design in the arrangement and positioning of spinneret holes (to ensure uniform cooling), controlling the spinning line tension, lower throughput and to increase the filtration. These potential answers to the problems of melt spinning of fine PEEK fibres have been partly investigated by Beyreuther [2001] and Brünig [2002] and the three following solutions were specified: high take-up velocity, very low mass throughput and high draw down ratio.

Despite taking precautions, the fibre breakage increases by fineness less than 1 dTex. Melt spinning of fine filaments is often a sensitive process, especially combined with filament breakage. Increasing the draw down ratio can initiate necking in the profile of the spinning line, which is important for the internal structure and the stability of process. The maximum allowed take-up speed to produce the minimum fine filament is especially dependent on the viscoelasticity and temperature distribution along the spinning line. The problems which must normally be covered can be summarised as forth: the instability of the spinning line (such as the necking effect), variation of filaments' fineness in a bundle, and the breakage of fibre.

Fine fibres are defined according to convention in diameter or fineness of fibre. The Textile Committee of Germany defines micro fibres as follows: fibres finer than 1.2 dTex as Polyester and finer than 1.0 dTex as Polyamide. However, other definitions [Fourné 1995] classify a micro-filament as lying between 0.3 and 1.1 dTex. Alternatively, fine fibres are also defined as fibres of less than 0.7 denier ($0.7 \cdot 1.11 \sim 8$ dTex) [Okamoto 1994]. Fibres less than 0.55 dTex are considered ultra-fine and fibres finer than 0.11 dTex are sometimes referred to as super ultra-fine. Beyreuther [2001] has defined the so-called micro fibres as filaments with a fineness of <1 dTex and diameter of $<10 \mu\text{m}$. This thesis concerns itself with the fibres holding diameter of $10 \mu\text{m} < D < 30 \mu\text{m}$; however, other fibres with a diameter lower than $10 \mu\text{m}$ and up to $60 \mu\text{m}$ have also been investigated in order to complete the discussions.

1.2 Specific application of fine PEEK fibres for hybrid yarn

To produce Fibre Reinforced Composites (FRC) or Reinforced Thermoplastics Composites (RTC), the filaments are the base components. These types of composites have high strength and lightweight properties, and are used in many fields of engineering including aerospace, automotive and other industries. FRC are designed to have both creep as well as fatigue resistance at a high operating temperature. The first step in the production of FRC is the selection and preparation of proper fibres. The second step is to mix the fibres in a commingled hybrid yarn, which is a textured yarn consisting of continuous reinforcement fibres (for example carbon or glass) and thermoplastic fibres (for example PEEK or PP). Since the hybrid yarn is soft, it is very suitable for producing fibre pre-forms using almost any textile technology. In the subsequent heating and consolidation process, the thermoplastic fibres melt and become the matrix material, and the reinforcement fibres are impregnated with the matrix in the formed fibre composite material (see Figure 1.1). Two cases of hybrid yarn, PEEK/CF and PP/GF, are briefly explained as follows:

Case 1 Commingled hybrid yarns PEEK/CF (carbon fibre) [Hufenbach 2002]: PEEK fibres as a thermoplastic matrix material and carbon fibres as a reinforcement are used to produce high

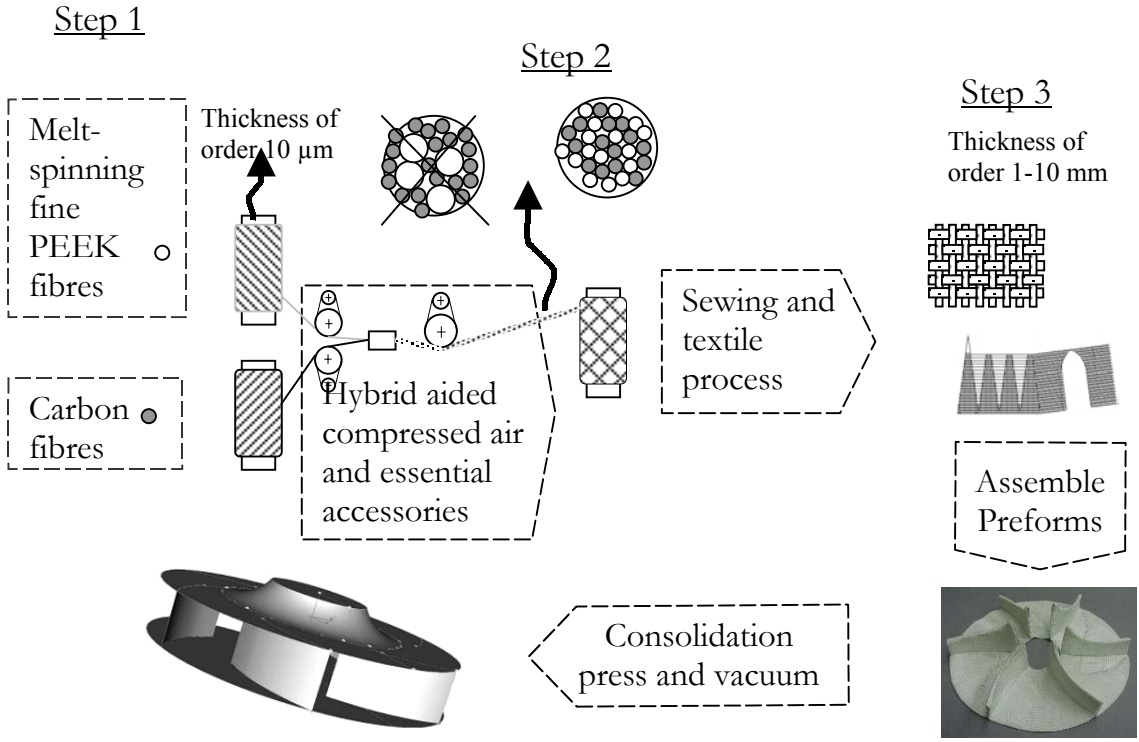


Figure 1.1 Melt spinning as starting process to produce the Fibre Reinforced Composite [DFG Project FOR278/2]

performance rotors from reinforced textile composite to use in complex applications. Carbon fibre is selected as a reinforcement material due to its high strength. The PEEK fibre is selected as the thermoplastic matrix material for its relative high operating temperature and a stable chemical resistance. An advanced composite rotor was developed for high rotation speeds up to $100,000 \text{ min}^{-1}$. Construction of the net shape rotor pre-form is achieved by means of different stitching processes. The machines of the ready-made-clothing technology allow the specific sewing-up of the semi-finished textile products into a three dimensionally reinforced multi-layer composite structure [Herzberg 2001].

Case 2 Commingled hybrid yarn PP/GF: In this case the glass fibre is produced with special lubricant to be used as reinforcement and the low viscous polypropylene is used as a matrix polymer. This makes for fast and simple processing of hybrid yarn.

Theoretical investigations concerning the diameter ratio of two-fibre system (reinforcement and matrix) to design the hybrid yarn were summarised by Beyreuther [2001] using the following criteria:

- Filament Surface/Volume Ratio (FSVR) criterion: if the FSVR ratio of reinforcing fibres (CF or GF) come near to matrix fibres FSVR Ratio, then the better laminate can be obtained.
- Each Other Touch (EOT) criterion: If the number of matrix filaments are at least as high as the number of reinforcement in the hybrid yarn, bonding with less defect can be achieved.

Following these two criteria, the optimal consolidation can be obtained if the hybrid yarn has a uniform and homogeneous mixture of reinforced fibres and matrix. This can be realised if both components have the same diameter and same cross section area. Classical reinforcements (CF/GF) have a relatively small diameter in the order of $10 \mu\text{m}$. Brünig [2002] explained that the available PEEK yarn with a diameter of $20 \mu\text{m}$ and the commercial CF with a diameter of $7 \mu\text{m}$ makes a hybrid yarn with 40/60 volume ratio (see Step 2 in Figure 1.1). In this type of hybrid yarn components, the thermoplastic molten can not reach every reinforcing fibre during press and consolidation. This can lead to unbounded reinforcement and a FRC with defects. Therefore, in order to have a better reinforcement, the diameter of the PEEK fibre must reach $12 \mu\text{m}$ or even $10 \mu\text{m}$ when possible.

1.3 Goals and methods of this work

In order to supply the fine PEEK filaments to use later as hybrid yarn for reinforced thermoplastics, the following two goals have been established:

The first goal is the investigation of fine PEEK filaments produced by the melt spinning process. In order to produce the fine filaments, it is necessary to find the proper spinning conditions such as take-up speed, throughput, draw down ratio, melting temperature and take-up point. To obtain a more fundamental understanding of the spinning conditions on the melt spinning process, on-line measuring of fibre speed and temperature is carried out in order to examine the cooling rate, extensional viscosity, necking effect and stress along spinning line. Based on the on-line measurements and the proposed new model of extensional viscosity and cooling rate, the mathematical model is improved to compare with the experimental results. In the theoretical part, the steady state equations of melt spinning are submitted to cover PEEK properties such as density and a specific heat as a function of temperature, and viscosity as a function of temperature and strain rate. The equations are solved after the implementation of the constitutive equations of viscous (Newton model) and viscoelastic (Maxwell model). The suitable model describes the fibre formation of fine PEEK fibre, which confirms close results to online measurements, is also used to study the effect of different spinning conditions. The effect of the spinning conditions on properties of filaments such as fineness, stress-strain curve, tenacity and structure (birefringence and crystallinity) are parts of this analysis. The so-named off-line measurements characterise the properties of as-spun fibres.

The second goal is to find the limits of spinnability by repeating the process in a trial form and by also repeating the spinning conditions for spinnable region of the fine filaments. In this part, the take-up speed and the mass throughput of material are changed to find the stable spinning conditions. The design of arrangement of holes, the number of spinneret holes, melting temperature and effect of heating tube are changed to improve the spinnability in practice. To decrease the take-up point (distance from spinneret to winder), a special moveable winder was used.

To overcome the problems and to find the unknowns, this work is supported by experimental and analytical methods. In the experimental part of the work, a large number of equipment and methods are incorporated; Melt spinning equipment in the laboratory and the semi-production scale are used.

1.4 Outline of the thesis

Based on the above stated goals, the thesis is divided in five chapters as follows:

The experimental methods and equipment used are summarised in Chapter 2. The first section of Chapter 2 concerns the melt spinning equipment, the apparatus for on-line measurements, the base of measurement and the required temperature corrector. The last section of Chapter 2 describes the off-line measurements of as-spun fibre and contains the selected materials' properties of PEEK and PP used in this thesis.

The first section of Chapter 3 describes the shear melt rheology of PEEK and PP, and the material function. In the second section of the Chapter 3, the extensional viscosity of PEEK is estimated by on-line measurements. The proper expression for extensional viscosity is found using the three models: viscous, viscoelastic and non-linear viscoelastic.

Chapter 4 contains the structural and mechanical properties of as-spun fine PEEK fibres. Therefore, this chapter can be dealt separately. The fineness and diameter of as-spun PEEK filaments are compared to as-spun PP filaments. The optical birefringence and degree of crystallinity of as-spun PEEK fibre are measured and discussed over spinning conditions. The final section of Chapter 4 covers the stress strain curves and the modulus elasticity for different spinning conditions.

In Chapter 5, the equations of steady state melt spinning and the implementation of constitutive equations (Newton, Maxwell and upper-convected Maxwell) are explained. The fibre formation model using the material function and other properties for PEEK is also applied in this chapter. Comparison of fibre temperature and speed profile, both experimentally and theoretically, are given. The last section of Chapter 5 deals with the tension and stress profile along the spinning line.

Chapter 6 investigates the spinnable regions and the spinnability limits (under different spinning conditions such as throughput and take-up speed, etc.) for PEEK and PP. The effect of melt temperature and viscosity are explained briefly and the optimisation of spinning conditions for fine PEEK filaments are explained (based on the fibre formation modelling and experiments).

2 Experiments and measurements

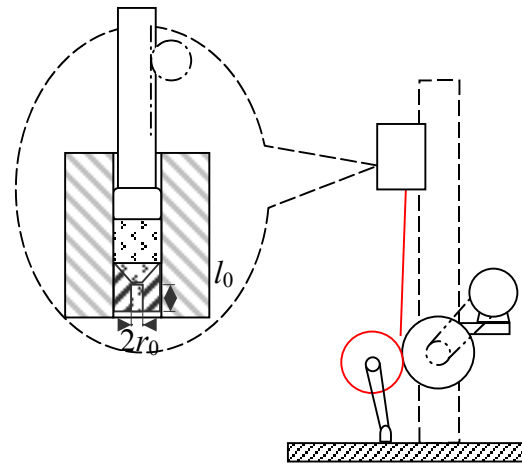
Chapter 2 consists of four sections which describe the experimental methods, measurements and the melt spinning equipment used in this thesis. The first section describes the main parts of the melt spinning equipment and their various functions. On-line measurements including fibre speed, temperature and diameter along the spinning line are discussed thoroughly in the second section. Off-line measurements for the structural and mechanical properties of the as-spun fibre at room temperature are explained briefly in the third section. Finally, the rheometry and the properties of original materials for both PEEK and PP thermoplastics are summarised in the fourth section.

2.1 Melt Spinning equipment

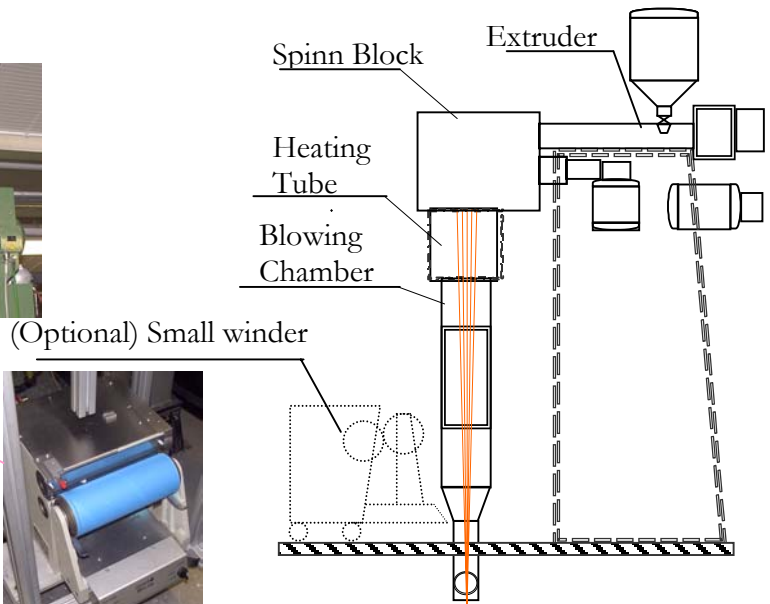
Two types of spinning equipments are used in this thesis and these are introduced simply by general specifications and geometrical arrangements. Two different equipment arrangements are used for melt spinning experiments at the Institute of Polymer Research Dresden e.V.: one using piston equipment and the other using extruder equipment. Both arrangements consist of two major units: (a) an extrusion unit to melt the polymer and to supply definite throughputs, and (b) a wind-up unit to supply the take-up speed.

Piston equipment: The piston ($D_p=10$ mm) equipment is designed for small scale spinning and can support mass throughputs from 0.01 g/min up to 10 g/min and take-up speeds from 5 m/min to 1200 m/min, see Figure 2.1.1 (a). This small scale arrangement is basically able to spin with a few grams of polymer and can be applied for some flexible spinning conditions. Piston spinning allows one to quickly realise the desired conditions (mainly a very low mass throughput) and to optimise the spinning conditions for the special material.

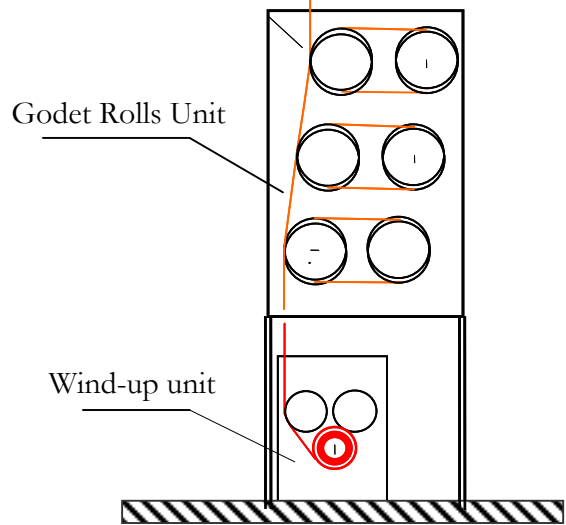
Extruder equipment: In the extruder equipment, the extruder geometries are ($D_e=18$ mm and $L_e/D_e=25$) and a gear spinning pump supports the throughput of the polymer melt in the spinneret. It can supply mass throughputs ranging from 5 g/min up to 50 g/min and take-up speeds ranging from 50 m/min to 6000 m/min. Figure 2.1 (b) shows the three major units of extruder equipment. The godets unit only exists in extruder equipment for the drawing after the fibre formation process, which can be heated and rotated separately up to 7000 m/min. For more details about melt spinning equipment specifications, the references under Beyreuther, Brüinig, Vogel and Schmack are recommended.



(a)



(Optional) Small winder



(b)

Figure 2.1.1 (a) Piston equipment (b) extruder equipment for melt spinning in IPF Dresden

2.2 On-line measurements (along the spinning line)

The on-line measurements of fibre speed, temperature and diameter are used in the thesis as non - contact measurement methods [Golzar et al. 2002]. The same methods are also reported by Ohkoshi et al. [2000] and Götz et al. [2001]. Contacting methods for temperature measurements such as thermocouples are used for glass fibre [Xiang et al 2001], but can also disturb the polymer melt and the cooling process in the fibre formation zone.

2.2.1 Fibre speed measurements

The laser Doppler anemometry device named 'LaserSpeed LS50M' (TSI Inc., USA) measures the speed of moving filament, see Figure 2.2.1. The device works principally as follows: a laser beam produced in the device is separated into two convergent parts and is focused on the running fibres. When two laser beams intersect, an interference pattern of both light and dark fringes is created. The distance between the fringes is a function of wavelength and the angle between the beams.

Nearly all materials (including synthetic fibre and plastics etc) have light scattering sites-particle and minute facts that make up the surface microstructure. As a light-scattering site passes through the measurement region, light is scattered every time it passes through a light fringes. The scattering-light is collected and converted to an electrical signal that has a frequency proportional to the material velocity. The reflected beams are detected by an optical system. The control unit receives the signals, evaluates by fast transformation and gives an absolute speed value. The fibre speed is obtained by dividing the distance between the fringes by the time it takes for the light scattering site to move from one fringe to the next. The distance between the device and fibres is approximately 280 mm, and can be adjusted in such way that two laser beams meet each other exactly at the fibre surface. The laser device is mounted onto a vertical stand and can be moved up and down along the spinning line. The measurements of fibre speed contain uncertainties at high speeds due to the fluctuation of moving fibre. The data is displayed on a connected computer and can be saved for evaluation.

2.2.2 Temperature thermography and emission correction

The temperature measuring system consists of three subsystems: an infrared camera, a monitoring subsystem and a newly developed processing subsystem to calibrate and correct the infrared temperature measurements.

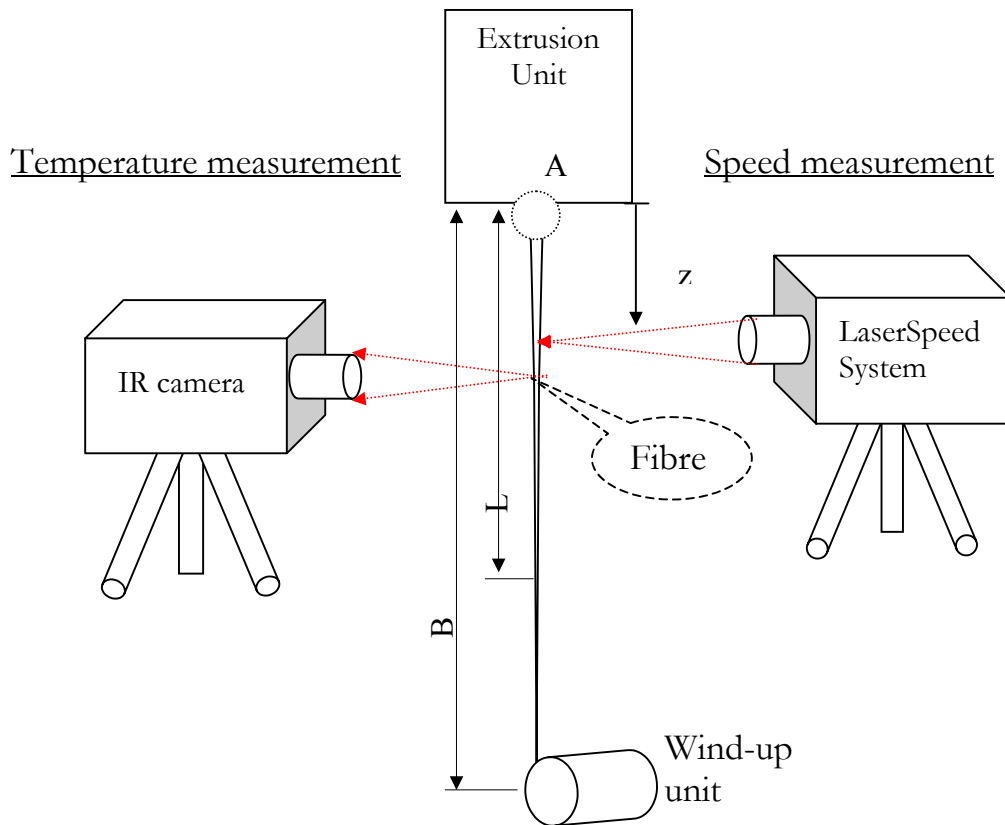


Figure 2.2.1 On-line measurements of fibre temperature and speed along the spinning line

Infrared camera: The VarioTHERM™ is a portable infrared camera designed for precise real time thermography applications by Jenoptik AG, Jena, Germany. The spectral sensitivity of the camera ranges from 3.4 μm to 5.0 μm and can renew the measurement every 20 ms. A precise microscope lens MWIR f/4.4 is added to make our special measurement possible. Another essential accessory is the stable and portable tripod that fixes the camera and can adjust it vertically and horizontally.

Monitoring subsystem: The monitoring subsystem includes various hardware components such as a personal computer connected to the camera, some interfaces and converters. The special IRBIS® software package is supported by InfraTec GmbH, Dresden, Germany. It is possible to receive the digital data from the camera and with regards to the target on the monitor live, to take snapshots, open and save the thermography as files etc. [InfraTec 1998].

Correction subsystem: As shown in Figure 2.2.2, the on-line measurement of temperature along the spinning line can be used to estimate the diameter. The temperature will be corrected using an emissivity correction factor depending on the fibre diameter (see Figures 2.2.3 and 2.2.4).

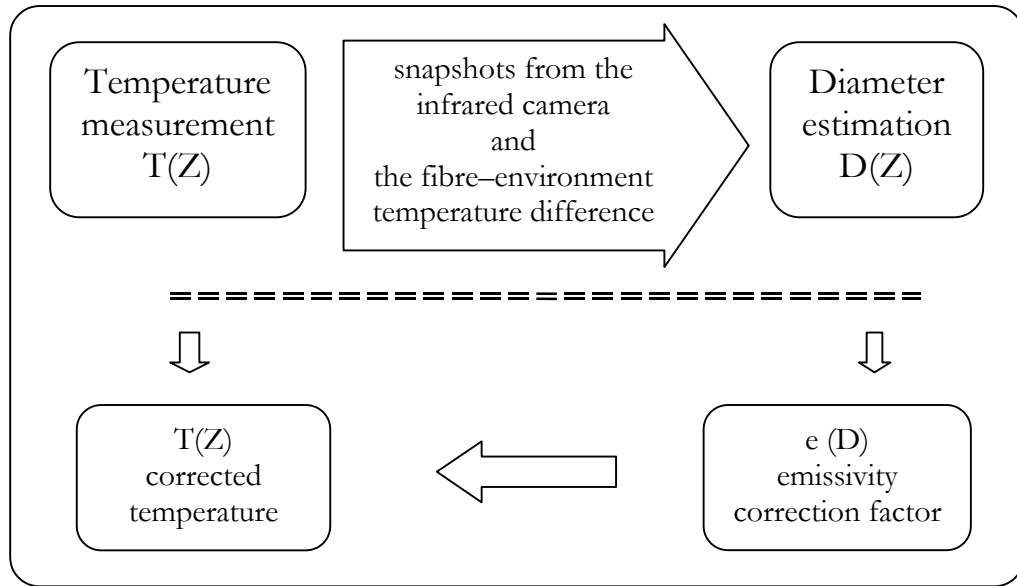


Figure 2.2.2 General principles of the on-line temperature measurements and correction

Temperature correction: As already mentioned, the infrared thermography is a non-contacting measurement method. The total value of energy received by the infrared camera splits into three components and can be expressed in the following simplified formula:

$$em + re + tr = 1 \quad , \quad (2.2.1)$$

where $em = W_e/W$ is the emissivity, which indicates the ability to send infrared energy; $re = W_r/W$ is the reflectivity, which indicates the ability to reflect infrared energy and $tr = W_t/W$ is the transmittivity, which indicates the ability to transmit infrared energy (other symbols are referred to the list of symbols from this point onwards). It is obviously that: $0 \leq em, re, tr \leq 1$.

Emissivity: Black bodies can exclusively emit radiation and do not reflect or transmit infrared waves, therefore, as given in Equation (2.2.1), the emissivity value for a black body has a maximum of one ($em=1$ and $re=tr=0$). In reality, the fibre is not an ideal black body, and as a result, the emissivity of the fibre is less than one ($em < 1$). The emissivity of a target generally depends on many parameters such as material composition, surface oxide layer thickness, surface roughness, the normal axis angle, temperature and polarization direction. The thermography of polymers is classified into two different thicknesses: solids with a thickness of at least a few millimetres, and very thin films or fibres. It can be generally observed that the polymers as solids give an emissivity of close to one ($em \approx 1$), but the emissivity of fibres behaves in a more

complicated manner in infrared measurements, because the emissivity as a correction factor depends on the fibre thickness. In addition, just like other materials, polymers have a spectral emission or transmission according to their chemical composition [InfraTec 1998].

In the present work, the emissivity as a correction factor was found for different fibre diameters and different temperatures. The following two methods were arranged experimentally:

- a) Heated chamber and black background
- b) Heated, polished and fixed drum.

Heated chamber and black background: In the first experimental method, a dark, closed heated chamber was prepared, and a fibre was hanged in front of a heated background, see Figure 2.2.3 (a). The temperature in the chamber is supplied by hot air assumed to be a fibre temperature. The experiment was carried out for different fibre diameters and different chamber temperatures. The background temperature was measured and could be adjusted lower or higher than the fibre temperature. The energy that the camera received, as shown in Figure 2.2.3 (a), can be simply written in the following form:

$$W = \epsilon_m f \cdot W_f + \text{tr}_f \cdot W_h + \text{re}_f \cdot W_f \quad , \quad (2.2.2)$$

where the index f refers to the fibre and the index h refers to the heated black background. The following conditions were assumed: no or small fibre reflection ($\text{re}_f \approx 0$), equal fibre and hot air temperatures ($T_f = T_a$) and that the heated background is a black body ($\epsilon_m h \approx 1$). According to the aforementioned assumptions, Equation (2.2.2) and Equation (2.2.1) can be simplified:

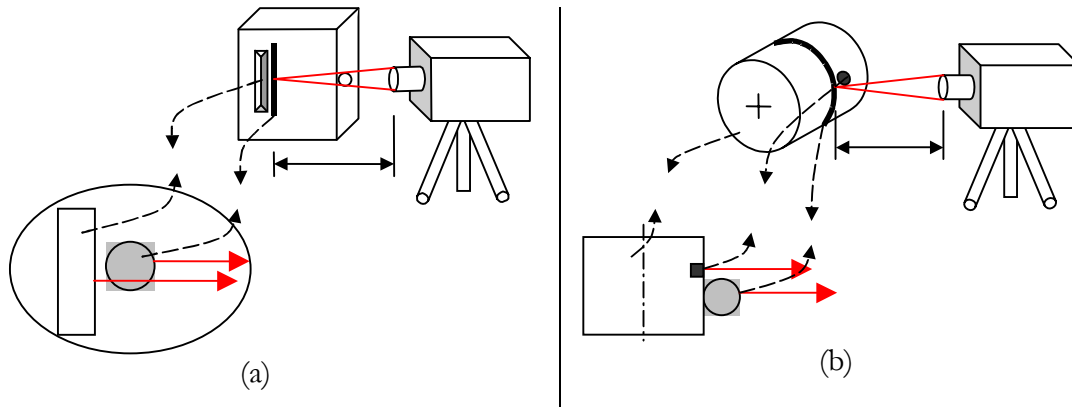


Figure 2.2.3 Two methods to find the emissivity corrector for thermography of fibre
(a) heated chamber (b) polished drum [Golzar et al. 2004]

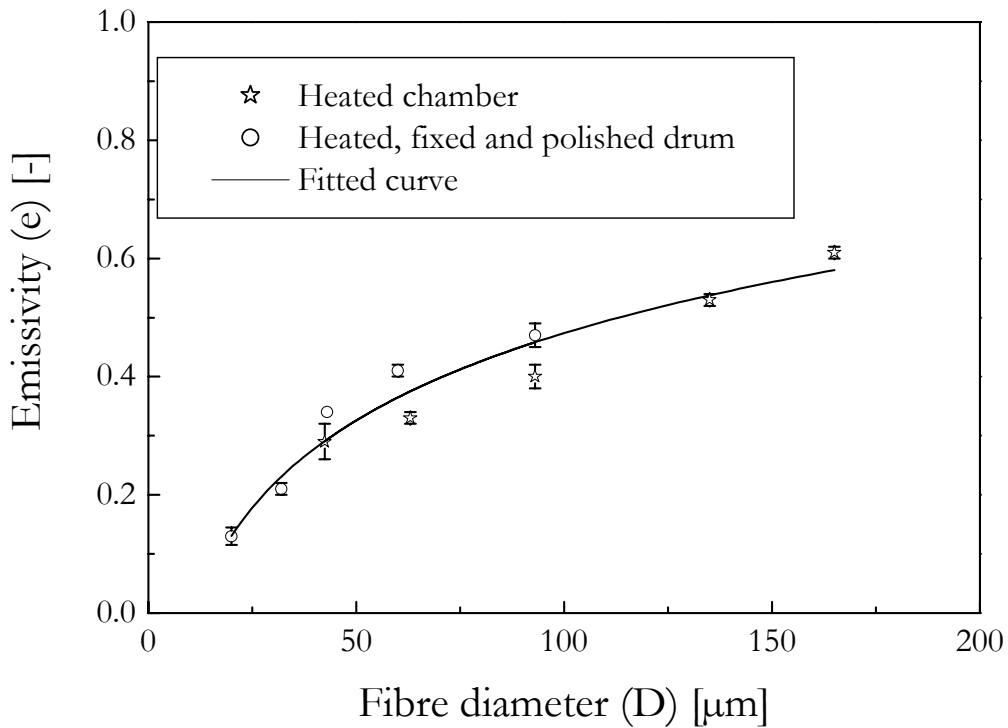


Figure 2.2.4 Results for the emissivity correction factor using two experimental methods

$$W = \text{em}_f \cdot W_f + (1 - \text{em}_f) \cdot W_h \quad (2.2.3)$$

Equation (2.2.3) can only be used to find the emissivity of the fibre (em_f) if the fibre and background temperatures are differently assigned. The results were calculated using the IRBIS[®] computer program, supported by the infrared camera by varying the emissivity (em_f) until the measured fibre temperature had reached the real temperature value.

Heated, polished and fixed drum: In the second experiment, as shown in the Figure 2.2.3 (b), the polished drum (diameter 193 mm) was heated electrically, and part of the fibre was bound around the drum. The fibre and drum temperatures were measured with the infrared camera at different temperatures and fibre diameters. The assumptions for this experiment are as follows: no or only slight emissivity of polished drum ($\text{em}_d \approx 0$), equal fibre and drum temperature (conduction heat balance) and a reference point painted black, as the drum was assumed to be a black body ($\text{em}_p \approx 1$). In this case, the following equation is valid:

$$W = \text{em}_f \cdot W_f \quad (2.2.4)$$

The two experiments mentioned above were conducted in order to determine the emissivity correction factor. It was observed that the fibre temperature had no or only a very slight effect on the measured emissivities. Figure 2.2.4 summarises the comparison with the emissivities dependent on the PEEK fibre diameter, derived from the two experiments. The emissivities for the fibre diameters (20, 32, 42.4, 60, 63, 93, 135, 165) μm , which are presented in Figure 2.2.4, were fitted with a general simple logarithm expression showing a difference of less than 5 %.

The emission corrector for polybutene was found and reported by Joshua [2000]. He found the correction factor for a different material type and with another experiment but the emissivity correction factor still shows the same tendency as given in Figure 2.2.4

2.2.3 Diameter estimation via infrared measurements

The LaserSpeed LSM 50 (TSI Inc.) measures the fibre speed, and the fibre diameter can be calculated by using the continuity equation (throughput and density are assumed to be known). The fibre diameter can also be calculated from the on-line fibre speed measurement and the continuity equation, Equation (5.1.2). Using a new approach, the diameter of the fibre was estimated along spinning line by gauging on-line temperature measurement via infrared camera; this was reported successfully by Vogel et al. [2003]. A brief literature review to on-line fibre diameter measurement and more detail about this new method is given by Golzar et. al. [2004]

The infrared camera displays the temperature of the fibre and the surroundings as shown in Figure 2.2.5 (left). This figure contains the temperature as a digit in every pixel. The temperature distribution of an arbitrary line perpendicular to the spinning line is shown in Figure 2.2.5 (right).

As explained in Section 2.2.2, the IRBIS[®] software package instantaneously shows the temperature measurement along the spinning line and also takes snapshots. Every snapshot contains 256×254 pixels, and every pixel refers to a known temperature. Therefore, the output ASCII file corresponding to the snapshot contains 256×254 temperature values. Every pixel occupies 25 μm , which means that every snapshot displays a temperature area of about 6×6 mm^2 . The camera was adjusted to move vertically using the elevator of the tripod. The snapshots were taken at desired vertical distances to the spinneret.

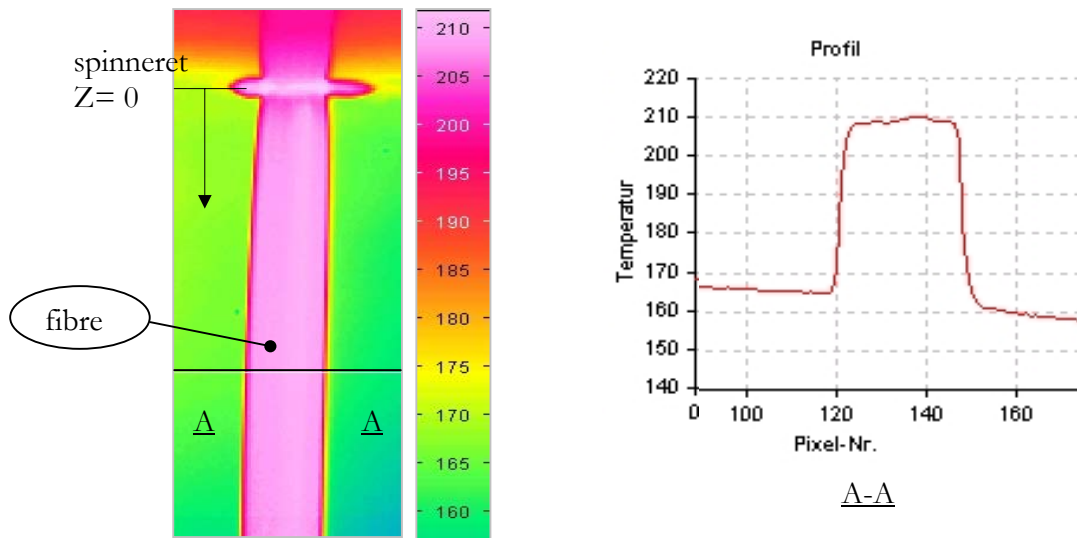


Figure 2.2.5 (left) Snapshot of the fibre after leaving the spinneret
(right) the cross temperature profile

The estimation of the fibre diameter using temperature measurement was automated using own subroutines. The NADIA¹ computer program was developed in the Visual Basic language with active X and associating a MS-Excel spread sheet. The output of IRBIS[®] is the input of the NADIA program. The program needs the following additional information: the number of snapshots, the vertical distance between two neighbouring snapshots and the respective names of the ASCII files. After starting the NADIA program, it works according to the flowchart shown in Figure 2.2.6. It reads the temperature at every point with distance (z) and also finds the maximum value. The maximum value is assumed to be the fibre temperature; the other temperature values on the same line are compared with the maximum, and the number of pixels (temperatures), which are higher than the ambient temperature, are found. The total number of counted pixels now indicates the fibre diameter after multiplying by $25 \mu\text{m}$. In other words, the key of the method is the difference between the fibre and ambient temperature as shown in Figure 2.2.5 (right). The measured maximum temperature is the fibre temperature, but this temperature varies across the fibre diameter and in turn drops to ambient temperature. This drop of the temperature from fibre to ambient is used to estimate the fibre diameter. Using this method, the estimated fibre diameters are to be accurate about $\pm 25 \mu\text{m}$, and are limited from $25 \mu\text{m}$ up to $5000 \mu\text{m}$ (the limit of IR-camera resolution).

¹ New Approach of DIAMeter measurement

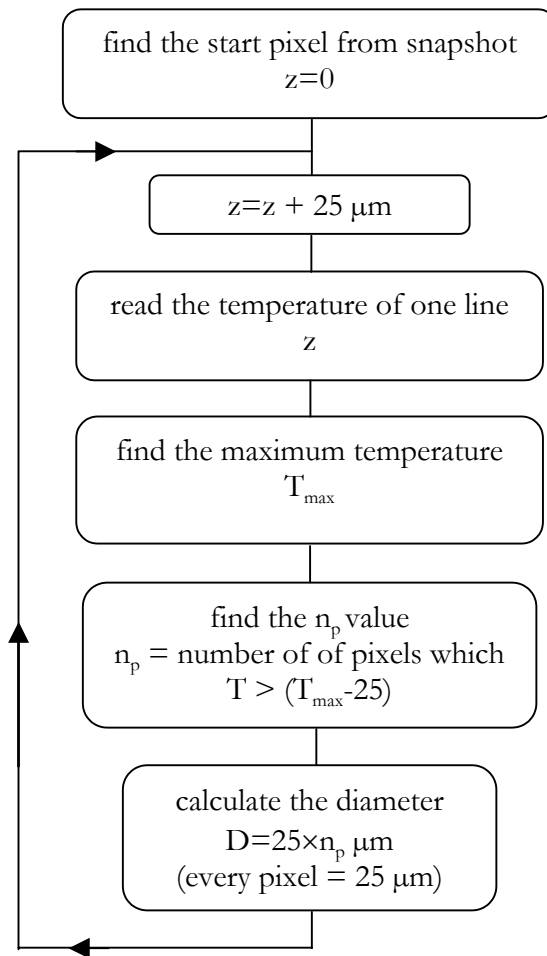


Figure 2.2.6 Flowchart of diameter estimation via the infrared temperature measurement

2.3 Off-line measurements (as-spun fibre characterisation methods)

This section briefly describes the different methods used to characterise the as-spun fibre (as a product of melt spinning). It contains a general description of the equipment, the accuracy and the formula used to find the mechanical and geometrical properties (diameter, fineness, tenacity, stress-strain) and the structure of end product (as-spun fibre orientation and degree of crystallinity).

2.3.1 Fineness and diameter measurements

To determine the filament fineness, two methods have been used in this work according to DIN53834:

- Gravimetric method: measuring the mass of 100 m fibres, or 1 m for 10 samples. The mass scale used (Sartorius BP 110 S) has an accuracy of ± 0.0001 g;
- Optical method: measuring the filament diameter by means of microscope with an accuracy of ± 0.2 μm .

The fineness is a combination of mass and length of fibre and is normally assigned by titre (Γ_t). The titre unit is presented in Tex (1 g/1 km) or dTex (1 g/10 km). The following formulas can be simply derived [Fourné 1995] and are often used for textile fineness:

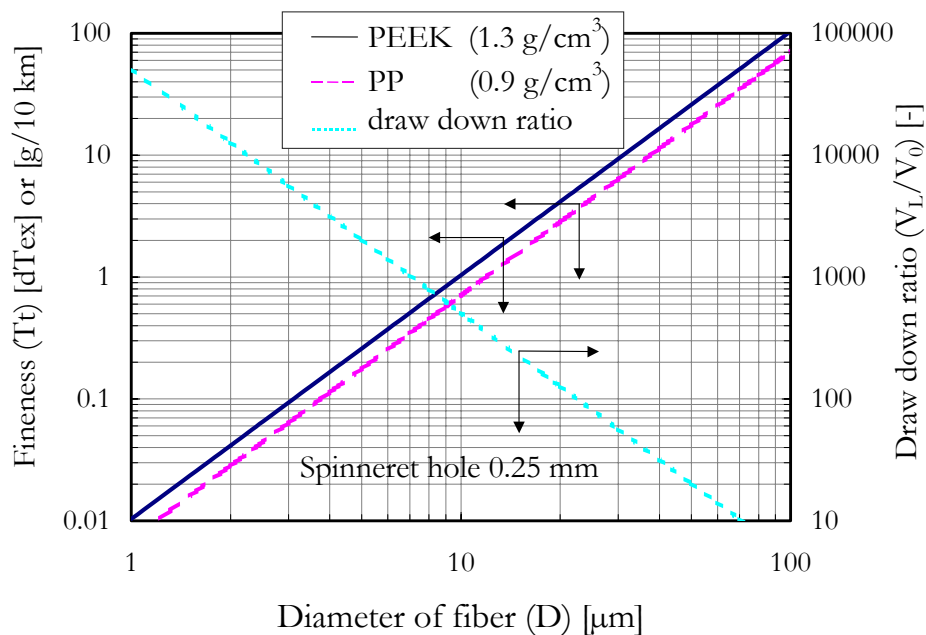


Fig 2.3.1 Fineness and draw down ratio of PEEK and PP as a function of fibre diameter, the effect of polymer density ($\rho_{\text{melt}}/\rho_{\text{solid}}$) is for fibre diameter over draw down ratio considered.

$$(a) T_t = 0.01 \cdot \frac{\pi \cdot D^2}{4} \cdot \rho \quad (b) D = 20 \sqrt{\frac{T_t}{\rho \cdot \pi}} \quad , \quad (2.3.1)$$

where D is the diameter of fibre in μm , ρ is the density of fibre in g/cm^3 and T_t is the fineness of fibre in dTex. Fineness and draw down ratio of two polymers (PEEK and PP) are compared graphically in Figure 2.3.1. The fineness (T_t) can be expressed as a spinning parameter in Equation (2.3.2) (a):

$$(a) T_t = 10000 \cdot \frac{Q}{V_L} \cdot \frac{1}{DR} \quad (b) T_t = 10000 \cdot \frac{\rho_0 \cdot A_0}{V_L/V_0} \quad , \quad (2.3.2)$$

where T_t is the fineness in dTex, Q is the mass throughput in g/min , V_L is the take-up speed in m/min and DR is the possible draw ratio. By neglecting the drawing after the spinning and replacing the mass throughput from the continuity equation, the fineness as a function of draw down ratio is found and expressed in Equation (2.3.2) (b). In this equation, T_t is the fineness in dTex, (V_L/V_0) is the draw down ratio, the ρ_0 is the melt density in g/cm^3 and A_0 represents the spinneret hole area in mm^2 .

2.3.2 Tensile test

The tensile test (force-deformation test) was carried out in accordance with DIN 53834 by the tensile strength testing device GOODBRAND MICRO 350. The error raised in the test device for force measurement is about ± 0.01 N. The test used a sample fibre length of 100 mm, and the fineness determined from the gravimetric method in Section 2.3.1 was used as an input. Other important input data were the test speed 200 mm/min , which is dependent on the elongation of the fibres and the pre-stress, which is dependent on the fineness.

Tenacity can be defined as the tensile strength with relation to the fineness of fibre, and can be calculated as follows:

$$R_{\text{cN/dtex}} = F/T_t \quad R_{\text{cN/dtex}} = 0.1 R_{\text{GPa}} / \rho \quad , \quad (2.3.3)$$

where $R_{\text{cN/dtex}}$ is the tenacity in cN/dTex , R_{GPa} is the tensile strength in GPa , ρ is the density in g/cm^3 . The physical tenacity is defined as: $R_u = R_{\text{cN/dTex}} \cdot (1 + 0.01 \delta_u)$, where δ_u is the elongation at the break in %. The tensile device measures and displays the force (F) versus the deformation (δ). The following equations are used to find the true stress σ (Pa) and true strain ε (Hencky's strain):

$$\varepsilon = Ln\left(1 + \frac{\delta}{100}\right) \quad \sigma = F \cdot \left(1 + \frac{\delta}{100}\right) / A_i \quad , \quad (2.3.4)$$

where δ is the deformation in %, F is the tensile force in N and A_i is the initial area of fibre in m^2 . Equation (2.3.4) is normally not valid when the necking is occurred. The elasticity modulus (E) was found in the linear elastic range ($\varepsilon < 0.01$) from general relation $E = \sigma / \varepsilon$.

2.3.3 Crystallinity and birefringence measurements

Crystallinity: The degree of crystallinity can be measured using the following three methods: (a) by measuring the density of as-spun fibre, (b) using the on-line temperature measurement along the spinning line and (c) using DSC measurement. However, in order to compare the methods (a) and (c), they should be carried out at the same time after spinning, and the method (b) can give the on-line crystallinity along the spinning line until the solidification point.

a) The volumetric degree of crystallinity (X) can be calculated from the density of as-spun fibre (ρ_p), the amorphous density (ρ_{am}) and crystalline density (ρ_{cr}) of polymer, which is found using

the simple formula $\rho_p = X \cdot \rho_{am} + (1 - X) \cdot \rho_{cr}$ or $X = \frac{\rho_p - \rho_{am}}{\rho_{cr} - \rho_{am}} \left(\frac{\rho_{cr}}{\rho_p} \right)$ [Ziabicki 1985]. The

density of fibre (ρ_p) is determined by measuring the titre and diameter of fibre from Formula 2.3.1 (b). For PEEK, ρ_{cr} and ρ_{am} are given in Tables 2.4.1 and 2.4.4.

b) Using the on-line temperature measurement which discussed later in Chapter 5, Section 5.2.4.

c) Using the DSC method to determine the melting and glass temperature and degree of crystallinity of the melt-spun fibres by TA Instrument. The enthalpy of fusion of fully crystalline PEEK is taken as $\Delta H = 130 \text{ J/g}$ [Blundell 1983]. The degree of crystallinity is calculated as follows: finding the difference between the endothermic peak area and the post-crystallization area (the area under the exothermic crystallization), which is divided by the fully crystalline enthalpy (ΔH). The DSC measurements are carried out in following steps with heating rate of $20^\circ\text{C}/\text{min}$:

For PEEK

1. First heating from 30°C to 380°C in order to find the cold-crystallization
2. Cooling down from 380°C to 30°C
3. Second heating from 30°C to 380°C to find the maximum crystallinity

For PP

1. First heating from 30°C to 230°C in order to find the cold-crystallization
2. Cooling down from 230°C to 30°C
3. Second heating from 30°C to 230°C to find the maximum crystallinity

Birefringence measurements: Total orientation can be measured as birefringence (Δn) using a polarized optical microscope with a 30 order tilting compensator. To determine the birefringence value, 10 measurements in different points for every sample are carried out. The diameter measured by the same microscope and the mean value and standard deviation are determined. The birefringence is calculated after determining the diameter and the two angles in the opposite direction in the proper formula.

2.4 Material properties of original granules

In this section, the properties of original material granules of both PEEK and PP polymers are collected. The experimental method related to melt behaviour by rheometry is given first.

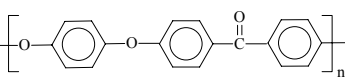
2.4.1 Rheometry

The rheological measurements in this work are found by using rotational shear rheometry carried out by the Rheometer ARES-PA[®] from the company RheometricScientific, USA. The software, named the Orchestrator[®] 6.5.1 evaluates the results in Windows 95[®]. The configuration used was cone plate geometry with \varnothing 25 mm and cone \angle 0.1 rad. The heating gas for all measurements was dried nitrogen. The samples were prepared as follows: drying 3 h in the air circulating oven at 150°C to normal atmosphere. The water content was determined by coulometric titration at 120°C [Schmack 2000]. The samples were heated in an oven and the water was transported to the titration vessel. The following data was adjusted to the specifications of each individual test.

- Small angle oscillating sweeps for the domain 0.1-100 s⁻¹ with an oscillating amplitude of 10%. The three melting test temperature were 360°C, 380°C and 400°C for PEEK and 200°C, 230°C and 260°C for PP respectively. The reference temperatures of master curve were 380°C for PEEK and 230°C for PP.

- Time dependence for 1 rad/s, 30 min, with an amplitude of 10 %, using a temperature of 400°C for PEEK and 230°C for PP respectively.

2.4.2 General material properties of PEEK (in comparison with PP)

PEEK (poly (ether ether ketone)):  Common types from the company Victrex PEEK are used for the experiments of this thesis. Typical properties of Victrex® PEEK™ 151 G are listed in Table 2.4.1. The general properties of PEEK are as follows: excellent chemical resistance, very low moisture absorption, inherently good wear and abrasion resistance and that it is unaffected by continuous exposure to hot water or steam.

Property	Test Method	PEEK	Units
Density (crystalline)	ISO 1183	1.32	g/cm ³
(amorphous)		1.26	
Typical crystallinity	N/A	35	%
Water absorption (24 h, 23°C)	ISO 62	0.5	%
Melting point	DSC	334	°C
Glass transition temperature	DSC	143	°C
Melt operating temperature		375-400	°C
Specific heat capacity (melt)	DSC	2.16	kJ/kg/K
Thermal conductivity	ASTM C177	0.25	W/m/K
Tensile strength (23 °C)	ISO 527	100	MPa
(250 °C)	50 mm/min	12	
Tensile elongation (Break 23°C)	ISO 527	U _p to 60	%
(Yield 23°C)	50 mm/min	5	
Secant Modulus (1% strain 23°C)	ISO 527	3.5	GPa
Flexural Modulus (23°C)	ISO 178	4.1	GPa
(120°C)		4.0	
(250°C)		0.3	
Flexural strength (23°C)	ISO 178	170	MPa
(120°C)		100	
(250°C)		13	
Shear strength (ultimate, 23°C)	ASTM D3846	53	MPa
Shear Modulus (23°C)	ASTM D3846	13	GPa
Poisson's ratio (23°C)	ASTM D638	0.4	-
Shear viscosity (400°C)	In 1000 s ⁻¹	350	Pa.s
(380°C)		400	
(360°C)		480	

Table 2.4.1 Properties of PEEK 151 G according Victrex®

PEEK 450G	PEEK 380G	PEEK 150G
34,000	26,000	20,000

Table 2.4.2 Molecular weight obtained by the intrinsic viscosity [Ohkoshi 1996] based on [Devaux et al 1985]

Polypropylene HF445FB (from Borealis): The polypropylene used here was modified in order to have the proper surface condition for the hybrid yarn. A double screw extruder (ZSK30) was used to mix in 98 % PP HF 445 FB and 2% polybond 3200. Polybond is a type of additive used to decrease the viscosity of polypropylene and mainly to increase the bond of PP matrix to Glass fiber. The melt spinning of both elements in a double screw extruder did not directly satisfy the required condition. The Melt Flow Index (MFI) for the PP and the modifier are carried out and compared in Table 2.4.3. Borealis's other properties of PP HF445FB are listed in Table 2.4.4.

Material		Melting Index (MFI)	
1	PP HF 445 FB	18.2	gr/10 min
2	98% PP HF 445 FB +2% polybond 3200	20.1	gr/10 min
3	polybond 3200	121.6	gr/10 min

Table 2.4.3 Melting index of two types of polypropylene unmodified and modified

Property	PP	Units
Density (Crystalline)	1.0	g/cm ³
(Amorphous)	0.7	
(melt in 200°C)	0.712	
Typical crystallinity	65	%
Water absorption (24 h, 23°C)	<0.1	%
Melting point	161-165	°C
Glass transition temperature	4	°C
Melt operating temperature	200-270	°C
Preferred	230-240	
Specific heat capacity (melt)	3.18	kJ/kg/K
Thermal conductivity	0.12	W/m/K
Tensile strength (23 °C)	32	M Pa
Tensile elongation (Break 23°C)	400	%
(Yield 23°C)	9.8	
Secant Modulus (1% strain 23°C)	-	GPa
Flexural Modulus (23°C)	1.35	GPa
(120°C)	1.4	
Poisson's ratio (23°C)	0.32	N/A
Shear zero viscosity (200°C)	1200	Pa.s

Table 2.4.4 Properties of PP HF 445 FB according to producer (Borealis)

The specific volume, specific heat and the shear viscosity as a function of temperature: The specific volume is graphically given as both a function of temperature and pressure in Figure 2.4.1 (a), taken from the company Victrex. The density is found as a reciprocal of specific volume, which is shown in Figure 2.4.1 (b). To find the proper expression of density, there are two expressions reported: for a melt state, $\rho(T,X)=\rho_0/(1+\delta.(T-T_0))$ [Menges 1998], and for a solid state, $\rho(T,X)=\rho_0(X)+\alpha.(T-T_0)$ [Zieminski 1986]. Fitting to the density curve in Figure 2.4.1 (b) is given in Equation 2.4.1.

$$\rho(T) = \left\{ \begin{array}{ll} \frac{1310}{(1 + 0.000174 \cdot T)} & \text{if } T < T_g \\ \frac{1410}{(1 + 0.000793 \cdot T)} & \text{if } T > T_m \\ (-0.0037 \cdot T^2 + 1.112 \cdot T + 1181.6) & \text{if } T_g < T < T_m \end{array} \right\} \text{ in kg/m}^3, \quad (2.4.1)$$

where T is the desired temperature and T_g is the glass transition temperature and T_m is the melting temperature (all in °C). Density in the solid state is only taken as a function of temperature.

Specific heat of PEEK is assumed to be a linear function of temperature. Equation (2.4.2) is fitted to PEEK 151 G from the data given by Victrex[®], see Figure 2.4.2 (a).

$$Cp_p(T) = \begin{cases} 3.6 \cdot T + 1100 \\ 3.2 \cdot T + 1200 \end{cases} \rightarrow \text{if } T > T_g \quad \text{Where } T \text{ in } ^\circ\text{C} \text{ and } Cp_p \text{ in J/kg/K} \quad (2.4.2)$$

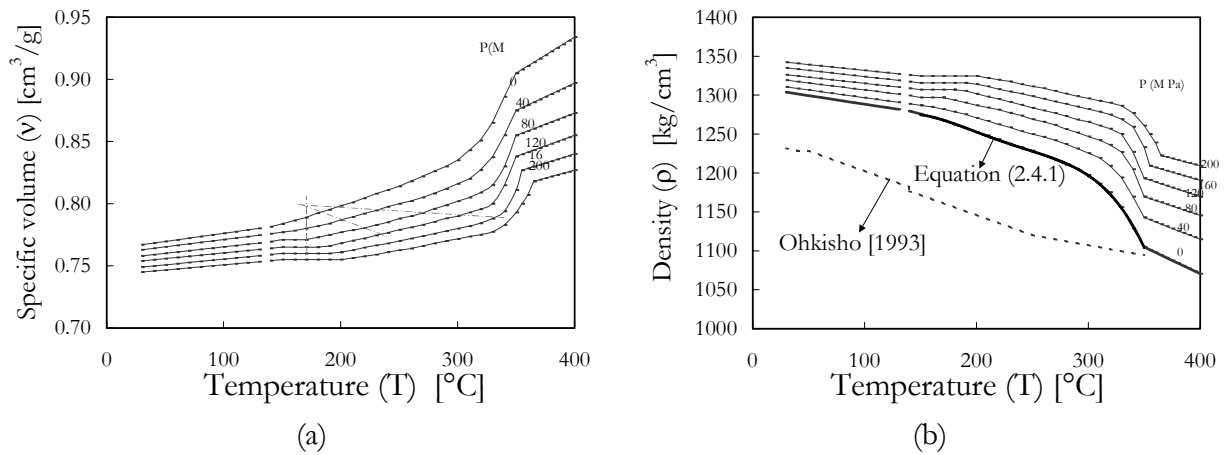


Figure 2.4.1 (a) PEEK specific volume as a function of temperature from producer (Victrex) (b) PEEK density vs. temperature in solid and melt calculated from specific value

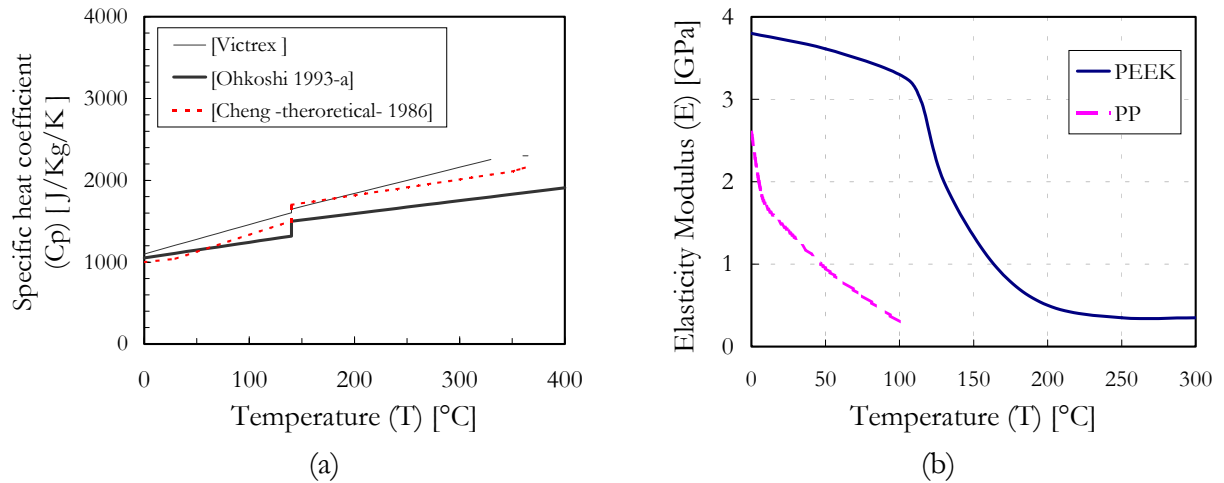


Figure 2.4.2 Diagrams over temperature for (a) Specific heat of PEEK (b) Elasticity Modulus for PEEK by crystallinity X~35 % and PP by crystallinity X~60-70 % [Ehrenstein 1999]

Typical elasticity modulus over temperature of partially crystalline PEEK and PP are given in Figure 2.4.2 (b). Figure 2.4.3 gives an overview of PEEK and PP shear viscosity in the melt condition compared to other polymers. PEEK has a high processing temperature, but the shear viscosity is in the same order as those of PP, Nylon 6,6, Soft PVC and LDPE.

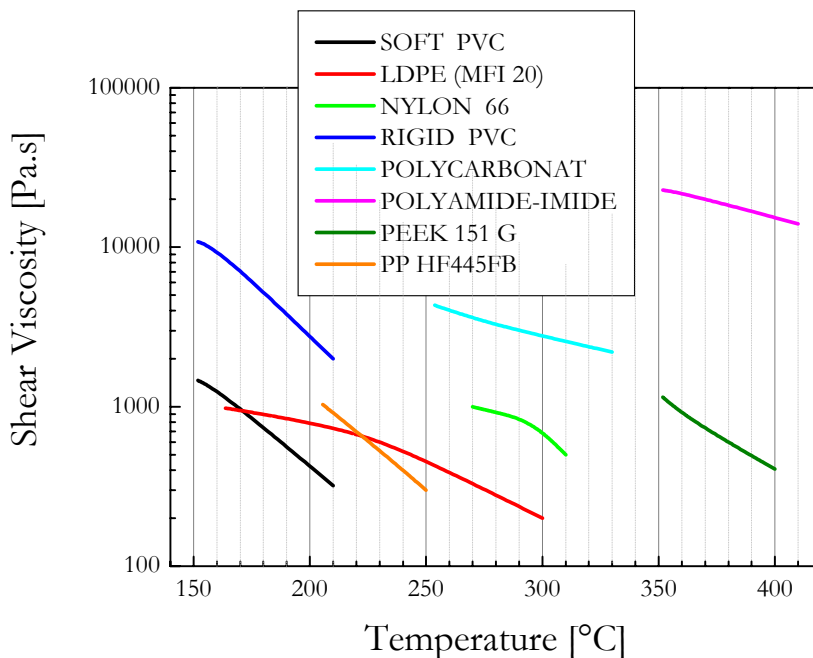


Figure 2.4.3 Shear viscosity over temperature in comparison with different polymers [Victrex]

3 Rheological studies in the melt spinning as extensional flow

Melt spinning involves various deformation and flow conditions: shear flow mainly in the spinneret channel and extension in the fibre formation zone. Therefore both shear rheology and extension rheology are considered. However, Schöne [1980] has also considered the solid deformation rheology after the solidification point. The polymer melts in the extruder, and the spinning pump (gear pump type) supplies the constant volume throughput through the spinneret. The polymer undergoes shear and extension in the extruder to spinneret capillary. Therefore stress and strain prehistory exists at the outlet of the spinneret, but in order to simplify the investigations, this prehistory is not considered here at first. The fibre formation zone is itself a free surface deformation process and can be assumed to be a pure uniaxial extension between the spinneret and wind-up unit.

The intent of rheological studies in this chapter is to provide two aspects. The first is to find the properties and parameters in the constitutive equation, and then submit these into the fibre formation model. The second is to investigate the spinnability, improve the material selection and melt spinning process parameters. As mentioned above, the polymer in the melt spinning process, especially in the fibre formation zone (from the spinneret to solidification point), mainly undergoes extension, but the shear rheology provides properties for the extension studies such as: the material function and material properties such as zero shear viscosity (η_0), temperature dependence viscosity ($\eta_0(T)$), and the shear strain rate dependence of viscosity ($\eta_0(\dot{\gamma})$). The shear relaxation strength (g_i) and relaxation time (λ_i), evaluated from the shear rheology, can also be used in the extension. Both the above properties from shear rheology and also the on-line measurements along the spinning line are used to modify the extensional viscosity. Chapter 3 includes some background on extensional rheology aided melt spinning, which is essential especially for (fine) fibre formation zone. Section 3.1 deals with the basic concept of shear viscosity, which is applied in the melt spinning model. Shear rheology is generally quite widely discussed in literature; by contrast, the extensional viscosity in Section 3.2 encounters some difficulties. The constitutive equations and their application are studied in Chapter 5, but in this chapter, the experimental methods and some results are discussed. The material function determined from shear rheology is replaced in the constitutive equations for the viscous, viscoelastic and nonlinear behaviour of material. The nonlinear behaviour is evident in time dependent measurements, and the damping function can be found from the shear rheology and also implemented in extension.

3.1 Rheological characterization and material function from shear flow

Shear rheology is basically the first polymer characterization, because in the shear rheometer, the deformation is homogenous and can simulate all cases: small, large and steady state deformation. The rough estimations used here for the flow behaviour of melt spinning are the small amplitude oscillatory shear, the steady state shear and the strain sweep test.

The simple constitutive equation for the simple shear flow is the Newton law for fluid ($\tau = \eta \cdot \dot{\gamma}$), which relate the shear strain rate ($\dot{\gamma}$) and shear stress (τ) by the shear viscosity (η), see Figure 3.1.1. Newton law is for a perfect viscous fluid but can describe most low viscous fluids and can also apply to extensional flow. But for high viscous fluids such as the polymer melts, more additional interesting phenomena appear such as time dependent properties (viscoelastic), the normal stress in the shear flow for high shear strain (non-linearity) and the decrease in viscosity when increasing the shear strain rate (shear thinning). Therefore, the more complex constitutive equations are developed and applied in order to describe the polymer behaviour.

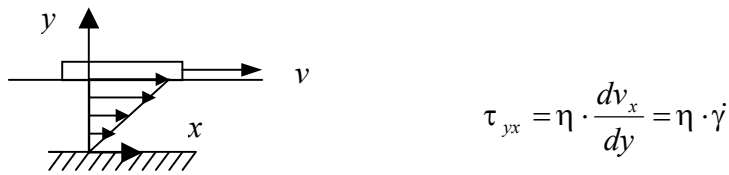


Figure 3.1.1 Shear flow, a homogeneous and uniform deformation

3.1.1 Shear viscosity and spinnability using the small amplitude oscillatory shear test

The shear viscosity for small shear strain rate is approximately constant. The zero shear viscosity is defined as the limit of shear viscosity when the shear strain rate approaches zero ($\lim_{\dot{\gamma} \rightarrow 0} \eta_s = \eta_0$). However, the polymer melt shows linear behaviour in accordance with Newton law only for a small shear strain rate; for a high shear strain rate, the polymer melt shows a lower shear stress, meaning that the shear stress needed for a high deformation rate is smaller than the shear stress estimated by Newton's law. In other words, one can say the shear viscosity drops down with a higher shear strain rate. This is what is known as shear thinning and it is a non-linear rheological behaviour. To establish the zero shear viscosity dependent on shear strain rate, different experimental methods have been used through the literature. A common method to

estimate the zero shear viscosity using shear rheology is the small amplitude sinusoidal oscillation. The apparatus used here and the test conditions are given in Section 2.4.1. This is the suitable method to investigate the shear viscosity over a wide range of rotational frequency (ω). Reminding now some important relations in this method: The polymer sample is melted and a small amplitude frequency deformation ($\gamma = \gamma_0 \cdot \sin(\omega \cdot t)$) is applied to the polymer melt, see Figure 3.1.2. A transducer transforms the shear force initiated ($\tau = \tau_0 \cdot \sin(\omega \cdot t + \delta)$), and the viscosity and loss and storage modulus will be calculated as follows:

$$\begin{array}{l}
 \text{Elastic modulus} \quad G_E = \frac{\tau_0 \cdot \cos(\delta)}{\gamma_0} \\
 \text{Viscous modulus} \quad G_V = \frac{\tau_0 \cdot \sin(\delta)}{\gamma_0}
 \end{array}
 \left. \vphantom{\begin{array}{l} G_E \\ G_V \end{array}} \right\}
 \begin{array}{l}
 G^* = \sqrt{G_E^2 + G_V^2} \\
 \tan(\delta) = \frac{G_V}{G_E}
 \end{array}
 \quad (3.1.1)$$

$$\text{Complex viscosity} \quad \eta = \frac{\tau}{\dot{\gamma}} \Rightarrow |\eta^*(\omega)| = \sqrt{\left(\frac{G_E}{\omega}\right)^2 + \left(\frac{G_V}{\omega}\right)^2} = \frac{1}{\omega} |G^*(\omega)|$$

The shear rate, as given in Figure 3.1.2, is a cosine function and is comparable to the extension rate in the fibre formation zone, which is similar to a half sine periodic function, see Figure 6.2.8. The constitutive equation relating to the above test can be extended to the viscoelastic case where the elastic behaviour of polymer is considered. The viscoelastic model means that the material relaxes over a significant time and the strength is therefore time-dependent. In this model, the relaxation strength ($G(t)$) and the zero shear viscosity (η_0) can be approximated as a series of relaxation strengths (g_i) and relaxation times (λ_i) as follows:

$$G(t) = \frac{\tau(t)}{\gamma_0} \quad \text{or} \quad G(t) = \sum_{i=1}^N g_i \cdot e^{-t/\lambda_i} \quad \eta_0 = \int_0^{\infty} G(t) \cdot dt \quad \text{or} \quad \eta_0 = \sum_{i=1}^n g_i \cdot \lambda_i \quad (3.1.2)$$

In this case however, the first relaxation times have more effect on the material relaxation than the next one and the discrete distribution of elastic and viscous strength from the small amplitude

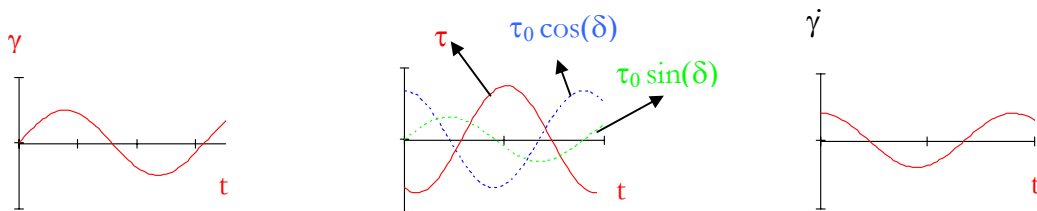


Figure 3.1.2 Small amplitude oscillation shear and the material response

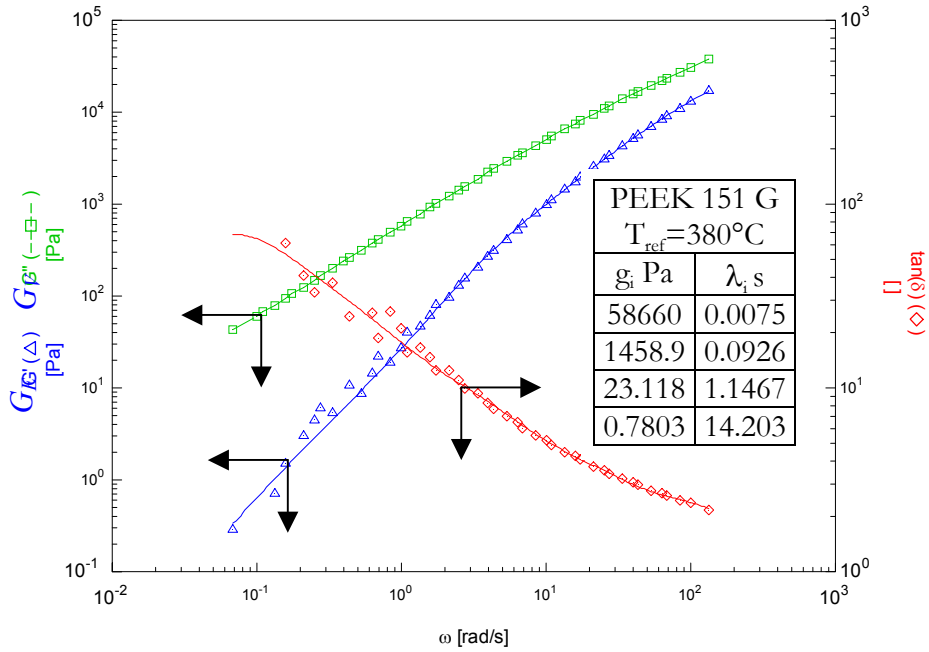


Figure 3.1.3 Master curve of elastic modulus G_E , viscous modulus G_V and $\tan(\delta)$ of melt PEEK 151G at 380°C experimentally by rheometer and fitted by strength spectrum g_i and λ_i (lines)

oscillation can be summarised as Equation (3.1.3):

$$G_V(\omega) = \sum_{i=1}^n g_i \cdot \frac{\omega \cdot \lambda_i}{1 + \omega^2 \cdot \lambda_i^2} \quad G_E(\omega) = \sum_{i=1}^n g_i \cdot \frac{\omega^2 \cdot \lambda_i^2}{1 + \omega^2 \cdot \lambda_i^2} \quad (3.1.3)$$

The temperature master curves in Figures 3.1.3, 3.1.4 and 3.1.5 show the result of small amplitude oscillatory shear test. The relaxation strengths and times are listed in every named figure, and are found by fitting the Maxwell model to experimental results of oscillation test. The zero shear viscosity and the temperature dependent viscosity are determined by the temperature master curve concept that is described in the next section (Section 3.1.2).

Spinnability: Spinnability of polymers can also be predicted by the master curves shown in Figures 3.1.3, 3.1.4 and 3.1.5. The main idea was reported by Beyreuther et al. [1996] and was verified later for other polymers by Hoffmann [2002], based on the correlation between the shear rheology in small angle oscillation and loss angle ($\tan(\delta)$) and spinnability of polymer. The different polymers which were examined were classified in three categories: well, poor and non-spinnable polymers. Following this classification, a polymer is well spinnable if loss angle $\tan(\delta) > 10$ for $G_E > 100$ Pa in the master curve.

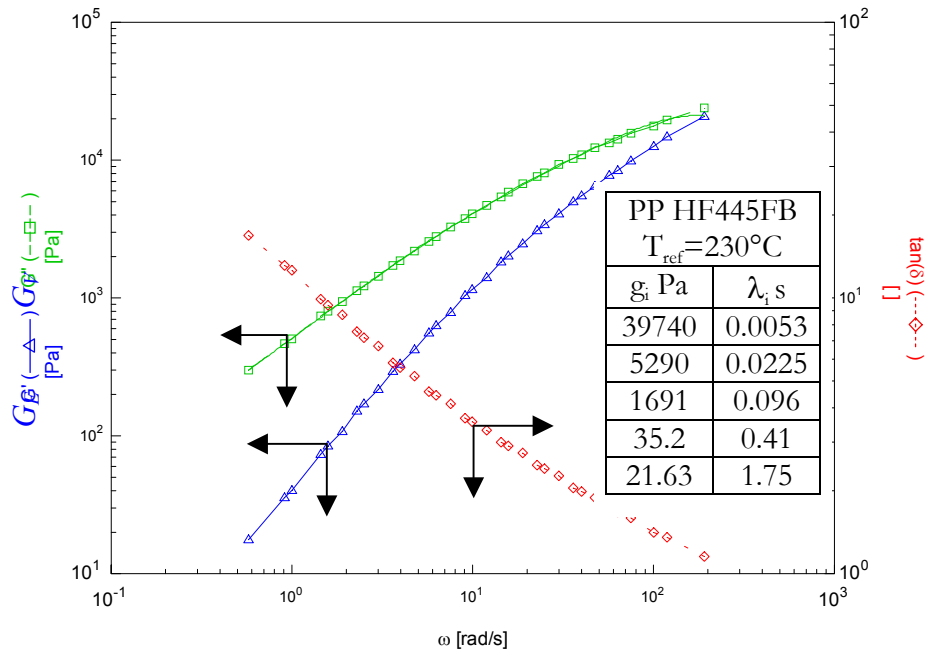


Figure 3.1.4 Master curve of elastic modulus G_E , viscous modulus G_V and $\tan(\delta)$ of melt PP at 230°C experimentally by rheometer (symbols) and fitted by strength spectrum g_i and λ_i (lines)

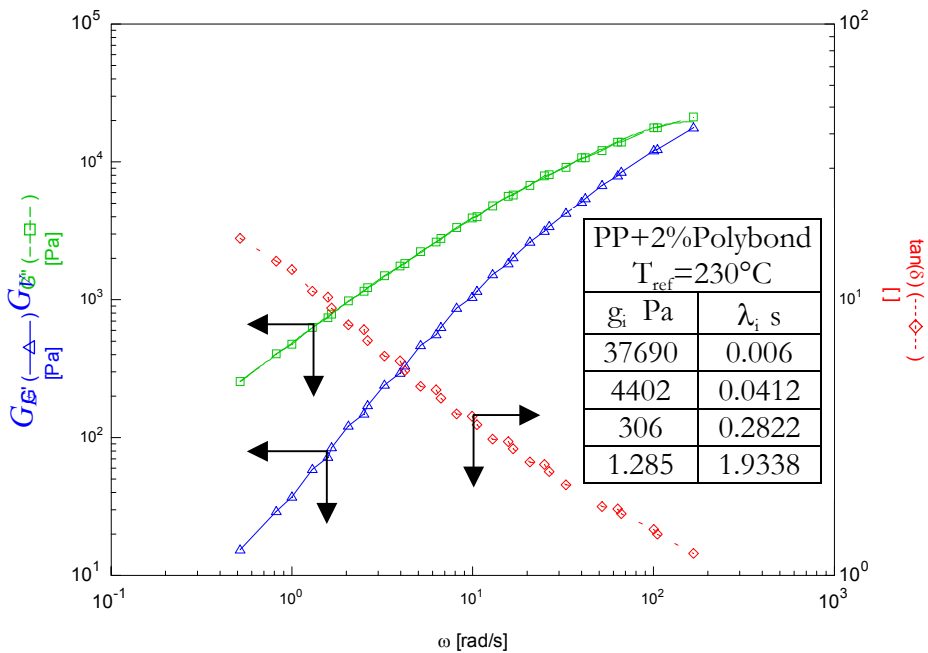


Figure 3.1.5 Master curve of elastic modulus G_E , viscous modulus G_V and $\tan(\delta)$ of melt PP+2%Polybond at 230°C experimentally by rheometer (symbols) and fitted by strength spectrum g_i and λ_i (lines)

Comparisons of the master curves of PP in Figure 3.1.4 and Figure 3.1.5, show that a $\tan(\delta) < 5$ for $G_E > 100$ Pa. Therefore, according to these criteria, they are non-spinnable, although experiences shows that both polymers are well spinnable. If the first criterion is improved to $\tan(\delta) > 10$ for $\omega = 1$ rad/s, then it will be valid for the PEEK and PP master curves (Figures 3.1.3, 3.1.4 and 3.1.5). More experiences in the melt rheology lead to a simple new rule that predicts the spinnability of polymer by primitive observation, i.e. if the melt is pulled manually to a distance of 1 m to 2 m and still connected to the melt and makes a continuous fibre, the polymer can be spinnable. In other words, the ability to extend a polymer melt to high strain (~ 5) is a good qualitative signal of a spinnable polymer, but this cannot recommend in this form for quantitative testing.

3.1.2 Temperature dependence of viscosity

The effect of temperature on viscosity is high, because the polymer chains will move easier at a high temperature. Therefore, the shear viscosity decreases by increasing the polymer temperature, and the viscosity decreases by using the empirical model in an exponential temperature function. The temperature dependent viscosity measurement is carried out using rotational rheometer measurements by means of the small oscillatory frequency sweeps. The PEEK was tested at three temperatures (360, 380, 400)°C and PP (200, 230, 260)°C. All samples showed similar rheological properties at the relevant processing temperature, as can be seen in Figures 3.1.3 to 3.1.6. In other words, the polymers approach a constant zero shear viscosity at a low shear rate and the shear viscosity decreases with a high shear rate. All samples tested also showed no degradation for more than 30 minutes and the complex viscosities were constant. The complex viscosity ($\eta^*(\omega)$), was calculated from Equation 3.1.1. According to the time-temperature-superposition principle, the master curves of complex viscosity were constructed for each sample at the reference temperature specified as in Figure 3.1.6. The shift factor (a_T) was fitted using the Arrhenius-equation:

$$a_T(T, T_{ref}) = \exp\left(\frac{E_a}{R} \left(\frac{1}{T} - \frac{1}{T_{ref}}\right)\right) \quad (3.1.4)$$

These fits provide the flow activation energy (E_a), as can be seen in Table 3.1.1. The master curves for three PEEK types and two PP samples are shown in the Figure 3.1.6. The temperature dependence of viscosity can now be represented as in Equations 3.1.5 (a) and (b):

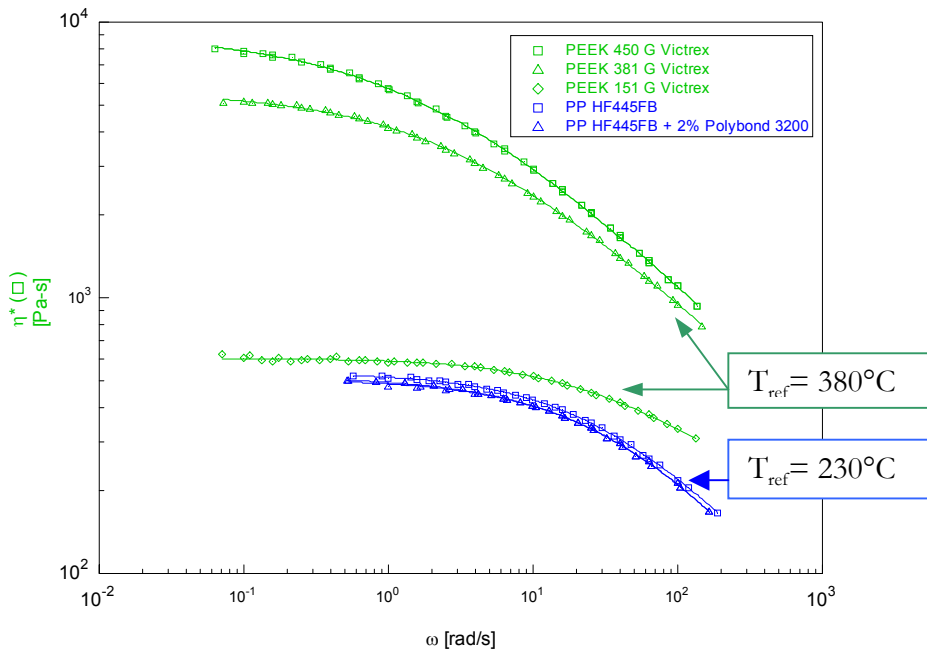


Figure 3.1.6 Master curve of shear viscosity η of melt three PEEK types, PP and PP+2%Polybond experimentally by rheometer (symbols) and fitted

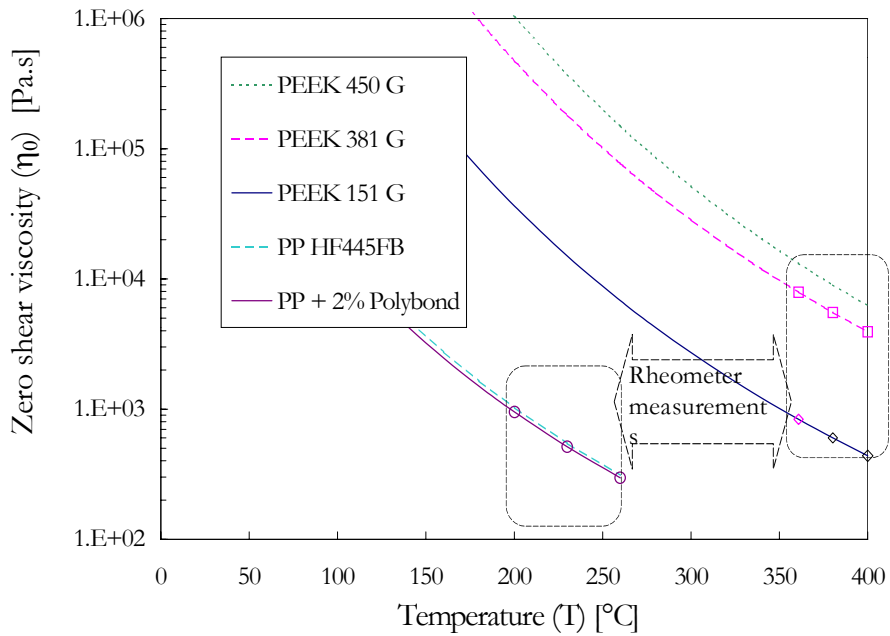


Figure 3.1.7 PEEK & PP zero shear viscosity as a function of temperature from the small angle oscillation shear rheology test (symbols), according Arrhenius (solid lines)

$$\begin{aligned} \eta_0(T) &= \eta_0 \cdot \exp\left(\frac{E_a}{R} \left(\frac{1}{T} - \frac{1}{T_{ref}}\right)\right) & (a) \quad \text{Arrhenius above melting point } T > T_m \\ \log\left(\frac{\eta}{\eta_r}\right) &= \frac{-C1 \cdot (T - T_r)}{C2 + (T - T_r)} & (b) \quad \text{"WLF" for } T_g \leq T \leq T_g + 100 \end{aligned} \quad (3.1.5)$$

In Arrhenius equation (Equation (3.1.5)(a)), $R=8.321$ J/mol/K is the molar gas constant and the Parameters η_0 and E_a are determined at the reference temperature (T_{ref}) as explained previously in this section. The temperature dependent viscosities found by this method are shown in Figure 3.1.7. As noted in Equation (3.1.5), the Arrhenius equation gives a good approximation at the temperatures ranging above melting point and the "WLF" equation at temperature near glass temperature. In the "WLF" equation the subscript r refers to the condition at some arbitrary reference condition, the best fit is reported as $T_r=T_g+40$ [Macosko 1994]. Using the "WLF" shift factor, the coefficients $C1$ and $C2$ could be found by master curves constructed near the reference temperature T_r . From this point onwards the Arrhenius equation is used.

3.1.3 Shear rate and molecular weight dependence of shear viscosity:

The so-called shear thinning (the decrease of the viscosity in high shear strain rate) can be investigated by the result of small amplitude shear oscillation test, as given in Figure 3.1.6. Because the power law fails to describe the low shear rate region, in order to find a simple model of shear viscosity, another viscosity model was fitted to the experimental data in Figure 3.1.6. To give regions at both low and high shear rates, the three-parameter Bueche model, or modified Cross model, is proposed as in Equation (3.1.6). Applying the more complex viscous models requires more numerical efforts. Fitting the master curve of viscosity, three constants of the Equation (3.1.6) are found and listed for the steady shear viscosity in Table 3.1.1.

$$|\eta^*(\omega)| = \frac{\eta_0}{1 + k \cdot \omega^m} \quad (3.1.6)$$

	E_a [kJ/mol]	η_0 [Pa.s]	k	m
PEEK 151 G	58.512	611.30	0.0402	0.6597
PEEK 381 G	63.469	5831.9	0.4150	0.5498
PEEK 450 G	67.706	9307.3	0.6253	0.5408
PP	41.872	546.70	0.0560	0.7113
PP+ 2%Polybond	40.685	514.08	0.0517	0.7233

Table 3.1.1 Activation energy and coefficients of shear viscosity as a function of strain rate

In the shear flow, there is a very useful relationship between material functions often observed to hold approximately. The empirical relationship, called the Cox-Merz rule, often holds fairly well at high shear strain rates:

$$\eta(\dot{\gamma}) = |\eta^*(\omega)| \quad \text{for } \dot{\gamma} = \omega : (\text{rad} / \text{s}) \quad (3.1.7)$$

This rule states that the shear strain rate dependence of the steady state viscosity (η) is equal to the frequency dependence of the complex linear viscoelasticity (η^*), see Figure 3.1.2. According the Cox-Merz rule (Equation (3.1.7)), Equation (3.1.6) can be extended to present the steady shear viscosity as a function of temperature and shear strain rate in Equation (3.1.8):

$$\eta(\dot{\gamma}, T) = \frac{\eta_0(T)}{1 + k \cdot \dot{\gamma}^m} \quad (3.1.8)$$

The temperature effect of the zero shear viscosity can be used from Arrhenius equation (Equation (3.1.2)(a)). In the next section (Section 3.2), this expression is compared with the extensional viscosity.

Molecular weight dependence of shear viscosity: The longer the molecular chain the more entanglements exist. As a result, the viscosity increases by increasing the molecular weight. The zero shear viscosity (η_0) and the average molecular weight (M_w) are valid in the relationship Equation (3.1.9):

$$\eta_0 = K \cdot M_w^j \quad j \approx 3.4 \quad \text{if } M_w > M_c \text{ and } j \approx 1 \text{ if } M_w < M_c, \quad (3.1.9)$$

where M_c is the critical molecular weight for the entanglement and the two parameters K and j can be determined experimentally. The long chain length allows for entanglements, as shown in the Figure 3.1.8. The chains entanglements cause the viscosity to rise quite significantly.

High molecular weights usually lead to higher activation energies of viscous flow. If the polymer exhibits a higher glass transition temperature, it will show higher activation energies and will consequently show higher sensitivity to temperature (see Table 3.1.1 and Figure 3.1.7). The comparison between the estimated activation energies in Table 3.1.1 and the viscosities in Figure 3.1.6 show a result of: $\eta_0^{\text{PEEK 450G}} > \eta_0^{\text{PEEK 381G}} > \eta_0^{\text{PEEK 151G}} > \eta_0^{\text{PP}} > \eta_0^{\text{PP+2\%polybond}}$. It can also be concluded according Equation (3.1.9) that: $M_w^{\text{PEEK}} > M_c^{\text{PEEK}}$, $M_w^{\text{PP}} > M_c^{\text{PP}}$

Ohkoshi et al. [1993] investigated the molecular weight effect on melt spinning of PEEK. For polypropylene, an expression of viscosity was given by Ghijssels [1994]:

$$[\eta]_{PP} = 2.49 \times 10^{-16} \cdot (M_w)^{3.57} \quad (3.1.12)$$

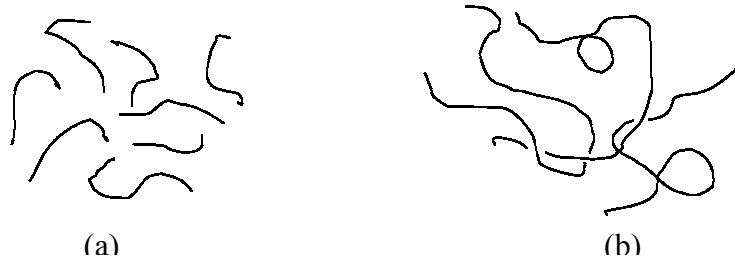


Figure 3.1.8 Entanglement of the molecular chains (a) low molecular weight (b) high molecular weight [Sperling 1992]

3.2 Extensional viscosity in the melt spinning process

It is known that the polymers behave according to loading. Consequently the different constitutive equations, which relate the deformation and the internal force, can describe the polymer behaviour. Also the polymers show different behaviour in the extension and in the shear deformation, because the long chains of polymer molecules exhibit resistance to extension deformation, therefore the extensional viscosity is more than shear viscosity. The primary reason for the poor prediction of an extension dominated flow is the low viscosity of the material in generalized Newton model. Experiments and theories have been proved that the extensional viscosity for a small extension rate is three times that of shear viscosity ($\lim_{\dot{\epsilon} \rightarrow 0} \eta_e = 3 \cdot \eta_0$).

However, extensional viscosity is a true material property, independent of both techniques of measurement and of any assumption concerning the constitutive behaviour of the fluid [Shridar 1988]. To measure the extensional viscosity, a lot of extensional rheometers have been proposed [Macosko 1994]. The current state of extensional measurements and their limitations were summarized by Rides et al. [1996]. The upper limits of the reported extensional measurements were for the Hencky's strain up to 4, and a strain rate up to 30 s^{-1} , and temperature up to 200°C , but the availability of such equipments is still limited.

The extensional viscosity in the melt spinning along the spinning line and in the fibre formation zone cannot be extracted from common extensional rheometry measurements for many reasons. Firstly, the extension strain rate reaches a high value and varies along the spinning line like a bell function (or half period of sine function) and the stress also increases, but the important aspect of measuring extensional properties is that the testing shall be carried out using either constant strain or constant stress in order to generate the quantitative data which is independent of the test method. Secondly, the extension Hencky's strain increases along the spinning line. Thirdly, the temperature decreases due to air cooling and the possible crystallisation along the spinning line, but in extensional rheometry, the temperature uniformity is essential for a uniform deformation of the test specimen. Therefore, an estimation of the extensional viscosity using on-line measurement of speed and temperature is recommended [Rides 1996]. Results from such estimations are not expected to be qualitatively correct for all polymer melts, however, the melt spinning can be used as technique to measure the extensional viscosity for the melts of lower viscosities [Gupta 1988], and the obtained extensional viscosity from melt spinning will give the best approximations of true material properties [Revenu 1993].

Sano et al. [1968] estimated the extensional viscosity by means of melt spinning process and measurements of fibre temperature and diameter along the spinning line. The viscosity was obtained for an isotactic polypropylene filament by measurements and speed-drag force calculations. He compared the non-Newtonian behaviour, from the so-called Bird equation $\eta=3.\eta_0.(1+(\lambda-\tau).V')$ with the Newtonian behaviour ($\eta=3.\eta_0$). He concluded that for $V' < 30 \text{ s}^{-1}$ there is no non-linear effect that is valid for $(\lambda-\xi) < 10^{-3} \text{ s}$ (the difference of the relaxation time constant (λ) and the retardation time constant (ξ)). Laun [1989] widely studied the extensional viscosity by the Rheotens test. With relation to his especial equipment, he concluded that extensional viscosities calculated from the Rheotens tests are not expected to be qualitatively correct because the Rheotens test is a non-homogenous and non-isothermal stretching. However, the laboratory extension flow studies by Meissner rheometer tried to supply constant strain rate in order to have precise measurements. The master curve idea has recently allowed a direct and quantitative comparison of the extensional behavior of different polymers in different processing conditions using the hyperlink die [Collier 2002] and Rheotens test [Brennat 2001]. Some producers also supply a portable universal testing platform, named SER (Xpansion Instruments, LLC, USA), to allow the shear rheometer a uniform extensional deformation. For the PEEK melt spinning process, other extensional or shear rheological test results have still not applied.

3.2.1 Estimation of extensional viscosity along spinning line

In order to estimate the extensional viscosity, the on-line fibre speed measurement, the estimated speed gradient and the internal force calculated from the momentum balance are replaced in Equation (3.2.4). Figure 3.2.1 shows a flow diagram and indicates the procedure used for the estimation of extensional viscosity. Internal force along the spinning line is calculated using the momentum equation, see Chapter 5. Difficulties are however raised in the initial value of internal force (F_0) and the speed gradient $((dV/dz)_0)$ at the spinneret outlet. Both of these values were estimated using different approaches which are discussed in Chapter 5. In this section, the estimated extensional viscosity along the spinning line (according to Equation (3.2.1)) is discussed, and then some mathematical expressions of extensional viscosity are also suggested. The estimated extensional viscosities over distance to spinneret are presented in Figures 3.2.2 and 3.2.3. The on-line speed and temperature measurements are included in Chapter 5. The spinning conditions are tabulated in the appendix Table A1. Looking to the distribution of extensional viscosity along the

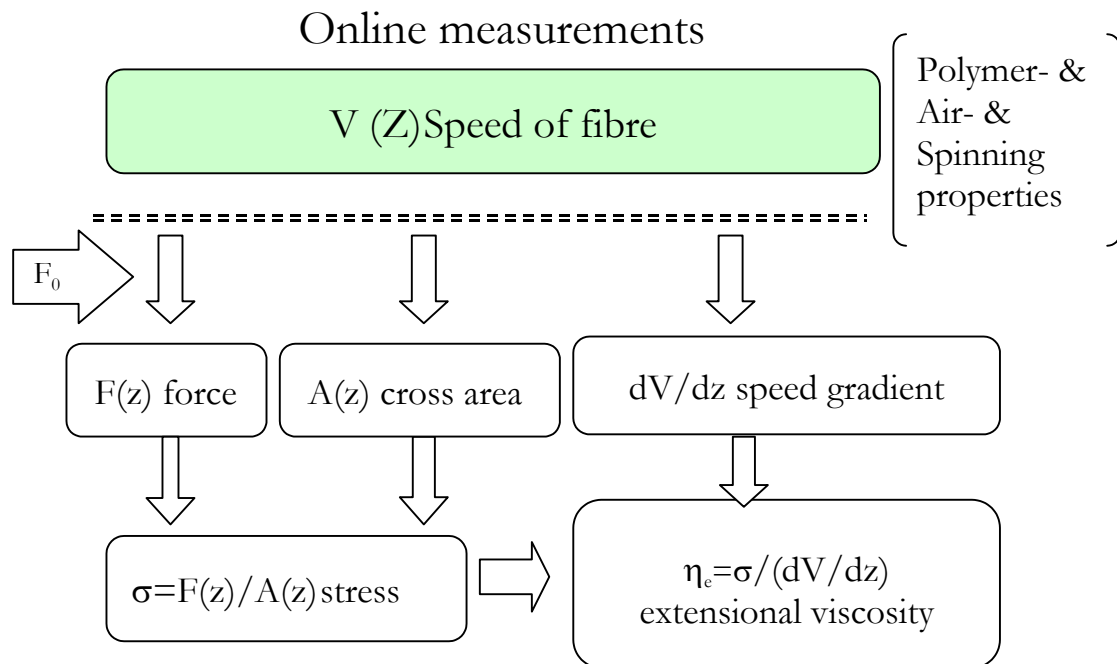


Figure 3.2.1. Flow diagram for estimation of elongation viscosity from online measurements.

distance from spinneret initially keeps a constant value near the spinneret, but then increases with distance. The extensional viscosity can later drop locally at a certain distance and then increases rapidly. This drop can be a sign of the so-called necking in the fibre profile. This drop is obvious in Figures 3.2.2 and 3.2.3. Such drop in the region of a take-up speed of 5000 m/min was more than take-up speeds 4000 m/min and 3000 m/min, which was investigated by Ishizuka [1985] for PE. This means that the reduction of the extensional viscosity becomes larger as the draw down ratio increases. Figures 3.2.2 and 3.2.3 also show that the necking point shifts upstream along the spinning line due to an increase of mass throughput, as Murase [1994] investigated for PET. The necking can be initiated by increasing the spinning speed at the same throughput. A rapid increase in the extensional viscosity is found at the end of the fibre formation zone, where the fibre has lower temperature. The rapid increase of extensional viscosity can be forced by the crystallisation along the spinning line. This increase becomes higher for take-up speeds greater than 2000 m/min. In addition to the spinning speed, however, a combination of the throughput and the take-up speed (draw down ratio) can be taken as a dimensionless criterion for crystallisation. This suggests that the polymer along spinning line undergoes structural changes accompanied by a rapid increase in viscosity of extensional flow. The structural changes involved are related to molecular ordering in the effective entanglement network, or in other words, to the change of the size of flow units or cohesive forces between neighbouring molecules. Off-line orientation and crystallisation of fibres are discussed in Section 4.1

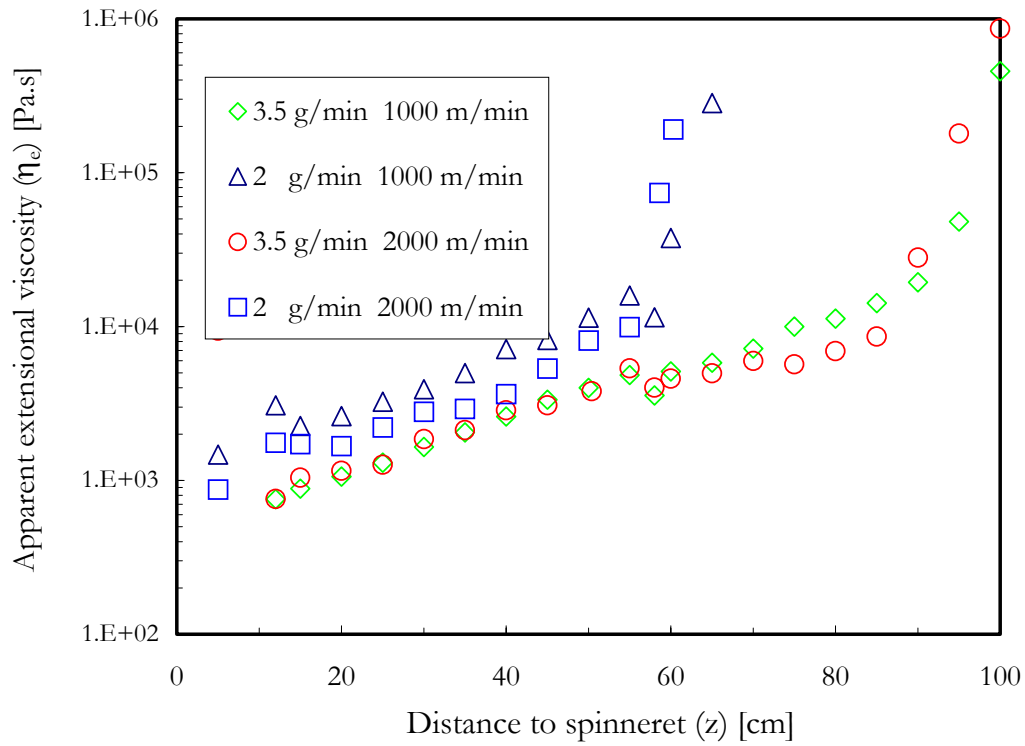


Figure 3.2.2 Estimated apparent extensional viscosity along spinning line of PEEK 151G, from melt spinning, $T_0=385^\circ\text{C}$ spinneret 3 holes ($d=0.25$ mm, $l=0.5$ mm).

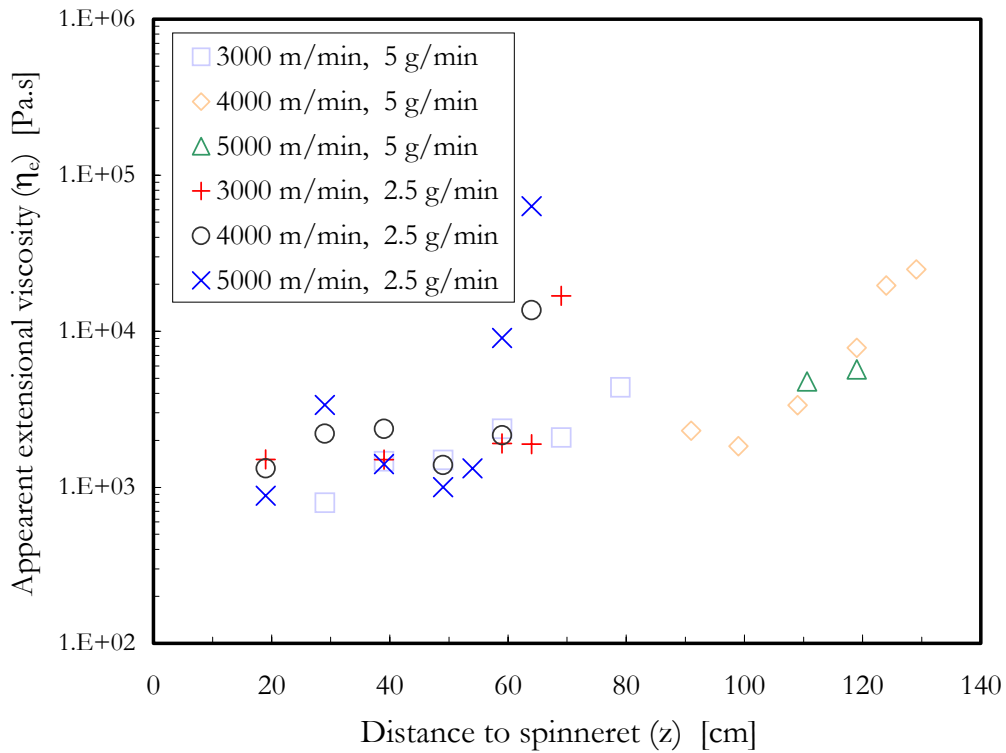


Figure 3.2.3 Estimated apparent extensional viscosity along spinning line of PEEK 151G, from melt spinning, $T_0=400^\circ\text{C}$ spinneret 3 holes ($d=0.25$ mm, $l=0.5$ mm)

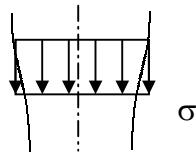
3.2.2 Strain rate dependence of extensional viscosity

The extensional viscosity estimated from Figure 3.2.1 contains all spinning line effects such as the temperature dependence of the viscosity and varies from one point to point along the spinning line; it is therefore sometimes called the transient viscosity. Because the temperature (T), the strain rate ($\dot{\epsilon}$), and the crystallisation (X) also vary along the spinning line, the extensional viscosity varies with these quantities ($T, \dot{\epsilon}, X$). Therefore the extensional viscosity can be expressed as function of distance along spinning line:

$$\eta_e(z) = \eta_e(T(z), \dot{\epsilon}(z), X(z)) = \eta_1(T, \dot{\epsilon}) \cdot \eta_2(X) \quad (3.2.1)$$

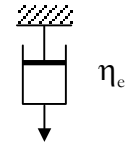
Different expressions for η_1 and η_2 in Equation (3.2.1) are proposed in the literature of Ziabicki [2002], Spruiell [2001] and Shimizu [1985]. In order to find the proper form, a brief introduction is given.

Apparent extensional viscosity: For the pure extensional viscous behaviour of polymer melt, the stress (σ) and the strain rate ($\dot{\epsilon}$) are related according to the Newtonian constitutive equation by:



σ

$\sigma = \eta_e \cdot \dot{\epsilon}$



η_e

$$(3.2.2)$$

This is the so-called mechanical model of polymer behaviour as dashpot where the factor η_e describes the extensional viscosity. The strain rate, $\dot{\epsilon}$, can be replaced by the speed gradient, V' , in Equation (3.2.2), therefore the extensional viscosity can be expressed along the spinning line as Equation (3.2.3)

$$\eta_e = \frac{\sigma}{dV/dz} \quad (3.2.3)$$


By replacing the definition of the normal stress ($\sigma = F/A$) in Equation (3.2.3), and from continuity equation ($Q = \rho \cdot A \cdot V$), the cross section area ($A = Q/\rho \cdot V$) leads to:

$$\eta_e = \frac{1}{dV/dz} \cdot \frac{F}{A} = \frac{F \cdot V \cdot \rho}{V' \cdot Q} \quad (3.2.4)$$

To estimate the extensional viscosity from Equation (3.2.4), the internal force (F), the fibre speed (V), and speed gradient (V') must be known along the spinning line. In order to find the final form of strain rate dependent extensional viscosity as discussed above, it is useful to be reminded of the definition of Trouton ratio in the uniaxial extension. The dimensionless extensional

viscosity known as the Trouton ratio is often reported as: $Tr = \sigma / (\eta_0 \cdot \dot{\epsilon}) = \eta_e / \eta_0$. For melt spinning under low and constant extension strain rates, the Trouton ratio will be equal to three and therefore, $\eta_e = 3 \cdot \eta_0$, as for the Newton viscous model.

For low strain rates (below 600 s^{-1} according to Cuculo [2001], although this seems very high), the extensional viscosity is predominantly a function of temperature only and is reasonably close to three times the shear viscosity (η_0) predicted by the Newtonian fluid model. In the case of a high strain rate (high speed gradient), both the elastic and the viscous behaviour of polymer melt must be taken into consideration. The simplest approximation of the viscoelastic model is expressed by the Maxwell constitutive equation as a series combination of Hooke's spring (elastic behaviour) and Newton dashpot (viscous behaviour). Because the viscous deformation is dominant in the fibre formation zone for temperature higher than glass transition temperature, and also by decreasing the temperature, the elastic deformation is dominant; therefore the Maxwell model (one spring and one dashpot) is applied for melt spinning [Shimizu 1985(a)] as followed in Equation (3.2.5):



$$\dot{\epsilon} = \frac{\dot{\sigma}}{E} + \frac{\sigma}{\eta_e} \quad (3.2.5)$$

It should be mentioned, however, that the mechanical model of viscoelastic behaviour in Equation (3.2.5) can indeed simplify the calculation, but cannot help to understand the polymer behaviour from molecular events in any way. In order to combine the viscous and elastic effect into a single variable quantity, the apparent extensional viscosity (η_{app}) has been defined as the ratio of stress to the extension rate from Equation (3.2.5), and can be derived as:

$$\eta_{app} = \frac{\sigma}{V'} = \frac{\eta_e}{1 + (\eta/E) \cdot V'} \cdot \left(1 - \frac{V \cdot F'}{E \cdot A \cdot V'}\right)^{-1} \quad (3.2.6)$$

The second fraction in Equation (3.2.6) tends to zero and can be ignored, if the air drag and all other forces, except the inertial force, are negligible. On replacing ($F' = Q \cdot V'$) and the continuity equation ($Q = \rho \cdot A \cdot V$), and assuming for spin polymers ($E \gg V^2 \rho$) then ($\frac{V \cdot F'}{E \cdot A \cdot V'} = \frac{V^2 \cdot \rho}{E} \rightarrow 0$).

The Maxwell viscoelastic Equation (3.2.5) leads to the simple form [Ziabicki 1985]:

$$\eta_{app} = \frac{\eta_e}{1 + De(z)} = \frac{\eta_0(T)}{1 + \lambda \cdot \dot{\epsilon}} = \eta_1(T, \dot{\epsilon}), \quad (3.2.7)$$

where $De(z) = \lambda \cdot V'$ is the Deborah number and $\lambda = \eta/E$ is the extension relaxation time. Stelter [2002] emphasized that both the relaxation time and the steady terminal extensional viscosity are needed for describing the extensional viscoelastic behaviour. The Deborah number, $(De(z))$ characterizes the strength of extensional flow, equal to the longest characteristic relaxation time ($\lambda(z)$) of the polymer multiplied by the characteristic timescale of the kinematics ($V'(z)$). To state it briefly, the Deborah number indicates the relative importance of elastic effects to viscous effects [Rothstein 2002]. If the Deborah number is very small ($De \rightarrow 0$), Equation (3.2.7) will be same as Equation (3.2.3) and $\eta_{app} = \eta_e$, which means that the polymer behaves viscous. However, a small relaxation time ($\lambda(z)$) as for spinnable polymer, and sufficiently high strain rate ($\dot{\epsilon}$) as for along the spinning line can produce a high Deborah number that should not be ignored. When the Deborah number increases, the effect of elastic part will appear. In other words, the Deborah number indicates if the polymer behaves viscously, linear viscoelastically or non-linear viscoelastically and also indicates which constitutive equation is suitable for the fibre formation zone.

Considering the simplest incorporated non-linearity Maxwell model (Upper-Convected Maxwell) in the steady state uniaxial extension and rewrite the $\eta_1(T, \dot{\epsilon})$ in Equation (3.2.1) [Macosko 1994]:

$$\eta_1(T, \dot{\epsilon}) = \frac{\eta_0(T)}{1 + \lambda \cdot \dot{\epsilon}} + \frac{2 \cdot \eta_0(T)}{1 - 2 \cdot \lambda \cdot \dot{\epsilon}} = \frac{3 \cdot \eta_0(T)}{(1 + \lambda \cdot \dot{\epsilon}) \cdot (1 - 2 \cdot \lambda \cdot \dot{\epsilon})} \quad (3.2.8)$$

It is also noteworthy that for the case ($\dot{\epsilon} \geq 1/2 \cdot \lambda$) the prediction of an infinite or negative value of viscosity has no physical significance, it is the limit of validity of Equation (3.2.8).

If Equations (3.2.7) and (3.2.8) are fitted to the extensional viscosity estimations, the relaxation time (λ) must be known. The relaxation time can be found by fitting the Maxwell model to the shear rheology measurements, but the temperature dependence of relaxation time makes it difficult to work with Equations (3.2.7) and (3.2.8).

Since the zero viscosity (η_0) varies depending on temperature and temperature itself varies along the spinning line, η_0 is replaced by $\eta_0(T)$. The temperature dependence of viscosity $\eta_0(T)$ from Arrhenius Equation (3.1.2) (a) is presented in Figure 3.1.7, and can also be implemented for extension. Therefore, by replacing Equation (3.2.7) with $\eta_{app}/\eta_0(T)$, the strain rate dependent

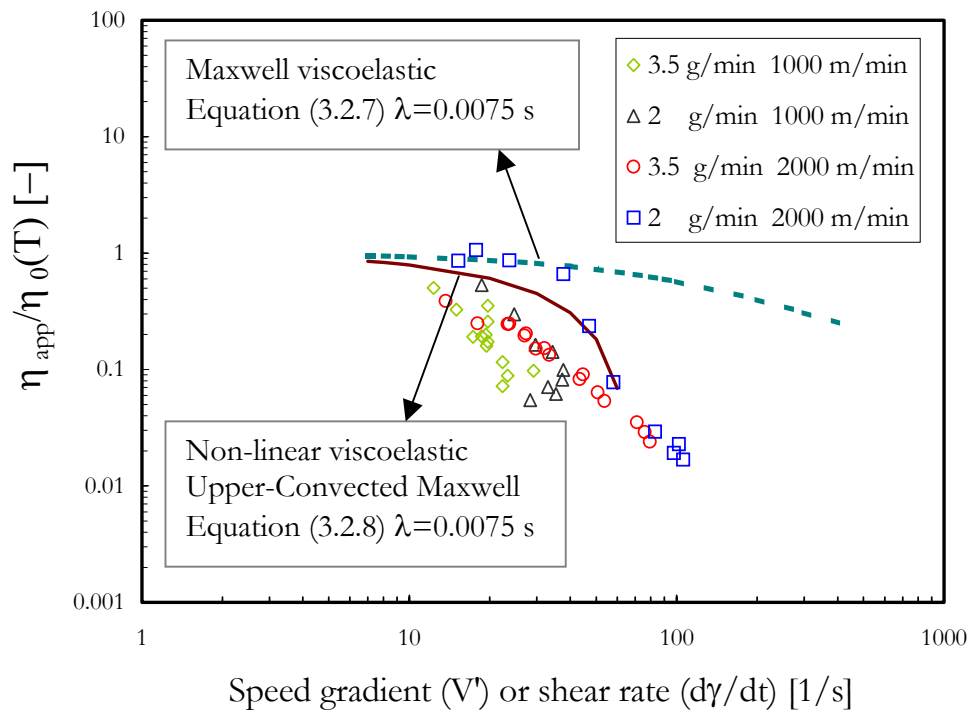


Figure 3.2.4 Dimensionless apparent extensional viscosity over strain rate along spinning line of PEEK Victrex 151 G, $T_0=385^\circ\text{C}$ spinneret 3 holes ($d=0.25$ mm, $l=0.5$ mm)

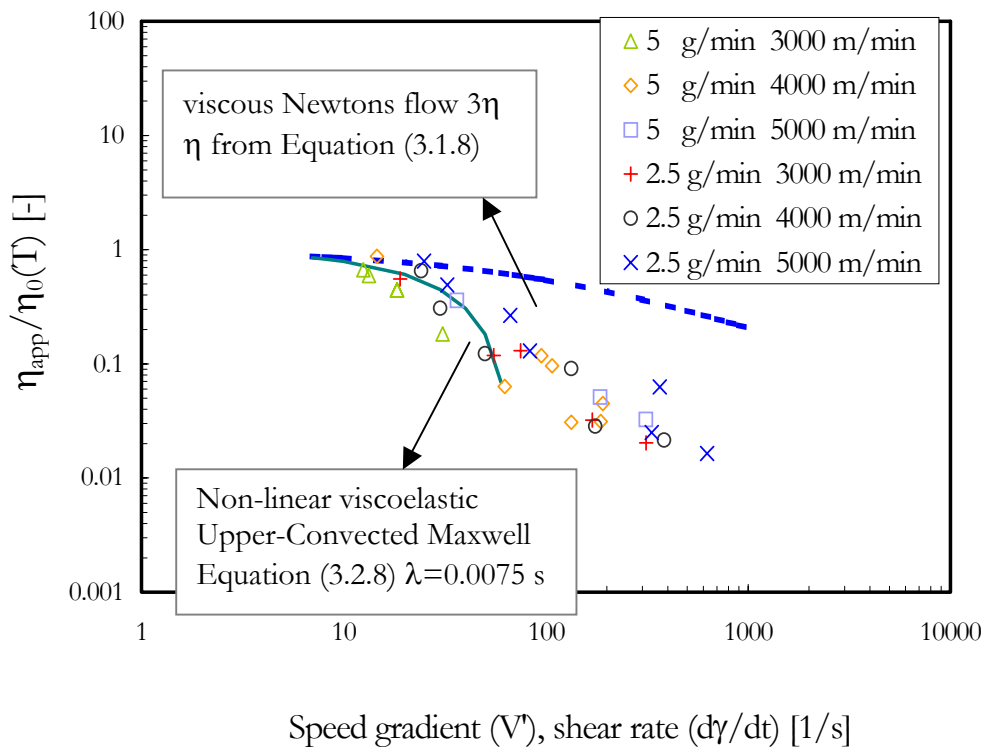


Figure 3.2.5 Dimensionless apparent extensional viscosity over strain rate along spinning line of PEEK Victrex 151 G, $T_0=400^\circ\text{C}$ spinneret 3 holes ($d=0.25$ mm, $l=0.5$ mm).

extensional viscosity can be displayed over the strain rate. The ratio $\eta_{\text{app}}/\eta_0(\mathbf{I})$ from on-line measurements over the strain rate gives a lower value than from Equations (3.2.7) and (3.2.8) at high strain rate, see Figures 3.2.4 and 3.2.5. The relaxation time in Equations (3.2.7) and (3.2.8) was found using the shear rheology of PEEK, see Figure 3.1.3. The reduced apparent extensional viscosity over the strain rate fitted by the linear and non-linear viscoelastic behaviour gives a good explanation, but it is nonetheless still depending on the relaxation time constant and the spinning conditions as seen in Figures 3.2.4 and 3.2.5. To improve the strain rate effect on extensional viscosity, the generalized viscous fluid $\sigma = \eta_1(T, \dot{\epsilon}) \cdot \dot{\epsilon}$ and the following constitutive equation was proposed [Ding 1995].

$$\eta_1(T, \dot{\epsilon}) = \frac{\eta_0(T)}{1 + (a \cdot \eta_0(T) \cdot \dot{\epsilon})^b} \quad (3.2.9)$$

In this case, the $\eta_1(T, \dot{\epsilon})$ approaches a constant value for a low strain rate and decreases by increasing the strain rate (thinning effect). In other words, Equation (3.2.9) is similar to modified Cross model, Equation (3.1.6). In contrast to Equation (3.2.7) and (3.2.8), Equation (3.2.9) contains a temperature effect under the fraction, and the constants a and b can be found directly by fitting Equation (3.2.9) to the estimated extensional viscosity from on-line measurements. Equation (3.2.9) is a special case of Equation (3.2.7), in which $b=1$ and $a = 1/E$.

To find the final form of extensional viscosity from Equations (3.2.1) and (3.2.9), either no or negligible level of crystallinity in PEEK melt spinning for low draw down ratios is assumed [Spruiell 2001]. According to Figure 3.2.1, the estimated extensional viscosity (η_{app}) is reduced in relation to the temperature dependent viscosity ($\eta_0(\mathbf{I})$) from Equation (3.1.2). The vertical axis $\eta_{\text{app}}/\eta_0(\mathbf{I})$ is subsequently dimensionless in Figures 3.2.6 and 3.2.7 and the horizontal axis is the product of speed gradient and the estimated temperature dependent viscosity from Equation (3.1.2). Parameters a and b are found by fitting Equation (3.2.9). It may be of interest to report that the exponents of shear and extension rate, parameter b in Equation (3.2.5) and parameter m in Equation (3.1.5) are found to be very close. The other parameters a and k are different in regards to the temperature variation considered along spinning line in Equation 3.2.5.

The first region of spinning, where the strain rate is smaller than 10 s^{-1} , is not included in Equation (3.2.9) because the on-line measurements were out of the range.

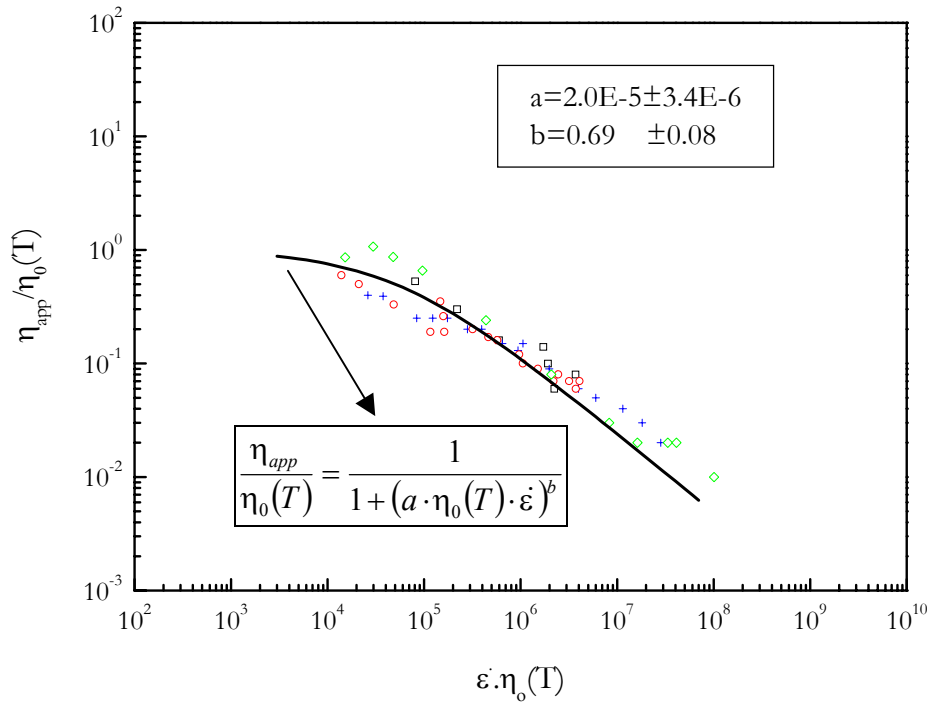


Figure 3.2.6 Dimensionless extensional viscosity estimated from online measurement (symbols) and function fitted (solid line) for test series B1 to B4 (see Table A1)

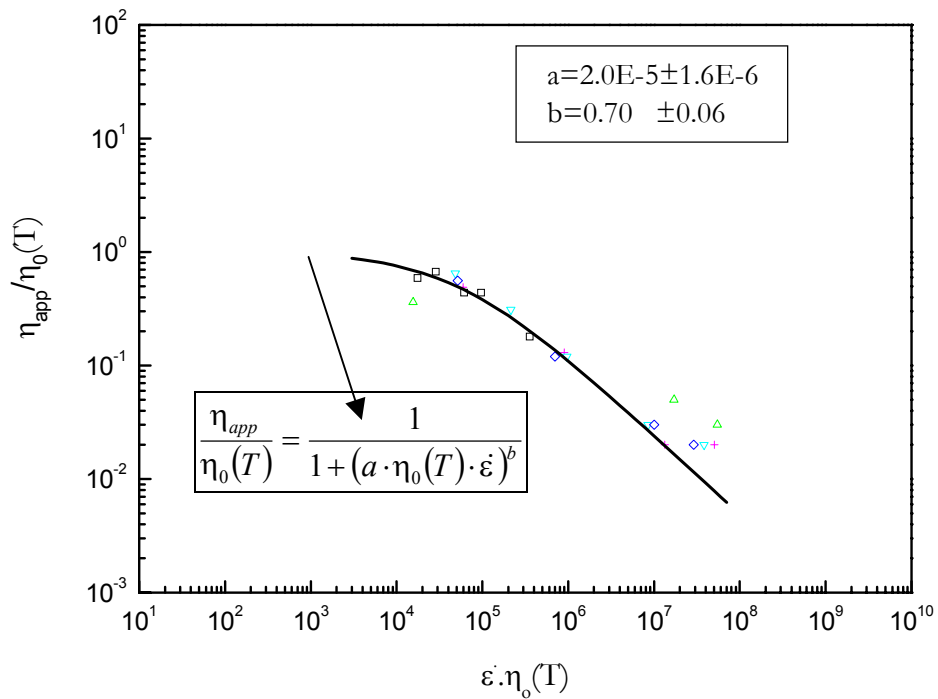


Figure 3.2.7 Dimensionless extensional viscosity estimated from online measurement (symbols) and function fitted (solid line) for test series C1 to C6 (see Table A1)

Crystalline-controlled viscosity: If the polymer crystallises in the fibre formation zone, several anticipated relationships between viscosity and crystallinity were discussed and compared by Ziabicki et al. [2002], they have proposed an empirical relation in the form:

$$\eta_2(X) = \left(\frac{1}{1 - (X/X_{cr})} \right)^a \tag{3.2.10}$$

If the crystallinity X approaches X_{cr} , fluid melt is converted into elastic solid and viscosity asymptotically approaches infinity and the material becomes incapable of flowing. The effect of this function is out of the scope of this article; this is neglected from the estimation of extensional viscosity as a result. Assume no crystallinity ($X=0$), the viscosity along the spinning line will only be a function of temperature (T) and the extension rate ($\dot{\epsilon}$). Figure 3.2.8 shows how the temperature dependent viscosity varies if the material is fully crystallised during cooling. For the partially crystallised polymers, it can be imagined that the viscosity goes to infinity between T_g and T_m at the freezing temperature. It can be shown that if the fully crystallised polymer is melted, it becomes very thin after crystals melt temperature. It is obvious that this crystallisation leads to an increase in polymer viscosity and then completes the solidification of material. The increase of viscosity should be applied to the fibre formation modelling for melt spinning.

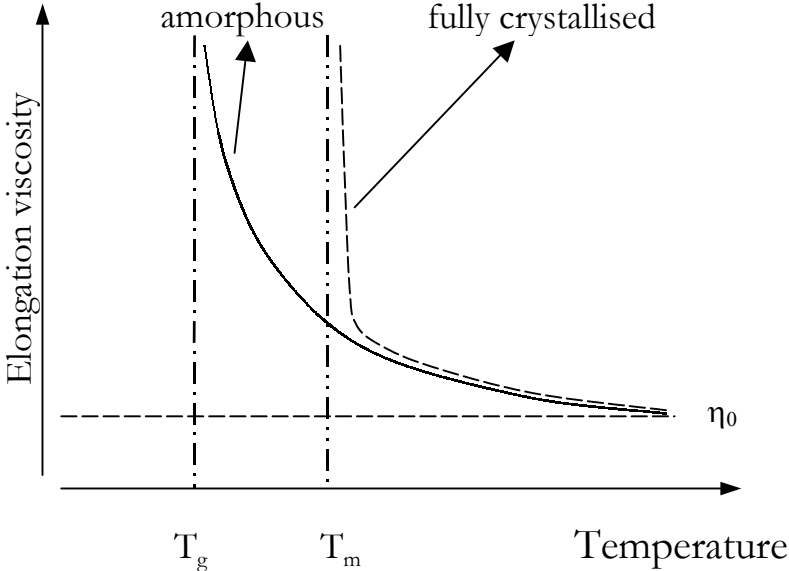


Figure.3.2.8 Effect of crystallisation on the polymer viscosity over temperature [Menges 1998]

3.2.3 Conclusion

The extensional viscosity along the spinning line is a complex, which varies from point to point. The estimation of the extensional viscosity from on-line measurements of the fibre speed and temperature is only qualitative, but for a low viscous polymer, a quantitative estimation can also be used along the spinning line. It can be concluded from the estimated extensional viscosity along the spinning line that the viscosity gradient ($d\eta/dz$) in the range of stable spinning controls the stress and molecular orientation (see Figures 3.2.2 and 3.2.3); therefore, a stronger viscosity gradient initiates the necking, and later, the instabilities. The stress along the spinning line for PEEK filament [Ohkoshi 1996] is discussed in Chapter 4 and 5.

It is obvious from results in Figures 3.2.4 and 3.2.5 that two regions of polymer behaviour exist (neglecting the region of decreasing the speed gradient along the spinning line). In the region in which the polymer assumed to have a viscous behaviour for an extension strain rate higher than 10 s^{-1} , the extensional viscosity decreases by increasing the extension strain rate. However, the second region near the spinneret for a strain rate smaller than 10 s^{-1} can proceed with viscoelastic behaviour during die swelling, which is a relaxation of polymer from upstairs flow [Brennat 2001]. The above observation simply confirms the following general statements along the spinning line of the melt spinning process. If the filament temperature is higher than the glass transition temperature, the viscosity term dominates. The viscous deformation decreases with decreases in temperature. The elastic deformation on the other hand dominates after solidification. The viscosity seems to be constant in low strain rate up to 10 s^{-1} and drops rapidly in the high strain rate as estimated for PEEK 151 G.

The deviations in the experimental estimations could be raised from measuring errors, due to inhomogeneous deformation, and also in the estimation of initial internal force and speed gradient.

To study the extensional rheology, the dimensionless apparent extensional viscosity is introduced. The extensional viscosity over strain rate can be interpreted in three regions, see schematic drawing in Figure 3.2.9. In the first region, the polymer has a high temperature, low extension strain and low strain rate, for PEEK 151 G: $\dot{\epsilon} < 10 \text{ s}^{-1}$. However, an increase in the extensional viscosity for low strain rate could not be detected by this study as reported by Rheotens [Laun 1989]. By decreasing the temperature along the spinning line, the viscosity increases exponentially according to the Arrhenius formula and the extension strain rate increases when

the fibre speed is also increased. This is the second region, where the dimensionless viscosity decreases by increasing the extension strain rate, but the apparent viscosity here is more than three times the shear viscosity, see Figures 3.2.2 and 3.2.3. This is the region for viscous deformation behaviour of polymer. In the third region after the peak of extension strain rate, the strain rate decreases, and the fibre solidifies. The temperature dependent extensional viscosity then increases quickly and approaches infinity near the solidification point. Therefore the dimensionless extensional viscosity in the third region is small in comparison to the same extension rate in the second region. After the solidification point, the extension strain rate becomes zero.

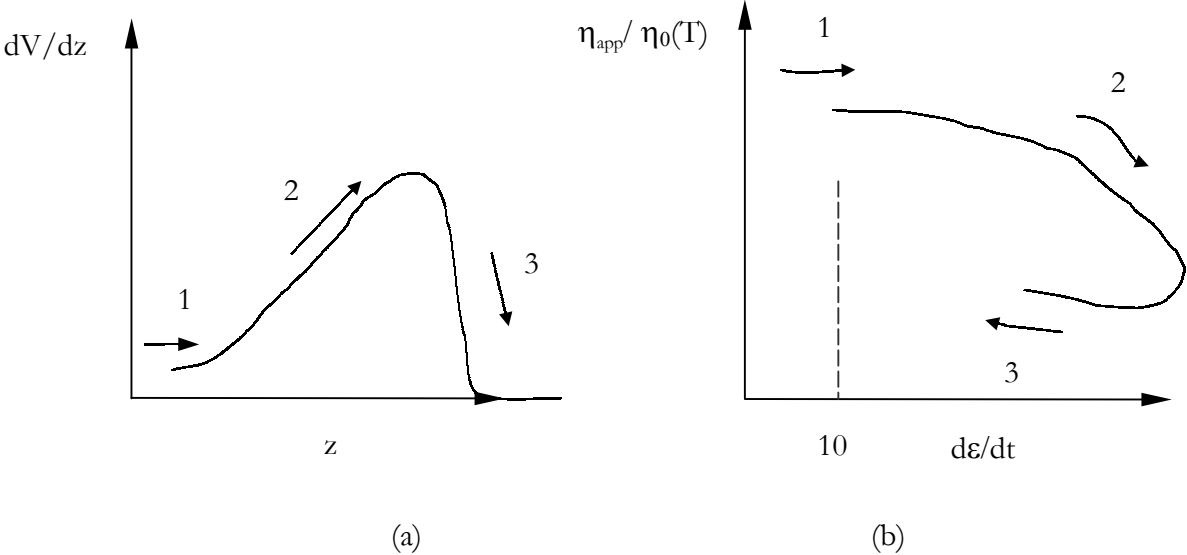


Figure 3.2.9 Schematic drawing of (a) fibre speed gradient along spinning line (b) dimensionless viscosity over extension strain rate along spinning line

4 Structural, mechanical and geometrical properties of the as-spun fibres

The structural and mechanical properties of as-spun fine PEEK and PP fibres are briefly dealt with in the following two sections in Chapter 4. It is worthwhile to fully study the structure of as-spun fine fibres of PEEK in order to understand and control the final properties in various spinning conditions. Various spinning conditions such as the take-up speed (V_L), throughput (Q), and the draw down ratio, (V_L/V_0) are discussed in relation to how they in turn affect the structural and mechanical properties of the fibres. The first section (Section 4.1) focuses mainly on structural investigations such as the orientation using off-line birefringence measurements (Δn), and the degree of crystallinity (X) using DSC measurements of as-spun fibres. The second section (Section 4.2) deal with mechanical and the geometrical properties such as fineness (Tt) and the end fibre diameter (D_1), and also stress-strain investigations such as elongation, strain and stress at break, tenacity and elasticity modulus.

4.1 Structural properties of the as-spun fine PEEK fibres

As the spinning speed increases along the spinning line in the fibre formation zone, the polymer chains orient and crystallise, and the fibre structure develops. The total orientation measured by birefringence could be correlated with the spinning line stress. The major variables affecting the molecular orientation are known to be those that have the greatest effect on the spinning line stress; namely polymer viscosity (and molecular weight), the spinning speed and mass throughput. The extrusion temperature also affects to a less extent the molecular orientation [Salem 2001].

4.1.1 Orientation investigations

The mechanical properties of as-spun fibres are strongly affected by the molecular orientation of polymer. The orientation of fibres has been widely investigated and it is of interest both for relation of orientation and properties of fibre, and also to find the melt spinning conditions that will result in the desired properties. Chain orientation is developed using polymer deformation; the deformation is either carried out in the melt or in the solid state. In the melt spinning process, the orientation of polymer molecules is developed in three regions: in the capillary, in the fibre formation zone during the stress-induced crystallisation and by drawing the crystallised fibre [Ehrenstein 1999]. However, the orientation of the shear flow in the capillary is lower than the orientation of polymer melt when extended along the spinning line. The main requirement is that

the molecular relaxation time of the deformed molecules must be longer than the experimental time allowed for relaxation. The partial crystallised polymer contains two phases: the amorphous phase and the crystalline phase, which can be independent from each other. However, the orientation of crystallised fibre is difficult to investigate because the simultaneously existing cases of orientation are dependent on each other. Therefore, all of the orientation measurements contain two mentioned parts, and a third additional part which covers the interaction of the two phases. Assuming that the interaction phase is negligible (the so-called birefringence form), the molecular orientation can be evaluated separately for the crystalline phase and amorphous phase by using the total birefringence (Δn). The birefringence (Δn), which is found in fibres due to molecular orientation, can be defined as the difference between the index of parallel refraction (n_{\parallel}), and perpendicular refraction (n_{\perp}) to the fibre axis ($\Delta n = n_{\parallel} - n_{\perp}$). The birefringence of partial crystalline fibre can be expressed as:

$$\Delta n = X \cdot \Delta n_{cr} + (1 - X) \cdot \Delta n_{am}, \quad (4.1.1)$$

where $\Delta n_{cr} = f_{cr} \cdot \Delta n_{cr}^{\max}$ and $\Delta n_{am} = f_{am} \cdot \Delta n_{am}^{\max}$,

X is the degree of crystallinity, which can be determined by DSC measurements.
 $\Delta n_{cr}^{\max}, \Delta n_{am}^{\max}$ are the fibre birefringences of the total crystalline and amorphous phases respectively. They are adopted using the sonic module parameter [Schmack 1997]. The maximum possible birefringence corresponds to all molecules aligned parallel to the fibre axis.
 f_{cr}, f_{am} are “crystalline” and “amorphous” orientation functions (order parameters) respectively, and can be evaluated by X-ray scattering.

According to the definition of the orientation function, $f = 1$ means that all of molecules are aligned parallel to the fibre axis, and $f = 0$ describes the random dispersed (isotropic) system and $f = -0.5$ is valid if all the molecules are perpendicular to the fibre axis. The total birefringence (Δn), and the degree of crystallinity (X) are dependent on the spinning conditions. The orientation of amorphous part increases slightly when the spinning speed is increased. The orientation of crystalline phase is known to begin with a definite spinning speed; however, the effect of the draw down ratio on the orientation was only recently reported in the investigations for Polypropylene [Choi 2002] and for Nylon-6,6 [Joo 2002].

Birefringence of as spun PEEK fibres: The on-line birefringence of PEEK was measured by interference [Shimizu et al. 1985]. The reported total birefringence was 0.199 and the crystal orientation factor found $f_{cr} = 0.9$. The reported birefringence of the amorphous region of as-spun

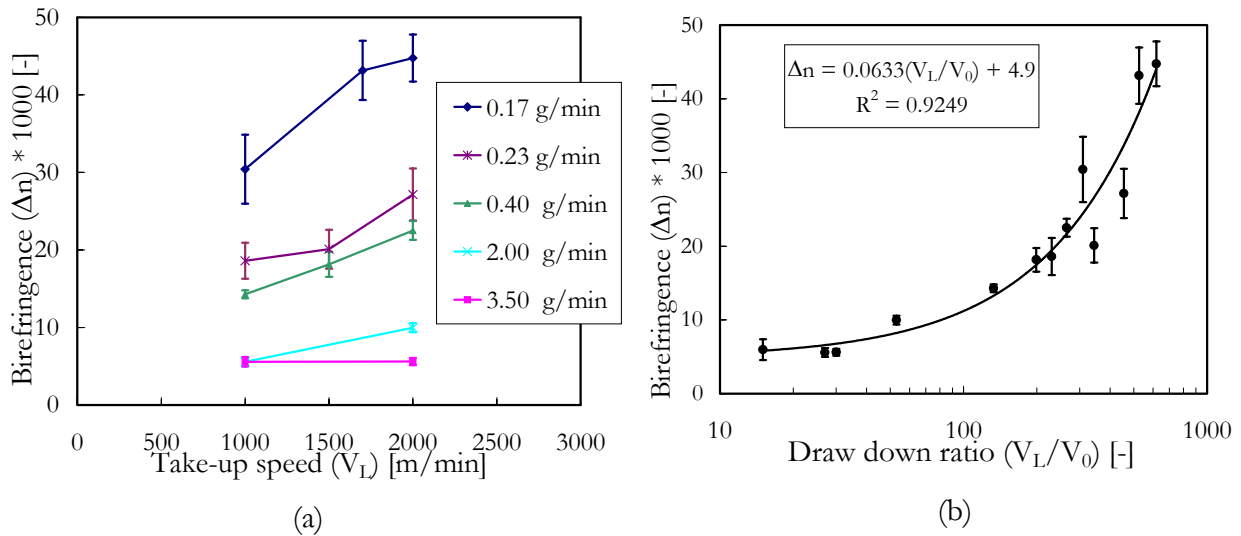


Figure 4.1.1 Birefringence measured in different throughput conditions of spun fibre PEEK 151 G (a) over take-up speed (b) over draw down ratio, measurement (symbols), fitted (solid line)

PEEK fibres was more than ten times of the crystalline region. Increases in the birefringence caused by increasing the spinning speed are well known for different melt-spun fibres [Shimizu 1985] and also for PEEK fibres [Ohkoshi 1999]. For a range of take-up speeds up to 100 m/min, the molecular orientation of as-spun fibres increases with an increasing take-up speed [Shimizu 1987].

The birefringence was measured here aided by an optic microscope, as explained in Section 2.3. Figure 4.1.1 (a) demonstrates the measured birefringence of as-spun PEEK fibres over take-up speed for different mass throughputs. It is evident from the Figure 4.1.1 (a) the birefringence increases by increasing the take-up speed, but in a constant take-up speed, increasing the mass throughput leads to decreases in the orientation. For example, with a take-up speed of 2000 m/min, by making the throughput twenty times as small (3.5 g/min to 0.17 g/min), the orientation increasing tenfold. With a constant throughput, increasing the take-up speed increases the orientation, but the slope of the increase becomes more gradual when increasing the throughput. For a constant mass throughput of 0.17 g/min, the measured birefringence for different take-up speed shows a sharp increase. At a mass throughput of 0.17 g/min, the maximum possible take-up speed for stable spinning is about 2000 m/min (see Chapter 6 for spinning limits). It can be concluded that for these spinning conditions, the maximum orientation for PEEK expressed as birefringence is $\Delta n^{\max} \approx 0.05$. For the higher throughput of 3.5 g/min, the orientation seems to be only weakly dependent on the take-up speed.

To discuss the combined effect of the mass throughput and the take-up speed, the results of the birefringence measurements over the draw down ratio are presented in Figure 4.1.1 (b). With the smaller draw down ratio values, the birefringence can approach a constant value of $\Delta n \rightarrow 0.005$, extrapolated by the solid line fitted to orientation. In the specified region of draw down ratio >200 , the as-spun PEEK fibres show comparatively high molecular orientation. If the draw down ratio is above 200, high levels of orientation are obtained. By increasing the draw down ratio, the birefringence increases and the fineness (diameter) is known to decrease. The stress development (especially the stress at solidification point) along the spinning line mainly initiates and controls the orientation of molecule chains.

Orientation and stress along the PEEK spinning line: Above the glass transition temperature for the low initial stress level, the birefringence of an as-spun amorphous polymer filament is proportional to the applied stress. This is expressed with an experimental linear relation between birefringence (Δn) and the internal tensile stress (σ) as follows:

$$\Delta n = C \cdot \sigma \tag{4.1.2}$$

The constant C is inversely proportional to the absolute temperature. However, it is frequently

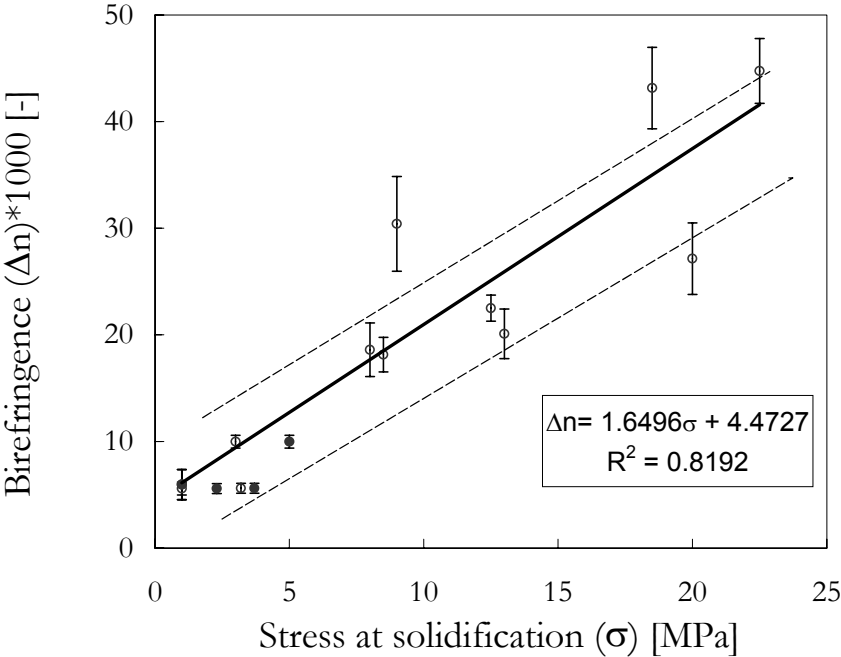


Figure 4.1.2 Birefringence (measured) over stress (calculated) at solidification point for PEEK 151 G fibre

found that C can be treated as a constant over the range of the temperature where the birefringence of the spinning polymer develops. C can be either positive or negative, depending on the relative value of the two components of polarity. By increasing the spinning speed the stress becomes higher and higher, but the birefringence reaches its maximum (Intrinsic) value Δn^* .

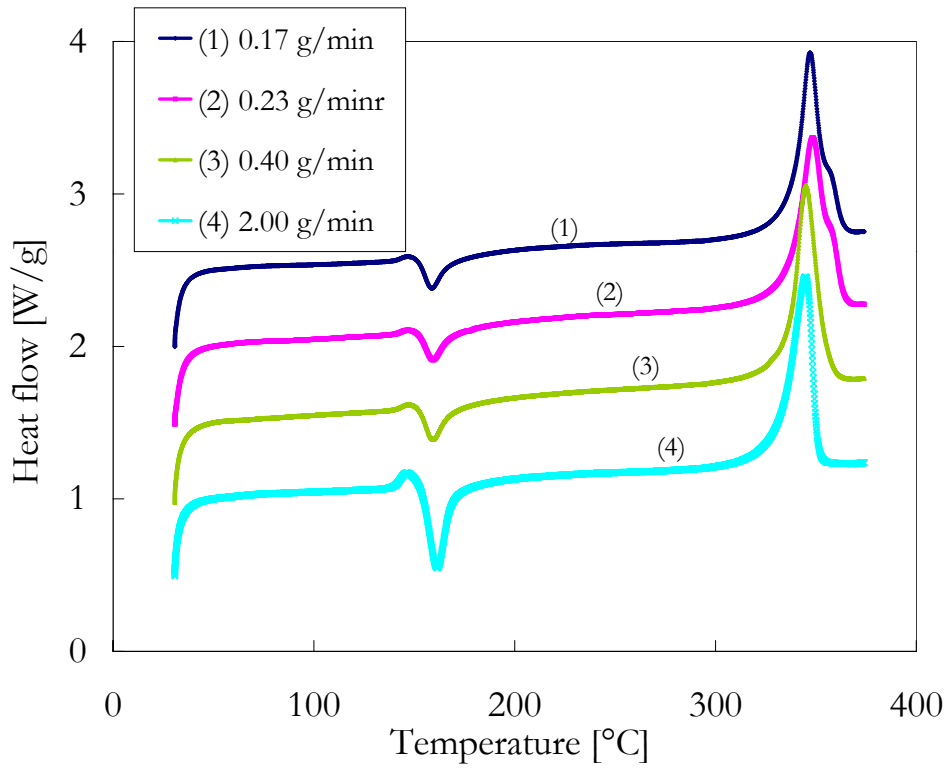
Ohkoshi [1996] reported some on-line birefringence measurements and stresses along the PEEK spinning line and concluded that the stress-optical law, which is a good approximation for some polymers, is not valid for PEEK. At the beginning of the spinning line the birefringence was just 2 % of the intrinsic birefringence. He concluded that because of the long relaxation time and the high thinning rate, stable viscous deformation could not occur. The molecular chain deformation has rather elasticity with little relaxation, and then it freezes with orientation-induced crystallisation. Figure 4.1.2 represents the off-line measured birefringence over the estimated internal stress at the solidification point, calculated from model of fibre formation of PEEK (see Section 5.4). The linear relation as Equation (4.1.2) shows still a good agreement, but shows some deviations to the orientation measurements.

4.1.2 Crystallisation of the as-spun PEEK fibres

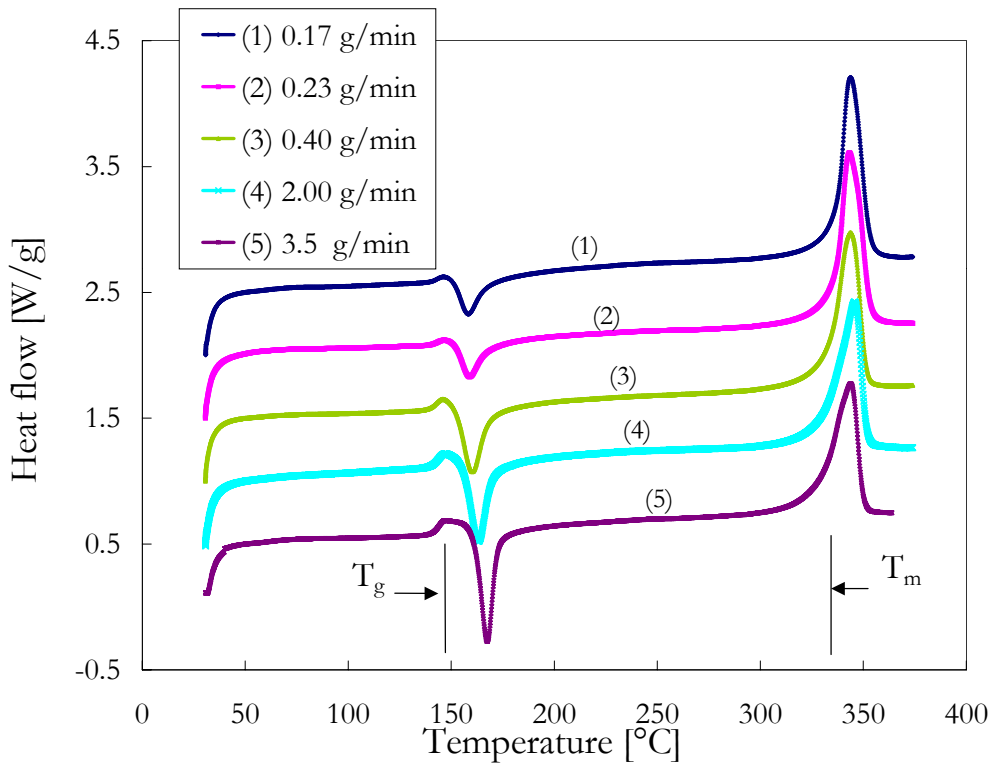
Crystallisation is a term used for both nucleation and crystal growth. The nucleation rate of polymers at a constant temperature is greatly accelerated by the molecular orientation. Crystallinity plays an important role in determining the strength, stiffness and dimensional stability of synthetic fibres. Crystallisation occurs only within a specific temperature range that is bounded by melting point and the glass transition temperature ($T_m > T > T_g$). Along spinning line the polymer cools from a molten to a solid state, and subsequently passes through this aforementioned temperature range. It should be noted that materials having a T_g below ambient temperature, such as polypropylene, would continue to crystallise (post-crystallisation) even after the spinning process is completed. It is known that the crystallisation that occurs under molecular orientation may be different from ordinary not-oriented crystallisation. Ziabicki et al. [1985] concluded in the theory of orientation and crystallisation in the fibre spinning that the primary factor controlling the structural formation is the internal tensile stress (σ) along the spinning line in the fibre and not the draw down ratio (V_L/V_0) or deformation rate (V). However, the internal tensile stress depends on the spinning speed (V_L), extensional viscosity, the cooling rate and the fibre cross-section area. The spinnable polymers can be classified into three groups: not-

crystallising (e.g. atactic polystyrene), slowly crystallising (e.g. PET) and fast crystallising (e.g. Nylon 6,6 and PP). The relationship between structure and spinning conditions for polymers capable of effectively crystallising at low spinning speed such as polypropylene are different. A large number of crystals are formed in a low-stress part of spinning line at a high or low take-up speed. To a large extent, molecular and crystal orientations are developed independently and are controlled not by the oriented nucleation, but by the rotation of crystals and chain segments in the deformation flow field. This means that the crystal orientation factors (f_c) will be smaller and the amorphous orientation factor (f_{am}) will be much higher than predicted for orientation-induced crystallisation. Amorphous orientation will not be considerably reduced as a result of crystallisation. Therefore, PEEK and PP can crystallise at a low take-up speed and in a part of the spinning line where the stress is low. The amorphous and crystal orientations are developed independently. This means that, at the same stress level ($\sigma = K$), the crystal orientation factors will be smaller and amorphous orientation factors will be much higher than those predicted for orientation-induced crystallisation.

The Degree of Crystallinity for as-spun PEEK fibre using DSC measurements: The crystal structure of PEEK has been investigated by wide angle X-ray diffraction from melt-spun fibres [Shimizu 1985]. Some information of kinetics of non isothermal crystallisation of PEEK was reported by Zhang [2003]. In this thesis the degree of crystallinity of the as-spun fibre was determined using DSC measurement, as explained in Section 2.3.3. The DSC scanning curves for samples selected at first heating show a difference (as shown in Figure 4.1.3 (a),(b)). The first heating step of as-spun fibres shows a glass transition followed by post-crystallisation region and a melting peak. The glass transition temperature (T_g) shows no distinct difference under different spinning conditions. The post-crystallisation, which appears in the first heating, takes place directly after the glass transition. However, the beginning of as-spun PEEK fibre post-crystallisation is shifted to higher temperature using higher throughputs or lower draw down ratios of the melt spinning process. The melting points (T_m) of as-spun PEEK fibres are not affected (no high difference) by different spinning condition, see Figure (4.1.3) (a) and (b). The degree of crystallinity of a-spun PEEK fibres was determined using the first heating step of DSC measurements by subtracting the melting and post-crystallisation areas. The result (enthalpy of crystallisation) is divided by the enthalpy of 100% crystallisation. The area of post-crystallisation shows an increase with a lower draw down ratio; this is a spinning condition in which the stress is low and the induced crystallisation consequently lower than for higher draw down ratio.



(a)



(b)

Figure 4.1.3 DSC measurement, first step heating flow over temperature
 (a) take-up speed 2000 m/min (b) take-up speed 1000 m/min

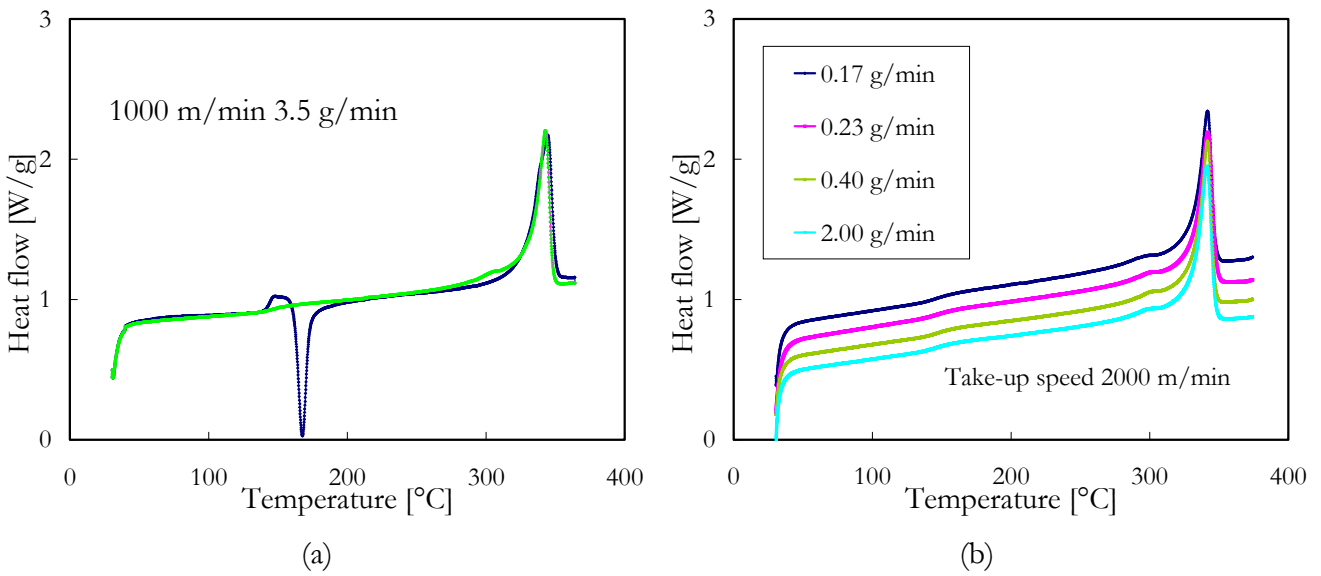


Figure 4.1.4 (a) First and second step heating to find crystallinity (b) second heating step

The second heating step shows no post-crystallisation and only a light relaxation in the glass transition temperature, see Figure 4.1.4 (b). After a cooling stage of 20°C/min, the second heating of DSC measurement shows the totally same behaviour at the glass temperature and the same melt temperature. The crystallisation at second heating indicates that the maximum possible crystallinity of PEEK is about 40%.

Nr.	Q g/min	V _L m/min	D _L μm	V _L /V ₀ -	ΔH J/g	X %	Δn*1000 -
1	3.5	1000	58	15	20	15	5.58
2	2	1000	44	27	23	17	5.61
3	3.5	2000	41	30	22	17.5	5.58
4	0.225	200	33	47	22	17	-
5	2	2000	31	53	23	17.9	9.9
6	0.225	400	23	94	23	18	-
7	0.4	1000	19.6	133	29	22	14.3
8	0.225	600	19	141	29	22	-
9	0.225	800	16.5	189	32	25	-
10	0.4	1500	16	199	39	30	18.2
11	0.231	1000	14.9	230	33	25	18.6
12	0.4	2000	13.9	265	43	33	22.5
13	0.17	1000	12.8	309	40	31	30.4
14	0.225	1500	12	350	42	32.4	20.1
15	0.231	2000	10.6	455	45	35	27.2
16	0.17	1700	9.8	526	45	34.5	43.2
17	0.17	2000	9.1	619	46	35	44.8

Table 4.1 birefringence and degree of crystallisation from DSC for as-spun PEEK

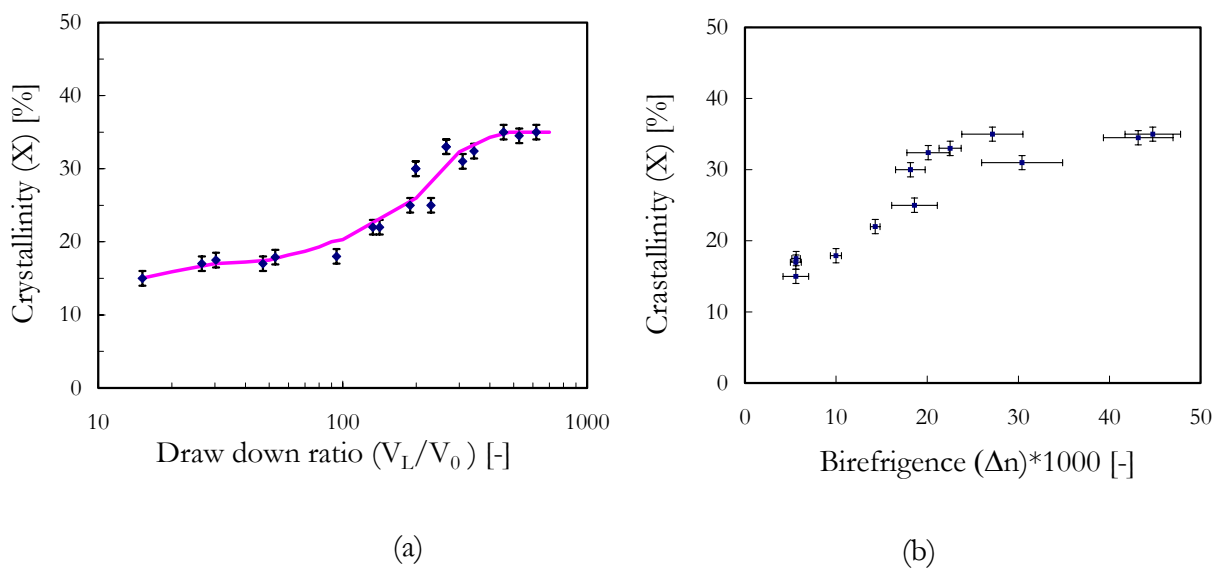


Figure 4.1.5 Crystallinity from DSC of as-spun fibre PEEK 151 G
(a) over diameter and (b) over birefringence

In Figure 4.1.5 (a), the degrees of crystallinity from DSC measurements are plotted over the draw down ratio. The crystallinity increases by increasing the draw down ratio slowly, but if the draw down ratio reaches the value ~ 200 , it increases rapidly until it reaches a maximum value of draw down $ddr \sim 350$. The maximum crystallinity of as-spun fibre measured from DSC is about $\sim 35\%$ for a draw down ratio greater than 350. One should be remind that increasing the draw down ratio is known to lead to decreasing the fibre diameter and fineness. This means that the fine PEEK fibres show a high degree of crystallinity. If the crystallinity is extrapolated at a very small draw down ratio ($ddr \rightarrow 0$), the crystallinity can reach a constant value of $X \sim 15\%$. It is obvious that the crystallinity also exists for a very small draw down ratios. The effect of crystallinity on geometrical and mechanical properties of fibres is discussed in the Section 4.2.

Crystallinity of as-spun PEEK 151G vs. Birefringence (Δn) is plotted in Figure 4.1.5 (b). The total birefringence starts at low take-up level speed but shows a little dependence on degree of crystallisation. The crystallinity and birefringence both simultaneously reach a maximum. The extrapolation for the maximum orientation does not reach the 100% crystallinity. PEEK is known to be a polymer that crystallises at a lower molecular orientation and the crystallinity produced inhibits further progression of molecular orientation.

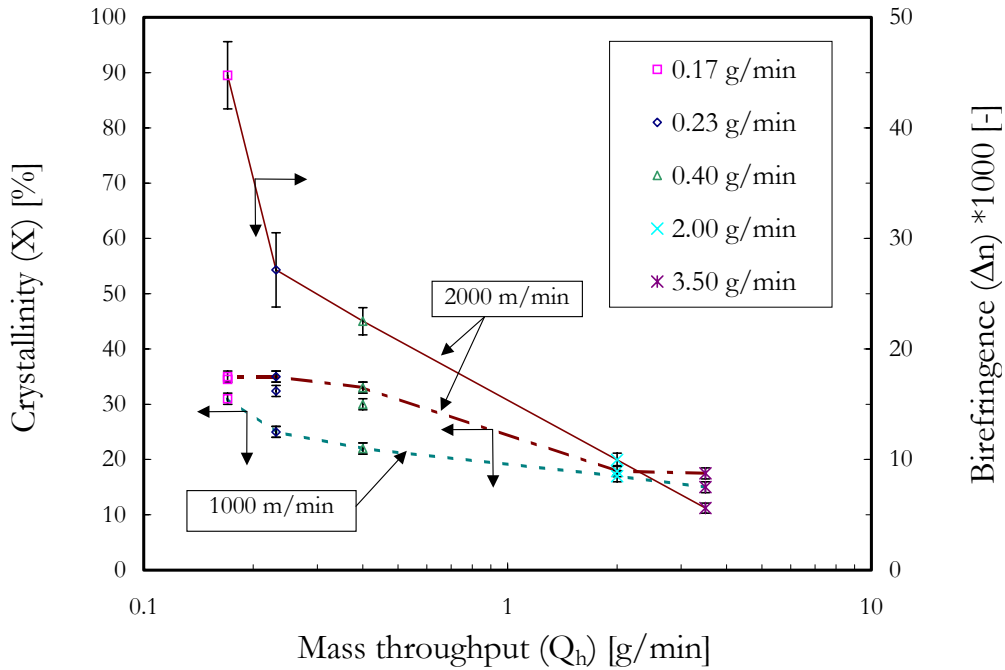


Figure 4.1.6 Degree of crystallinity and total birefringence measured (symbols) over throughput for different take-up velocities of PEEK 151G

According to the DSC measurements of the as-spun PEEK fibre, the degree of crystallinity reaches a maximum value of about 35 % at a spinning speed 2000 m/min and falls to below 15 % at the same spinning speed but for a higher throughput (>2 g/min), see Figure 4.1.6. The same maximum degree of crystallinity can be reached using a spinning speed 1000 m/min, but this can be only for a very low throughput. The total birefringence of as-spun PEEK fibre at 2000 m/min shows a decrease by increasing the throughput as discussed previously in Figure 4.1.1 (b).

Some considerations for on-line crystallisation and orientation: The increase in take-up speed produces a major increase in the crystallisation kinetics, and it is expected, the crystallisation temperature will also increase. If the crystallisation kinetics is saturated, an increase in take-up speed will still increase the cooling rate and that will produce lower crystallisation temperature. Increasing the molecular weight increases the polymer viscosity and leads to a greater stress and molecular orientation in the spinning line. This usually leads to higher crystallisation temperature. Crystallisation of polypropylene in the spinning line occurs at a lower temperature than for polyethylene, despite the higher melting point of polypropylene. The crystallisation in melt spinning of PEEK proceeds in a highly oriented structure region of fibres on the spinning line [Shimizu 1987]. According to the oriented crystallisation, the molecular orientation causes an increase in the crystallisation rate but reduces the average crystal size [Salem 2001].

4.2 Mechanical and geometrical properties of as-spun fine fibres

4.2.1 Fineness and Tenacity (PEEK and PP fibres)

Fineness: In Figure 4.2.1, the fineness and diameter of as-spun PEEK fibres over the take-up speed for different throughputs are compared. The solid lines are the calculated values of fineness and the symbols are the measured values of fineness. It can be seen that the values of fineness measured and calculated are close together and show a good agreement. The deviations of measurements from theoretical calculation may be due to the process parameters, i.e. mass throughput, take-up speed deviations, polymer impurities and the die inaccuracies [Beyreuther 1998]. If the fineness and diameter values are presented over the draw down ratio, the curves can be reduced with respect to throughput as shown in Figure 4.2.2. It is obvious from this presentation that in order to produce fine fibres, the draw down ratio has to increase quadratic. For example, to reduce the diameter from 60 μm to 20 μm , the draw down ratio has to increase from 10 to 90. But to decrease the diameter from 10 μm to 8 μm the draw down ratio must increase from 500 to 780, which is not easy to spin stable because of such high draw down ratio. More investigations about the spin stability and the limit of fineness to produce the fine fibres are discussed in the Chapter 6.

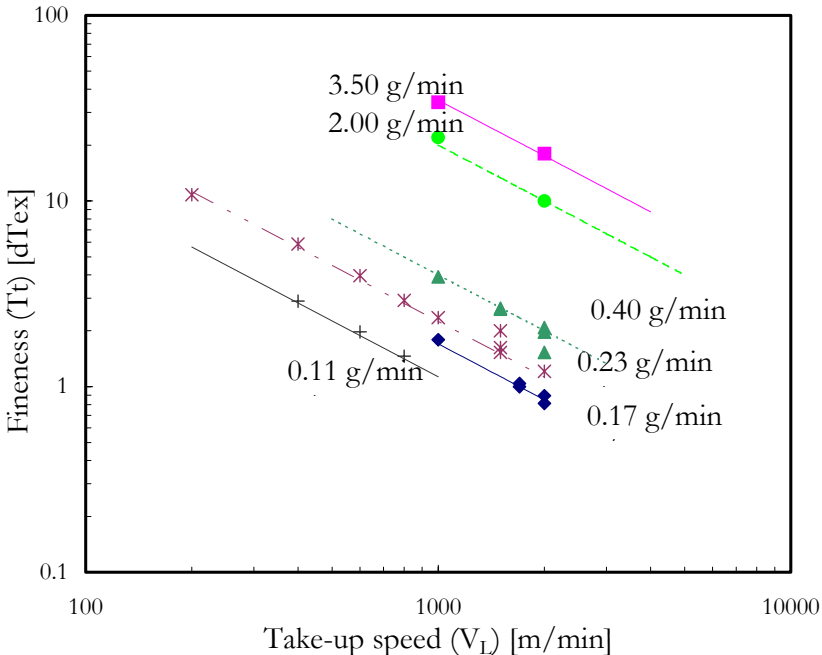


Figure 4.2.1 Fineness and diameter measured and calculated of as-spun PEEK 151G fibres for different spinning conditions over take-up speed

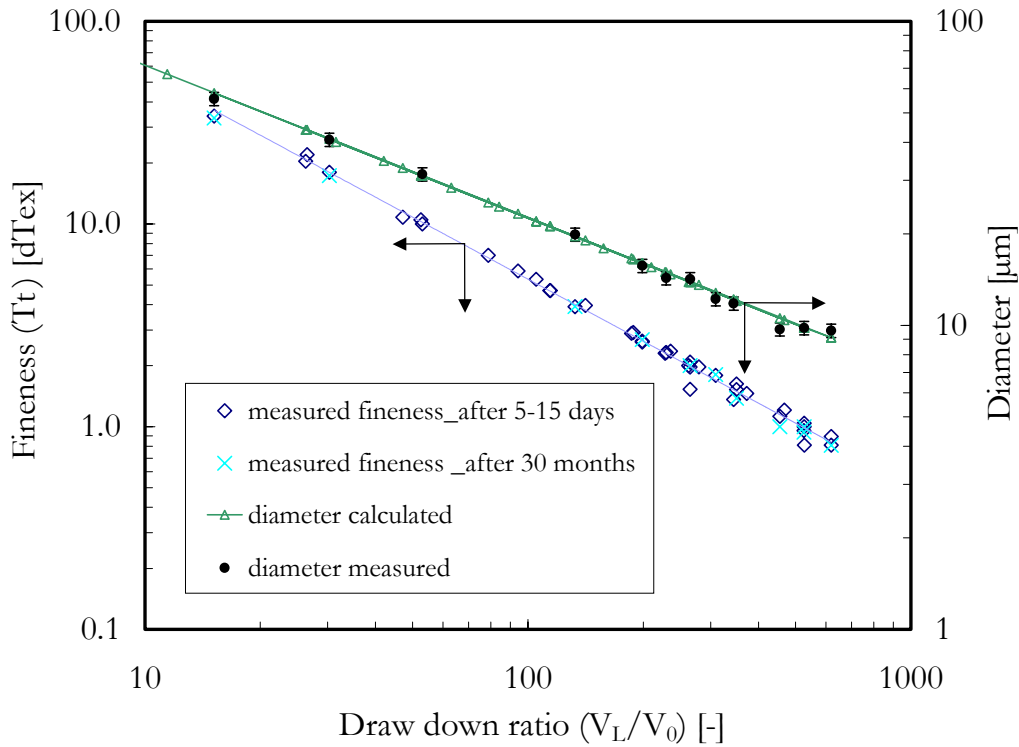


Figure 4.2.2 Fineness and diameter measured and calculated of as-spun PEEK 151 G fibres for different spinning conditions over draw down ratio

The fineness was measured according to gravitational method as described in Section 2.3.1. In Figure 4.2.2, the diameter measurements were carried out using an optic microscope described in Section 2.3, and the fineness measurements were done directly after spinning and again later after 30 months, and showed no significant difference.

Elongation at break: As explained in Section 2.3.2 the elongation measured by a tensile test can be used to calculate the Hencky's strain. The elongation and Hencky's strain are only identical for a very small deformation (<0.01). Figure 4.2.3 shows the elongation at break over the take-up speed for as-spun PEEK fibres. In comparison to the general observation of many spinning thermoplastic fibres, Figure 4.2.3 verifies that the high stress at the solidification point along the spinning line for PEEK fibres leads to decrease the elongation at break [Brünig 1999]. Of course, the Hencky's strain shows the same trend as the elongation over take-up speed. As the take-up speed increases and approaches 5000 m/min, the elongation at break will reach 40 % and the Hencky's strain will equal 0.4. If the take-up speed is extrapolated for ($V_L \rightarrow 100$) the elongation at break appears to approach 300 % and the Hencky's strain at break (ϵ) will approach 1.4. As explained, the elongation at break decreases by increasing the take-up speed, however, at the constant take-up speed, a different value for measured elongation exists, see Figure 4.2.3.

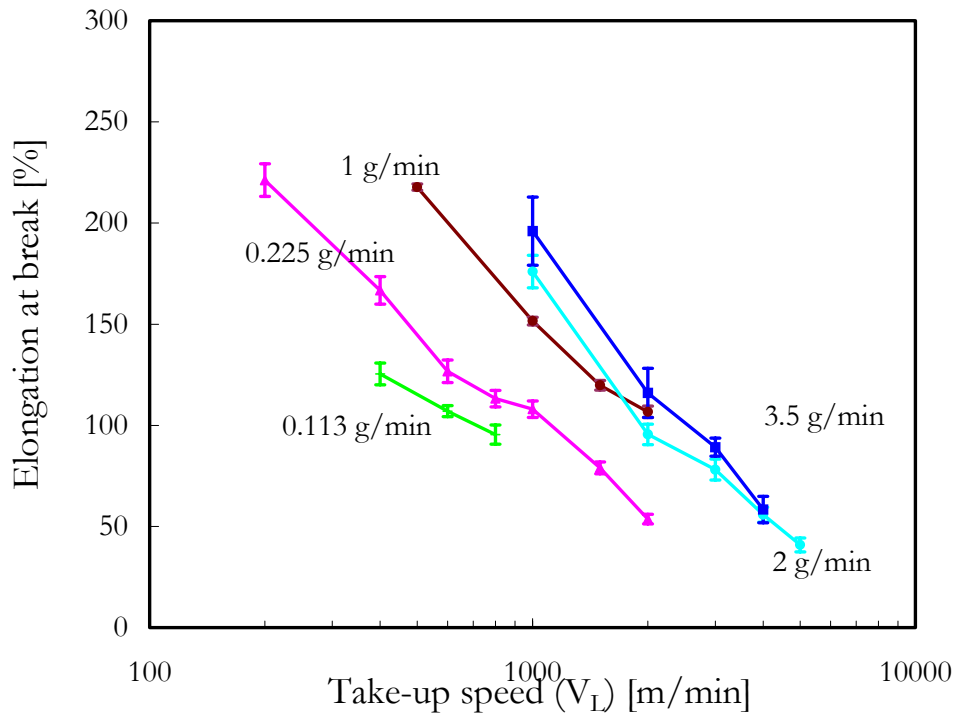


Figure 4.2.3 Elongation at break over take-up speed of as-spun fibres of PEEK 151G Victrex from tensile test

Different elongations are caused by different draw down ratios for one take-up speed, in other words, it is due to different throughputs. Higher throughput means lower solidification stress value and smaller throughput leads to a higher elongation at break [Beyreuther 1991]. The elongation at break decreases more when increasing the draw down ratio, see Figure 4.2.4 (b). Whilst the elongation at break is more than 100 % for $ddr \sim 10$, it can decrease to 40 % as the draw down ratio approaches 1000. This can be due to the structure of PEEK fibres; for a higher draw down ratio, the crystalline part approaches its maximum, and the amorphous part can be stretched and oriented along the fibre axis.

Tenacity: The effect of the take-up speed on the physical tenacity is presented in Figure 4.2.4 (a). The line fitted to physical tenacity of PEEK fibres slowly decreases from 6-7 cN/dTex down to 4 cN/dTex for a take-up speed approaching 5000 m/min. It is necessary to notice that, for the production of fine filaments, the elongation and the physical tenacity are lower for the same take-up speed. A low melting temperature also leads to a higher value of physical tenacity. This can be due to increased crystallization and lower orientation. One should consider that the variation of physical tenacity of fibres with respect to draw down ratio shows a relative constant tenacity 5 cN/dTex for a draw down ratio of $(V_L/V_0) < 200$, see Figure 4.2.4 (b). For a higher draw down ratio (to produce fine fibres), the physical tenacity decreases slightly to a smaller value; for

$ddr \rightarrow 1000$, the physical tenacity can possibly reach 4 cN/dTex (see Figure 4.2.4 (b)). Figure 4.2.4 (b) also shows another set of measurements taken after 30 months of spinning. However, the tenacity itself over the draw down ratio shows a slight increase for as-spun PEEK fibers, as shown in Figure 4.2.5 (a) and (b). For a low draw down ratio about 10, the tenacity is about 2 cN/dTex , and for a high draw down ratio close to 1000, it is greater than 4 cN/dTex . This means that to produce more fine filaments in the melt spinning, the tenacity increases, but the physical tenacity decreases, as shown in Figure 4.2.4. The increase of tenacity was also reported for other polymer, e.g. by Murase [1994] for PET. The deviation in the tenacity measurements is caused by different structural properties, i.e. crystallization and orientations. Other reason for physical tenacities deviations is the effect of multifilament tensile test. This means that the single filaments of multifilament under stress breaks one by one, and the stress and the strain of break differs for every filament, therefore the physical tenacities, as a true stress at the breakage can not be totally reliable as for the tensile test of single filament.

By comparing the polypropylene to PEEK in Figure 4.2.6 (a) and (b), this confirms that physical tenacity decreases if the draw down ratio is increased. The elongation at the PP break is higher than for PEEK, and decreases rapidly with the increase of the draw down ratio. However, the elongation at break of PP is higher than for PEEK and the physical tenacity is also higher. The polypropylene fibres show a higher deviation in fineness and diameter in the measurements given in Figure 4.2.6 (a); this could be interpreted as due to the different structure formation of polypropylene compared with PEEK.

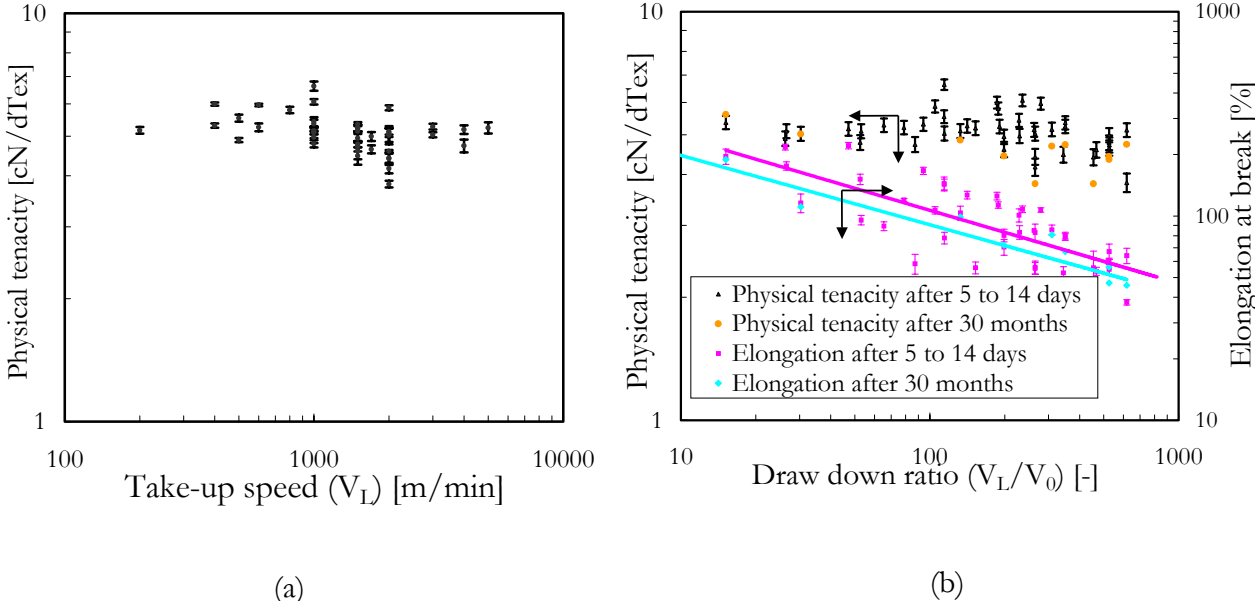
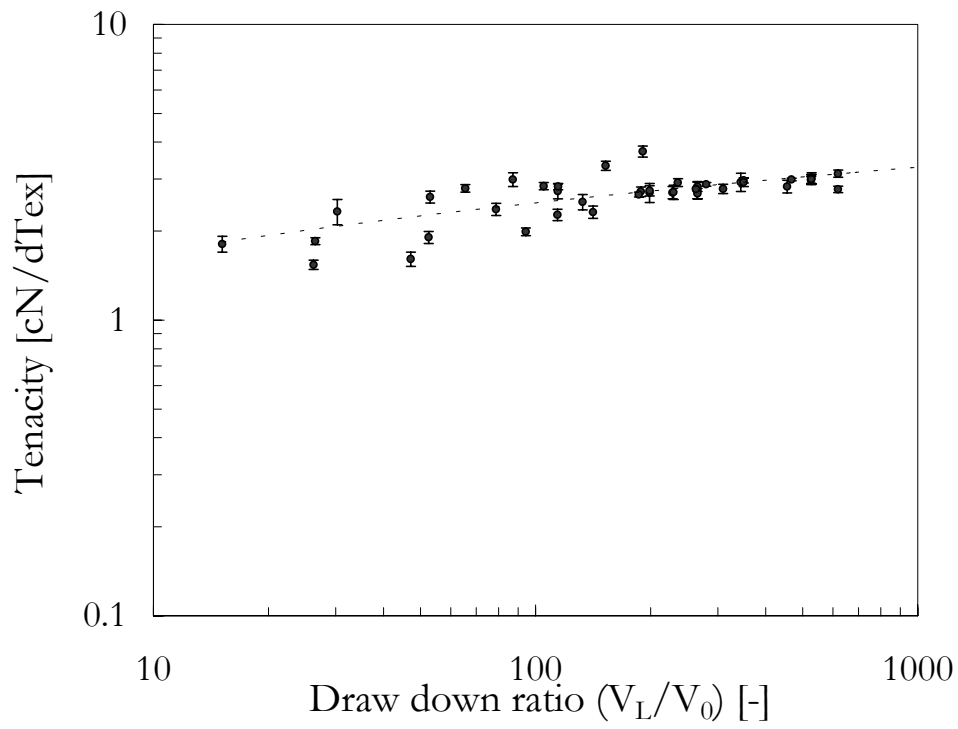
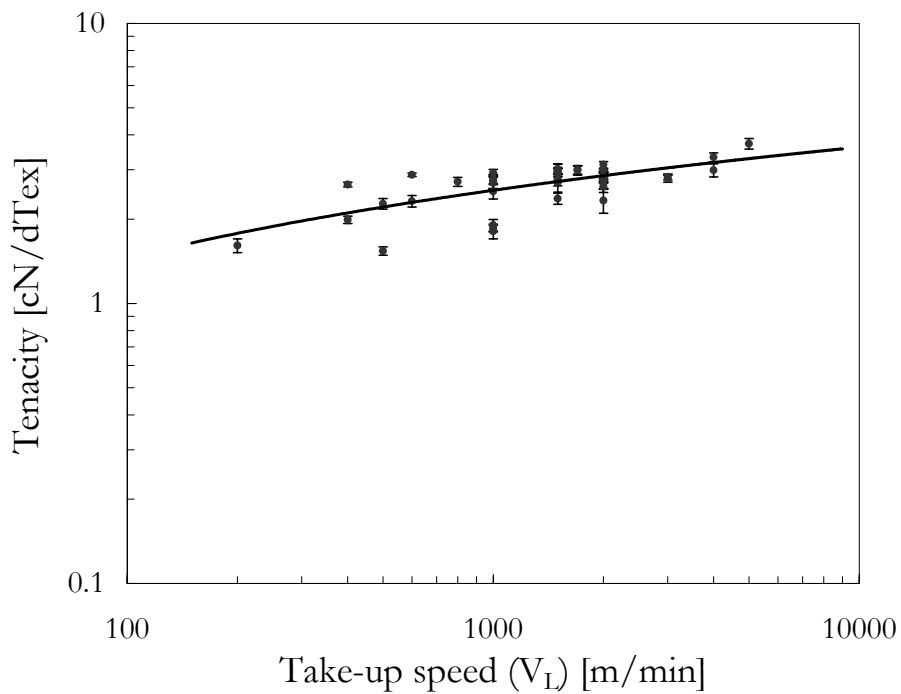


Figure 4.2.4 (a) Physical tenacity over take-up speed (b) Physical tenacity and elongation at break over draw down ratio for different spinning conditions of PEEK 151 G (solid line fitted)

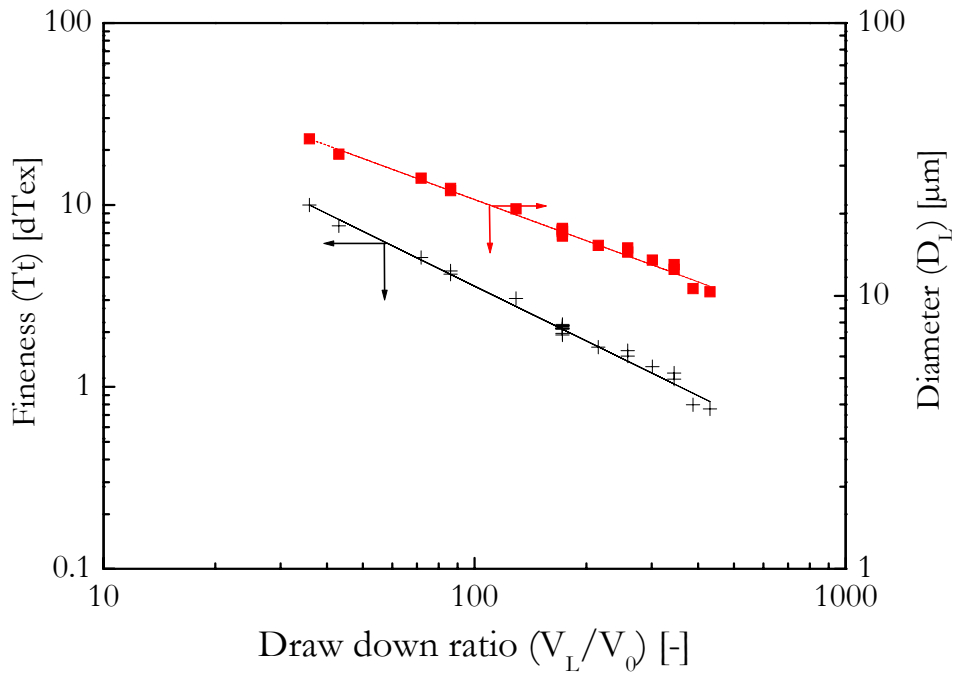


(a)

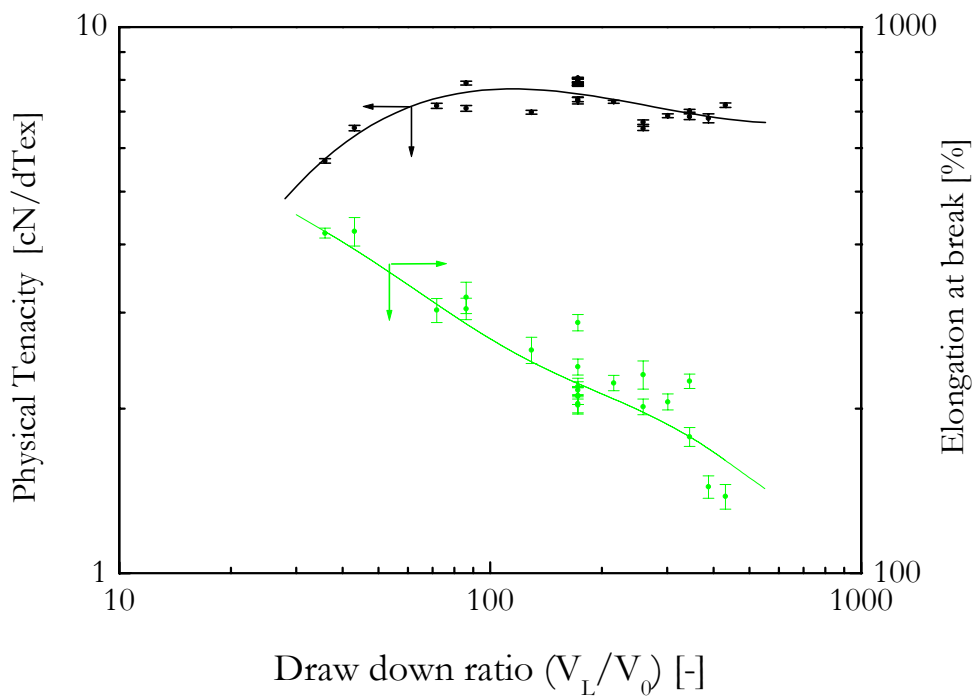


(b)

Figure 4.2.5 Tenacity for as-spun fibre of PEEK 151G
 (a) over draw down ratio and (b) over take-up speed
 (solid line fitted)



(a)



(b)

Figure 4.2.6 (a) Fineness and diameter measured (symbols) and calculated (solid lines)
 (b) Physical tenacity and elongation at break of PP HF445FB over take-up speed, measured (symbols), fitted (solid lines)

4.2.2 Elasticity modulus and stress strain curves

The room-temperature fibre structure properties discussed here are the initial elasticity modulus and the tensile strength. The following discussion of the structure-property relationship provides a simplified outline of the subject. The modulus of fibres from flexible chain polymers is usually much lower than the ultimate value, because chains in the non-crystalline regions are far from being fully aligned. The modulus of polymers in the amorphous state (E_{am}), with randomly oriented chains, is generally one to two orders of magnitude lower than its (chain axis) modulus in the crystalline state (E_{cr}). For a simple series arrangement of amorphous and crystalline region assuming crystals fully oriented along fibre axis the overall elasticity modulus is given by

$$\frac{1}{E} = \frac{(1-X)}{E_{am}} + \frac{X}{E_{cr}} \tag{4.1.3}$$

It is clear that the not-oriented amorphous regions have the dominated influence on the fibre elasticity modulus, even at very high levels of crystallinity. If the crystalline regions are surrounded by the amorphous phase in a parallel series arrangement, and $E_{cr} \gg E_{am}$, the influence of E_{am} is again predominant. Only when there is crystal continuity (amorphous and crystalline

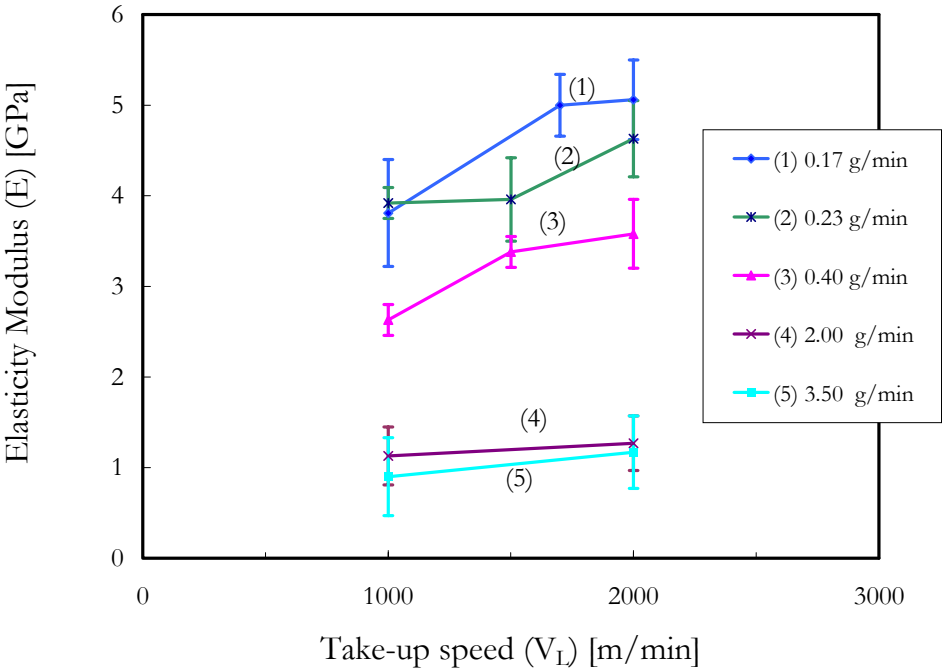


Figure 4.2.7 Elasticity modulus from true stress-strain curves in room temperature of melt-spun PEEK 151 G fibres over take-up speed

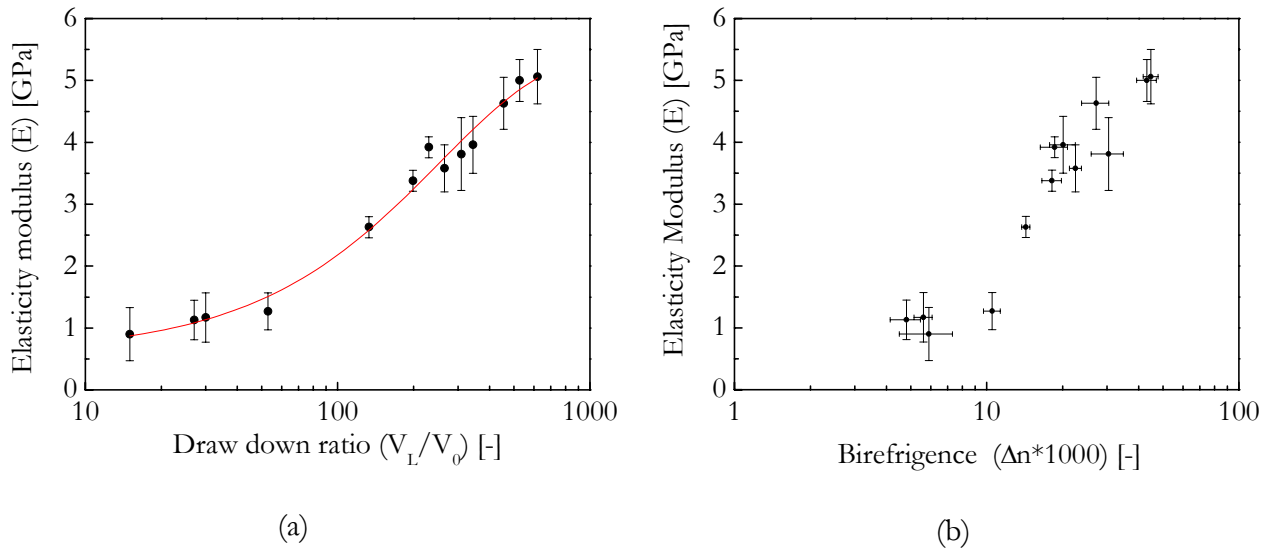


Figure 4.2.8 Elasticity modulus from true stress-strain curves in room temperature of melt-spun PEEK fibres (a) over the draw down ratio (b) over birefringence in different spinning conditions, (solid line fitted to measurement)

phase in parallel, or amorphous regions surrounded by crystalline regions) can E approach E_{cr} . [Salem 2001].

Elasticity modulus of as-spun PEEK fibres: The theoretical tensile modulus of a fully extended PEEK molecule was calculated by Shimizu et al. [1987] and the module of the crystalline and amorphous regions were obtained. They applied a two-phase model by combining the crystalline and amorphous regions in series for various PEEK fibres, and they have been established that the initial compliance of the amorphous region can be represented as a linear function of amorphous orientation.

In this thesis, the total elasticity modulus of PEEK fibres is investigated in Figures 4.2.7; the elasticity modulus is calculated from tensile tests for the linear behaviour of PEEK fibres and presented over the take-up speed. Increasing the take-up speed leads to increases in the elasticity modulus of as-spun PEEK fibres. The different values of modulus at one take-up speed are referred to different mass throughputs in the melt spinning process. This is similar to the orientation variation over take-up speed investigated in Figure 4.1.1; therefore it is verified that the elasticity modulus of as-spun PEEK fibres depends on the orientation of the filaments. In Section 4.1, it was also mentioned that the orientation depends on the internal stress in the solidification point.

Figure 4.2.8 (a) presents the elasticity modulus over the draw down ratio. For a draw down ratio ranging within $10 < (V_L/V_0) < 1000$, the elasticity modulus increases by increasing the draw down ratio. With a draw down ratio of less than 100, the elasticity modulus increases slowly around 1 GPa and then quickly increases to reach 6 GPa. Figure 4.2.8 (b) presents the elasticity modulus over orientation expressed in birefringence. It is clear that orientation mainly controls the elasticity module value, and more molecular chains oriented along the fibre axis make a high elasticity modulus. With a birefringence of less than 0.01, the elasticity modulus is about 1 GPa and for the birefringence between 0.01 to 0.05, the elasticity modulus increases approximately linear from 1 GPa to 6 GPa. However, Shimizu et al. [1987] have examined the PEEK and found that the initial modulus of PEEK fibres of varying crystallinity can be related to the orientation of the corresponding amorphous region.

Stress strain curves of as-spun PEEK fibres: Two important points are here necessary to remind: Firstly, it is time consuming to measure stress and strain (σ - ϵ) of all isolated filaments in a yarn bundle, and especially in the case of fine fibres, it is impossible to isolate the fine filaments. Because the multifilament is broken in different levels, some theoretical and practical investigations of (σ - ϵ) curves of multifilament yarn bundle have been discussed by Beyreuther et al. [1998]. Based on this work, the simple (σ - ϵ) curve for single filament are compared to the multifilament yarn bundle in order to estimate the cross unevenness of multifilament without test all individual filaments. In the multifilament (σ - ϵ) curve, the single filaments break at specific stress and elongation levels, and the remaining filaments break at lower stress one after other. In the end, all the filaments are broken at the maximum elongation where the force is zero. Comparing single fine filament to multifilament is very difficult to achieve.

Secondly, tensile strength, extensibility, and modulus depend not only on the test temperature but also on the strain rate imposed, e.g. at low rates of deformation, the polymer chains in isotactic polypropylene have time to rearrange before failure, in a way that the final structure at failure is the same for all samples irrespective of the starting orientation, and that all samples break at the same true stress [Salem 2001]. If the deformation rate increases, the samples will break at lower stresses and lower extensions, because the chains cannot redistribute the stress fast enough, and at very high strain rates the breaking stress is directly related to the starting orientation.

Keeping in mind the two above mentioned points, typical true stress-strain curves for as-spun PEEK filaments in room temperature are shown in Figure 4.2.9 (a), (b), (c) and (d). The true

strain at break increases by decreasing the draw down ratio as seen in different curves. However, for the same throughput, increasing the take-up speed leads to increases in the strain at break, because of stress increases in the solidification point and orientation as previously discussed in Section 4.2.1.

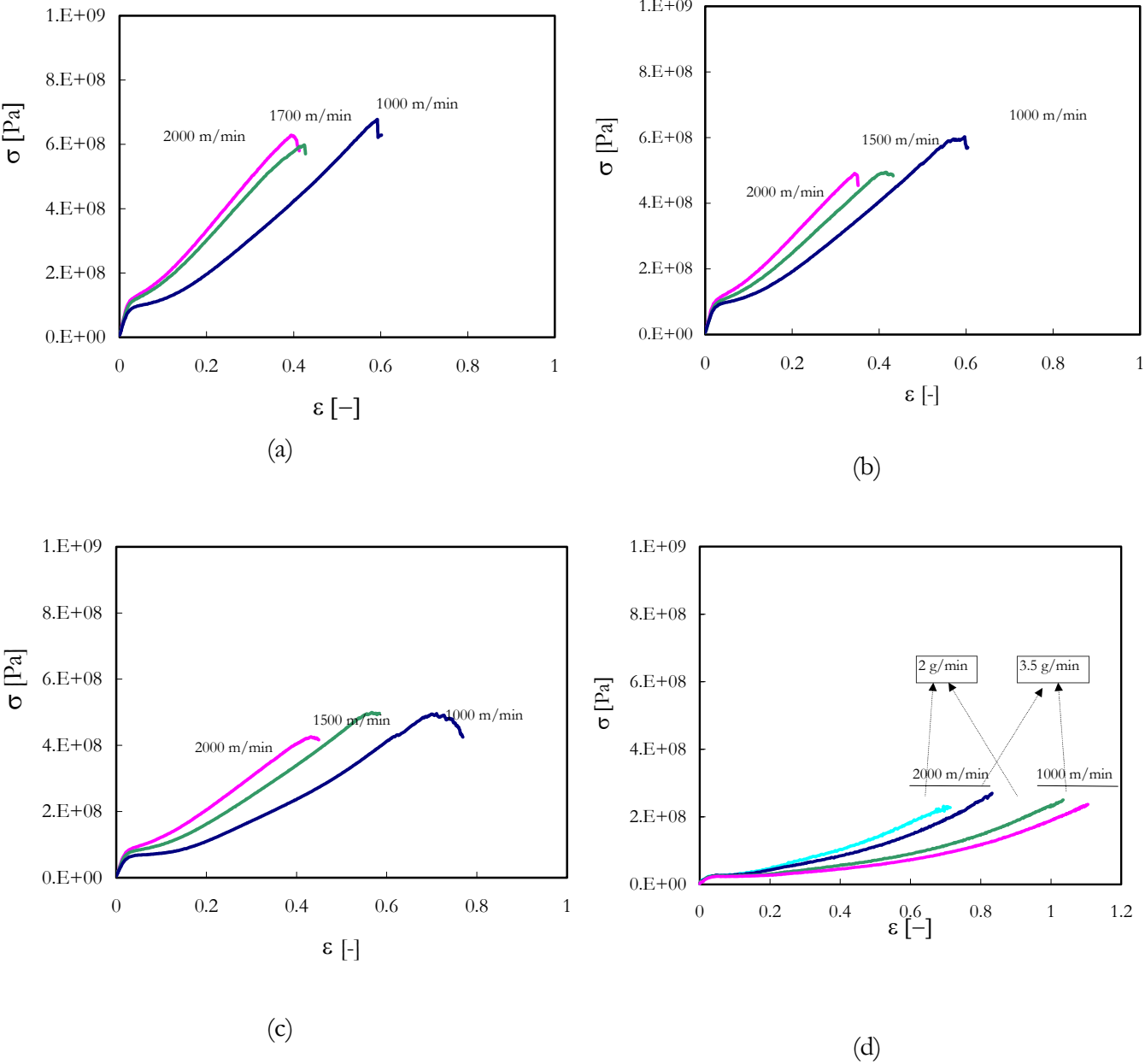


Figure 4.2.9 True stress strain of spun PEEK 151G fibre of different take-up speed and throughputs (a) 0.17 g/min, (b) 0.231 g/min, (c) 0.4 g/min, (d) 2 and 3.5 g/min

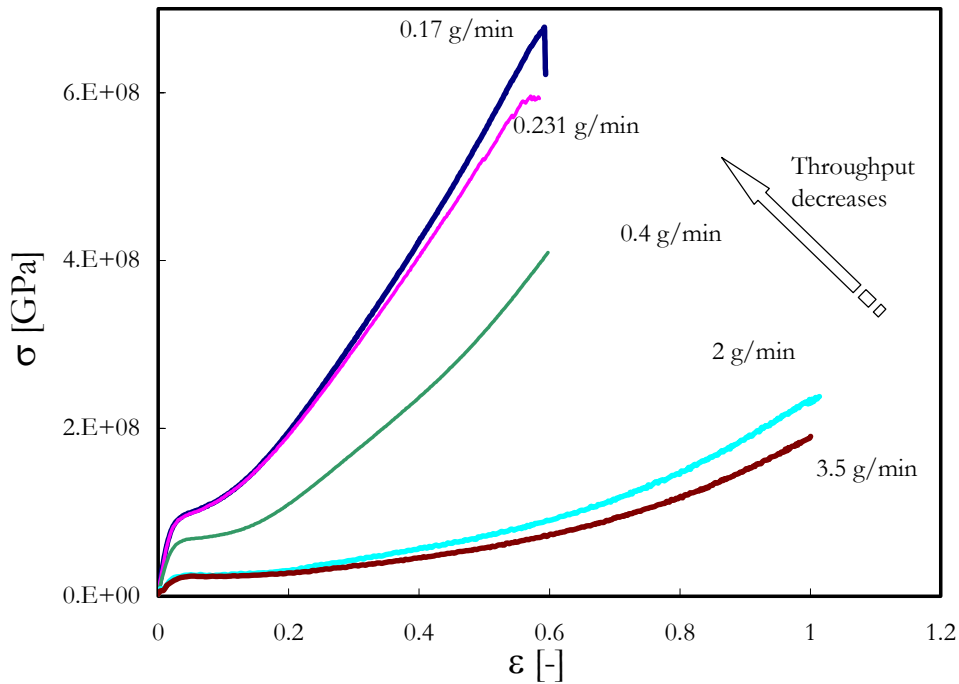


Figure 4.2.10 Effect of throughput on the true stress strain of as-spun PEEK 151G fibres at the same take-up speed 1000 m/min

The true stress at break increases by decreasing the melt throughput, see Figure 4.2.10. But with the same throughput, increasing the take-up speed leads to a slight decrease in stress at the break. It can be concluded that if the draw down ratio increases (to produce the fine PEEK fibres), the room temperature as-spun fibre will be yield at a higher tensile stress, but with a lower elongation, see Figure 4.2.10. In the other words, the fine fibres produced by a high draw down ratio, high crystallization and orientation become tougher and cannot deform plastic, because their elastic deformation is fully developed by the high draw down ratio. Filaments with low orientation show the yield, necking and extension at a relatively constant load, followed by a work hardening and high elongation at break. Because of its ductility, this filament can be drawn. The filaments with higher orientation have a higher yield strength, tenacity and lower elongation at break.

5 Applying the model of fibre formation to PEEK

In Chapter 5, the mathematical simulation of fibre formation is applied for the special thermoplastic PEEK Victrex 151 G. The first section (Section 5.1) is devoted to the differential equations, the boundary conditions and how to solve the equations. In Sections 5.2 and 5.3, the on-line measurements of temperature and speed are compared to the solution of the applied model, in order to examine the heat transfer and the viscosity effect on the structure formation of PEEK along the spinning line. In Section 5.4 the force calculation, internal stress and effect of skin drag force are discussed, which affect the orientation of chains in fibre.

5.1 Fundamental equations of steady state melt spinning

Fibre spinning is an example of steady state but non-uniform flow. This means that for a stationary observer the process is steady state, and variables such as the speed and deformation rate also remain constant at each point (z) of the spinning line. From the point of view of a small particle of polymer moving along the spinning line, the deformation is dependent on time, and the particle experiences different velocities and different strain rates as it moves along its trajectory. Figure 5.1.1 shows the distance dependent view of melt spinning process, which is often used in the modeling. The fibre formation zone begins from the spinneret where the polymer melt is supplied by the extruder, and then continues to solidification point where the melt cools down through exposure to air and where the fibre is transported as solid to wind-up unit.

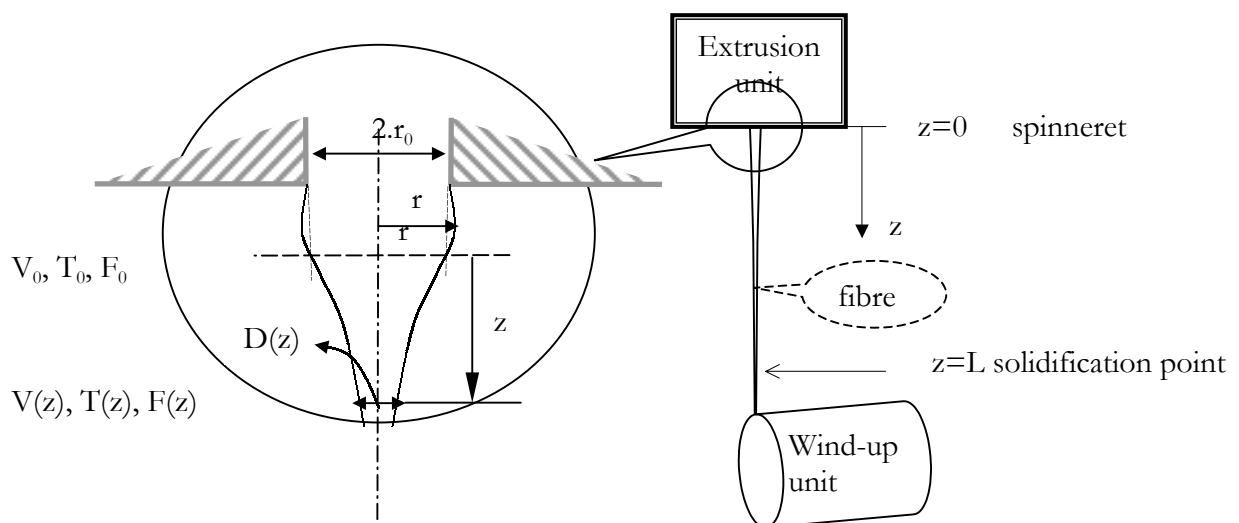


Figure 5.1.1 The one-dimensional model of melt spinning process and the coordinate

Unknown variables	Axisymmetric	$V_r=V_\theta=0$	This work	
$V (V_z, V_r, V_\theta)$	3	2	1	V_z
$\sigma (\sigma_{zz}, \sigma_{rr}, \sigma_{\theta\theta}, \tau_{zr}, \tau_{z\theta}, \tau_{r\theta})$	6	3	1	σ_{zz}
P, T, ρ	3	3	3	T
$X, \Delta n$	2	2	2	-
Total	14	10	7	3
Equations				
Equation for conservation of energy	1	1	1	1
Equation for conservation of matter	1	1	1	-
Equation for conservation of momentum	3	2	1	1
Constitutive equations	6	3	1	1
Equation of crystallisation kinetics	1	1	1	-
Equation concerning molecular orientation	1	1	1	-
Equation of state	1	1	1	-
Total	14	10	7	3

Table 5.1 Unknowns and equations in the model of melt spinning process

The general case for the melt spinning process in the three-dimensional polar coordinate has fourteen unknowns, which in turn needs a system of fourteen equations. Table 5.1 contains all of the unknowns and equations as summarized by Katayama [1994]. Solving the system of fourteen equations is in fact possible, but it is quite time consuming and not always necessary because the difficulties are at any rate normally present in the parameters and coefficients of equations. One can also use the two-dimensional approach (axisymmetric in polar coordinates) which reduces the system of unknowns and equations down to ten, by neglecting the variation in the angular coordinate, θ , from the geometrical symmetry. Recently, more new methods are reported to contain complex application and the use of non-linear constitutive equations. Joo et al. [2002] developed a model and simulation method for two-dimensional melt spinning of a viscoelastic melt (from non-isothermal Giesekus constitutive equation [2001]) and the crystallisation kinetics is described in the model proposed by Nakamura [1973], whereas the crystallisation rate is, as proposed by Ziabicki [1976], a function of both temperature and molecular orientation. Two different thermoplastics, amorphous polystyrene and fast crystallising Nylon-6,6 are simulated, and the non-linear governing equations are solved by using the finite element method and by including the die (composed of a contraction region and a capillary length), the molten zone, the spinning line and the solidification point in the calculation. The one-dimensional approach, which reduces the system of unknowns and equations to seven, is a much used method. Mitsoulis et al. [2000] analysed the melt spinning by means of a unidirectional approach and take apart the prehistory of the material in the die aided viscoelastic polymer melt behaviour (K-BKZ integral constitutive equation). They compared the experiments with the simulation results for

polypropylene (PP), Poly(ethylene terephthalate) (PET) and low density polyethylene (LDPE) melts at low and high speeds. They used an isothermal and non-isothermal simulation, and the die swell near the spinneret was not taken into consideration. The crystallisation effect was also not considered.

5.1.1 One-dimensional model for fibre formation

In this chapter the simple model of equations is assumed and solved. The equations of steady state melt spinning are derived from the three fundamental equilibrium equations: the conservation of energy, the conservation of momentum and the conservation of matter. Because there have been no adequate studies for PEEK including general information about the material's properties, the accurate and detailed physical property relationships must be at first developed (Chapters 2, 3 and 4), without adding further unknown and complexity to the model. In addition, the reported on-line measurements for PEEK fibre in the literature are of a very limited nature. Because of this, a lot of this thesis concerns itself with the on-line measurements, and their calibration as stated in Chapter 2. Hence the equations of state in fibre formation can be summarized in three one-dimensional equations. The three equations consist of momentum or force balance, and the energy, and the constitutive equation combined with continuity.

To simplify the simulation of the melt spinning process, the model is used with the following assumptions:

- a One-dimensional steady state and stable melt spinning process
- b The temperature and velocity are independent of radial position
- c The density and specific heat are functions of temperature
- d Stress-induced crystallisation is not taken into consideration at all
- e Cooling occurs in stationary air T_a (convective and radiation heat transfer)
- f The Newtonian model for fluid flow and Maxwell viscoelastic model
- g The die swell is small or negligible
- h The elongation viscosity is dependent on temperature and extension rate
- i The prehistory of polymer flow is ignored.

The assumption (a) and (i) means that the fibre speed gradient (V') is approximated by the strain rate ($\dot{\epsilon}$) of polymer as:

$$\frac{d\epsilon}{dt} = \frac{dV}{dz} \quad \text{or} \quad \dot{\epsilon} = V' \quad (5.1.1)$$

The one-dimensional model is based on the small slope of fibre in the axial direction, i.e. ($dD/dz \ll 1$). This fails near the spinneret where the flow is more complex and therefore

requires two-dimensional analysis. Although the small slope approximation imposes some restriction, it is still worth undertaking the one-dimensional analysis.

Continuity equation:

$$Q = \rho \cdot A \cdot V, \quad (5.1.2)$$

where the density (ρ) cross-section area (A) and fibre speed (V) vary from point to point along the spinning line but their product, the throughput (Q) stays constant.

Momentum or force balance:

$$\frac{dF}{dz} = Q \cdot \frac{dV}{dz} + \pi D \cdot \left(C_f \cdot \frac{1}{2} \cdot \rho_a \cdot V^2 \right) - \rho \cdot g \cdot A, \quad (5.1.3)$$

where the internal force gradient is (dF/dz) at every section along spinning line and the inertia force gradient is $F'_i=Q \cdot (dV/dz)$, the skin drag force gradient is $F'_s=\pi \cdot D \cdot (C_f \cdot \rho_a \cdot V^2/2)$ and the gravity force gradient is $F'_g=\rho \cdot g \cdot A$.

Energy equation:

$$\frac{dT}{dz} = -\frac{\pi \cdot \lambda_a}{Q \cdot C_{p_p}} \cdot \left(Nu \cdot (T - T_a) + \sigma_{SB} \cdot \epsilon_m \cdot (T^4 - T_a^4) \cdot \frac{D}{\lambda_a} \right) + \frac{\Delta H}{C_{p_p}} \cdot \frac{dX}{dz}, \quad (5.1.4)$$

where the Nusselt number (Nu) refers to heat convection, ϵ_m is the emissivity of radiation and the crystallisation (X) should be defined as a function of z , but is neglected by solving the equation.

5.1.2 Constitutive equations

Viscous and viscoelastic constitutive equation were used separately for the model. This section provides a brief introduction to the method used to implement the constitutive equation in the model.

Viscous or Newton Model: As explained in Section 3.2, the constitutive equation of viscous model is $\sigma = \eta_e \cdot (d\varepsilon/dt)$ or $\sigma = \eta_e \cdot (dV/dz)$. In the viscous model the stress (σ) can be eliminated, where $\sigma=F/A$ and the cross section area (A) from continuity Equation (5.1.2) can be replaced. Therefore, the velocity gradient in viscous model works out to be as follow:

$$\frac{dV}{dz} = \frac{F \cdot \rho \cdot V}{\eta_e \cdot Q} \quad (5.1.5)$$

Viscoelastic Maxwell Model: One must note that by using the viscoelastic Maxwell, Equation (3.2.2), and replacing the definitions $\dot{\varepsilon} = V \cdot \varepsilon'$ and $\dot{\sigma} = V \cdot \sigma'$ in $\dot{\varepsilon} = \dot{\sigma} / E + \sigma / \eta_e$ leads to:

$$\varepsilon' = \frac{\sigma}{\eta_e \cdot V} + \frac{\sigma'}{E} \quad (5.1.6)$$

If $\varepsilon' = V'/V$, $\sigma = F/A$ and $\sigma' = (F' \cdot A - F \cdot A')/A^2$ are replaced in Equation (5.1.6) and F', A' is eliminated by using Equations (5.1.3) and (5.1.2), the velocity gradient for Maxwell viscoelastic is:

$$V' = \frac{dV}{dz} = \frac{E \cdot F + \eta_e \cdot V \cdot (F_s - F_g)}{\eta_e \cdot (E \cdot A - F - V \cdot Q)}, \quad (5.1.7)$$

where F_s and F_g are defined in the Equation (5.1.3).

Non-linear Viscoelastic equation: The simple form of nonlinear viscoelastic used in melt spinning process is the upper-convected Maxwell model, and in cases for the one-dimensional steady state, Yarin [1993] suggested the following constitutive equation:

$$\sigma + (\eta/G) \cdot (V \cdot \sigma' - 2 \cdot \sigma \cdot V') = 2 \cdot \eta \cdot V' \quad (5.1.8)$$

Using the same replacement explained above for Maxwell model in Equation (5.1.8) leads to the following:

$$V' = \frac{dV}{dz} = \frac{G \cdot F + \eta \cdot V \cdot (F_s - F_g)}{\eta \cdot (2 \cdot G \cdot A + F - V \cdot Q)} \quad (5.1.9)$$

Solving the equations of steady state melt spinning: The general form of the equations of state in the fibre formation zone can be summarised using the following matrix form.

$$\begin{Bmatrix} V' \\ T' \\ F' \end{Bmatrix} = \begin{Bmatrix} f_1(V, T, F) \\ f_2(V, T, F) \\ f_3(V, T, F) \end{Bmatrix} \quad (5.1.10)$$

The equation $f_1(V,T,F)$ is replaced by Equation (5.1.5) for viscous behavior, Equation (5.1.7) for viscoelastic behavior, or Equation (5.1.9) for nonlinear viscoelastic behavior. The equation $f_2(V,T,F)$ and $f_3(V,T,F)$ are replaced by Equations (5.1.4) and (5.1.3), respectively. Other material properties used in the above equations are given in Chapter 2 and 3. The three unknowns in the three governing equations are the velocity (V), the temperature (T) and the internal force (F). This means that to find the three variable V, T and F, these three equations must be solved simultaneously with the following boundary conditions:

Boundary conditions: the boundary conditions of melt spinning process are as follow:

<u>Initial values</u>			<u>Boundary values</u>			$\left\{ \begin{array}{c} V_0 \\ T_0 \\ F_0 \end{array} \right\}$ <p style="text-align: center;">? ←</p>
initial velocity	$z=0$	$V_0=V_0$	take-up speed	$z=L$	$V_L=V_L$	
initial temperature	$z=0$	$T_0=T_m$				
initial force	$z=0$	$F_0=?$				

Two initial values and one boundary value are known. The three initial values $\{V_0, T_0, F_0\}$ are needed in order to start the solution of the three differential equations. Since the spinning line tension F_0 is not known, an initial guess is necessary. More about initial force estimation is discussed in Section 5.4.

Integral type of constitutive equations: The usual form of linear viscoelastic and non-linear viscoelastic constitutive equations is, with respect to time, the integral type, which include the memory function and also the prehistory of polymer in the extrusion unit and spinneret channel. The integral form is used to include prehistory from spinneret. However, the differential form of the constitutive equation explained above is considered relatively easy to implement numerically. The equations of steady state in melt spinning mentioned above are derived with respect to distance (z) but the constitutive equations are derived with respect to time (t). This in turn means that the variation of state for one point moves along the spinning line. Rauschenberger [1997] used the time dependent equations and K-BKZ integral model for Rheotens. He solved the equations of steady state with a recursive method with respect to time. However, he neglected the inertia and friction force due to the relatively low speed spinning. Recently, Misououlis et al. [2000] combined the one-dimensional non-isothermal differential equation with respect to distance (z) with the integral constitutive equation (K-BKZ integral) with respect to time (t). The finite element approach and the relation between velocity, distance and time made it possible to solve the problem. The calculations, to change the time to distance and vice versa make the problem more complicated; they are only useful in cases the die swell near the spinneret or the take-up force is important to deal with.

5.2 Heat transfer and fibre temperature along spinning line

The cooling procedure and heat transfer of fibres are investigated in the fibre formation zone of the melt spinning process. The aim of Section 5.2 is to correct the measured temperature of PEEK fibre in order to examine the type of heat transfer to its surrounding. It was spun at piston and extruder equipment, the last combined with a single screw high-temperature extruder by Rieter Automatic.

Heat transfer along spinning line: To characterize the heat transfer from filaments, two approaches have normally been used, (a) the theoretical approach, which is based on boundary layer heat transfer, thermodynamics and fluid mechanics; and (b) the experimental approach, which includes design and fabrication of an experimental setup that adequately simulates the conditions experienced by a fibre formation. In this section, the heat transfer investigation is based on the energy balance equation and on the on-line measurements along the fibre formation zone. In other words, a complexity of boundary layer theory and a laboratory simulation are to be avoided.

The boundary layer on a spun fibre, however, has three specific features [Kubo 1985]:

1. The filament is usually very thin compared to the boundary layer around it,
2. There is a large temperature gradient across the boundary layer,
3. The surface of the filament undergoes acceleration in the longitudinal direction.

The basic problem of boundary layer growth and heat transfer from continuous cylinders moving through a still fluid has been studied quite extensively. It is evident that the boundary layer in the fibre formation zone is different to ordinary boundary layer theory. In the boundary layer theory, the flow along spun filament must divide into two regions: the first one from spinneret to solidification point, and the second one the flow after solidification point. In order to reduce the complexity of this problem, some assumptions are necessary. In most previous research, two essential assumptions were made: the polymer melt is assumed to be solid and cylindrically, and that the air is incompressible.

The heat transfer from the melt-spinning line to an ambient medium involves several mechanisms: radiation, free (natural) convection, forced convection [Ziabicki 1976] and conduction [White 2001]. Depending on spinning conditions, one or more mechanism are dominated. In a low speed spinning, the free convection dominates [Ohkoshi 1993]. In a relative thick filament, the heat conduction part cannot be ignored, and for high fibre temperature, the radiation especially near the spinneret is of utmost importance.

Nusselt number from on-line measurement: The Nusselt number (Nu) is the most important dimensionless number in the convective heat transfer; it is defined as $Nu=h \cdot D/\lambda_a$, where h is convection heat coefficient, D is diameter of fibre and λ_a is the heat conduction coefficient of air. The Nusselt number represents the ratio of heat convection to heat conduction (both in fluid) [Tucker 1989]. The heat transfer coefficient for melt spinning requires further study, although, several theoretical and empirical efforts were made to find a general relationship for Nusselt number [Ziabicki 1976]. For the same spinning conditions, different values occur from relationships suggested, in turn affecting the calculated fibre temperature profile along the spinning line. The energy equation, Equation (5.2.1), contains all form of heat transfer and the heat from crystallisation in the melt spinning process:

$$\frac{dT}{dz} = -\frac{\pi \cdot \lambda_a}{Q \cdot Cp_p} \cdot \left(Nu \cdot (T - T_a) + \sigma_{SB} \cdot \varepsilon_m \cdot (T^4 - T_a^4) \cdot \frac{D}{\lambda_a} \right) + \frac{\Delta H}{Cp_p} \cdot \frac{dX}{dz} \quad (5.2.1)$$

Assuming that the radiation energy can be ignored, Equation (5.2.1) in dimensionless temperature, $\Theta = (T - T_a)/(T_0 - T_a)$, and dimensionless distance to spinneret, $Z = z/L$, is reduced to the following equation:

$$\frac{d\Theta}{dZ} = -\frac{\pi \cdot \lambda_a \cdot Nu}{Q \cdot Cp_p} \Theta + \frac{\Delta H}{Cp_p \cdot (T_0 - T_a)} \cdot \frac{dX}{dZ} \quad (5.2.2)$$

Equation (5.2.2) can be solved and was reported by Nakamura [1972]:

For $Z < Z_X$ before the crystallisation occurs where $(dX/dZ)=0$, see Figure 5.2.1

$$\Theta = \exp\left(\frac{-\pi \cdot \lambda_a}{Q} \int_0^Z \frac{Nu}{Cp_p} dZ'\right) \quad (5.2.3)$$

For $Z_X < Z < Z_X + \Delta Z$ assume a plateau if crystallisation occur $(d\Theta/dZ)=0$

$$\Theta_X = \frac{Q \cdot \Delta H}{\pi \cdot \lambda_a \cdot Nu \cdot (T_0 - T_a)} \cdot \frac{dX}{dZ} \quad (5.2.4)$$

For $Z > Z_X + \Delta Z$ after the crystallisation ends where $(dX/dZ)=0$

$$\Theta = \Theta_X \cdot \exp\left(\frac{-\pi \cdot \lambda_a}{Q} \int_{Z_X + \Delta Z}^Z \frac{Nu}{Cp_p} dZ'\right) \quad (5.2.5)$$

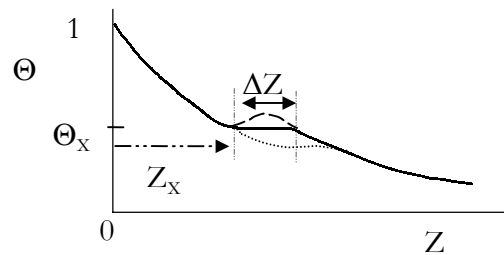


Figure 5.2.1 Typical dimensionless fibre temperature over dimensionless distance to spinneret

To solve the energy equation, Equation (5.2.1), numerically or to find the temperature analytically as in Equations (5.2.3), (5.2.4) and (5.2.5), the value of the Nusselt number must be known. If the crystallisation along the spinning line is ignored ($dX/dZ=0$ in Equation (5.2.1)), the Nusselt number is found out from measured variable such $T(z)$ and $D(z)$:

$$Nu = \left(\frac{Q \cdot C_p}{-\pi \lambda_a} \cdot \frac{dT}{dz} \cdot \frac{1}{(T - T_a)} \right) - \sigma_{SB} \cdot \varepsilon m \cdot \frac{T^4 - T_a^4}{T - T_a} \cdot \frac{D}{\lambda_a} \quad (5.2.6)$$

After the substitution of known parameters and on-line measured variables such as the diameter of filament (calculated from measured velocity in different distance to spinneret) and the corrected temperature in the above equation, the Nusselt number can be calculated. The Nusselt number (Nu) is normally expressed in dimensionless groups such as the Reynolds number (Re), Rayleigh number (Ra), Prandtl number (Pr) and Grasshof number (Gr). The Reynolds number is defined as $Re = V \cdot D / \nu_a$, where V is fibre speed, D is the fibre diameter and ν_a is the kinematic viscosity of air. The Reynolds number is the ratio of the internal force of the air to the viscous flow. When the Reynolds number is large, the effect of air viscosity is relatively small.

The Nusselt number in melt spinning process is a combination of natural and forced convection

$$Nu = Nu(Nu_f, Nu_n) \quad (5.2.7)$$

Free (natural) convective heat transfer is known to be the typical heat transfer mechanism for stationary system, and it is concerned with the movement of air due to the temperature gradient around the cooling body. The dimensionless free convective Nusselt number around the fibre is generally reported as a function of two other dimensionless numbers, the Grasshof number (Gr), and the Prandtl number (Pr) [Kast 1974]

$$Nu_n = Nu_n(Gr, Pr), \quad (5.2.8)$$

where the Grasshof number is $Gr = g \cdot \beta \cdot (T - T_a) \cdot D^3$ and the Prandtl number of air is $Pr = \eta \cdot C_p / \lambda_a$. In order to find the specific correlation for free convection, an experimental investigation must be carried out.

In the melt spinning process, the Grasshof number indicates that the natural convection is dependent on temperature difference of fibre and ambient air, which depends on both take-up speed and throughput. The cooling by natural convection becomes dominant factor for a low take-up speed [Ziabicki 1976]. Schöne [1980] has explained that a large share of heat transfer is expected near the spinneret due to free convection, but the high temperature of spin block brings

forth additional complication. Recently, Ohkoshi [2000] also confirmed this effect for PEEK aided experimental measurements when the fibre temperature is high and the fibre speed is low.

Forced convective heat transfer occurs due to the relative movement of an immersed body in an ambient medium. The relative movement in the melt spinning refers to the axial speed of fibre, or the cross airflow. In high speed spinning lines, the convective heat transfer in the melt spinning process is dominant. The Nusselt number for the convective heat transfer depends on three dimensionless numbers: Reynolds (Re), Prandtl (Pr), and dimensionless distance (z/D),

$$Nu_f = Nu_f(Re, Pr, z/D), \quad (5.2.9)$$

where the Reynolds number is based on fibre diameter, $Re = V.D/v_a$. In both theories and experimental studies, other dimensionless numbers are also introduced to provide a general relationship of the Nusselt number. The Reynolds number, based on distance, $Re_z = V.z/v_a$, can be expressed as $Re_z = Re.z/D$. The dimensionless distance that appears in the theoretical boundary layer studies as $\zeta = z.v_a/VD^2$ can be expressed as $\zeta = Re^{-1}.z/D$.

Therefore the Nusselt number, Equation (5.2.7), can be expressed as a function of three dimensionless numbers by combining Equation (5.2.8) and (5.2.9) in the following way

$$Nu = Nu(Re, Gr, z/D) \quad (5.2.10)$$

In Equation (5.2.10), it is also assumed that the Prandtl number of air is equal to unity. The Nusselt number can now be expressed as $Nu = a Re^b . Gr^c . (z/D)^d$, and if the four constants a, b, c and d are found using experimental correlation, the empirical relation will be provided.

5.2.1 Fibre temperature and Nusselt number for PEEK fibres

Some melt spinning experiments with the spin equipments were designed and carried out using a single screw extruder and a movable wind-up unit. The wind-up unit was placed about 1.5 m from the spinneret. PEEK Victrex 151 G was used as the spinning material. The melt was drawn through a three holes spinneret, and the melt temperature was 385°C.

To measure the fibre temperature, 100 snapshots were taken with the infrared camera at every desired vertical distance to the spinneret. As shown in Figure 5.2.2 and Figure 5.2.3, the recorded temperatures have different values at every location because the fibres go out of the focal point of the lens. This occurs due to the motion of the fast running fibre and its subsequent lateral vibration. Therefore, the maximum of the measured temperature values was assumed as the fibre temperature at every location.

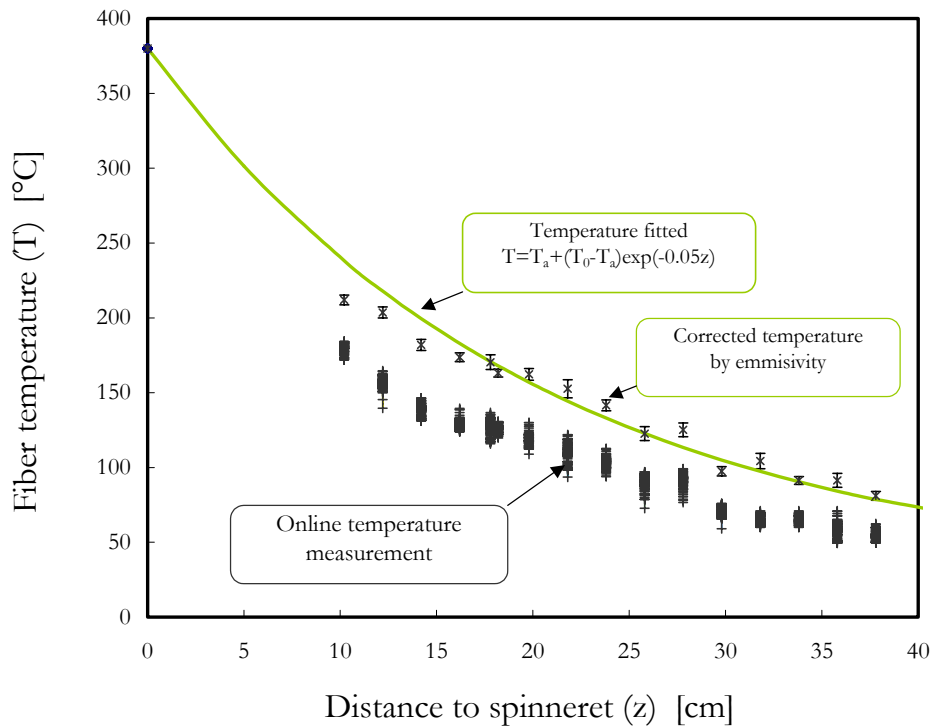


Figure 5.2.2 Fibre temperature along spinning line, on-line temperature measurement of PEEK Victrex 151G, $T_0=380^\circ\text{C}$, $Q=0.465\text{ g/min}$, $V=25\text{ m/min}$, spinneret 1 holes ($d=0.3\text{ mm}$, $l=0.6\text{ mm}$)

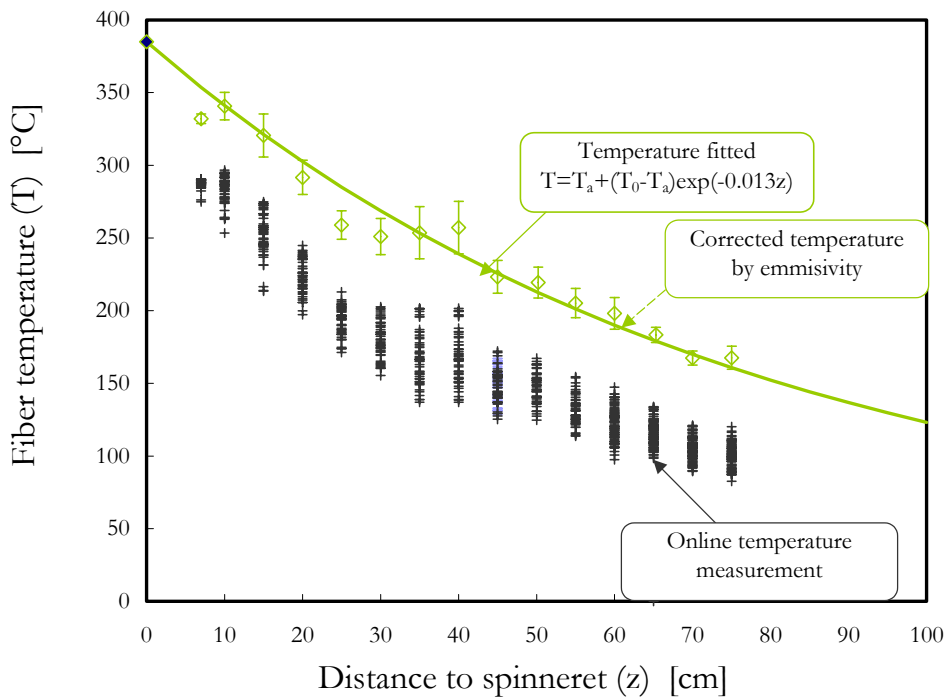


Figure 5.2.3 Fibre temperature along spinning line, on-line measurement for PEEK Victrex 151 G, $T_0=385^\circ\text{C}$, $Q=3.5\text{ g/min}$, $V=1000\text{ m/min}$, spinneret 3 holes ($d=0.25\text{ mm}$, $l=0.5\text{ mm}$)

The measured temperature has to be corrected using the emissivity correction factor, which is a function of the fibre diameter (see Section 2.2.2). These procedures were repeated with different take-up speeds and different throughputs as shown in Figure 5.2.3. The melt spinning equipment, the material conditions, the melt temperature and the spinneret were the same for all experiments. From the results it is obvious that the corrected temperatures are higher than 10% of the measured maximum temperature. Therefore the effect of the emissivity correction factor to justify the true fibre temperature cannot be discounted. The corrected temperatures were fitted to a curve and compared with measurements of Ohkoshi [1993] in Figure 5.2.4. Although the material is the same as in Ohkoshi's experiment [1993], the spin conditions and the melt temperature are different.

The temperature from on-line measurements and the temperature gradient of fibre are replaced in the Equation (5.2.6) to investigate the fibre heat transfer coefficient. Replacing the expression fitted to the corrected temperature is recommended in order to smooth the temperature and temperature gradient estimation from on-line measurement. The fibre temperature along the spinning line decreases due to cooling, therefore one should assume an exponential decreasing function using the applications of Equations 5.2.3 to 5.2.5 as follow:

$$\Theta = \exp(-B.\zeta) \quad \text{or} \quad T(z) = T_a + (T_0 - T_a) \cdot \exp(-A.z), \quad (5.2.11)$$

where the dimensionless temperature is $\Theta = (T - T_a) / (T_0 - T_a)$ and the dimensionless distance to the spinneret is $\zeta = z v_a / VD^2 = \pi z v_a \rho_p / 4Q$. A and B are found by fitting the Equation (5.2.11) to the corrected on-line fibre temperature in Figures 5.2.2 to 5.2.5 (see Table 5.2.1). The dimensionless temperature, $\Theta = (T - T_a) / (T_0 - T_a)$, is normally used to reduce the temperature of fibre, and the dimensionless distance to spinneret, $\zeta = z v_a / VD^2$, appears from the boundary layer studies around the long cylinder. However, Figure 5.2.5 demonstrates that the effect of different spinning conditions, especially the low draw down ratio, could not be reduced as simply as expected.

	Throughput Q g/min	Take-up speed V _L m/min	Draw down ratio V _L /V ₀	A cm ⁻¹	B -
1	0.465	25	4	0.05	0.0024
2	3.5	1000	15	0.013	0.0048
3	2	1000	27	0.021	0.0044
4	3.5	2000	30	0.014	0.0052
5	2	2000	53	0.025	0.006

Table 5.2.1 Melt spinning process of PEEK and fitting parameter to fibre temperature profile

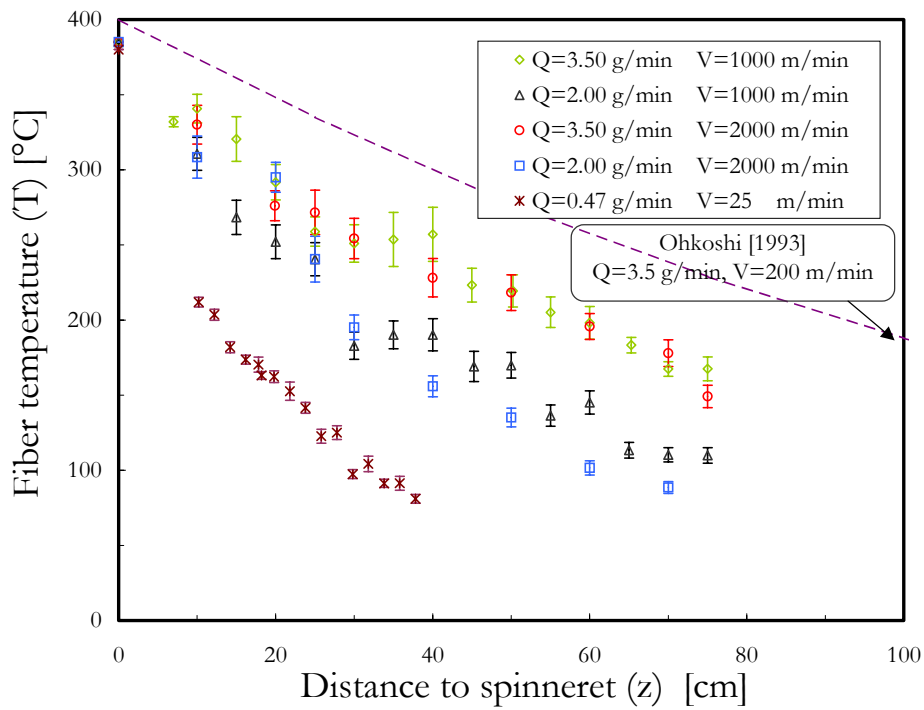


Figure 5.2.4 Fibre temperature along spinning line, online corrected for different spinning conditions of PEEK Victrex 151 G, $T_0=385^\circ\text{C}$, spinneret 3 holes ($d=0.25$ mm, $l=0.5$ mm)

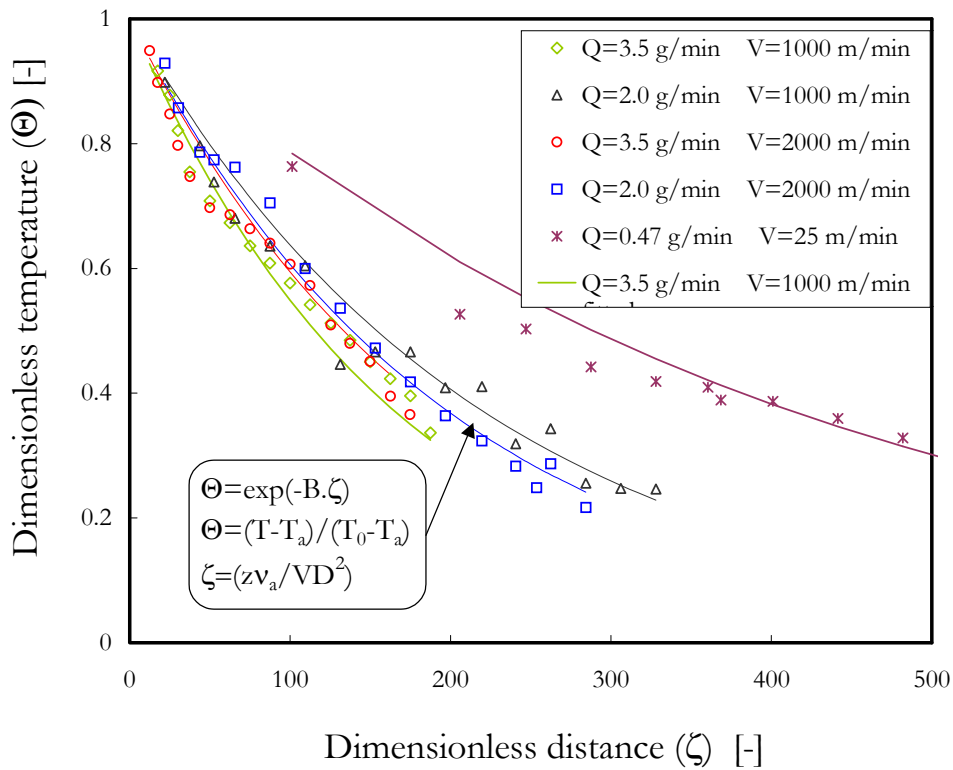


Figure 5.2.5 Dimensionless temperature over dimensionless distance, measured (symbols), fitted (solid lines)

The empirical Nusselt number for PEEK melt spinning: The heat transfer of PEEK has been studied by Ohkoshi et al. [2000, 1993]. Ohkoshi [1993] concluded that the heat radiation is predominant near the spinneret and leads to an empirical formula of $Nu=0.16Re^{0.520}$. Later Ohkoshi [2000] took both the natural convection and heat radiation into consideration, and concluded that the Nusselt number should be a function of not only the Reynolds number but also the Rayleigh number by assuming the empirical formula $Nu=k.Re^a.Ra^b$. The obtained Nusselt numbers were higher than the reported values by Kase and Matsuo [1965], especially when the fibre temperature was higher than 300°C. The higher cooling rate on the spinning line is caused by natural convection.

Using Table 5.2.1 and the Equation (5.2.11), the fibre temperature and fibre temperature gradient can be calculated and replaced using Equation (5.2.6) to estimate the Nusselt number for every distance to spinneret. Figure 5.2.6 gives the end result of the Nusselt number over the Reynolds number calculated for four spinning conditions. The Nusselt number decreases as the Reynolds number increases along the spinning line. The absolute values lay between 1 and 2 and it seems that with a higher throughput, the Nusselt number is higher. However, it is not to be expected that the various take-up speeds influence the Nusselt number. The Nusselt number and the Reynolds number for the four experiments estimations in Figure 5.2.6 are for the melt spinning of PEEK and can be used under following conditions:

$$1 < Nu < 2 \quad \text{for} \quad 10 < Re < 100 \quad \text{and} \quad 10 < \zeta < 300$$

$$Nu = 3.Re^{-0.22} \quad (5.2.12)$$

The Equation (5.2.12) is found by fitting the equation $Nu=a.Re^b$ to experimental Nusselt values found in Equation (5.2.6). The Nusselt number, as in Equation (5.2.10) with four parameters, is not easy to apply.

As previously mentioned, the Nusselt number has several relationships from different approaches, which give different Nusselt values for the same spinning condition. Table 5.2.2 and Figure 5.2.6 shows the variation clearly. For the above spinning condition the Kase and Matsuo relationship increases, see Figure 5.2.6 (A). The only relationships decrease in Table 5.2.2 are (C) and (F). The estimated Nusselt number shows a slight increase at the end of spinning line in Figure 5.2.6. This in turn means that by increasing the fibre speed and the Reynolds number, the force convection increases, but near the spinneret, the decreasing effect can be interpreted as effect of radiation and natural heat convection.

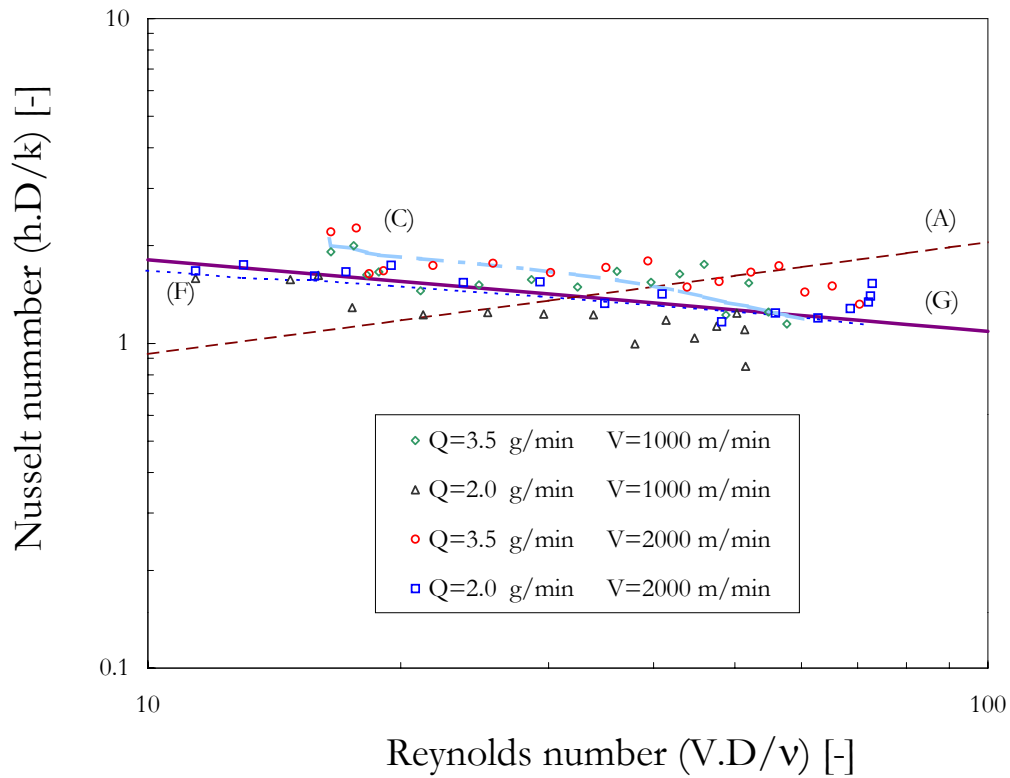


Figure 5.2.6 Nusselt number estimated from online temperature measurements along spinning line of PEEK 151 G Victrex, $T_0=385^\circ\text{C}$, spinneret 3 holes ($d=0.25$ mm, $l=0.5$ mm)

Relationship	Application	Application
A $Nu=0.42.Re^{0.344}$	Kase and Matsuo [1965]	Found by simulation of electrically heated 0.2 mm heated wire for $0.5 < Re < 50$
B $Nu=0.91Q^{0.21}D_0^{0.29}V_L^{0.05}$	Schöne [1980]	From processing parameter
C $Nu=11.6e-6(T-T_\infty)/k_a$	Moris [1997]	Found by simulation of electrically heated wire
D $Nu=0.16.Re^{0.50}$	Ohkoshi [1993]	Proposed for slow PEEK melt spinning
E $Nu=a.Re^b.Ra^c$	Ohkoshi [2000]	Proposed for PEEK melt spinning a, b, and c were not given.
F $Nu=0.42.Re^{0.344}.Ra^{0.13}$	This study	Fitted to PEEK spinning line 2 g/min and 3.5 g/min and 1000 m/min and 2000 m/min
G $Nu=3.Re^{-0.22}$	This study	

Nusselt number ($Nu=hD/\lambda_a$), Reynolds number ($Re = VD/v_a = 4Q/\pi\rho_p v_a D$)
Rayleigh $Ra=D^3 \cdot \rho_a \cdot Cp_a \cdot \beta \cdot g \cdot (T-T_a)/v_a \cdot \lambda_a$, $Ra=Pr \cdot Gr$
Grasshof number $Gr=g \cdot \beta \cdot (T-T_a) \cdot D^3$, Prandtl number $Pr=\eta \cdot Cp/\lambda$

Table 5.2.2 Comparison of some relations for Nusselt number

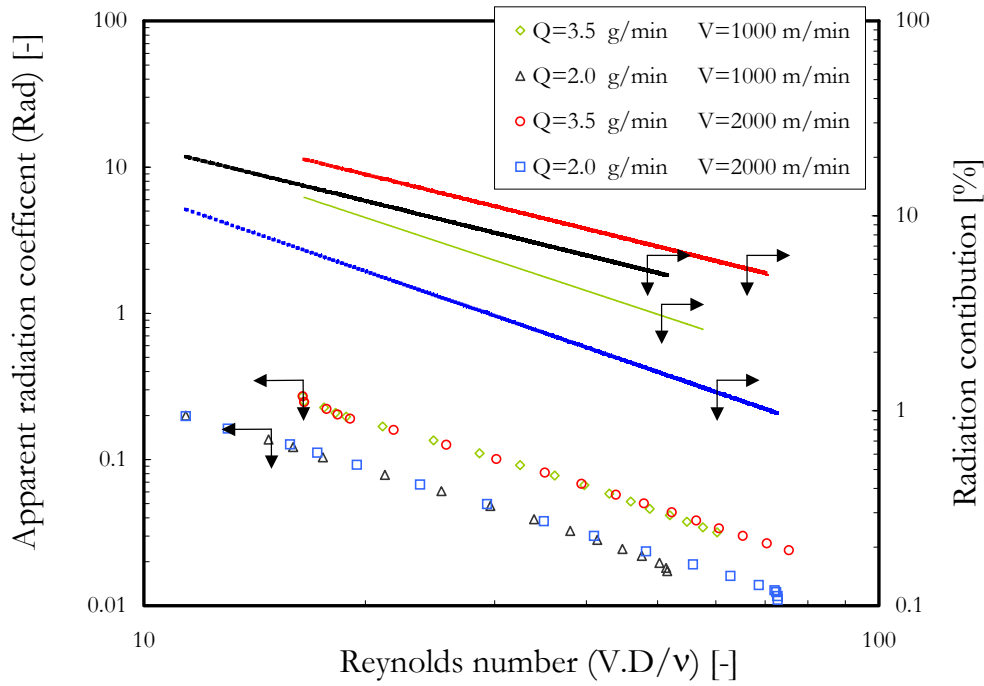


Figure 5.2.7 The radiation effect and the radiation contribution of heat transfer along spinning line of PEEK, $T_0=385^\circ\text{C}$, 3 holes spinneret

Radiation effect along the PEEK spinning line strongly depends on the temperature of the radiating body. Studies have been conducted which indicate that the radiation contribution ranges from 20% of the total heat flux near the die to less than 1% away from the die [Zieminski 1986]. The second term in Equation 5.2.6 is used to define the apparent radiation coefficient, Rad:

$$\text{Rad} = \sigma_{SB} \cdot \epsilon m \cdot \frac{T^4 - T_a^4}{T - T_a} \cdot \frac{D}{\lambda_a} \quad (5.2.12)$$

The radiation contribution, (Rad/Nu), is defined from Equation (5.2.12) and Equation (5.2.6). The maximum radiation contribution for PEEK is about 12% of all heat transfer along spinning line. The Figure 5.2.7 shows that as the Reynolds number decreases along the spinning line, the radiation contribution also decreases. This is evident due to fact that the fibre temperature decreases by the cooling.

5.2.2 Temperature comparison: model and on-line measurement

The PEEK fibre formation model, as stated in Section 5.1, is solved for various throughputs and take-up speeds. The results of the model and the online measurement temperature are compared in the dimensionless temperature over dimensionless distance in Figure 5.2.8. The suggested relationships for the Nusselt number in Table 5.2.2 (F) and (G) give a more accurate estimation

than the Kase and Matsuo formula in the fibre formation zone due to the radiation effect considered in the estimation of Nusselt number in Figure 5.2.5. On solving the model for dimensionless temperature, it can be concluded that:

- There is no significant difference between the Newton constitutive equation and for Maxwell viscoelastic model; the dimensionless temperature from Newton is just 1% more than Maxwell. There is also no difference present when using the extensional viscosity as a function of temperature or by adding the strain rate effect.
- The difference exists only if different Nusselt functions are used, as seen in Figure 5.2.8. The symbols shown in the Figure 5.2.8 are from temperature measurements.
- The Kase and Matsuo relationship for Nusselt number, $Nu=0.42.Re^{0.344}$, gives a better approximation for the distance $(z/L)>1$, i.e. for the distance after the solidification and out of the fibre formation zone, the temperature calculated after Kase and Matsuo is close to the on-line measurements.
- In the fibre formation zone, $(z/L)<1$, the proposed relationship $(Nu=3.Re^{-0.22})$ gives a better approximation, as this relation contains both forms of cooling, convection and radiation.

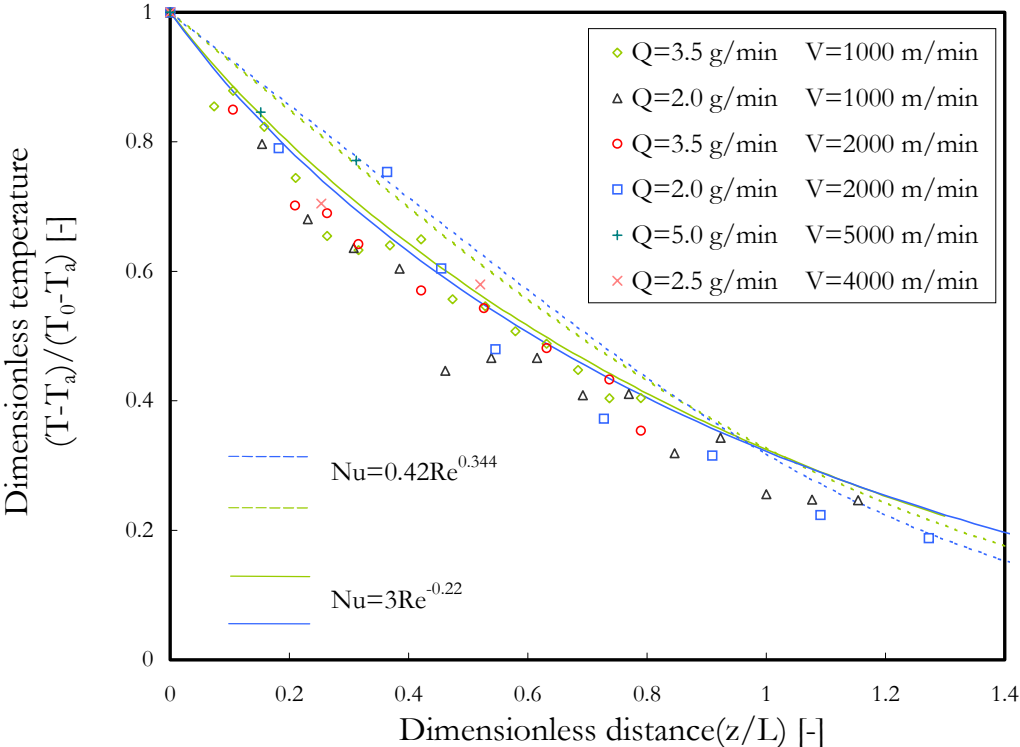


Figure 5.2.8 Dimensionless temperature measurement (symbols) and theory (solid lines) of the fibre along spinning line, PEEK 151 G Victrex, $T_0=385^{\circ}C$, spinneret 3 holes ($d=0.25$ mm, $l=0.5$ mm)

5.2.3 Crystallisation investigations by on-line temperature measurement

By neglecting the radiation heat transfer in the energy balance equation, Equation (5.2.1), and on assuming that crystallisation takes occur, then the energy equation becomes

$$\frac{dT}{dz} = \frac{-\pi \cdot \lambda_a}{Q \cdot Cp_p} \cdot Nu \cdot (T - T_a) + \frac{\Delta H}{Cp_p} \frac{dX}{dz} \quad (5.2.13)$$

The crystallisation term is found out and the Equation (5.2.13) is written in other form:

$$\frac{dX}{dz} = \frac{\pi \cdot \lambda_a}{Q \cdot \Delta H} \cdot Nu \cdot (T - T_a) - \frac{Cp_p}{\Delta H} \cdot \frac{dT}{dz} \quad (5.2.14)$$

Integration with respect to distance, both sides of Equation (5.2.14) give:

$$X = \int_0^z \left(\frac{\pi \cdot \lambda_a}{Q \cdot \Delta H} \cdot Nu \cdot (T - T_a) - \frac{Cp_p}{\Delta H} \cdot \frac{dT}{dz} \right) \cdot dz', \quad (5.2.15)$$

where ΔH is the enthalpy of fusion of fully crystalline, $\Delta H_{\text{PEEK}}=130$ (J/g) [Blundell 1983]. By knowing the Nusselt number and temperature along the spinning line, one can calculate the so-named stress-induced crystallisation along the spinning line from Equation (5.2.15). The area surrounded by the temperature profiles in Figure 5.2.9, is the total end crystallisation of PEEK fibres. However, no measurement was carried out to verify the result of Equation (5.2.15) and the

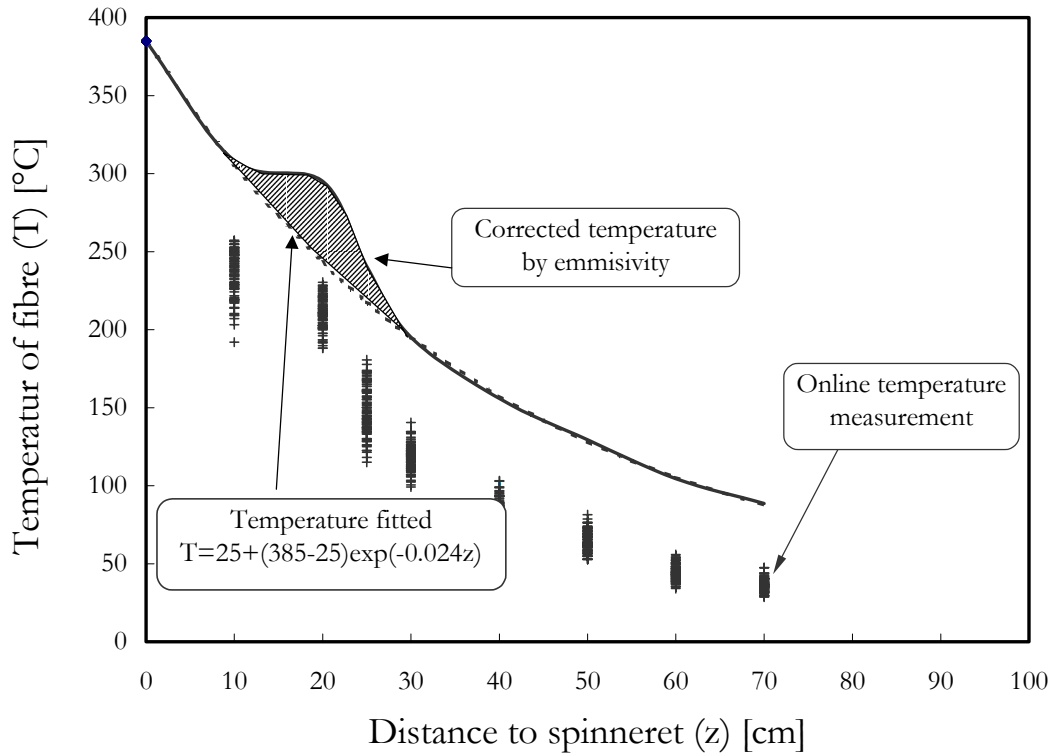


Figure 5.2.9 Fibre temperature along spinning line, on-line measurement (symbols) for PEEK 151 G Victrex, $T_0=385^\circ\text{C}$, $Q=2$ g/min, $V=2000$ m/min, spinneret 3 holes ($d=0.25$ mm, $l=0.5$ mm), fitting to corrected values (solid lines)

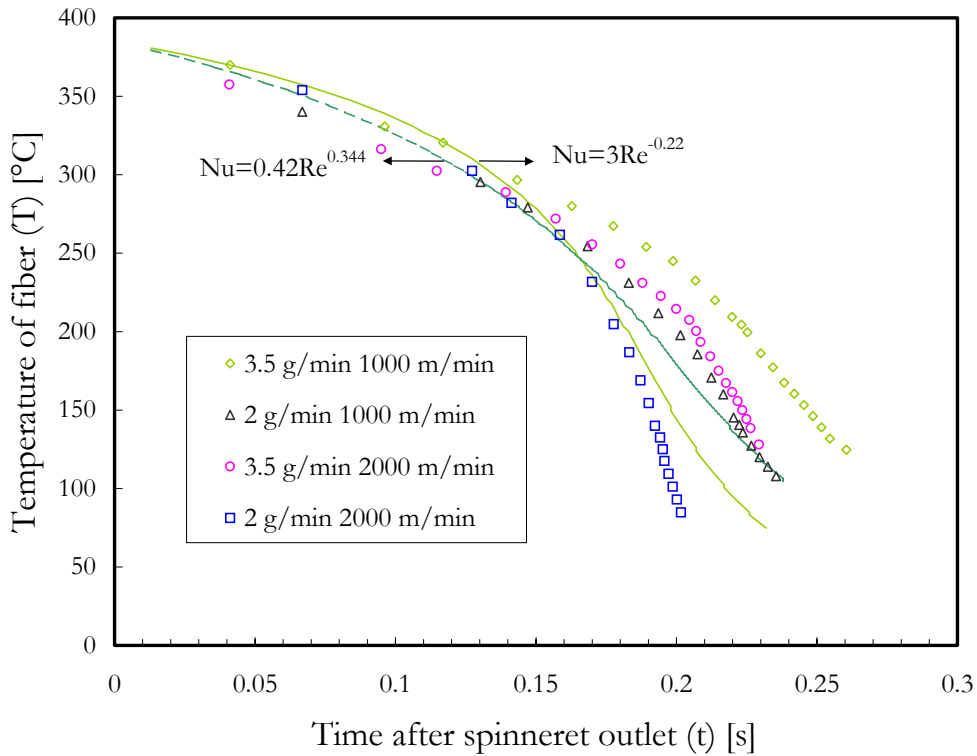


Figure 5.2.10 Continuous cooling transformation diagram for PEEK victrex 151 G, on-line measurement (symbols), calculated from model (solid lines)

on-line temperature measurement did not give sufficient information to examine the on-line stress-induced crystallisation along the spinning line. The temperature varies along spinning line and it is often displayed over the distance. However, in the crystallisation studies, the temperature (T) along time (t), and temperature rate (dT/dt) is of more importance. In the melt spinning process, the time for moving chain from the outlet spinneret to solidification point is very short ($t_s < 1$ s), but the time can be calculated from fibre speed measurements.

If the fibre speed defined as $V = \frac{dz}{dt}$, then the time can be integrated by:

$$t = \int_0^z \frac{dz'}{V} \quad (5.2.16)$$

Figure 5.2.10 demonstrates the temperature measured over time. Figure 5.2.10 obtains a good qualitative understanding of the important relationships between cooling conditions and crystallisation kinetics using the concept of a “continuous cooling transformation diagram” [Spruiell 1975]. This concept can be applied for PEEK and the cooling curves plotted versus times axis can also be used. It was illustrated that faster cooling produces a greater super cooling of the melt before crystallisation occurs.

5.3 Speed of PEEK fibre along spinning line

5.3.1 Fibre speed comparison: model and on-line measurement

The fibre speed profile along the spinning line shows the structure formation of fibre and is affected by various factors such as material behaviour, processing conditions and energy transfer. The model of fibre formation of PEEK was solved under the following assumptions, and the fibre speed was compared to on-line measurements:

- (a) Viscosity as a function of temperature, $\eta(T)$, and $Nu=0.42.Re^{0.344}$
- (b) Viscosity as a function of temperature, $\eta(T)$, and $Nu=3.Re^{-0.22}$
- (c) Viscosity as a function of temperature and speed gradient, $\eta(T,V')$, and $Nu=0.42.Re^{0.344}$
- (d) Viscosity as a function of temperature and speed gradient, $\eta(T,V')$, and $Nu=3.Re^{-0.22}$

The spinning conditions for the selected experiments are classified into four separated cases to simplify the discussions.

Case I $V_L < 2000 \text{ m/min}$ and $(V_L/V_0) < 50$: Two spinning conditions in Figures 5.3.1 and 5.3.2 were selected to discuss the on-line fibre speed measurements and the results of the mathematical model.

The extensional viscosity as a function of temperature and speed gradient, $\eta(T,V')$, improves the results of model assumptions (c) and (d) in comparison to the temperature dependent viscosity, $\eta(T)$, given in Figures 5.3.1 and 5.3.2 (a), (b). The extensional viscosity as a function of temperature, $\eta(T)$, causes an overestimation for the calculated fibre speed in comparison with the measured fibre speed. This is caused by high estimated viscosity, because the high temperature and low speed gradient cause $\eta(T) > \eta(T,V')$ near to spinneret.

The fibre speed profile from assumptions (c) shows two different types of behaviour. It means that near the spinneret, the fibre speed from (c) is less than the (d) for low Reynolds number, but later the fibre speed profile (c) is also more than (d) for low Reynolds number. The calculated fibre speed for (c) and (d) in the first part of fibre formation zone provides a slight overestimation with respect to the measurements. This could be due to higher temperatures near the spin block, where the velocity decreases and the diameter of fibre increases. The solidification point does not move when changing the cooling rate or extensional viscosity, as shown in Figures 5.3.1 and 5.3.2. This means that the total heat transfer and the average Nusselt number assumed for the model is approximately equal. Increasing the draw down ratio in Figure 5.3.1

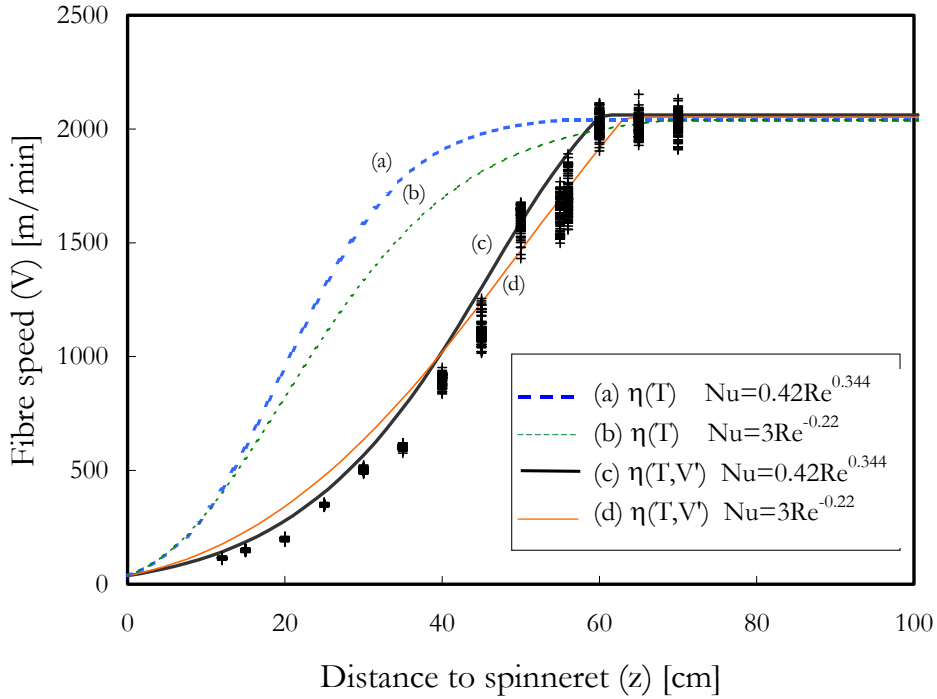


Figure 5.3.1 Fibre speed along spinning line measurement (symbols) and model comparison for PEEK 151 G Victrex, $T_0=385^\circ\text{C}$, $Q=2\text{ g/min}$, $V=2000\text{ m/min}$, spinneret 3 holes ($d=0.25\text{ mm}$, $l=0.5\text{ mm}$)

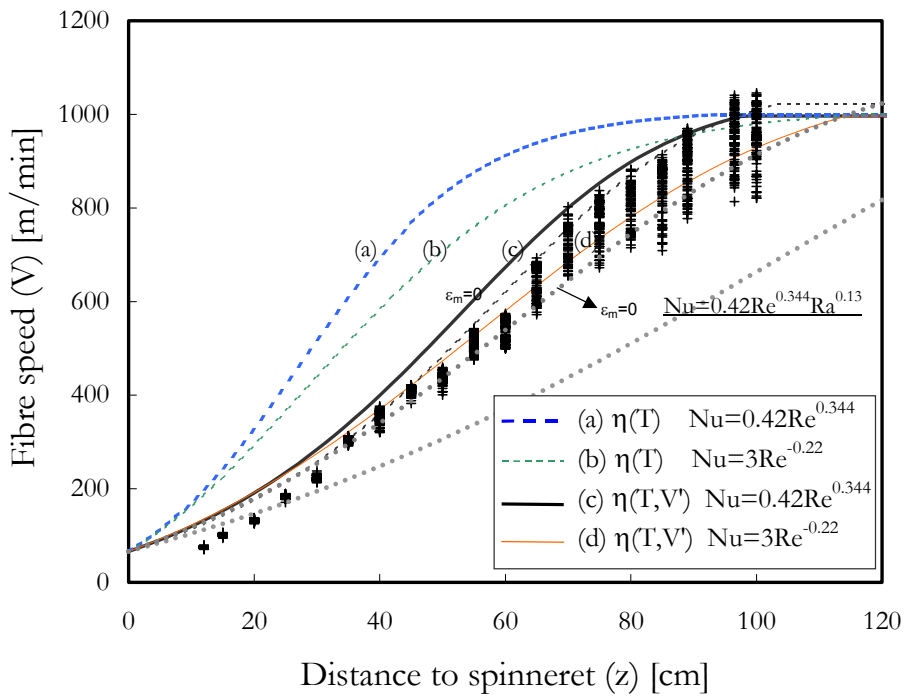


Figure 5.3.2 Fibre speed along spinning line measurement (symbols) and model comparison for PEEK 151 G Victrex, $T_0=385^\circ\text{C}$, $Q=3.5\text{ g/min}$, $V=1000\text{ m/min}$, spinneret 3 holes ($d=0.25\text{ mm}$, $l=0.5\text{ mm}$)

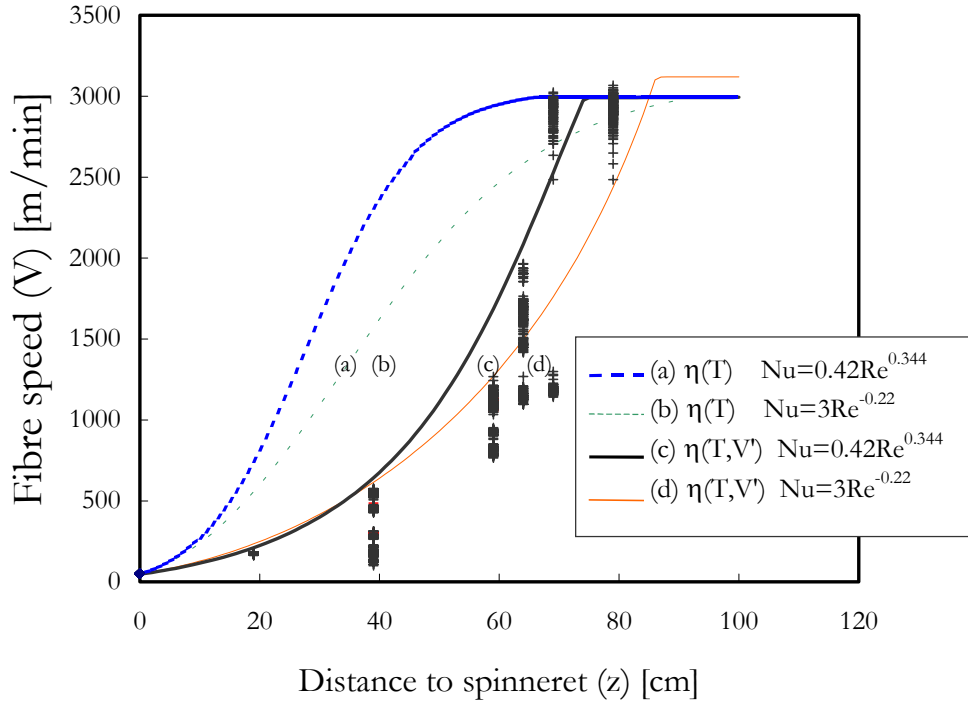


Figure 5.3.3 Fibre speed along spinning line measurement (symbols) and model comparison for PEEK 151 G Victrex, $T_0=385^\circ\text{C}$, $Q=2.5$ g/min, $V=3000$ m/min, spinneret 3 holes ($d=0.25$ mm, $l=0.5$ mm)

with respect to Figure 5.3.2 increases the fibre speed at the end of the fibre formation zone (from measurements and assumptions (c) and (d)). This is expected when increasing the speed gradient and consequently when increasing the extensional viscosity.

Case II $V_L > 3000$ m/min: The effect of high speed melt spinning on the fibre speed profile and the PEEK fibre formation are investigated in Figures 5.3.3, 5.3.4 and 5.3.5. As well as the considerations in Case I, other points are summarised as follow:

The high speed spinning encounters a high mass throughput of 2.5 to 5 g/min, however, when using these spinning conditions, it is difficult to measure the precise fibre speed at the end of fibre formation zone. The deviation of fibre speed measurements were especially recorded at the last part of the fibre formation zone, where the structure formation accelerates and necking effect normally can occur. In the first part of the fibre formation zone, the measured fibre speed is almost identical with constant mass throughput; increasing the take-up speed does not affect this region, i.e. there is no high cooling rate and structure formation near the spinneret. For the high speed spinning in Figure 5.3.3, the Reynolds numbers are in the range of ($10 < \text{Re} < 100$), and for Figures 5.3.4 and 5.3.5 the Reynolds numbers are ($25 < \text{Re} < 180$). The dimensionless distances for these three figures are $\zeta < 350$. These conditions are out of the range of validity for

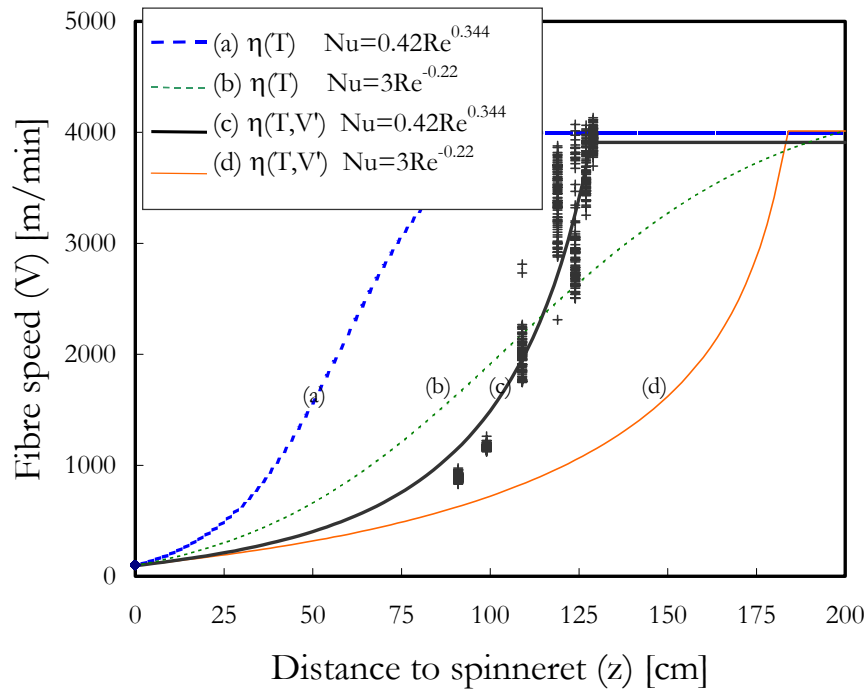
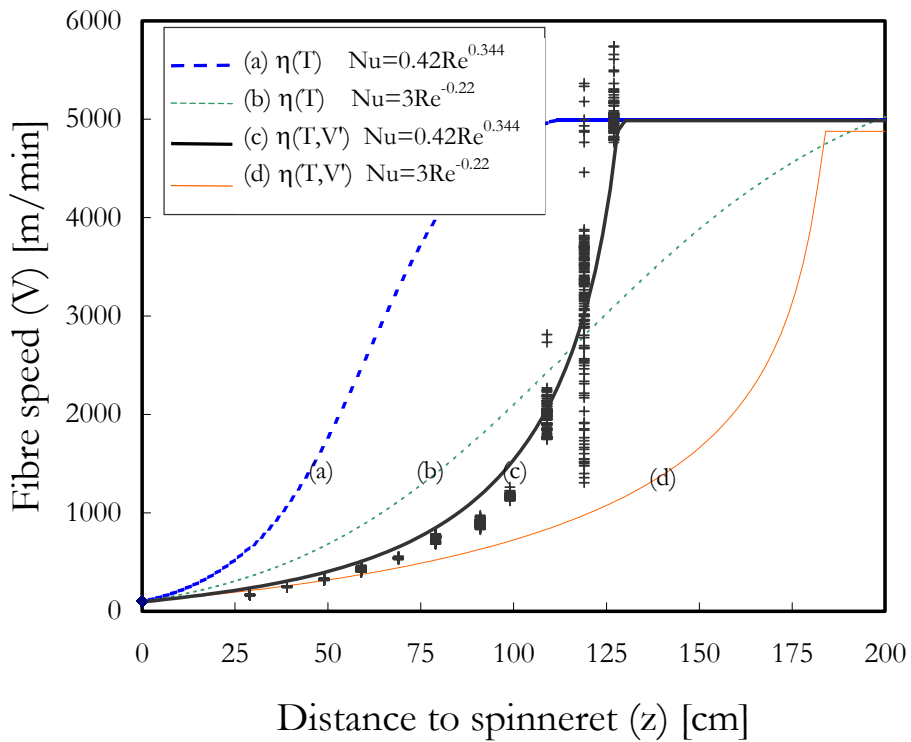


Figure 5.3.4 Fibre speed along spinning line measurement (symbols) and model comparison for PEEK 151 G Victrex, $T_0=385^\circ\text{C}$, $Q=5\text{ g/min}$, $V=4000\text{ m/min}$, spinneret 3 holes ($d=0.25\text{ mm}$, $l=0.5\text{ mm}$)



5.3.5 Fibre speed along spinning line measurements (symbols) and model comparison for PEEK 151 G Victrex, $T_0=385^\circ\text{C}$, $Q=5\text{ g/min}$, $V=5000\text{ m/min}$, spinneret 3 holes ($d=0.25\text{ mm}$, $l=0.5\text{ mm}$)

Equation 5.2.12, therefore the Nusselt number over Reynolds number ($Nu=3.Re^{-0.22}$) from Section 5.2 does not provide valid results.

Case III $Q<0.5$ g/min and $V_L<2000$ m/min: In Figure 5.3.6, by comparing the measured with calculated fibre speed for a very low mass throughput, and for take-up speed lower than previously discussed, it is important to notice here that the spinning conditions in Figure 5.3.6 leads to Reynolds number of <10 ($1<Re<4$ for $V_L=25$ m/min) and ($1<Re<8$ for $V_L=100$ m/min), therefore the relationship ($Nu=3.Re^{-0.22}$) gives a higher value than the estimations of Nusselt number using temperature measurements, however, the Nusselt number still decreases when increasing the Reynolds number. The cooling rate in the model with Nusselt relationship of ($Nu=3.Re^{-0.22}$) causes to two effects: the fibre speed is increased rapidly along the spinning line, and the solidification distance is decreased. Using a higher cooling rate in the model like ($Nu=3.Re^{-0.22}$) decreases the fibre diameter and increases the fibre speed; as a result, the solidification region will be short. The measurements in Figure 5.3.6 were carried out by the piston equipment. It is a different spinneret, spin block and take-up unit configuration in comparison with extruder equipment. The heat transferred by free convection especially close the spinneret (<1 cm), where the temperature of the air is high and the fibre speed is low. The effect of radiation at the beginning of the spinning line is not negligible, as discussed in Section 5.2.

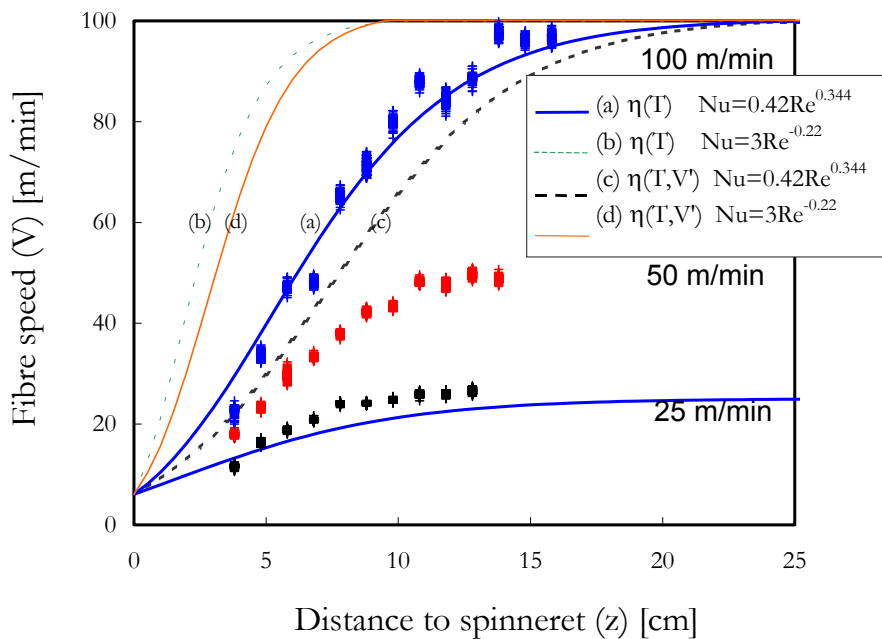


Figure 5.3.6 Fibre speed along spinning line measurement (symbols) and model comparison for PEEK 151 G Victrex, $T_0=380^{\circ}\text{C}$, $Q=0.465$ g/min, $V=100, 50, 25$ m/min, spinneret 1 holes ($d=0.3$ mm, $l=0.6$ mm)

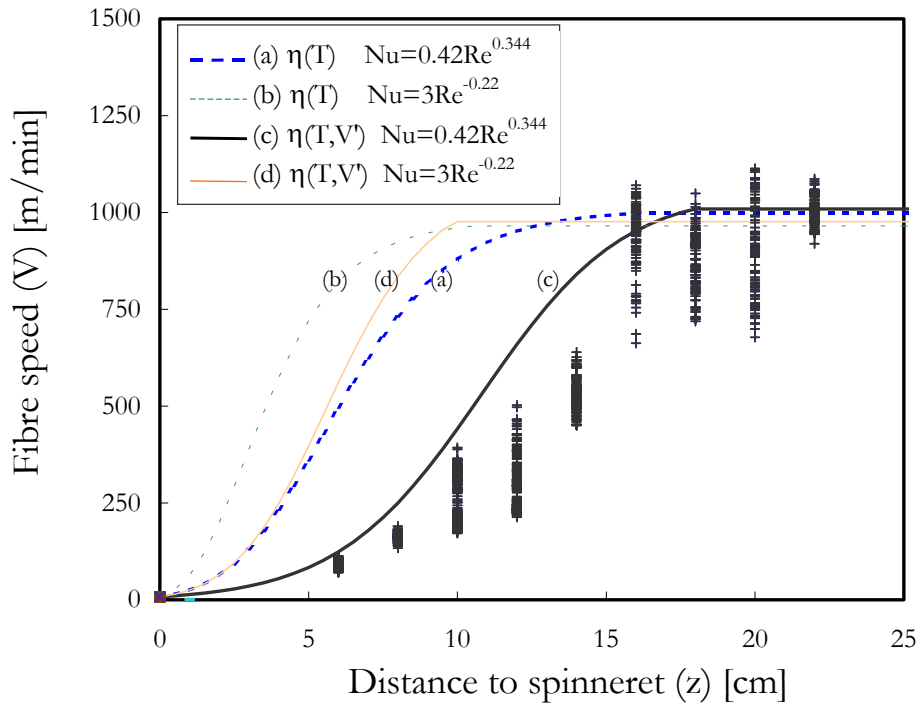


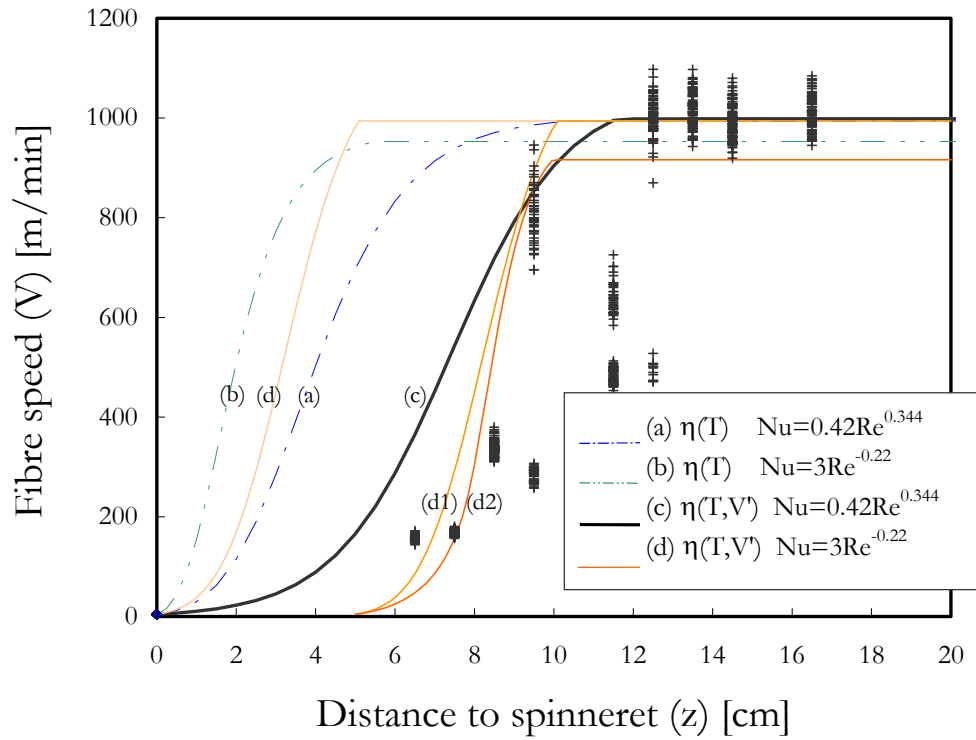
Figure 5.3.7 Fibre speed along spinning line measurement (symbols) and model comparison for PEEK 151 G Victrex, $T_0=385^\circ\text{C}$, $Q=0.4\text{ g/min}$, $V=1000\text{ m/min}$, spinneret 24 holes ($d=0.25\text{ mm}$, $l=0.5\text{ mm}$)

The viscosity as a function of temperature and speed gradient, $\eta(T,V)$, in Figure 5.3.6 shows there is no better agreement between calculated fibre speed and the measured fibre speed. This could be due to the low strain rate ($\dot{\epsilon} < 10$) along the spinning line, which does not fall within the validity of equation for viscosity, Equation (3.2.5).

In the relatively high take-up speed spinning $>1000\text{ m/min}$, and low mass throughput 0.4 g/min further effects are to be noticed:

The effect of multifilament melt spinning, as in the spinning condition of Figure 5.3.7, causes an increase in the fibre temperature in comparison to monofilament melt spinning. As a result, the Nusselt number and cooling rate will decrease, at least at the beginning of the spinning line.

The higher fibre temperature in multifilament spinning causes a lower extensional viscosity and a decreasing fibre speed. Therefore, the Kase and Matsuo relationship gives a better approximation in these circumstances, because it gives lower Nusselt number, as indicated in Figure (5.2.6). This can be interpreted to be caused by the multifilament effect.



5.3.8 Fibre speed along spinning line measurement (symbols) and model comparison for PEEK 151 G Victrex, $T_0=385^\circ\text{C}$, $Q=0.225\text{ g/min}$, $V=1000\text{ m/min}$, spinneret 48 holes ($d=0.25\text{ mm}$, $l=0.5\text{ mm}$)

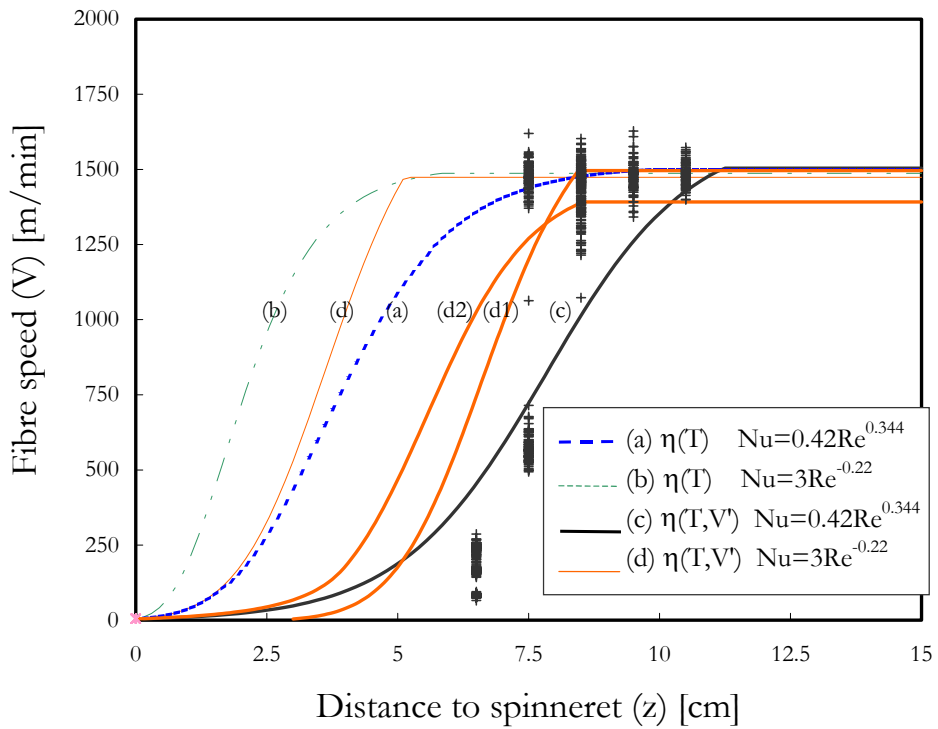


Figure 5.3.9 Fibre speed along spinning line measurement (symbols) and model comparison for PEEK 151 G Victrex, $T_0=400^\circ\text{C}$, $Q=0.225\text{ g/min}$, $V=1500\text{ m/min}$, spinneret 48 holes ($d=0.25\text{ mm}$, $l=0.5\text{ mm}$)

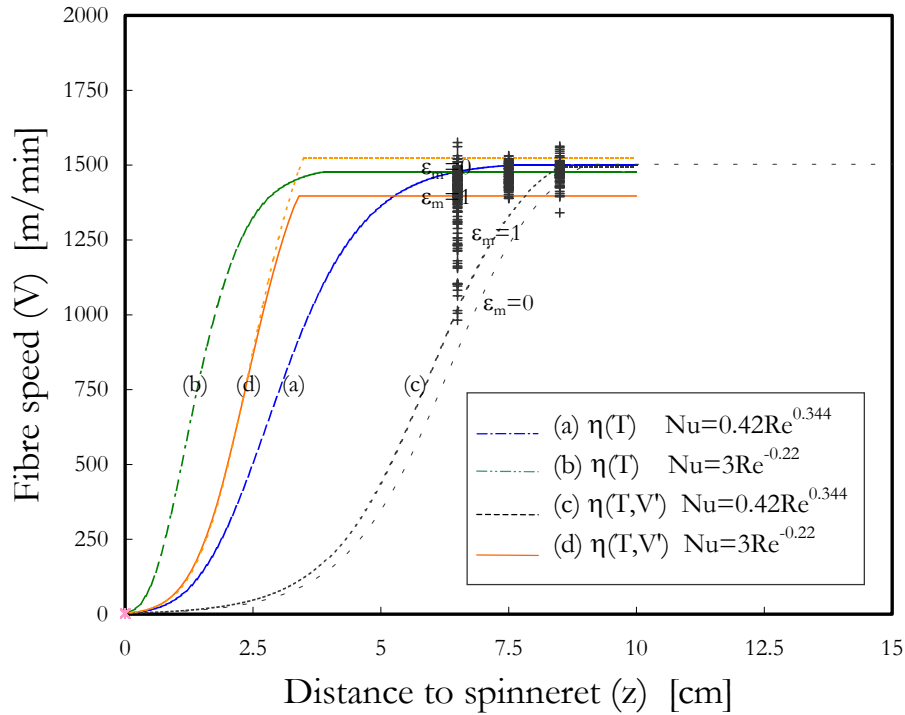


Figure 5.3.10 Fibre speed along spinning line measurement (symbols) and model comparison for PEEK 151 G Victrex, $T_0=400^\circ\text{C}$, $Q=0.15$ g/min, $V=1500$ m/min, spinneret 48 holes ($d=0.25$ mm, $l=0.5$ mm)

Case IV $Q < 0.23$ g/min and $V_L < 1500$ m/min: This case applies to very fine filaments of PEEK ($D_L \sim 10$ μm). The comparison is presented for the mass throughput 0.225 g/min and for take-up speeds 1000 m/min and 1500 m/min (see Figures 5.3.8 and 5.3.9). The measurement for the finest fibre was with a mass throughput of 0.15 g/min and a take-up speed of 1500 m/min, (see Figure 5.3.10). There are some comments in this case:

The fibre formation zone is very short, $L < 10$ cm, and the take-up speed is a relatively high speed of 1500 m/min, the on-line measuring therefore is difficult and it is in fact impossible to measure the fibre speed near the spinneret (< 5 cm), especially in Figure 5.3.10. The air temperature is high near the spinneret; the heat convection is therefore low and this can affect the fibre speed profile.

In Figure 5.3.8, the solution (d1) is shown with the same condition as for (d), but the origin of the calculation is shifted to $z_0=5$ cm. The solution (d2) was made for an air temperature of $T_a=200^\circ\text{C}$ near the spinneret ($0 < z < 5$) cm. Both solutions confirm that the air temperature is too high near the spinneret, and in the first half of the fibre formation zone, the effect of die swell can shift the course of fibre formation of the model, because the swelling effect was ignored in the model.

In Figure 5.3.9 the solution (d1) is shown with the same condition as for (d) but the origin of the calculation is shifted to $z_0=3$ cm. The solution (d2) was made for an air temperature of $T_a=250^\circ\text{C}$ near the spinneret ($0 < z < 4$) cm.

The effect of radiation in the energy equation on fibre speed profile: The effect of radiation is investigated in the last section (Section 5.2), and the radiation heat transfer contribution is calculated and compared to other heat transfer mechanisms, free convection and forced convection. The emissivity (ϵ_m) in the energy equation (Equation 5.2.1) was considered to be constant and equal to the maximum contribution of radiation, $\epsilon_m=1$. Other reported investigations used different values; for example Maebius [1985] investigated the spinning of glass fibre by studying the effects of radiation and employing one-dimensional model of a Newtonian fluid. He concluded that if the effect of convection is neglected, and if all the cooling is assumed to take place due to radiation, the small changes in emissivity could have a large influence on the shape of glass fibre, and consequently, the fibre speed profile. Schöne [1980] reported that for polymer, the emissivity value in literature ranges within $0.62 < \epsilon_m < 0.95$, and he used the value 0.8; recently Mitsoulis [2000] used the $\epsilon_m=0.5$. The emissivity should not be considered constant along the spinning line, however, in order to simplify the radiation investigation, the upper and lower values of emissivity are assumed, $0 \leq \epsilon_m \leq 1$.

Figure 5.3.10 shows two various effects of radiation. The maximum effect of radiation causes an increase in the local speed and also increases the Reynolds number. The Nusselt relationship as conducted by Kase and Matsuo was increased by increasing the Reynolds number, therefore the fibre speed in Figure 5.3.10 (c) for ($\epsilon_m=1$) became higher than for ($\epsilon_m=0$). This effect by Nusselt relationship ($Nu=3.Re^{-0.22}$) is the reverse. Because increasing the radiation ($\epsilon_m=1$) increases the local speed and the Reynolds number, but this decreases the Nusselt number and fibre speed in the model as seen in Figure 5.3.10 (d).

5.3.3 Solidification point

The solidification point is the region where the fibre becomes solid, i.e. the end of the fibre formation way, and can be found manually after taking following methods into consideration:

- a) from spinning speed profile: the first point along the spinning line which reaches the take-up speed,

- b) from temperature distribution: the first point along the spinning line which reaches the glass transition temperature.

From velocity measurements of different melt spinning processes, the distance from the spinneret to the solidification point over draw down ratio is presented in Figure 5.3.11. Based on the on-line measurements of fibre speed, the solidification way is dominated by the mass throughputs. The table on Figure 5.3.11 sets out the different take-up speeds for the given throughput. The fibre formation ways for throughputs < 0.1 g/min were too short, therefore the on-line measurements for speed and temperature could not be practically gauge with the measuring equipments.

The solidification point in the melt spinning of thermoplastics has been generally reported as $L=L(Q, V_L)$ [Shimizu 1985-a] or $L=L(Q, V_L, D_0, \Theta)$ [Beyreuther 1991]. The following relation is found for PEEK by fitting a simple $L \sim L(Q)$ to Figure 5.3.1

$$L \sim (26 \cdot Q + 6.4) \quad \text{for } (0.2 < Q < 5) \text{ g/min,}$$

where L in cm and Q in g/min.

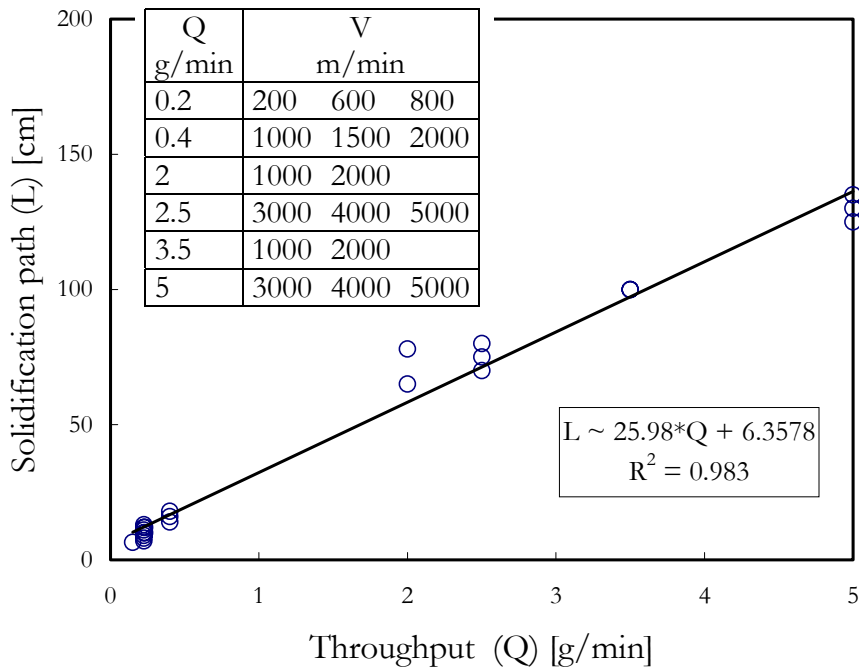


Figure 5.3.11 Solidification path over mass throughput from fibre speed measurements of PEEK 151 Victrex

5.4 Tension in the spinning line (force-stress estimation)

The internal force value along the spinning line can be calculated from Equation (5.1.3). The momentum balance at every section along the spinning line [Ziabicki 1976] leads to Equation (5.3.1), which is rewritten in Equation (5.4.1):

$$F' = Q \cdot V' + F'_s - F'_g \quad (5.4.1)$$

Integrating both sides of Equation (5.4.1), the following expression for internal force is obtained:

$$F(z) = F(0) + Q \cdot (V - V_0) + \frac{\pi}{2} \int_0^z D \cdot C_f \cdot \rho_a \cdot V^2 \cdot dz - \frac{\pi}{2} \int_0^z \rho_p \cdot g \cdot A \cdot dz, \quad (5.4.2)$$

where $F(z)$ is the internal force at every section along spinning line and

the inertia force is $F_i = Q \cdot (V - V_0)$,

the skin drag force is $F_s = \frac{\pi}{2} \int_0^z D \cdot C_f \cdot \rho_a \cdot V^2 \cdot dz$,

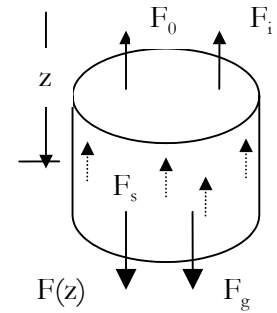
and the gravity force is $F_g = \frac{\pi}{2} \int_0^z \rho_p \cdot g \cdot A \cdot dz$.

Finally the fibre stress can be found by:

$$\sigma(z) = F(z) / A(z) \quad (5.4.3)$$

To find the tension force along the spinning line, the initial force $F_0 = F(0)$ at the spinneret ($z = 0$) must be known. The initial force F_0 is estimated using two approaches: an experimental approach by a new non-vertically melt spinning arrangement, and a theoretical approach.

Experimental approach to find F_0 : On-line internal force measurements along the spinning line have been investigated [Beyreuther 1999], and the experimentally and the theoretically calculated tensile forces have been compared. However, some restrictions encounter the measurement of force along the spinning line, for example the fibre force measurement by tensiometer is only possible after the solidification point and can only measure relative high internal force > 2 mN. Therefore, a new method was developed, where the spinning tension in the fibre formation zone was calculated with a geometric measurements. This method was based on the tensile force measurement of melt spinning of PEEK and was developed by Brünig [2003]. A non-contact method to determine the force tension of the spinning line was proposed by the non-vertically arrangement of a melt spinning equipment. The curvature caused by gravitation was determined experimentally by measuring the spinning line location. This is the



key to the determination of filament force by non-vertically arrangement of melt spinning equipment from non-contact measurements.

Theoretical approaches to find F_0 : The initial force is the limit of tension force in Equation (5.4.2) as $z \rightarrow 0$. Ziabicki [1976] found this limit value by assuming the simple model:

$$F(0) = 6 \cdot \eta(T_0) \cdot \int_{V_0}^{V_L} \frac{D \cdot h}{2 \cdot V} \cdot dV \cdot \frac{1}{\rho \cdot C_p \cdot \psi(T_0, T_L)}, \quad (5.4.4)$$

where $\psi(T_0, T_L) = \eta(T_0) \cdot \int_{T_L}^{T_0} \frac{dT}{(T - T_\infty) \cdot \eta(T)}$.

An other theoretical approach to find F_0 is based on solving numerically the initial value problem of coupled steady state equations of the melt spinning process simultaneously. The general form of differential equations of the fibre formation zone is well known and is summarised in Equation (5.1.10). The solution of three differential equations needs three initial values $\{V_0, T_0, F_0\}$. Since the initial spinning line tension F_0 is not known, an initial guess is necessary. This was done by the so-called shooting method.

The result of the estimated initial forces from non-contact experiments [Brünig 2003] and the two theoretical approaches used are listed in Table 5.4.1. The non-contact determination of initial force by non-vertically melt spinning is time consuming, but it give a better correlation with the Equation (5.4.4). However, for melt spinning of PEEK a Newton model in Equations (5.1.10) was applied. The initial force was calculated from mathematical model and is listed in Table 5.4.1. By applying the Maxwell viscoelastic model in Equation (5.1.10) and the elongation viscosity as function of temperature and strain rate, the initial value was underestimated.

Experiment conditions	F_0 mN		
	Ziabicki Equation (5.4.4)	Measurement Brünig [2003]	Equations (5.1.10) $\eta(T)$, Kase and Matsuo
A1	0.4643	-	0.303
B1	1.752	2.006	1.07
B2	1.861	-	1.25
B3	2.392	-	1.3
B4	2.452	-	1.51

Table 5.4.1 Comparison of different method to estimate the initial force

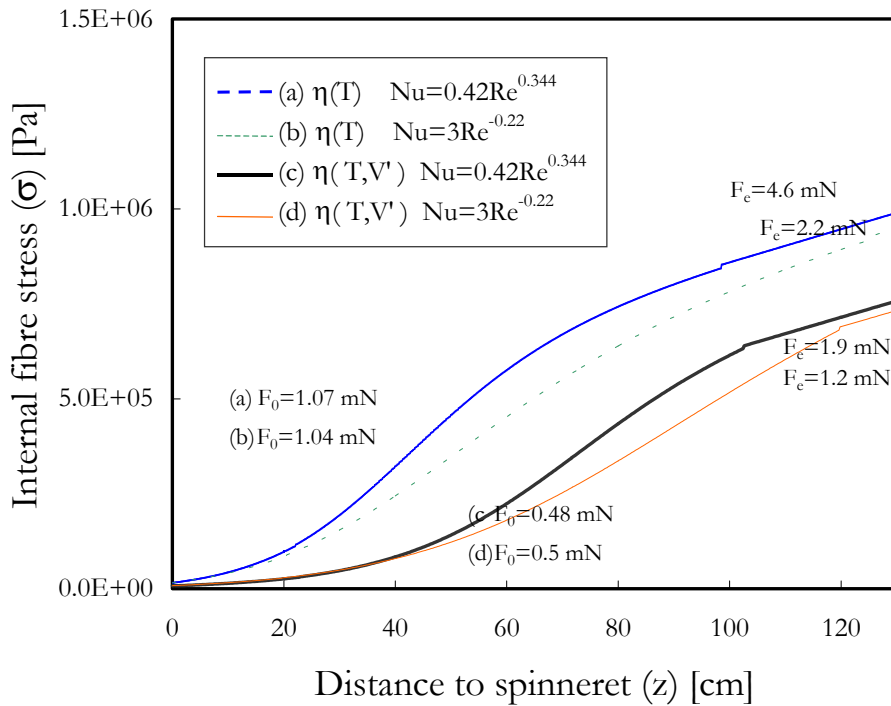


Figure 5.4.1 Calculated fibre stress from different model along spinning line for PEEK 151 G Victrex, $T_0=385^\circ\text{C}$, $V=1000$ m/min, $Q=3.5$ g/min, spinneret 3 holes ($d=0.25$ mm, $l=0.5$ mm)

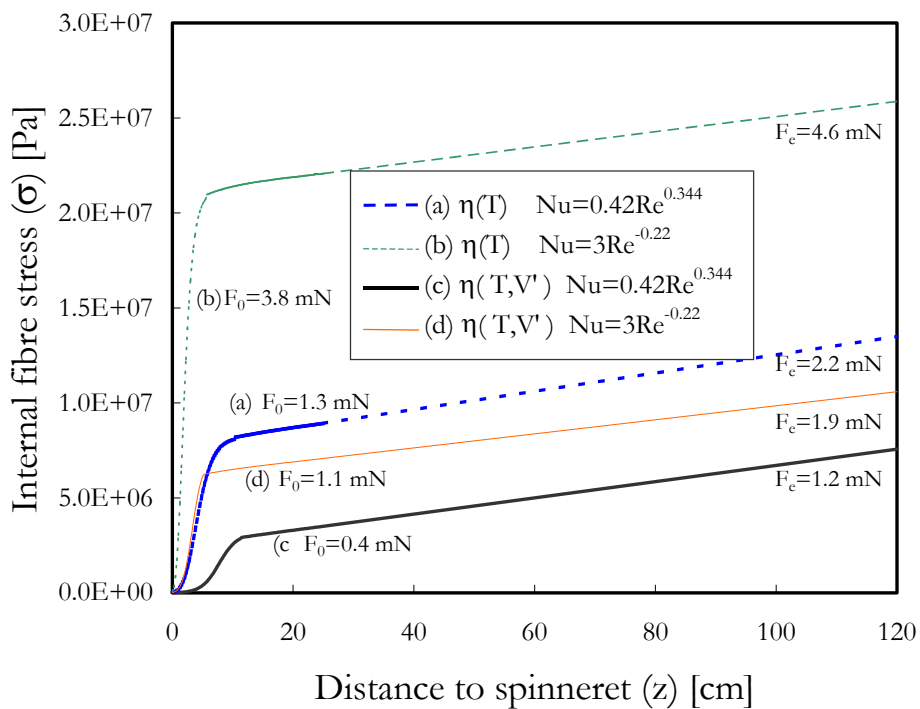


Figure 5.4.2 Calculated fibre stress from different model along spinning line for PEEK 151 G Victrex, $T_0=385^\circ\text{C}$, $V=1000$ m/min, $Q=0.225$ g/min, spinneret 48 holes ($d=0.25$ mm, $l=0.5$ mm)

Ziabicki [1976] concluded that the initial force (F_0) depends on upper flow conditions and the spinning conditions. This means that the relaxation of shear flow in spinneret channel and the cooling rate, throughputs and take-up speed can change the initial force value. From model increases in initial force (F_0) with increasing the take-up speed and decreasing the throughput.

In Figure 5.4.1, the calculated stress along the spinning line at low draw down ratio (ddr=15, $D_L=58 \mu\text{m}$) is presented. The effect of viscosity and Nusselt number were investigated for filament stress profile as in Section 5.3. The different models (a) to (d) in Figure 5.4.1 show different initial forces and take-up tensions. The calculated stress and internal force from model (a) and (b) are twice the other models (c) and (d). In Figure 5.4.2 the high draw down ratio (ddr=230, $D_L=15 \mu\text{m}$) makes a very different stress profile along the spinning line. The higher viscosity and higher heat transfer used, result a very high internal force and the stress becomes very high at the take-up point. Therefore it is necessary to compare the fibre speed profile of each model and filament speed measurement to choose the matching solution as discussed in Section 5.3.

Figure 5.4.3 shows the effect of take-up speed for constant throughput. Up to solidification point the stress growth dramatically as S-shape and after solidification the stress growth is linear due to the skin drag friction. The slope of stress line increases proportional to the square of take-up velocity. Figure 5.4.4 shows the effect of increasing the throughput at constant take-up speed. The slope of stress line after solidification is proportional to the inverse of root square of end fibre diameter. Therefore it can be concluded that:

$$\text{Slope of skin drag stress} \propto V_L^2 \cdot D_L^{-0.5} \propto V_L^{2.25} \cdot Q^{-0.25} \cdot \rho_p^{0.25} \quad (5.4.5)$$

The relation (5.4.5) is obtained from the calculated slope of stress after the solidification in the model of (c) of Figure 5.4.3 and 5.4.4.

Figures 5.4.5 and 5.4.6 present the fibre stress at solidification point over the take-up speed for different throughputs. The interesting results are due to different models of viscosity. Equation (4.1.2) states that the orientation of fibre is proportional to the fibre stress in solidification. This means that the result in Figure 5.4.5 calculated for $\eta(T)$ clarifies well the Equation (4.1.2), but in Section 5.3 the model of $\eta(T, V)$ shows better agreement to fibre speed profile. Figure 5.4.2 shows that the model (a) for $\eta(T)$ gives higher F_0 than (c). The correctness of stress estimations value could not be verified because no measurements were carried out.

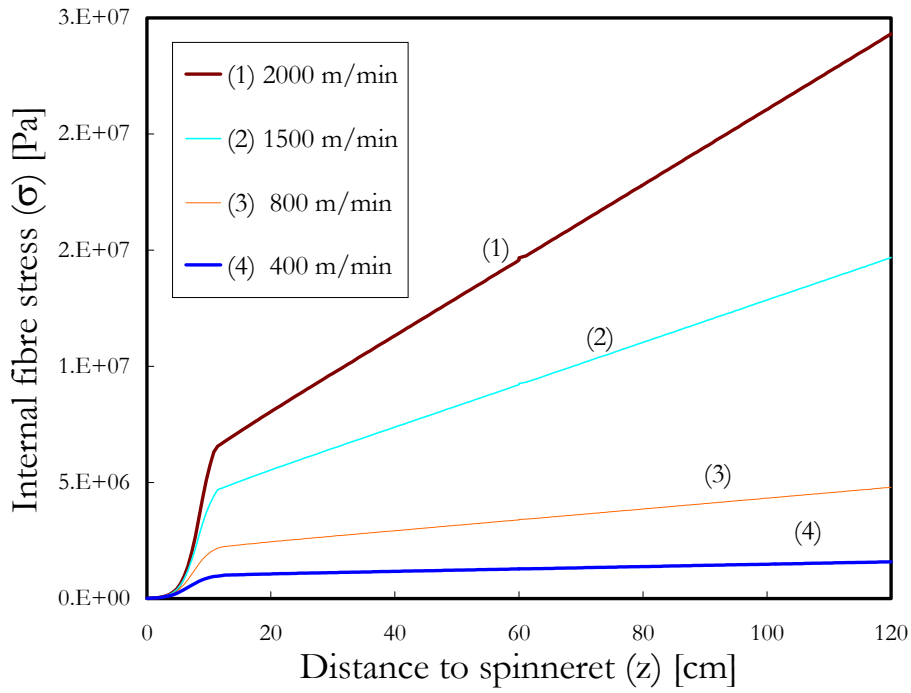


Figure 5.4.3 Calculated fibre stress from model $\eta(T,V)$ and Kase and Matsuo along spinning line for PEEK 151 G Victrex, $T_0=385^\circ\text{C}$, $Q=0.225\text{ g/min}$, spinneret 48 holes ($d=0.25\text{ mm}$, $l=0.5\text{ mm}$)

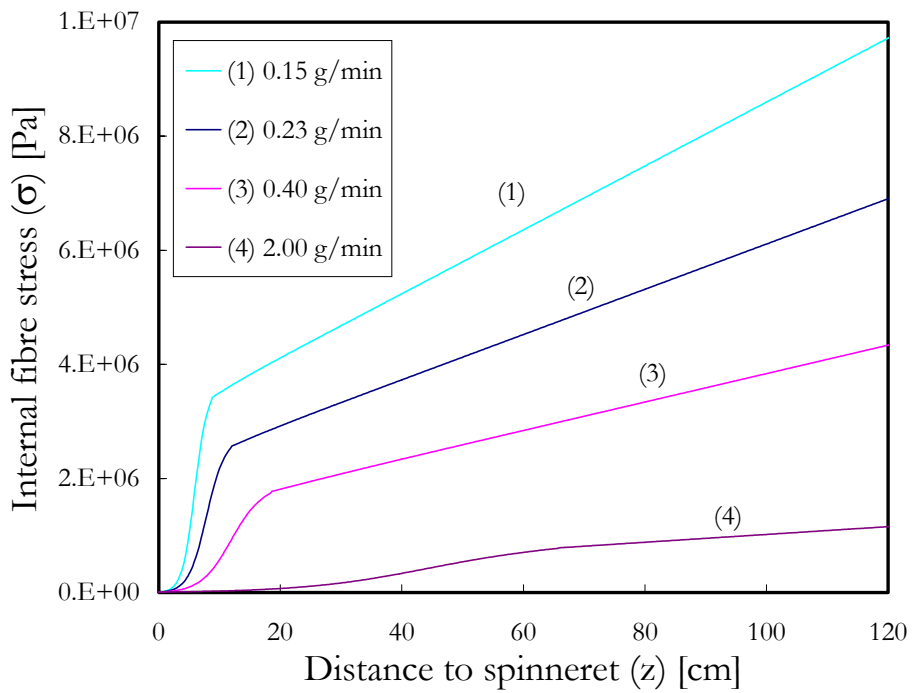


Figure 5.4.4 Calculated fibre stress from model $\eta(T,V)$ and Kase and Matsuo along spinning line for PEEK 151 G Victrex, $V=1000\text{ m/min}$, ($d=0.25\text{ mm}$, $l=0.5\text{ mm}$)

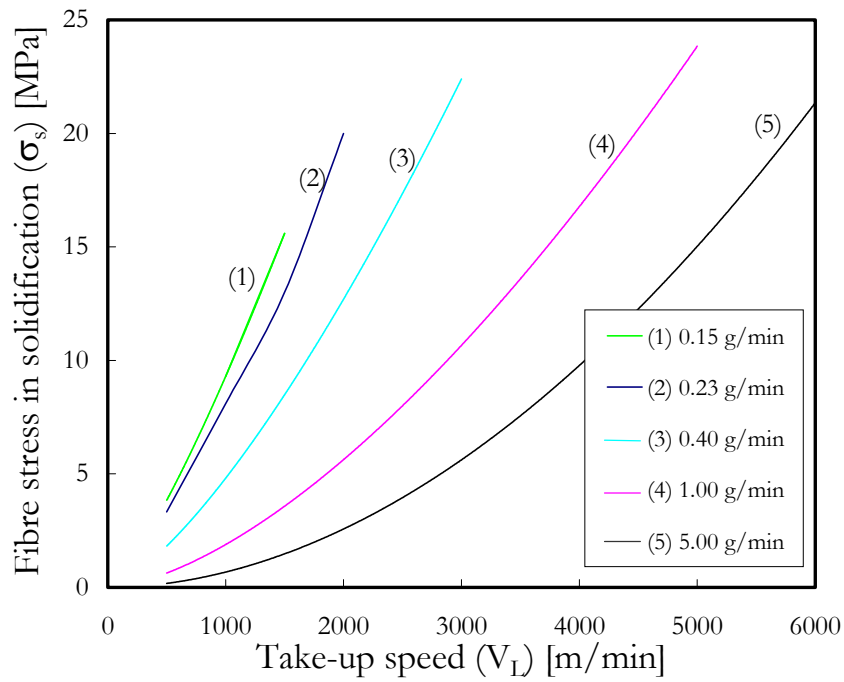


Figure 5.4.5 Calculated fibre stress at solidification point over take-up speed from $\eta(T)$ and Kase and Matsuo model of fibre formation of PEEK 151 G Victrex for different throughputs

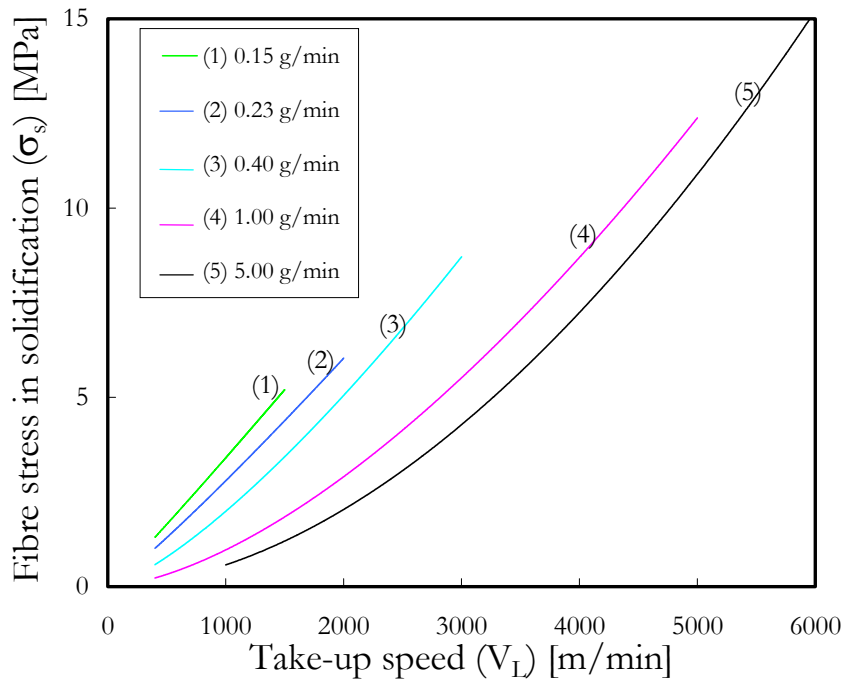


Figure 5.4.6 Calculated fibre stress at solidification point over take-up speed from $\eta(T, V)$ and Kase and Matsuo model of fibre formation of PEEK 151 G Victrex for different throughputs

6 Stability and fineness limitations of PEEK melt spinning

In this chapter, the failure theory is briefly introduced to discuss and understand the probable origin of instability in the melt spinning process. This introduction is followed by an examination into different spinning conditions in order to find the limits of stable spinning.

6.1 Failure theory in the melt spinning

Takasaki [2002] discussed the mechanism of fibre structure development in the spinning of ultra-fine Polylactides fibres. He concluded that the stability of spinning ultra-fine fibre is affected by two main failure mechanisms. The first is increasing surface tension, because for the ultra-fine fibres, the surface area over unit volume ratio becomes large. This outcome can cause the so-called capillary failure of the spinning line. The other possible failure mechanism is the effect of air-friction force, which also becomes high as the fibre fineness decreases, because the surface area is large. This effect may cause a cohesive failure of the spinning line in the down stream. Rauschenberger [2002] tried to summarise the criteria for the stable melt spinning of polymers by developing criteria for stability and applying them for LDPE, PA6 and two types of PP. Melt instability can occur in three different mechanisms: brittle, ductile failure and the necking. Both brittle and ductile failures can occur either in the melt or after the solidification. To distinguish between failure theories, general definitions are given here:

Brittle failure is a type of fibre breakage without any large plastic deformation. At the point of fracture, the fibre looks like a glassy break. The brittleness appears when the internal stress reaches a value near the critical tensile stress. This critical value for polymer melts is constant and tabulated for different polymers [Ghijssels 1997], although no value is reported for PEEK. For the fibre after solidification, the critical tensile stress can be assumed to be the minimum value of yield and ultimate stress.

Ductile failure is the type of fibre failure where the plastic deformation or strain becomes so large that the fibre material has stretched at one or more points, and the stress subsequently increases rapidly. If the strain increases and does not approach a constant value along the spinning line, the ductile failure leads to fibre breakage.

Necking is not a type of filament failure, but could initiate the instability in the melt spinning, which later leads to ductile or brittle breakage. If the fibre diameter decreases sharply at one point

along spinning line, the neck-like deformation takes occur, and the instability can lead to a failure. Ziabicki [1985] used the factor (V'_{\max}/V_L) to predict necking, and he also discussed the necking effect on the filament speed profile and on the extensional viscosity gradient (see Section 3.2). Rauschenberger [2002] defined the necking mathematically when the $(\partial^2 D/\partial z^2) < 0$.

6.2 Fineness limitations

6.2.1 Throughput, take-up speed and draw down ratio

In order to investigate the type of relationship between the three important spinning conditions: throughput (Q) take-up speed (V_L), and the draw down ratio (V_L/V_0), various experiments were carried out and compared with the theoretical calculation contained in Chapter 5.

It is to distinguish between the stability of melt spinning and the limits of spinnability. Stability is investigated in connection with time, and spinnability can be defined as the limits to which satisfactory spinning condition can be achieved in melt spinning process, independent of time. The following experiments can explain the difference:

- a) Conducting the melt spinning process with the same throughput, with an increasing take-up speed until the spinning line fails, determining the limit of spinnability.
- b) Melt spinning at the given spinning conditions without rupture or irregularity of as-spun fibre properties (for example the fineness, stress-strain curves...), making the melt spinning process stable.

Many methods were applied to establish relationships between the spinning conditions and the stability and spinnability [Ziabicki 1976, 1985]. Beyreuther et al. [1991] presented the limit of fineness over the take-up speed by applying two criteria: the maximum allowed internal fibre stress and the temperature limitation to solidify the fibre, and presented the maximum and minimum fineness over the take-up speed. In this thesis, a relatively new concept of a 'fibre spinning map' [Ghijssels 1994] is used. This concept was later successfully verified with the theoretical failure approach by Rauschenberger [2002], and was recently applied for PA6 and presented by Brünig [2002-b]. In order to graphically present the results, the maximum draw down ratio is presented over the take-up speed. By using constant mass throughput (the outlet velocity, V_0) it was spun with an increasing take-up speed (V_L). The take-up speed was increased until the spinning line is failed. This was repeated for the next throughput. The graph of (V_L/V_0)

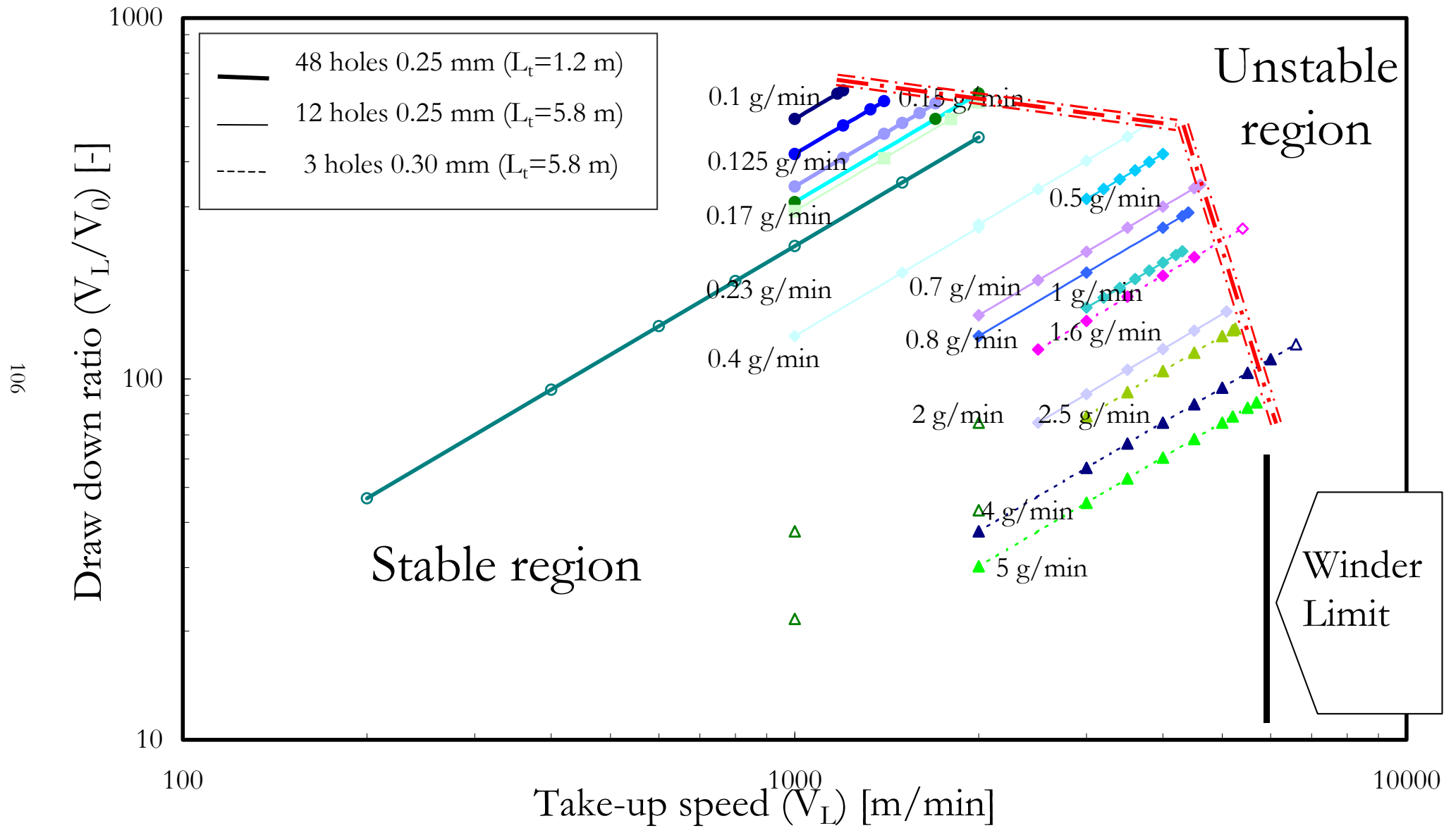


Figure 6.2.1 the fiber stability map for PEEK 151G Victrex under different spinning conditions

vs. V_L , shows the constant throughput as a straight line with the slope $(\rho_0 \cdot A_0 / Q)$. As explained in Section 2.2.1, the draw down ratio can be expressed by diameter of fibre as follows:

$$D = 1000 \cdot D_0 \cdot \sqrt{\frac{\rho_0}{\rho \cdot (V_L / V_0)}} \quad (6.2.1)$$

The draw down ratio over PEEK fibre diameter is already given in Figure 2.3.1. According to the Formula (6.2.1), it can be concluded that in order to produce fibre diameter of $7 \mu\text{m} < D_L < 12 \mu\text{m}$, the spinning conditions must be arranged to make the draw down ratio of $100 < \text{ddr} < 1000$.

The spinning limit experiments were carried out for PEEK and are shown in the so-called ‘fibre spinning map’ in Figure 6.2.1. The horizontal lines in the ‘fibre spinning map’ are of constant diameter, i.e. constant fineness. For a take-up speed of $V_L > 4000 \text{ m/min}$, the draw down ratio for stable spinning can reach maximum of $\text{ddr} < 300$. This means that with a filament diameter of less than $13 \mu\text{m}$, a fineness of 0.3 dTex can be reached for take-up speeds lower than 4000 m/min . The upper limit of take-up speed was limited to 6000 m/min by the wind-up unit, and when using the godets, can reach 7500 m/min . By decreasing the throughput, the stable melt spinning process was generally limited by take-up speed, because the stress and strain rate of the filament were increased and could not controlled by the structure formation of the polymer. These were the causes for ductile or brittle failure in the spinning line. The observed failures in a lot of melt spinning experiments, occurred in the region of the filament formation zone. In other words, the spinning line failures were not caused by an increase in stress beyond the solidification point to wind-up unit.

The region of stable spinning is divided into two limit lines (see Figure 6.2.1). The first limit range was identified for throughputs of more than approximately 0.7 g/min . For the throughputs range of about $0.8 \text{ g/min} < Q < 5 \text{ g/min}$, the take-up speed limit was increased and was observed within a range of $4000 \text{ m/min} < V_L < 6000 \text{ m/min}$. Brittle failure is the most plausible reason for failures in this range. The filament stress calculated from the PEEK fiber formation model, equals more than 20 MPa . Because no measuring limit value of melt break stress for PEEK was reported, an exact value for melt rupture could not be concluded. The second limits for stability were found to occur within a range of $1500 \text{ m/min} < V_L < 4000 \text{ m/min}$. A possible reason of these instability limits is that ductile failure may have also caused the allowable take-up speed to decrease. In this case the take-up speed was limited, where the strain rate of filament growth suddenly in the fibre formation zone when the throughput ranges between

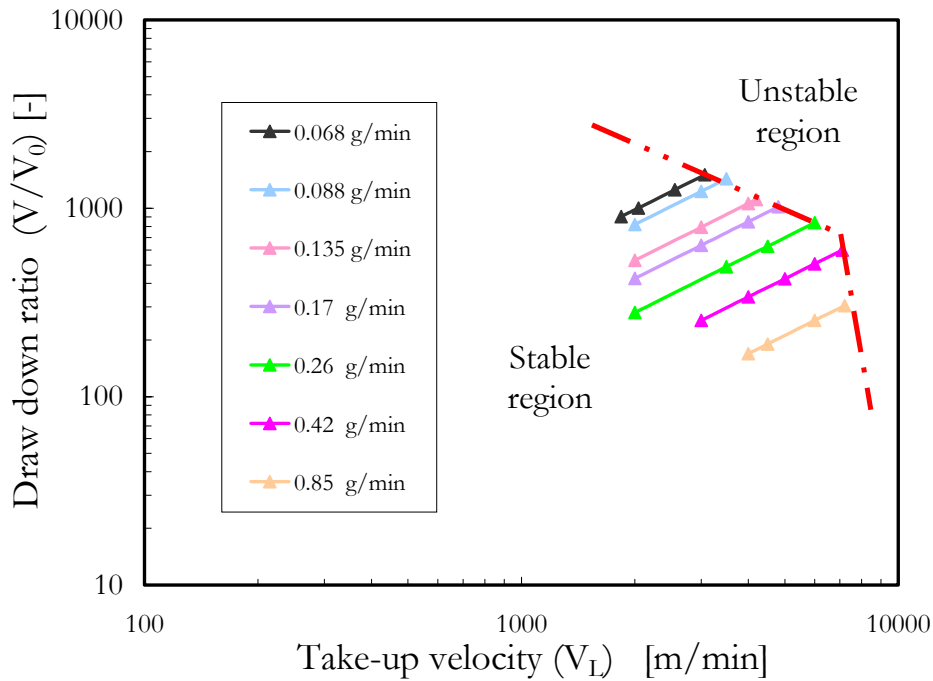


Figure 6.2.3 Fibre spinning map for PP HF 445 FB Borealis, $T_0=260^\circ\text{C}$, spinneret 48 holes, $D_0=0.25\text{ mm}$, $l_0=0.3\text{ mm}$, extruder melt spinning equipment

$0.1\text{ g/min} < Q < 0.5\text{ g/min}$. It was observed that upon decreasing the throughput, the strain rate increases suddenly along spinning line and the extensional viscosity decreases. The local decreasing viscosity caused a local filament speed increase and probably the necking. However, the necking is the beginning of instability, which can lead to ductile or brittle fracture. However, Rauschenberger [2002] suggested that the ductile failures could be occurred if the strain grows and does not approach a constant value. The Hencky strain is normally defined in the melt spinning as $\varepsilon = \ln(V/V_0)$. For draw down ratios in the range of fine filaments within $100 < ddr < 1000$, the Hencky strain is about $4.6 < \varepsilon < 6.9$.

The stability investigation was also carried out for polypropylene (PP HF 445 FB), and the results are presented in the fibre spinning map, see Figure 6.2.3. Fine PP filament demand a higher take-up speed. As investigated in Section 4.1 the as-spun polypropylene fibre has a higher elongation at break than PEEK in the tensile test. This is a probably reason why a high take-up speed is required to produce fine polypropylene fibres. In this thesis, no mathematical model was applied for a fibre formation of PP HF 445 FB, and no speeds or temperatures were measured. Therefore no further explanation about PP melt spinning failures can be pursued. PP HF 445 FB can generally be spun more easily in the temperature of 260°C and the draw down ratio reached (fine fibre) is higher than for PEEK spun in melt temperature of 400°C . This fact, which can be

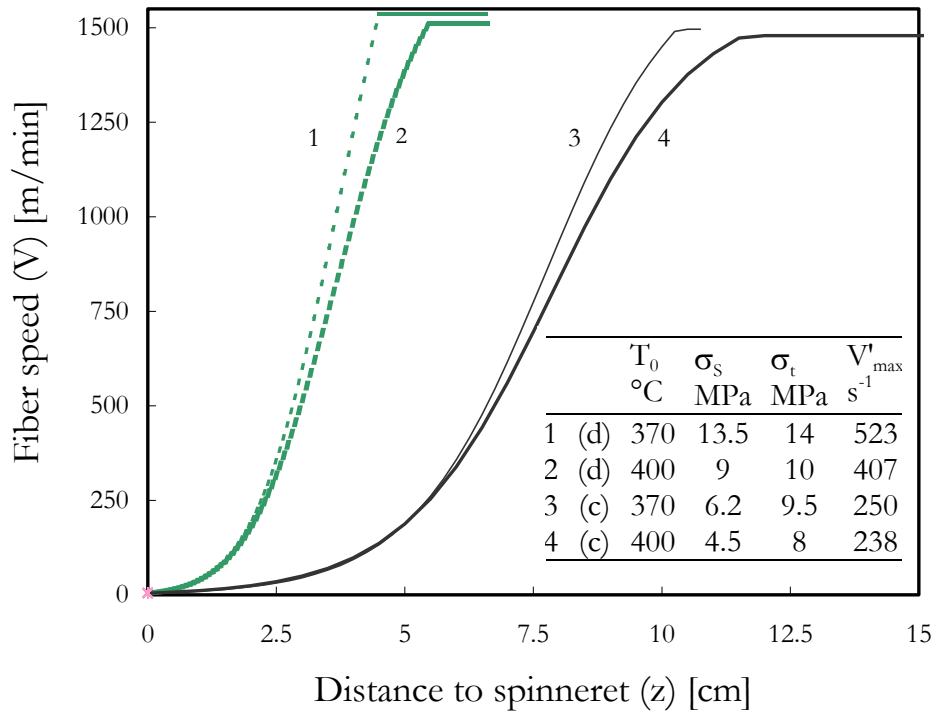


Figure 6.2.4 Effect of melt temperature on fibre speed profile, the solidification stress and the spinning gradient, calculated from model of PEEK 151 Victrex, (d) and (c) are assumptions used in Section 5.3, $V_L=1500$ m/min, $Q=0.225$ g/min, spinneret 48 holes ($d=0.25$ mm, $l=0.5$ mm)

expressed as $ddr_{PEEK}^{max} < ddr_{PP}^{max}$, can be explained due to the different melt temperatures and melt densities, and can also be attributed to the different fibre formation structures of the two aforementioned polymers, PEEK and polypropylene. The minimum throughputs achieved for polypropylene are lower than for PEEK using extruder equipment, see Figure 6.2.3. The slope for the PEEK probable ductile failure limit (ddr vs. V_L in Figure 6.2.1) is more gradual than the slope for brittle failure. The slope for PP probably ductile failure is also more gradual than for brittle failure.

6.2.2 Temperature of melt and viscosity

Increases in the processing temperature were recommended in order to improve the melt spinning process for production of fine filament [Fourné 1995]. However, increases in the melt temperature always have their limited, because it is known that the polymers degrade in too high temperature. On conducting experiments, it was observed during the melt spinning of PEEK 151 Victrex that increasing the melt temperature (temperature of processing) from 385°C to 400°C leads to improvements in the production of fine PEEK filaments. This change brought a reduction in spinning line breakages, and the stability of time variation variables was also improved. In the melt spinning of PP HF 445 FB, the increase in melt temperature from 230°C

to 260°C also improved the spinnability. The PEEK fibre formation model was used to investigate the effect of increased melt temperature on the melt spinning process. Figure 6.2.4 graphically demonstrates the effect on the filament speed profile when the PEEK melt temperature is increased from 370°C to 400°C. No spinning at 370°C was actually carried out, but this was taken in the PEEK fiber formation model to observe influence of low melt temperature.

Decreases in melt temperature also decreased the filament speed gradient at the end spinning line for both models (c) and (d). Figure 6.2.4 shows that the higher temperature enlarges the solidification way. The internal stress of filament at both the solidification point and the take-up point also decreases when the melt temperature is increased, as shown in the table contained in the Figure 6.2.4. The lower stress and enlarged solidification could be presumed to make a better structure formation. The effect on the take-up point can be seen in Section 6.2.3.

The temperature of the spinning line can be increased with a heat tube. It was observed during various experiments that adding the heat tube and increasing the temperature did not improve the stability of PEEK melt spinning. Increasing the air temperature in the model within the fibre formation zone decreased the initial force and also decreased the stress in the spinning line, but no effect on filament speed was observed. Additional effects were increases in the solidification way and the fineness of the filament. Decreasing the extensional viscosity in the applied model for PEEK lead to decreases in initial force. However, in this case, the velocity profile is changed as shown in Figure 6.2.5. More to the effect of viscosity was given in Section 5.3, where the fibre speed profile is discussed.

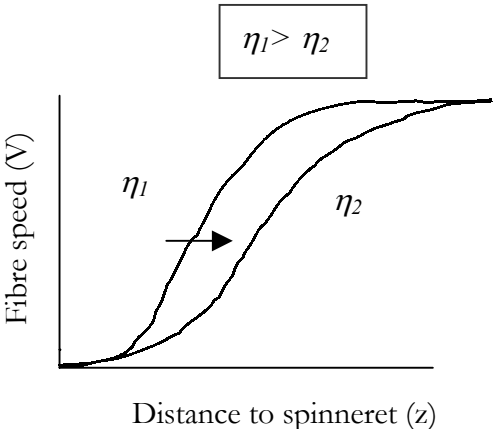


Figure 6.2.5 Effect of decrease of viscosity on the fibre speed profile along spinning line, calculated from PEEK fibre formation model

6.2.3 Take-up point

Figure 6.2.6 shows an example of melt spinning at a constant take-up speed of 1500 m/min, but with different running lengths of 50 cm and 120 cm at a constant throughput of 0.225 g/min. For a long running length, the fibre speed increases in two steps; the first step corresponds to the thinning process in the conventional melt spinning, and the second one is a deformation by plastic or elastic, since the filament is rather undeveloped in this step. This means that if the filament is running a long length and the air resistance is high, then the deformation in the second step would reduce the filament to a lower value than the short running length. The stress at the solidification point is increased by long spinning way and the maximum speed gradient of fibre is also increased. Although the PEEK fibre formation model does not contain the stress-induced crystallisation, the long take-up point was decreases the fibre speed at the end of the spinning line due to skin drag force.

The decrease of the spinning way (the distance from spinneret to wind-up unit) causes stable melt spinning for fine filaments, but is limited to a minimum value. Beyreuther et al. [1991] explained that the take-up point is limited by cooling conditions. This means that the fibres must reach the solidification temperature before first contact with the preparation; this limitation has to be consider for high throughputs and low take-up speed, which is different to melt spinning of fine PEEK fibers. The maximum allowed spinning way was defined by Beyreuthern et al. [1991] as a limit of fibre tensile stress along spinning line of $< (\frac{1}{2} \dots \frac{2}{3}) \cdot \sigma_s$. This means the fiber stress may not exceed the rupture stress along the spinning line, before and beyond the solidification point.

Figure 6.2.7 presents results of PEEK model calculations to illustrate the effect of increasing the take-up point on speed gradient. An example of melt spinning at a constant take-up speed of 1500 m/min and constant throughput of 5 g/min was selected. The distance of wind-up unit and the spinneret for the experiment was 580 cm. Two different running lengths are assumed; 200 cm and 580 cm. The speed gradients were calculated for different viscosity and heat transfer coefficient, as shown in Section 5.3. The speed gradient profile from models (a) and (b) is a typical form, and it appears to be a half periodic function. The models (b) and (c) show a depressed form and make a suddenly increase to a higher value. Such increases of speed gradient decrease the extensional viscosity in a small region and can be can be an indication of necking. This effect can later lead to brittle or ductile failure.

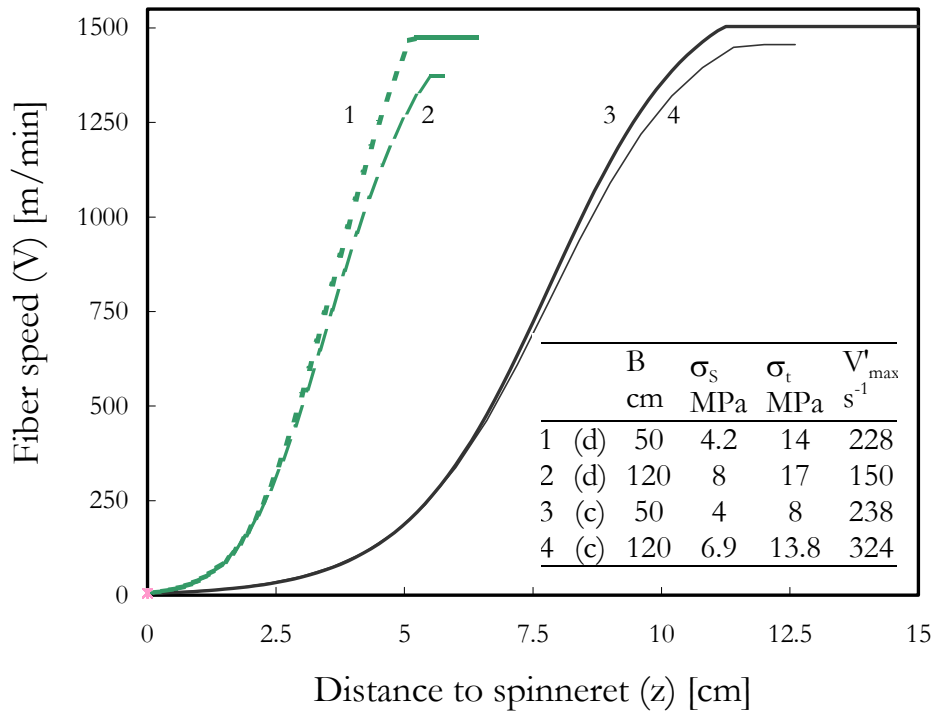


Figure 6.2.6 Effect of take-up point on solidification stress, take-up stress and speed gradient from model for PEEK 151 G Victrex, $T_0=400^\circ\text{C}$, $V_L=1500$ m/min, $Q=0.225$ g/min, spinneret 48 holes ($d=0.25$ mm, $l=0.5$ mm)

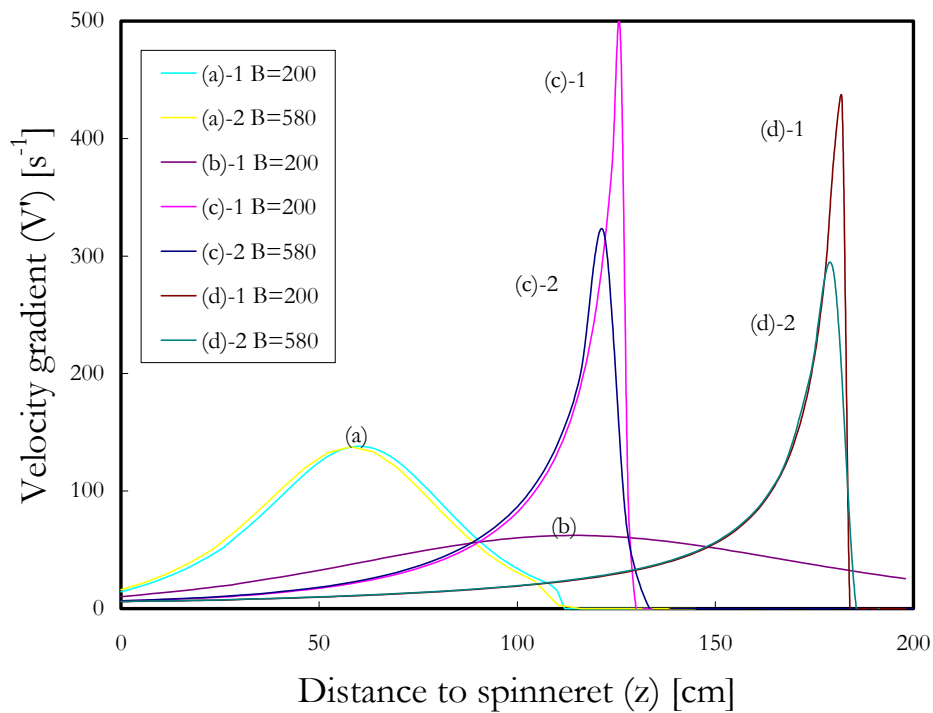


Figure 6.2.7 Effect of take-up point, B, on velocity gradient from model (c) and (d) for PEEK 151 G Victrex, $T_0=400^\circ\text{C}$, $V_L=5000$ m/min, $Q=5$ g/min, spinneret 3 holes ($d=0.25$ mm, $l=0.5$ mm)

6.3 Optimisation of spinning conditions for fine filaments

Beyreuther et al. [2001] mentioned that very fine filaments could be spun under a high take-up speed and with a very low mass throughput. They added a dependent condition namely the draw ratio. The spinning parameters to produce fine filaments are explained in this section. The most important parameters in this study are the take-up speed, the mass throughput and the draw down ratio. The melt temperature and viscosity are discussed briefly in the Sections 6.1 and 6.2.

Take-up speed, V_L : Fine as-spun fiber can be obtained under a relatively high take-up speed. Increasing the take-up speed is known to lead to conditions that arise in high speed spinning, such as increasing the drag force, and as a result, rheological force and induced filament stress. The strain rate increases rapidly and the necking effect appears. The strength limitations of material soon lead to filament breakages.

Draw down ratio, V_L/V_0 : Different studies have shown that decreasing the throughput leads to decreases in the maximum possible take-up speed. It is therefore better to use the ratio of take-up speed to speed of material at the outlet of the spinneret as dimensionless draw down ratio (ddr).

The different experiments carried out and the following parameters were varied to find the optimal conditions to produce fine filaments.

- a) Increases in the number of spinneret holes to decrease the mass throughput per holes were made, because the minimum mass throughput depends on extruder and spinning pump rotation speed (rpm) limitations. However, mass throughput decreases results in a smaller fibre formation zone, smaller solidification time and high temperature gradient. This effect can be seen in the fibre spinning map Figure 6.2.1.
- b) Increases in the take-up speed for the low mass throughput and find the take-up speed to spin in a stable and continuous conditions, can be seen Section 6.1
- c) Decreases the fibre path spinning line, i.e. distance between wind-up unit and the spinneret, can be seen in Section 6.2.3
- d) Increases the melt temperature are examined in Section 6.2.2
- e) Results of using the heating tube for different temperature and heating length are shown in Section 6.2.2

The first experiments were carried out with piston equipment in order to investigate PEEK melt spinning spinnability. A large amount of PEEK was later spun with the extruder equipment.

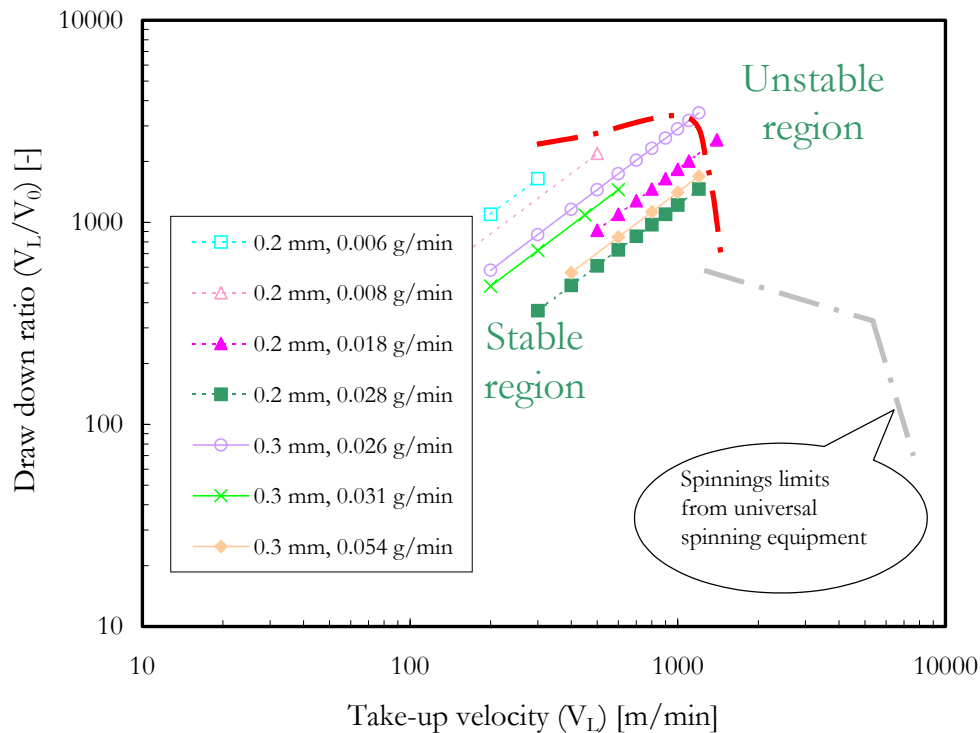


Figure 6.4.1 'Fibre spinning map' for ultra fine filament by piston melt spinning equipment, PEEK Victrex 151 G

6.4 Ultra-fine PEEK filaments ($D_L < 9 \mu\text{m}$)

The Section 6.3 explained how it is possible to optimise the spinning conditions to spin fine PEEK filaments with the extruder spinning equipment. The limits of fibre spinning come from a combination of the draw down ratio and the throughput. It is actually possible to spin with a high take-up speed in the extruder equipment, but decreasing the throughput under 0.1 g/min per holes is not possible, and therefore the piston spinning equipment must be used. Brünig [2002] reported that ultra-fine PEEK filament was spun aided with the piston equipment by decreasing the throughput, and the minimum filament diameter of $2.5 \mu\text{m}$ (0.2 dTex) was spun. He reported however that this experiment was not carried out under stable spinning conditions. To investigate the ultra-fine spinning, more experiments were carried out here with piston spinning equipment and represented in the 'fibre spinning map' in Figure 6.4.1. The limits of stable spinning by piston spinning were increased relative to extruder spinning equipment, and more fine filaments were produced. The slope of limits line for stable spinning by piston equipment was not longer the same as the extruder equipment. Neglecting the effect of time process variable variation (such as polymer melt, spinneret,...) in Figure 6.4.1 leads to important results. Firstly, decreases in mass throughput per holes are not necessary in order to spin even finer filaments, it means lower than certain throughput, no more finer fibres can be spun. Another important result is the draw down

ratio effect. A fine filament is produced with a high draw down ratio; this high draw down ratio can be obtained if the spinneret diameter is increased with the same throughput.

Low throughput and the melt pressure: It is generally not possible to generate very low throughput $Q < 0.1$ g/min per holes to spin fine filaments with the extruder equipment used here. The piston equipment is suitable for this purpose. The piston was derived once by direct movement, and once with a gearing system to change the rotation to a straight piston motion, and finally, the gas pressure was used to directly press the melt within the cylinder. The time variations of the polymer melt conditions and the pressure drop created a negative effect on the stability of ultra-fine melt spinning. Figure 6.4.2 presents the measured pressure drop over the throughput for low throughput experiments with piston equipment. The simple theoretical power law flow relation was fitted. As expected, the exponent of the classical power law is less than one ($n=0.9$) for the piston equipment. The exponent ($n=0.95$) was fitted for the extruder equipment. As already known the shear decreasing effect corresponds to exponent n less than unity, this means for the given throughput, the Δp can be many times lower than the calculated one with the equation in Figure 6.4.2.

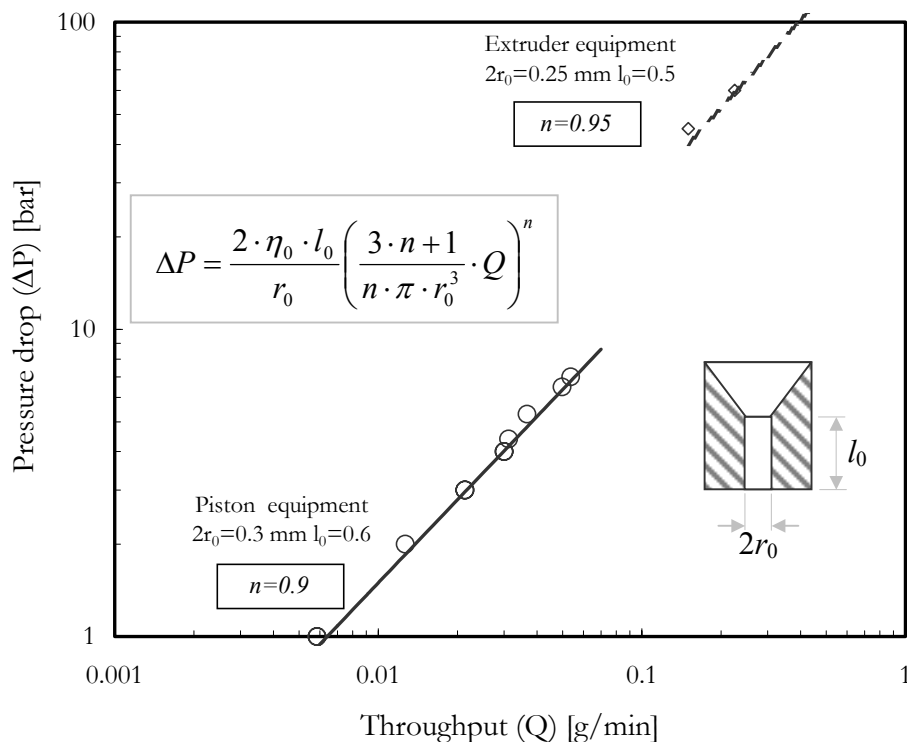


Figure 6.4.2 Pressure drop measured (symbols) for very low throughputs and the fitted power law exponent (lines), capillary flow by power law for PEEK Victrex 151 G

7 Conclusion and recommendations

7.1 Summary and Conclusion

No unique definition is given in the literature for fine filaments, this work mainly investigated the filaments with a diameter of $10\ \mu\text{m} < D_L < 30\ \mu\text{m}$, but higher and lower limits were included in order to complete the discussions. Although other fine polymer filaments have also been developed and patented, no extended and completed studies on fine PEEK fibres are cited in the literature. The special application of fine PEEK fibres are explained, such as the innovative product of commingling carbon reinforced fibres. This thesis investigated further features which concern the melt spinning process, e.g. textile properties and extensional melt rheology. The main goal of this thesis was to investigate the required spinning conditions (V_L, Q, T_0) to produce fine PEEK fibres using the melt spinning process. The effect of spinning conditions on final properties was investigated to explain the structure development ($\Delta n, X$) and its effect on mechanical properties in stress-strain curves. The model of PEEK fibre formation was applied to study the cooling and viscosity on fine filaments. The spinning limits for the production of fine PEEK filaments were investigated to optimise the spinning conditions.

Two methods were introduced to calibrate and correct the on-line temperature measurement by thermography. The related experiments were carried out under different temperatures and various filament diameters. The correction factor (related here to the emissivity factor) was established from two different methods, and it was mainly a function of filament diameter and the thermoplastic type. No dependence on any temperature difference of filament and environment of the correction factor was observed. A new method was developed to find the filament diameter along the spinning line by using infrared camera snapshots. This method can be helpful in measuring the filament diameter near the spinneret, especially when used to study the die swelling effect. The infrared camera used here was well-equipped to measure the usual filament diameter. Unfortunately, the camera led to limits, as it could not be used for all fine filament diameter, because the camera resolution could detect a minimum $25\ \mu\text{m}$ diameter and the measurements were limited just to $25\ \mu\text{m} < D < 5000\ \mu\text{m}$. The method used to measure the filament speed (Laser Doppler Anemometry device) is based on the reflected light-scattering and depends on the surface microstructure. As a result, the measurements at the end of the spinning line, where the structure is in formation, are subject to uncertainty (see Sections 2.21 and 5.3.1). The spinning equipment and the on-line and off-line test conditions were also explained in

Chapter 2. The filament characterizations and the collected material properties of PEEK were applied to the model of fibre formation in Chapter 5.

The material function of the PEEK melt (and PP in comparison) was found by shear rheometry, especially the small amplitude oscillatory test. The shear rheology of melt is necessary for the development of the constitutive equation in shear and can also be applied in extensional deformation. Zero shear viscosity, temperature dependent viscosity, strength relaxation, relaxation time and other properties are measured from shear rheology and implemented in the extensional constitutive equation. The shear thinning behaviour (the dependence of viscosity on shear rate) was fitted by the cross model, because the power law failed to fit the decreasing effect in a wide range of shear rates.

The apparent extensional viscosity was estimated by on-line filament speed and temperature measurements along the spinning line. The estimated apparent viscosity of PEEK versus the spinning line showed the important structure formation, especially the necking effect that occurs before the solidification. The effect of the speed gradient on extensional viscosity was approximated by using different expressions of the viscosity form in three approaches: viscous (Newton), viscoelastic (Maxwell) and simple non-linear viscoelastic (upper-convective Maxwell), but no total conformity was observed to the estimated extensional viscosity. The selected modified cross model $\eta(T, V') = \eta_0(T) / (1 + (a \cdot \eta_0(T) \cdot V')^b)$ was proven to be the best form of the extensional viscosity variation over the speed gradient. This was possible by displaying the estimated apparent extensional viscosity reduced by temperature viscosity, $\eta_{app} / \eta_0(T)$, over the time dependent speed gradient, $V' \cdot \eta_0(T)$. This turned out to be the most useful relation for the extensional rheological investigations in this thesis, which was subsequently applied successfully to the model of fibre formation outlined in Chapter 5. The strain rate dependent extensional viscosity investigated for PEEK shows a decreasing behaviour for $10 \text{ s}^{-1} < \dot{\epsilon} < 1000 \text{ s}^{-1}$. The mathematical expression fitted to the estimated extensional viscosity, Equation 3.2.9, could not include the thickening effect of extensional viscosity (non-linear behaviour) which normally appears after the outlet of the PEEK melt for smaller strain rate, $\dot{\epsilon} < 10 \text{ s}^{-1}$. Because of this, the equation cannot be considered valid to verifying the swelling effect.

The orientation of as-spun PEEK filaments was investigated by optical off-line measurements of birefringence. The results discussed in this thesis demonstrated that the birefringence of as-spun PEEK filaments increases on increasing the take-up speed from 1000 m/min to 2000 m/min

with a constant mass throughput. Increasing the throughput from 0.17 g/min to 3.5 g/min by constant take-up speed decreases the birefringence. However, It should also be made clear that the birefringence over draw down ratio increases exponentially and has an upper limit value; this means fine fibres are subsequently more oriented. The on-line birefringence and orientation development could not be investigated in this thesis, but it was verified that the total birefringence shows a linear relation to the stress at solidification point (calculated from the model contained in Chapter 5). The off-line crystallisation was investigated for as-spun PEEK fibre by DSC measurement. The results of the DSC measurement verified that the melting areas of as-spun PEEK filament are the same even with different take-up speed, but the post-crystallisation areas increase with increase in the take-up speed. The measured crystallinity in the first heating step lies between 15 % X 35%. After cooling with 20°C/min, the second heating step showed no heat release after the glass temperature and the maximum degree of crystallinity was about 40 %. The crystallinity degree increases when increasing the draw down ratio (ddr) and approaches a constant value $X \rightarrow 35\%$ for $ddr > 350$. This draw down ratio results in a fibre diameter of $D_L < 13\ \mu\text{m}$, of which the birefringence has its maximum value of $\Delta n_{\text{max}} \sim 0.05$.

The measured and calculated fineness for a wide range of spinning conditions was demonstrated to be a good agreement. For fine PEEK filaments the diameters were measured with a precision of $\pm 1\ \mu\text{m}$. The measured elongation at break proved that the high stress at solidification leads to the decrease of elongation at break (like other spin thermoplastics). The minimum measured elongation at break of as-spun PEEK filaments was 40 % with a take-up speed of 5000 m/min (for PP > 100 %). For the extrapolated take-up speed ($V_L \rightarrow 0$) the elongation at break seems to approach different values depending on the throughput. This means that not only the draw down ratio but also the mass throughput affect the elongation at break, although the elongation generally decreases when increasing the take-up speed. For higher throughputs and equal take-up speed, the elongation at break shows higher values. The tenacity of as-spun PEEK filaments increases slightly by increasing the take-up speed or increasing the draw down ratio. The tenacity lies between 1 cN/dTex and 2 cN/dTex (for polypropylene, the tenacity measured is between 5 cN/dTex and 8 cN/dTex).

The elasticity modulus of as-spun PEEK fibres showed the same trend as the orientation for different take-up speeds and constant throughput. This proved the dependence between the elasticity modulus and birefringence of as-spun PEEK fibres. The modulus of elasticity over draw down ratio for $10 < ddr < 100$ lies between $1\ \text{GPa} < E < 2\ \text{GPa}$, and for $200 < ddr < 400$, the

modulus increases linear up to 6 Gpa. The stress strain curve of as-spun PEEK fibre for different spinning conditions confirm the following facts: the fine fibres produced by high draw down ratio, high crystallisation and orientation become tougher and cannot deform plastic, because their elastic deformation is fully developed by the high draw down ratio in the melt spinning process. The fibres with lower orientation show the yield, necking behaviour and extension at relative constant load, followed by a work hardening and show high elongation at break. These filaments can be drawn because of its ductility. The PEEK fibres with higher orientation showed a higher yield strength, tenacity and lower elongation at break.

The one dimensional fibre formation model of PEEK was applied using the information collected from Chapter 2 and the result in Chapter 3 of this thesis. The three differential equations were used with different constitutive equations: Newton for viscous deformation, Maxwell for viscoelastic deformation and upper-convected Maxwell for non-linear viscoelastic deformation, in a differential form. The integral type of constitutive equations is an appropriate form to study both the effect of prehistory and swelling effect. Therefore applying the integral form of constitutive equation normally is accomplished by considering the upstairs flow in the spinneret channel as a part of the model. Although the PEEK crystallises along the spinning line, the stress-induced crystallisation was not considered in the model for two reasons; firstly, that no information about the crystallisation kinetics in the fibre formation zone of fine fibre especially for PEEK was available; and secondly, to implement the stress-induced crystallisation, the on-line measuring did not give enough information to verify the crystallisation behaviour (temperature measurement announced in Section 5.2.3).

By measuring the temperature along the spinning line, it was possible to examine the heat transfer mechanism in the air cooling of PEEK filament. A simple temperature profile was proposed in this thesis (Equation 5.2.11) to fit the measured data and to replace a smooth form in the estimation of the heat convection coefficient (Nusselt number). The Nusselt number over the Reynolds number decreased for $10 < Re < 100$ and was placed higher than the relationship suggested by Kase and Matsuo ($1 < Nu < 2$). Therefore a new (decreasing) Nusselt relationship, $Nu = 3.Re^{-0.22}$ (for $10 < Re < 100$ and $10 < \zeta < 300$) was developed. The suggested relationship gives a good agreement to the measured temperature in the fibre formation zone but after solidification it shows some overestimation. At the beginning of fine PEEK fibre formation, the effect of radiation is important and makes up about 12 % share of the total heat transfer. It decreases quickly to drop to 1 % at the end of the fibre formation zone. The Nusselt number increases at

the end of fibre formation due to forced convective heat transfer; therefore, near solidification point, the increasing Nusselt number relationship from Kase and Matsuo gives a better agreement to measurement.

The filament speed measurements and the solution of the PEEK model were also compared. For fine filaments, measuring the speed profile near the spinneret was not possible. The model was used for two different viscosities, $\eta(T)$ and $\eta(T,V)$ and two different Nusselt number relationships. The strain rate effect considered in the viscosity and the Kase and Matsuo relationship generally shows a better approximation. The one-dimensional model was solved by shifting the origin, the filament speed profile could give a better agreement to measurement. This could be due to the effect of high air temperature near the spinneret, or alternatively the swelling effect. The swelling effect was not considered in the model, as it did not affect the speed profile along the spinning line. Due to the fact that the origin of coordinate was assumed at the diameter equal to spinneret hole, the swelling effect could only shift the filament speed profile. Solving the equations of state in a two dimensional form near the spinneret maybe useful, but in this thesis it was proved that, in cases of melt spinning of fine filaments where the formation zone is very short, the one dimensional model can be successfully applied. The effect of cooling mechanism on filament structure formation was investigated, whilst also avoiding the complex formulation for the two dimensional model. At the beginning of the fibre formation zone, no high temperature decrease occurred, and structure of PEEK was still not oriented, because the filament speeds had conformed to different take-up speeds and constant throughput.

It was also proven that the initial rheology force F_0 dominates the stress along the spinning line of PEEK especially for fine filaments. The different cooling conditions and the different viscosity expressions changed the initial force value and the stress development. The calculated slope of skin drag stress from the model of PEEK after the solidification point is proportional to the square of the take-up speed and inverse to root square of the end filament diameter. The model results of filament stress at solidification were verified in the following manner: increase of stress at solidification exponentially with increasing take-up speed for constant throughput, and decrease of stress at solidification by increasing throughputs at constant take-up speed. The off-line measured birefringence and the calculated stress shows a linear relation.

The fibre spinning map (draw down ratio vs. take-up speed) developed for the spinning conditions of PEEK is very useful in understanding the mechanism of failure and the limits of spinning conditions for different throughputs. In cases for very low throughput (<0.5 g/min),

the ductile failure due to large strain and strain rate can be the reason behind spinning line breakages. The brittle failure takes occur in cases where the throughputs are >1 g/min. The fine fibre with a diameter of <13 μm can only be produced with a relative low take-up speed of <2000 m/min. Polypropylene PP HF445 FB showed a wide range of stability limits in relative high take-up speed of >2000 m/min and a low throughput of <0.1 g/min. Decreasing the melt temperature and increasing the take-up point (distance from spinneret to wind-up unit) was examined with fibre formation model of PEEK. It was proven that both effects increase the fibre stress and are therefore not suitable for satisfactorily producing fine fibres. Increasing the strain rate and changing of fibre speed profile are also proven using the model of fibre formation of PEEK. Very low throughputs for ultra-fine PEEK fibres were carried out, and the fibre with a diameter of <6 μm was produced. The melt spinning of ultra-fine fibres is very sensitive to the condition equipment and material; for example the way of supplying the low throughput, and also the effect of time variation parameter. The pressure drop vs. throughput was fitted for a low throughput of <0.1 g/min per hole by the power law relation for the flow in capillary.

7.2 Recommendations

The non-linear constitutive equation can be applied to the model of PEEK fibre spinning, especially in the first region of spinning line directly after the outlet of the spinneret. In this region the die swell can appear and influence the downward flow state of the fibre formation zone. This dilemma has been solved for other type of thermoplastics, but not for PEEK in two dimensions coordinate. Because the PEEK crystallises along spinning line the crystallisation kinetics and the orientation development, combined with some additional on-line measurements along the spinning line for birefringence and crystallisation, complete the model of the fibre formation. In this case the density and the viscosity should be treated as a function of crystallisation. For further studies the constitutive equation of linear viscoelastic Maxwell model of discrete spring and dashpot can be applied using the parameters in Figure 3.1.3. This is a recommendation on which further studies could be conducted. Different combinations of spring and dashpot in series and parallel may also provide interesting research work. In heat transfer, the fitting of Equation 5.2.10 will cover the free and forced convection. However, the lateral vibration of fibres observed along the spinning line disturbs the boundary layer and an additional heat transfer process should complete the description. The effect of the time dependent parameters must be especially considered for the stability of melt spinning of fine filament.

References

- Beyreuther 1991 Beyreuther R., Limitation of Elementary Fiber Finenesses in Melt spinning, International Fiber Journal, pp. 46-53, February 1991.
- Beyreuther 1996 Beyreuther R., Vogel R., Spinnability of Polymer Melts - a Complex Problem in Basic Research, International Polymer Processing XI, 2, pp. 154-158, 1996.
- Beyreuther 1998- a Beyreuther R., Brünig H., Hofmann H., Manufacture-Induced Inaccuracies of spinning Dies, International Polymer Processing, XIII, 4, pp. 365-368, 1998.
- Beyreuther 1998- b Beyreuther R., Brünig H. and Hofmann H., Use the Stress/Strain Curve of Multifilament Yarn Bundle for the Estimation of their Cross Unevenness, Chemical Fibers International, Vol. 48, pp. 126-127, 1998.
- Beyreuther 1999 Beyreuther R., Brünig H. and Hofmann H., Tensile Force Measurement in the PA6 High Speed Fiber Spinning and their Utility, Intern. Polymer Processing XIV, 4, pp. 326-330, 1999.
- Beyreuther 2001 Beyreuther R., Brünig H. and Vogel R., Preferable Filament Diameter Ratios of Hybrid Yarn Components for Optimized Long Fiber Reinforced Thermoplastics, 17th Annual Meeting of the PPS, Montréal, Canada, May 21st-24th, 2001.
- Beyreuther 2002 Beyreuther R., Melt spinning at the IPF Dresden - Quo Vadis?, Proc. of Symposium "Schmelzspinnen von Polymeren und Glas in der Polymerforschung", Institute of Polymer Research Dresden, pp. 233-243, 13.-14.05.2002.
- Bheda 1987 Bheda J. H., Mathematical Modeling and Experimental Study of Dynamics and Structure Development during High Speed Melt Spinning of Nylon-6, PhD Dissertation, Uni. of Tennessee, 1987.
- Blundell 1983 Blundell D. J., Osborn B. N., The Morphology of poly(aryl-ether-etherketone), Polymer, 24, pp. 953-958, 1983.
- Brennat 2001 Brennat A., Polymer Melt Rheology and the Rheotens Test, PhD Dissertation, Stuttgart University, IKT, 2001.
- Brünig 1999 Brünig H., Beyreuther R., Hofmann H., The Influence of Quench Air on Fibre Formation and Properties in the Melt Spinning Process, IFJ, pp. 104-107, April 1999.
- Brünig 2000 Brünig H., Beyreuther R., Melt Spinning of Polymers: Spinnability from Theoretical and Experimental Viewpoint, 5th IPF Colloquium, Dresden, November 14 and 15, 2002.
- Brünig 2002- a Brünig H., Beyreuther R., Vogel R., Tändler B., Melt Spinning of Fine and Ultra-fine PEEK-Filaments, Proceeding of Polymer Fibers, Manchester, 2002.
- Brünig 2002- b Brünig H., Beyreuther R., Vogel R., Tändler B., Golzar M., Schmelzspinnen von PEEK-Garnen mit feintitrigen Filamenten, Proc. of Symposium "Schmelzspinnen von Polymeren und Glas in der Polymerforschung", Institute of Polymer Research Dresden, pp. 251, 13.-14.05.2002.

- Brünig 2003 Brünig H., Tändler B., A new Method to Determine the Filament Force Tension within the Fiber Formation Zone, Intern. Polymer Processing XVIII, 1, pp. 41-45, 2003.
- Choi 2001 Choi B. D., Diestel O., Offermann P., Hübner T., Mäder E., Advancement for Commingling Hybrid Yarns for Fiber Reinforced Thermoplastics, Textil-Symposium, April 23-26, Frankfurt/Main, Germany, 2001.
- Choi 2002 Choi D., White J. L., Crystallisation and Orientation Development in Melt Spinning Isotactic PP of varying Tacticity, Intern. Polymer Processing, XVII, pp. 233-243, 2002.
- Choumilina 2001 Choumilina A., Visco-Elastic Models for Fiber Spinning, MSc Thesis, University of Kaiserslautern, 2001.
- Collier 2002 Collier J. R., Petroven S., Patil P., Collier B. J., Elongation Rheology of Fiber Forming Polymers, Polymer Fibers, Conference program & Extended Abstracts , UMIST, Manchester, 10-12 July 2002.
- Cragg 1999 Cragg A. J., Experimental Characterization of Heat Transfer from an Electrically Heated Thin Filament, Morgantown, West Virginia, MSc Thesis, 1999.
- Cuculo 2001 Cuculo J. A., Hotter J. F., Zhou Q., Advances in the Control of Spinline Dynamics for Enhanced Properties, Salem D. R., Structure in Polymeric Fibers, Carl Hanser, Munich, 2001.
- Devaux 1985 Devaux J., Delimoy D., Doust D., Legras R., Mercier P., Strazielle C., Nield E., On the Molecular Weight Determination of a poly(aryl-ether-ether-ketone) (PEEK), Polymer, Vol. 26, pp. 1994-2000, 1985.
- DFG DFG sub-Project TP7, Schmelzspinnen von PEEK-Garnen mit feintitigen Filamenten, FOR 278, Textile Verstärkungen für Hochleistungsrotoren in komplexen Anwendungen. .
- Ding 1995 Ding Z., Spruiell J. E., An Improved Mathematical Model of Melt Spinning Process, PhD Dissertation, University of Tennessee, 1996.
- Dutta 1984 Dutta A. and Nadkarni V. M., Identifying Critical Process Variables in Poly(ethylene Terephthalate) Melt Spinning, Textile Research Journal, pp. 35-42, January 1984.
- Ehrenstein 1999 Ehrenstein G. W., Polymer-Werkstoffe, Carl Hanser, München, 1999.
- Fourné 1995 Fourné F., Synthetische Fasern, Hanser Verlag, München Wien, 1995.
- Ghijssels 1994 Ghijssels A., Clippeleir J. De, Melt Strength Behaviour of Polypropylenes, International Polymer Processing, IX, pp. 252-257, 1994.
- Ghijssels 1997 Ghijssels A., Massardier C. H., Brandley R. M., Brittle Melt Rupture Phenomena in Polymer Processing, Int. Polym. Proc., 12, pp. 147-154, 1997.
- Golzar 2002 Golzar M., Beyreuther R., Brünig H., Tändler B. and Vogel R., Online Temperature Estimation and Simultaneously Estimation of Diameter of Fibres in Melt Spinning Process, Polydays 2002, Sept 30-Oct 02, TU Berlin, 2002.
- Golzar 2004 Golzar M., Beyreuther R., Brünig H., Tändler B. and Vogel R., Online Temperature Measurement and Simultaneous Diameter Estimation of Fibers by Thermography of the Spinline in the Melt Spinning Process, Advances in Polymer Technology, Vol. 23, No. 3, 2004.

- Golzar 2004 Golzar M., Brünig H., Beyreuther R., Tändler B. and Vogel R., Estimation of the Extensional Viscosity of PEEK by On-line Measurements along spinning Line, *Journal of Non-Newtonian Fluid Mechanics*, submitted, 2004.
- Grassman 1959 Grassmann P., *Physikalische Grundlagen der Verfahrenstechnik*, Salle & Sauerländer, pp. 908-910, 1959.
- Gupta 1988 Gupta R. K., Shridar T., "Elongational Rheometer" in *Rheological Measurement*, Ed. Collyer A. A., Collyer D. W., Elsevier Applied Science, London, 1988.
- Gupta 2002 Gupta M., Estimation of Elongational Viscosity of Polymers from Entrance Loss Data Using Individual Parameter Optimisation, *Advances in Polymer Technology*, Vol. 21, No. 2, pp. 98-107, 2002.
- Herzberg 2001 Herzberg C., Krzywinski S., Rödel H., Load-adapted 3D-reinforcement by means of Function-adjusted Ready-making Process, *ICCM 13*, Beijing, pp. 19-25 June, 2001.
- Herzberg 2002 Herzberg C., Krzywinski S., Rödel H., Montage Textiler Prefoms für Verbundwerkstoffrotoren, *Preform Sewing of Lightweight Composite Rotors*, TU Dresden, 6. Dresdner Textiltagung, 29-20 Juni, 2002.
- Hoffman 2003 Hoffmann M., *Schmelzspinnen Vernetzbarer Thermoplastischer Elastomere mittels Zweischneckenextrusion*, PhD Dissertation, TU Dresden, Shaker Verlag, Aachen, 2001.
- Hufenbach 2002 Hufenbach W., Offermann P., *Textile Verstärkungen für Hochleistungsrotoren in komplexen Anwendungen*, TU Dresden, 6. Dresdner Textiltagung 2002, 19-20 Juni 2002.
- InfraTec 1998 *Instructions for use, Berührungslose Infrarot-Temperaturmessung an Kunststoffen*, InfraTec GmbH, Dresden 1998.
- Isayev 1991 Isayev A. I., *Modelling of Polymer processing*, Carl Hanser, Munich, 1991.
- Ishizuka 1985 Ishizuka O., Koyama K., *Rheology and Dynamics of Melt Spinning: Viscoelastic Polypropylene and Polyethylens*, Ziabicki A., Kawai H., High-speed Fiber Spinning, John Wiley & Sons, Canada, 1985.
- Joo 2002 Joo Y. L., Sun J., Smith M. D., Armstrong R. C., Brown R. A., Ross, R. A., Two Dimensional Numerical Analysis of Non-isothermal Melt Spinning with and without Phase Transition, *J. Non-Newtonian Fluid Mech.* 102, pp. 37-70, 2002.
- Kase 1965 Kase S., Matsuo T., *Studies on Melt Spinning. I. Fundamental Equations on the Dynamics of Melt Spinning*, *Journal of Polymer Science*, Vol. 3, Part A, pp. 2541-2554, 1965.
- Kast 1974 Kast W., Kirscher O., Reinike H., Wintermantel K., *Konvektive Wärme- und Stoffübertragung*, Springer-Verl., Berlin, 1974.
- Katayama 1985 Katayama K., Yoon M., *Polymer Crystallisation in Melt Spinning: Mathematical Simulation*, pp. 1207-223, Ziabicki A., Kawai H., High-speed Fiber Spinning, John Wiley & Sons, Canada, 1985.
- Kubo 1985 Kubo S., *Air Boundary Layer on a Filament in High-Speed Spinning*, Ziabicki A., Kawai H., High-speed Fiber Spinning, John Wiley & Sons, Canada, 1985.
- Lunkwitz 2002 Lunkwitz K., *Polymerwerkstoffe*, Umdruck zur Vorlesung, TU Dresden, SS 2002.

- Laun 1989 Laun H. M., Schuch H., Transient Elongational Viscosities and Drawability of Polymer Melts, *J. Rheol.*, 33(1), 119-175, 1989.
- Macosko 1994 Macosko C. W., *Rheology*, VCH Publishers Inc., New York, 1994.
- Mäder 1998 Mäder E., Skop-Cardarella K., Mechanische Eigenschaften langfaserverstärkter Thermoplaste als Funktion der textilen Halbzeugstruktur, *Technische Textilien*, 41, pp. 37-40, Feb. 1998.
- Maebius 1985 Maebius R. E., The effect of Heat transfer in Melt Spinning, *Journal of Applied Polymer Science*, Vol. 30, pp. 1639-1652, 1985.
- Martyn 2002 Martyn M. T., Nakason C., Coates P. D., Measurement of Apparent Extensional Viscosities of Polyolefin Melts from Process Contraction Flows, *J. Non-Newtonian Fluid Mech.*, 92, pp. 203-226, 2002.
- Menges 1998 Menges G., *Werkstoffkunde Kunststoffe*, Carl Hanser, München, 1998.
- Mitsoulis 2000 Mitsoulis E., Beaulne M., Numerical Simulation of Rheological Effects in Fiber Spinning, *Advances in Polymer Technology*, Vol. 19, No. 3, pp. 155-172, 2000.
- Moris 1997 Morris G. J., Loth, J. L., Bond R. E., Cooling Rate of Filament, Final Contract report PPG Industries, Inc., Dec 1997.
- Murase 1994 Murase Y., Nagai A., Melt spinning, Nakajima T., chapter 2, *Advanced Fiber Spinning Technology*, pp. 25-64, 1994.
- Nakajima 1994 Nakajima T., *Advanced Fibre Spinning Technology*, Woodhead Publishing Ltd, England, 1994.
- Nakamura 1972 Nakamura K., Watanabe T., Katayama K., Amano T., *Journal of Applied Polymer Science*, 16, pp. 1077, 1972.
- Offermann 1995 Offermann P., Hybridgarne für neuartige Verbundwerkstoffe aus Thermoplasten, *Technische Textilien/ Technical Textiles*, 38. Jahrgang, pp. 55-57, Juni 1995.
- Ohkoshi 1990 Ohkoshi Y., H. Ohshima, T. Matsuhisa, N. Miyamoto, K. Toriumi, Konda A., Structures and Mechanical Properties of PEEK Filaments. *Sen'i Gakkaishi*, 46, (3), pp.87-92, 1990.
- Ohkoshi 1993- a Ohkoshi Y., Kikutani T., Konda A., Shimizu J., Melt Spinning of Poly ether-ether-ketone (PEEK) –Cooling, Thinning and Structural Development on Spin-line-, *Sen'i Gakkaishi*, 49, (5), pp. 211-219, 1993.
- Ohkoshi 1993- b Ohkoshi Y., Konda A., Ohshima H., Toriumi K., Shimizu Y., Nagura M., Molecular Weight Effects on Melt Spinning and Drawing of Poly Ether-Ether-Ketone Filaments, *Sen'i Gakkaishi*, 49, (4), pp. 151-156, 1993.
- Ohkoshi 1996 Ohkoshi Y., *Engineering Plastics, Melt spinning*, *Polymeric Materials Encyclopedia*, J. C. Salamone Ed., CRC Press, 1996.
- Ohkoshi 2000 Ohkoshi Y., Park C., Gotoh Y., Nagura M., Toriumi K. and Kikutani T., Cooling Behaviour of the Spinning Line of Poly (ether ether ketone), *Sen'i Gakkaishi*, 56, (7), pp. 340-347, 2000.
- Okamoto 1994 Okamoto M., Spinning of Ultra-fine Fibers, Nakajima T., Chapter 9, *Advanced Fiber Spinning Technology*, pp. 187-204, 1994.
- Petrie 1979 Petrie C. J. S., *Elongational Flows*, Pitman, London, 1979.
- Rauschenberger 2002 Rauschenberger V., Laun H. M., Spinnbarkeit und Versagensverhalten thermoplastischer Polymere aus rheologischer Sicht, *Symposium of Melt Spinning of Polymers and Glass in Polymer Research*, pp. 129-139, IPF Dresden, 13-14.05.2002.

- Rauschenberger 1997 Rauschenberger V. and Laun H. M., A Recursive Model for Rheotens Tests, *J. Rheology*, 41(3), May/June, 1997.
- Retting 1992 Retting W., *Mechanik der Kunststoffe*, Carl Hanser, München, 1992.
- Revenu 1993 Revenu J., Guillet J., Carrot C., *J. Rheology*, 37, pp. 1041-1056, 1993.
- Rides 1996 Rides M., Allen C. R. G., Chakravorty S., Review of Extensional Viscoelasticity Measurement Techniques for Polymer Melts, *Natl. Phys. Lab. rep. Center for Materials Measurement and Technology*, (A), 44 , 1996.
- Rothstein 2002 Rothstein J. P., McKlinely G. H., Inhomogeneous Transient Uniaxial Extensional Rheometry, *Journal of Rheology*, Vol. 46, Issue 6, Nov./Dec., pp. 1419-1444, 2002.
- Salem 2001 Salem D. R., *Structure in Polymeric Fibers*, Carl Hanser, Munich, 2001.
- Samon 2000 Samon J. M., Jerold M. S., Benjamin S. H., Jing W., Shirkant K., Structure Development during Melt Spinning and Subsequent Annealing of Polybutene-1 Fibers, *Journal of Polymer Science: Part B: Polymer Physics*, Vol. 38, pp. 1872-1882, 2000.
- Sano 1968 Sano Y., Orii K., Yamada N., Trouton Viscosity of Polypropylene in the Melt Spinning Process, *Sen-I Gakkaishi*, 24, pp. 147-154, 1968.
- Schäfer 2002 Schäfer K., Enders U., Neuere Anlagen- und Technologieentwicklungen für das Hochgeschwindigkeitsspinnen, *Proc. of Symposium "Schmelzspinnen von Polymeren und Glas in der Polymerforschung"*, Institute of Polymer Research Dresden, pp. 176-185, 13.-14.05.2002.
- Schmack 1997 Schmack G., Schreiber R., Veeman W. S., Hofmann H., Beyreuther R., Relation between Molecular Orientation and Mechanical Properties in Differently Processed Polyamid 4.6/6 Textile Yarns, *J. of App. Polymer Science*, Vol. 66, pp. 377-385, 1997.
- Schmack 2000 Schmack G., Jehnichen D., Vogel R., Tändler B., Biodegradable Fibres of Poly (3-hydroxybutyrate) Produced by High-speed Melt Spinning and Spin Drawing, *J. Polymer Sci., Part. B: Polymer Physics*, 38. 21, pp. 2841-2850, 2000.
- Schöne 1980 Schöne A., "Modellierung des Spinn- und Reckprozesses", Fadenbildungs- und -deformationsmodell, PhD Dissertation, ITF Dresden, 1980.
- Stibal 2002 Stibal W., Schwarz R., Schmelzspinnen von PET micro Filamenten nach dem INVENTA-Fischer Verfahren, *Proc. of Symposium "Schmelzspinnen von Polymeren und Glas in der Polymerforschung"*, Institute of Polymer Research Dresden, pp. 186-202, 13.-14.05.2002.
- Shimizu 1987 Shimizu J., Kikutani T., Ohkoshi Y., Akiro T., Melt-spinning of Poly Ether-Ether-Keton (PEEK) and the Structure and Properties of Resulting Fibers, *Sen'i Gakkaishi*, 43, (10), pp. 507-519, 1987.
- Shimizu 1985- Shimizu J., Okui N., Kikutani T., Simulation of Dynamics and Structure
a Formation in High-speed Melt Spinning, 173-201, Ziabicki, A., Kawai H., *High-speed Fiber Spinning*, John Wiley & Sons, Canada, 1985.
- Shimizu 1985- Shimizu J., Okui N., Kikutani T., Fine Structure and Physical Properties
b of Fibers Melt-Spun at High Speeds from Various Polymers, Ziabicki, A., Kawai H., *High-speed Fiber Spinning*, John Wiley & Sons, Canada, 1985.

- Shimizu 1985- Shimizu J., Kikutani T., Ohkoshi Y., Takaku A., The Crystal Structure and the Refractive Index of Drawn and Annealed Poly (ether-ether-ketone) (PEEK) Fiber, *Sen'i Gakkaishi*, 42, (11), pp. 461-467, 1985.
- Shridar 1988 Shridar T., Gupta R. K., Material Properties of Viscoelastic Liquids in Uniaxial Extension, *J. Rheology* 35(3), April 1991, pp. 363 Elsevier Applied Science, London, 1988.
- Sperling 1992 Sperling L. H., Introduction to Physical Polymer Science, John Wiley & Sons, Inc., 1992.
- Spruiell 1975 Spruiell J. E., White J. L., *Polm. Eng. Sci.*, 15, pp. 660, 1974.
- Spruiell 2001 Spruiell J. E., Structure Formation during Melt Spinning, Salem, D. R., Structure in Polymeric Fibers, Carl Hanser, München, 2001.
- Stelter 2002 Stelter M. and Brenn G., Yarin A. L., Singh R. P., Durst F., Investigation of the Elongational Behaviour of Polymer Solutions by Means of an Elongational Rheometer, *J. Rheol.* 46(2), pp. 507-527 March/April, 2002.
- Takasaki 2002 Takasaki M., Ito H., Kikutani T., Fiber Structure Development of Polylactides in High Speed Melt Spinning Process, pp. 93-104, Proc. of Symposium "Schmelzspinnen von Polymeren und Glas in der Polymerforschung", IPF Dresden, 13.-14.05.2002.
- Tucker 1989 Tucker C. L., Computer Modeling of Polymer Processing, Carl Hanser, Munich, 1989
- Vogel 1995 Vogel R., Schauer G., Beyreuther R., Melt spinning of Ultra-low-density Polyethylene Engage to Elastic Fibers, *Chemical Fibers Inter.*, Vol. 45, pp. 268-269, August 1995.
- Vogel 1999 Vogel R., Brünig H., Beyreuther R., Tändler B., Voigt D., Rheological and Theoretical Estimation of the Spinnability of Polyolefines, Part 1 Rheological Study, *Inter. Poly. Proc. XIV*, 1, pp. 69-74, 1999.
- Vogel 2003 Vogel R., Hatzikiriakos S. G., Brünig H., Tändler, B., Golzar M., Improved Spinnability of Metallocene Polyethylenes by Using Processing Aids, *Int. Polmer Proc.*, XVIII, pp. 67-73, 2003.
- White 2001 White J. L. and Choi C. -H., Modeling Heat Transfer with Crystallisation in Rods and Filaments, *International Polymer Processing*, XVI, 1, pp. 54-60, 2001.
- Xiong 2001 Xiang D., Lienhard V. J. H., Experiments on Convective Cooling of Continuously Drawn Glass Fiber, *Proceedings of NHTC'01*, California, June 10-12, 2001.
- Yarin 1993 Yarin A. L., Free Liquid Jet and Films in Hydrodynamics and Rheology, Longman Scientific & Technical, 1993.
- Yasuhiro 1994 Yasuhiro M., Naai A., Melt Spinning, chapter 2, Nakajima T, *Advanced Fibre Spinning Technology*, Woodhead Publishing Ltd, England, 1994.
- Zhang 2003 Zhang Y., Liu Q., Jiang Z., Nonisothermal Crystallisation Kinetics of Poly (ether ether ketone) (PEEK)-co-Poly(ether ether ketone) (PEEKK) block copolymers, *Polymer Materials: Science & Engineering* 88 , pp. 367-368, 2003.
- Ziabicki 1976 Ziabicki A., Fundamentals of Fiber Formation, Wiley. London, 1976.
- Ziabicki 1985 Ziabicki A., Kawai H., High-speed Fiber Spinning, John Wiley & Sons, Canada, 1985.

- Ziabicki 2002 Ziabicki A. and Jarecki L., The Role of Flow-Induced Crystallization in Melt Spinning, Proc. of Symposium "Schmelzspinnen von Polymeren und Glas in der Polymerforschung", Institute of Polymer Research Dresden, pp. 42-57, 13.-14.05.2002.
- Zieminski 1986 Zieminski K. F., Development and Application of a Mathematical Model for the High Speed Melt Spinning of Crystallizable Polymers, PhD Dissertation, Uni. Tennessee, 1986.

Patents (Japanese patents)

- Toray 1973 Toray, Fine Filament Manufacture, JP 73-17,703, 1973.
- Teijin 1979 Teijin, Production of Extremely Fine Fibers Polyester, JPA 79-30, 924, 1979.
- Unitika 1980 Unitika, Process for Producing Fine Polyamids Fibers, JPA 80-67, 007, 1980.
- Japan Ester 1980 Japan Ester, Process for Melt Spinning of Fine Multifilaments, JPA 80-60, 609, 1980..
- Unitika 1980 Unitika, Process for Producing Fine Polyamids Fibers, JPA 80-98, 816, 1980.

Appendix

Melt spinning of various PEEK using various spinning condition

In the first experiments, different products of Victrex® PEEK™ were selected and were spun using piston equipment. In these investigations the spinning conditions and the final properties were compared. In Table A1, three different as-spun fine PEEK filaments are compared.

		Q (g/min)	V _L (m/min)	T ₀ (°C)	ddr (V _L /V ₀)	Spinneret
1	PEEK 450G	0.465	350	400	72	1 hole 0.3
2	PEEK 381G	0.465	820	400	168	
3	PEEK 151G	0.465	1000	380	227	
4	PEEK 151G	0.233	500	380	227	
5	PEEK 151G	0.233	1000	380	454	

Table A1 As-spun for different type of PEEK by piston equipment

Considering the rheological investigations in Section 3.2 especially Figure 3.1.6 and the Table A1, it is obvious that PEEK 151 G can be spun more finer in the melt spinning. To verify the other specifications of filaments the final filaments produced in piston equipment tested for fineness, tenacity and elongation and compared to the standard product of Hoechst and Zyex in Table A2. As shown in Table A2 the as-spun from PEEK 151 G fibre shows higher deformation and ultimate strength but smaller tenacity. The physical tenacity appears to be the same for all types of PEEK. Therefore, the type PEEK 151 G is selected for the fine melt spinning. A series of test carried out to investigate the spinning conditions for fine Titer. The on-line measurements along the spinning line and off-line measurements for the as-spun PEEK fibre are listed in Table A3.

	D (µm)	T _t (dtex)	Ultimate strain (%)	Tenacity (cN/dTex)	Physical tenacity (cN/dTex)	Ultimate strength (M Pa)
1 PEEK 450G	36	13.3	90	1.72	3.26	227
2 PEEK 381G	27	5.8	49	1.6	2.39	211
3 PEEK 151G	22	4.7	143	2.73	6.63	355
4 PEEK 151G	21	4.7	144	2.27	5.53	299
5 PEEK 151G	14	2.3	101	2.7	5.42	324
6 Hoechst M	27	6.9	42	5.19	7.37	623
7 Zyex 4110	40	15.3	42	4.14	5.88	497
8 Hoechst 495 f72	-	495	32	3.86	5.1	464
9 Zyex 460 f30	-	460	38	3.6	4.96	431

Table A2 As-spun PEEK fibres properties

	Q_{hole} g/min	Q_t g/min	V_L m/min	T_0 °C	V_L/V_{00} ddr	Filaments		B cm	
A1	0.465	0.465	26.5	380	4.4	1	T*, V**	120	Pi.***
A2	0.465	0.465	50	380	8.2	1	V	120	Pi.
A3	0.465	0.465	100	380	16.5	1	V	120	Pi
A4	1	12	3000	401	157.5	12	T	120	
A5	1	12	4000	401	210.1	12	T	120	
B1	2	6	1000	385	26.5	3	T, V	120	Un****
B2	2	6	2000	386	53.0	3	T, V	120	Un
B3	3.5	10.5	1000	385	15.1	3	T, V	120	Un
B4	3.5	10.5	2000	385	30.3	3	T, V	120	Un
C1	2.5	7.5	3000	400	63.1	3	V	580	Un
C2	2.5	7.5	4000	400	84.1	3	V	580	Un
C3	2.5	7.5	5000	400	105.1	3	V	580	Un
C4	5	15	3000	400	31.5	3	V	580	Un
C5	5	15	4000	400	42.0	3	V	580	Un
C6	5	15	5000	400	52.5	3	V	580	Un
D1	0.4	9.6	1000	382	132.8	24	V	120	Un
D2	0.4	9.6	1500	385	198.8	24	V	120	Un
D3	0.4	9.6	2000	385	265.1	24	V	120	Un
E1	0.23	5.52	1000	385	230.5	24	V	120	Un
E2	0.23	5.52	1500	385	345.8	24	V	120	Un
E3	0.225	10.8	200	385	47.1	48	V	120	Un
E4	0.225	10.8	400	385	94.3	48	V	120	Un
E5	0.225	10.8	600	385	141.4	48	V	120	Un
E6	0.225	10.8	800	385	188.5	48	V	120	Un
E7	0.225	10.8	1000	385	235.7	48	V	120	Un
E8	0.225	10.8	1500	400	350.3	48	V	120	Un
E9	0.225	10.8	2000	400	467.1	48		120	
F1	0.17	5.44	1000	400	309	32	V	120	Un
F2	0.17	5.44	1700	400	526	32	V	120	Un
F3	0.17	5.44	2000	400	619	32	V	120	Un
G1	0.15	7.2	1500	400	525.5	48	V	120	Un

Table A3 List of experiments and the measurements of as-spun PEEK fibres

* Online temperature measurement

*** Piston equipment

** On-line speed measurement

**** Extruder equipment

Fibre speed and fibre speed gradient

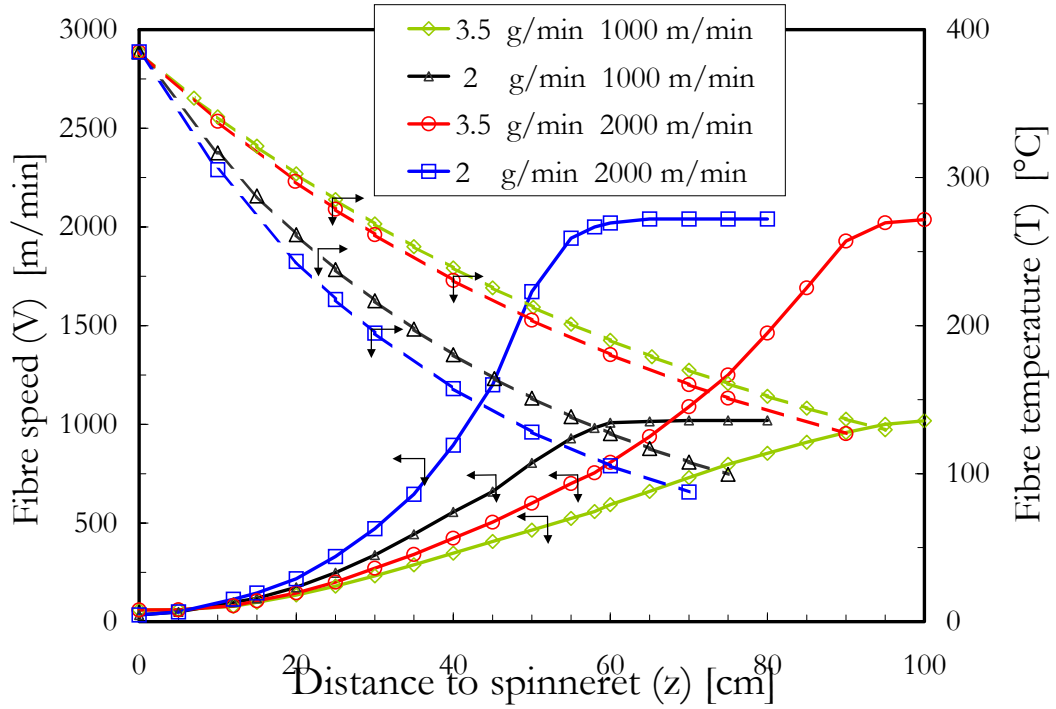


Figure A1 On-line speed measurements along spinning line PEEK 151G, $T_0=400^\circ\text{C}$, Spinneret 3 holes ($d=0.25$ mm, $l=0.5$ mm)

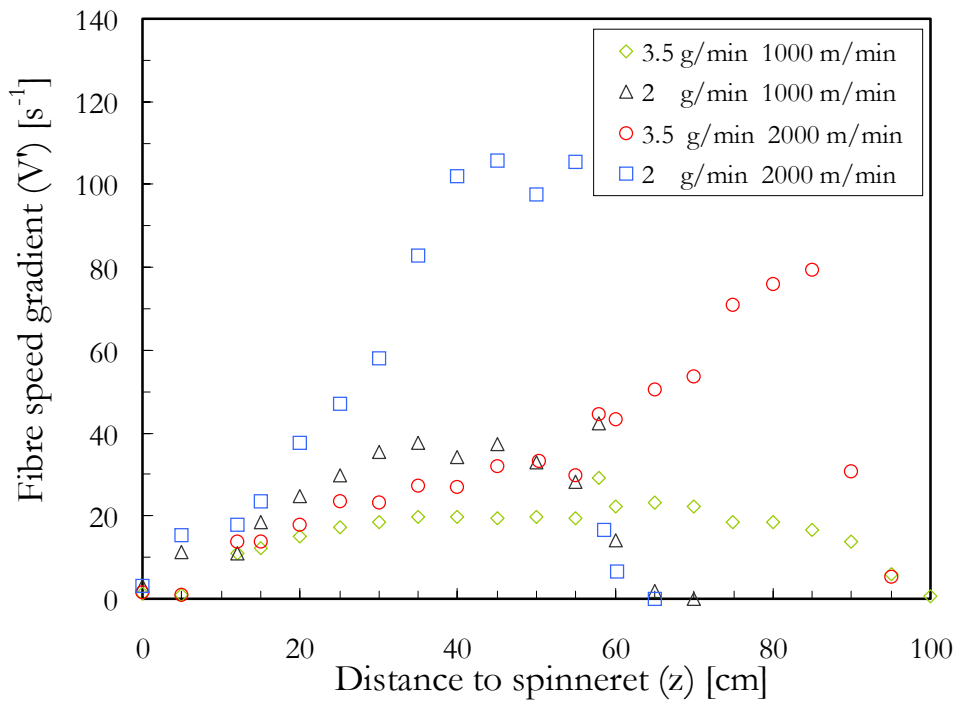


Figure A2 Speed gradient or strain rate of fibre along spinning line PEEK 151G, $T_0=385^\circ\text{C}$, spinneret 3 holes ($d=0.25$ mm, $l=0.5$ mm)

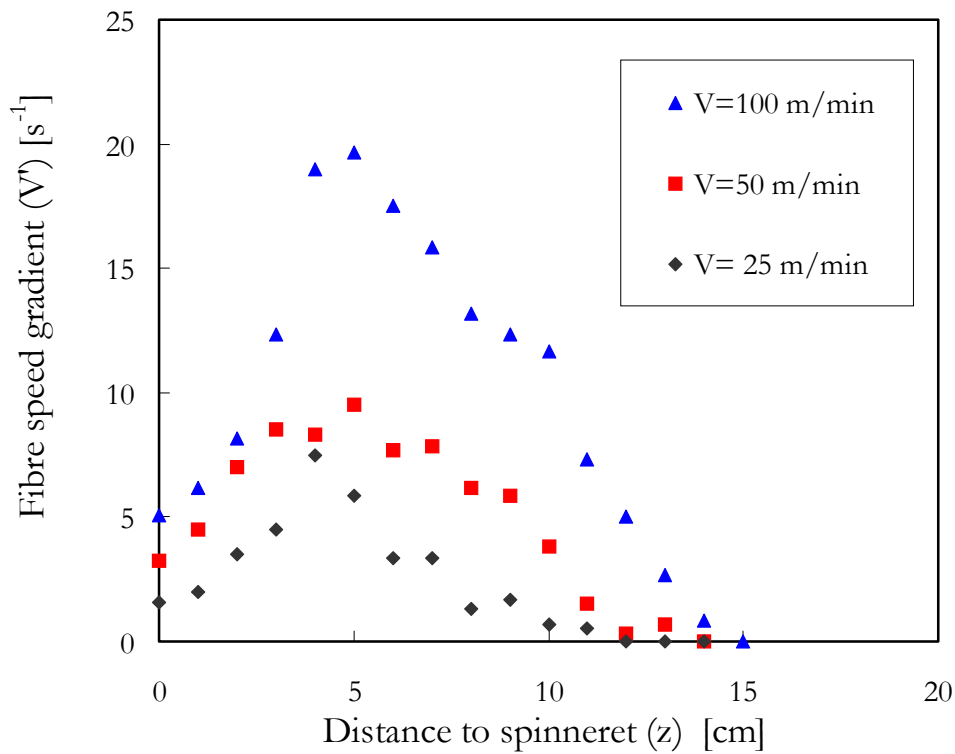


Figure A3 Speed gradient or strain rate of fibre along spinning line PEEK 151G, $T_0=385^\circ\text{C}$, spinneret 3 holes ($d=0.25$ mm, $l=0.5$ mm)

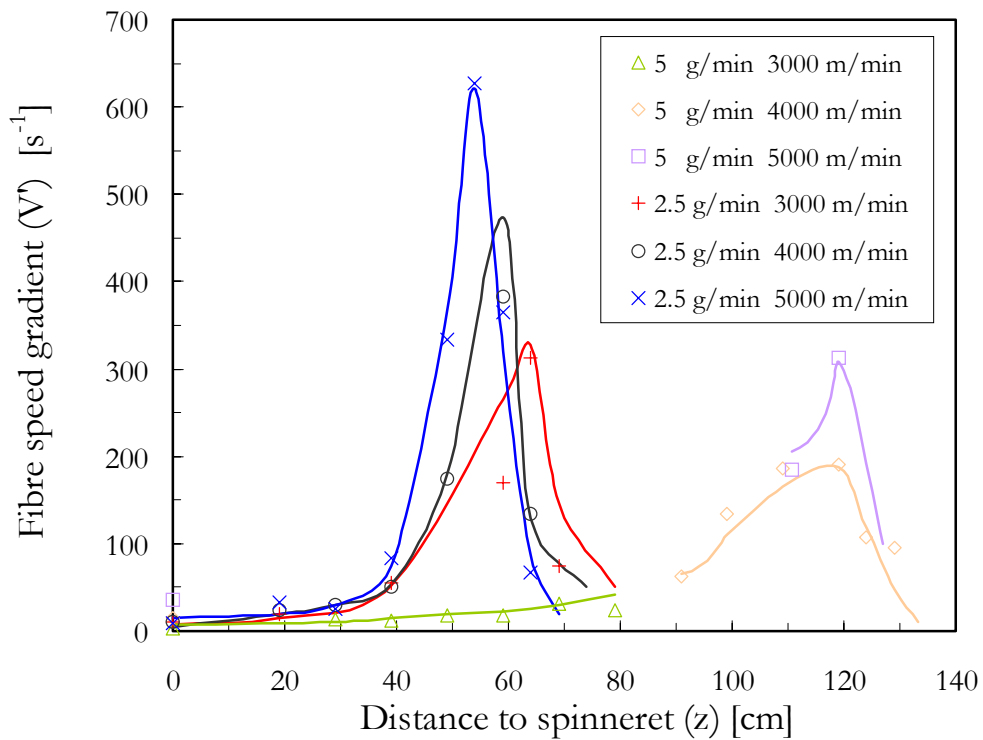


Figure A4 Speed gradient or strain rate of fibre along spinning line, PEEK 151G, $Q=0.465$ g/min, $T_0=380^\circ\text{C}$, spinneret 1 hole ($d=0.3$ mm, $l=0.6$ mm), piston equipment

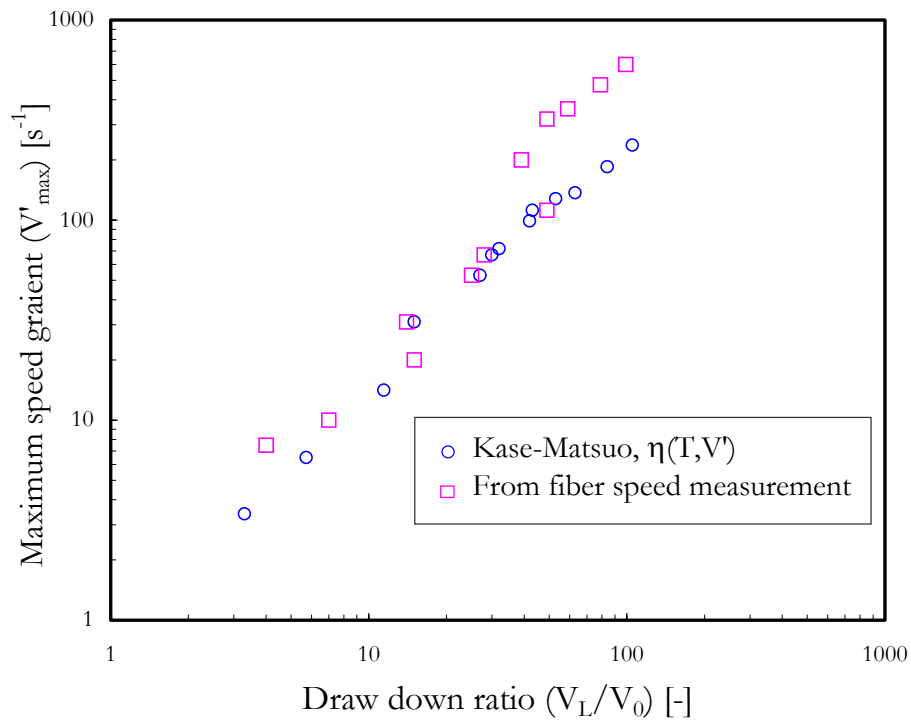


Figure A5 Maximum speed gradient or strain rate over draw down ratio along spinning line, PEEK 151G

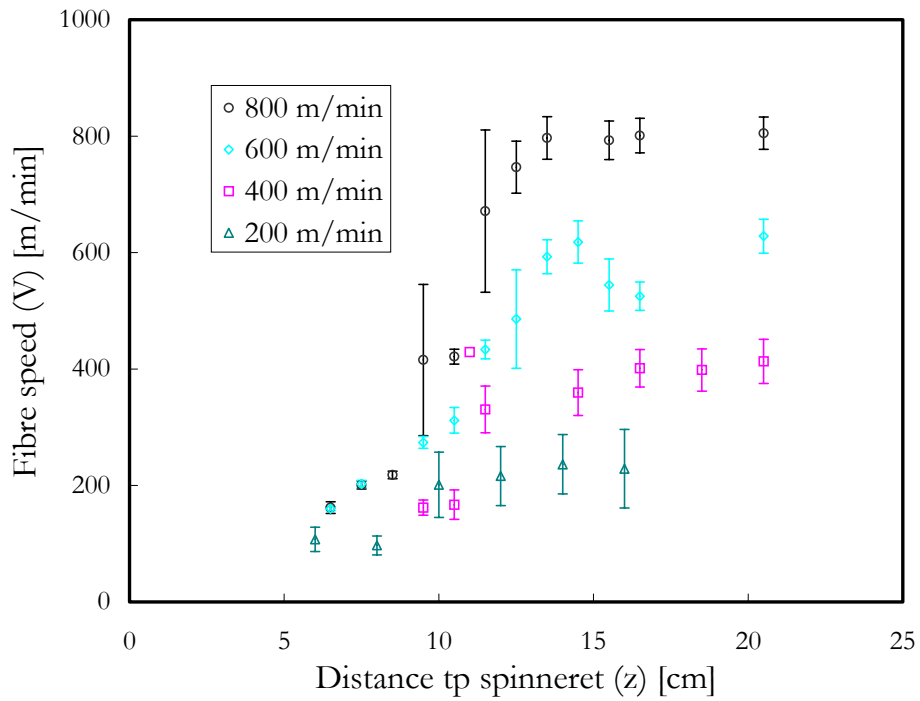


Figure A6 On-line speed measurements along spinning line PEEK 151G, $T_0=385^\circ\text{C}$, $Q=0.255\text{ g/min}$, spinneret 48 holes ($d=0.25\text{ mm}$, $l=0.5\text{ mm}$)

Temperature measured and corrected

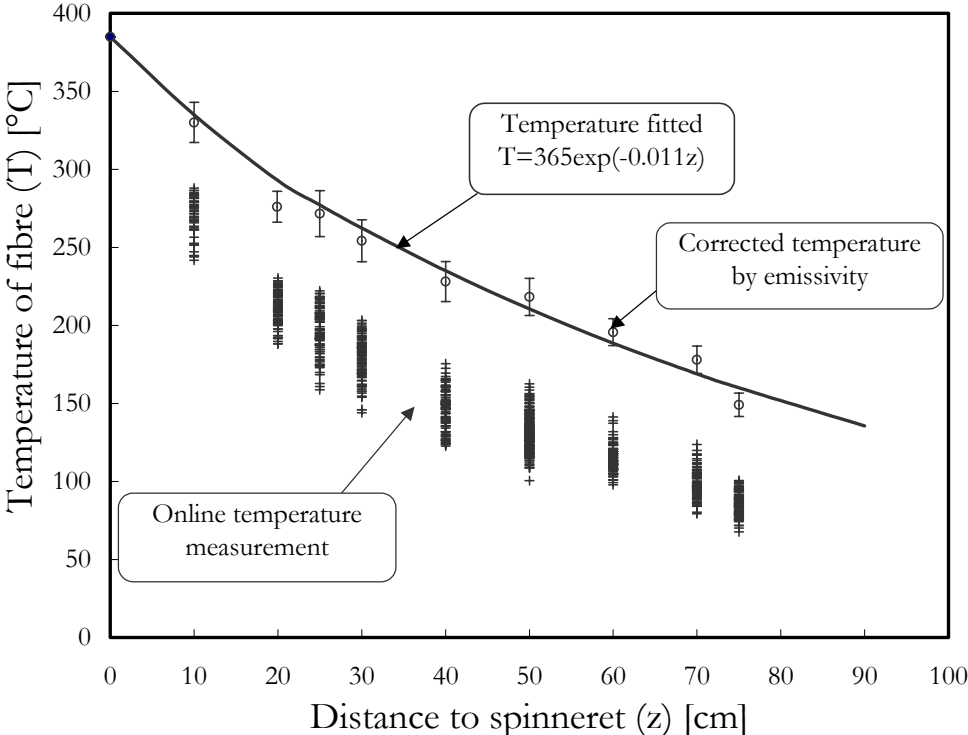


Figure A7 Measured and corrected fibre temperatures for the melt spinning of PEEK 151 G, $Q=3.5$ g/min, $V=2000$ m/min, $T_0=385^{\circ}\text{C}$, 3 hole spinneret, $2r_o=0.25$ mm, $1/2r_o=2$

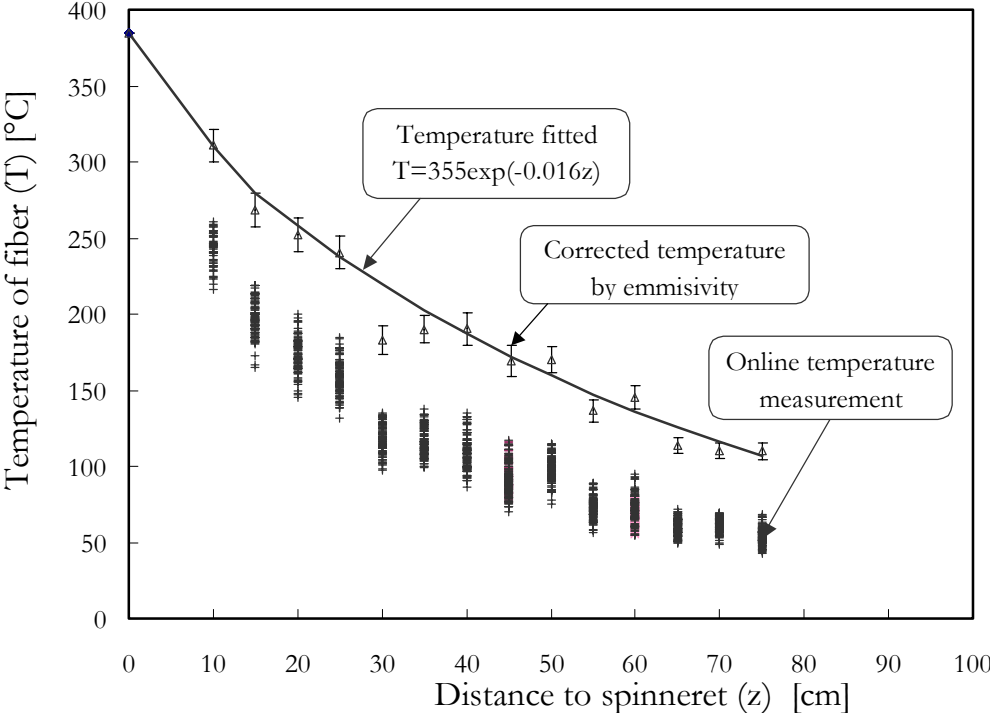


Figure A8 Measured and corrected fibre temperatures for the melt spinning of PEEK 151 G $Q=2$ g/min, $V=1000$ m/min, $T_0=385^{\circ}\text{C}$, 3 hole spinneret, $2r_o=0.25$ mm, $1/2r_o=2$

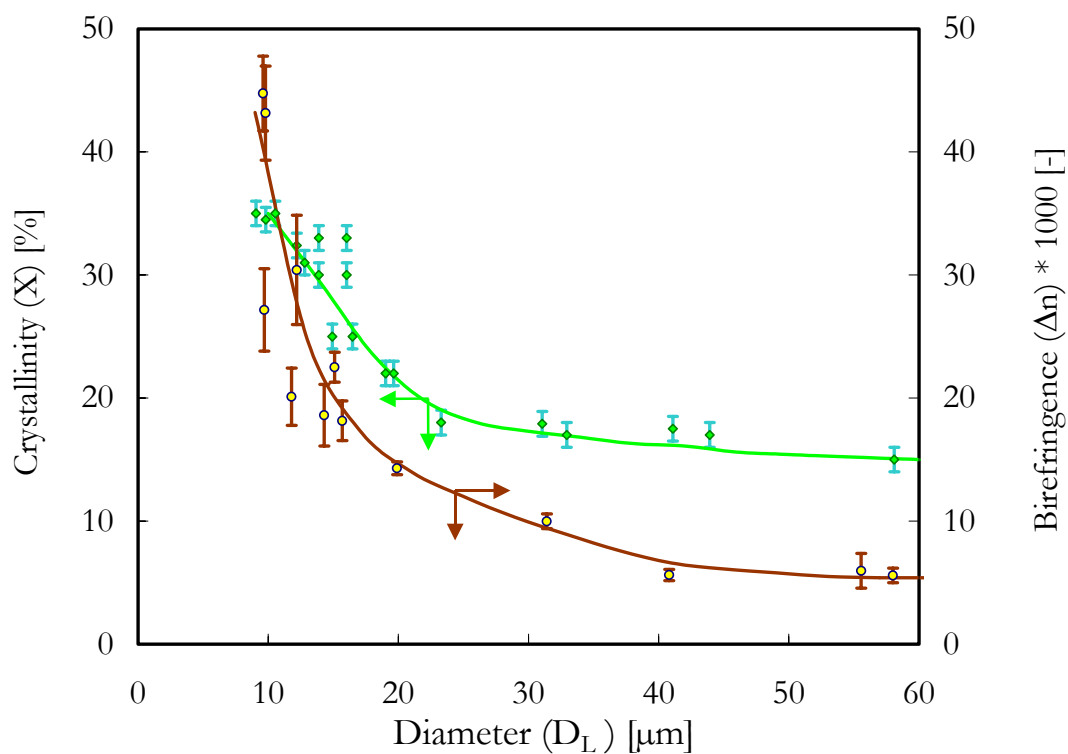


Figure A9 Crystallinity and Birefringence measured over diameter of as-spun PEEK fibre

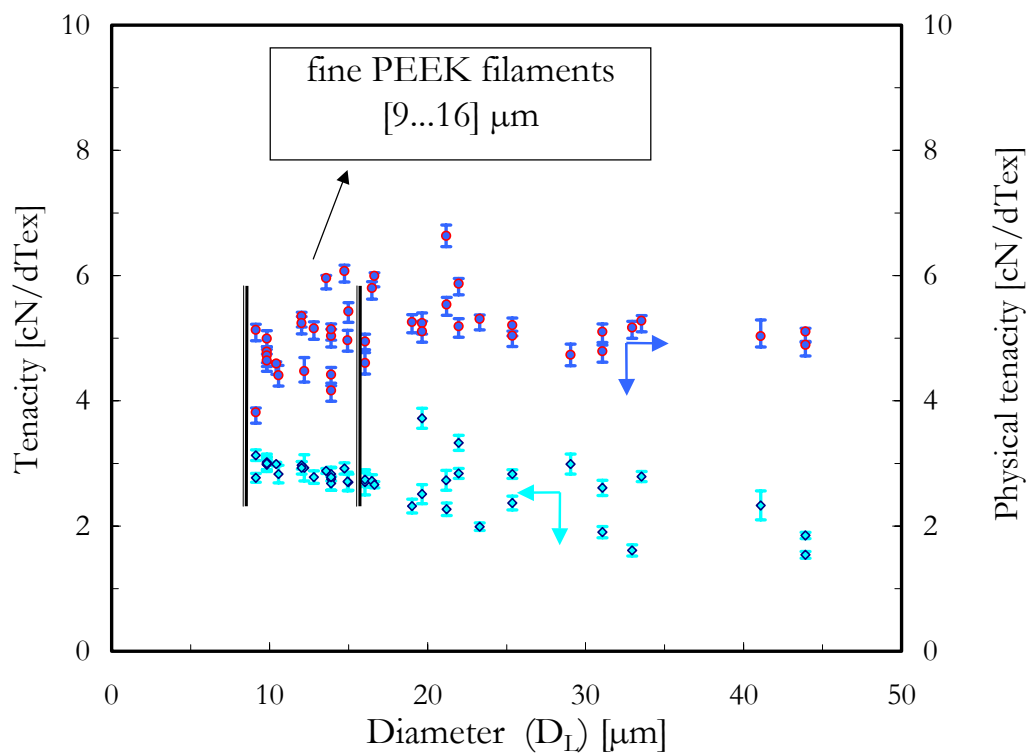


Figure A10 Tenacity and physical tenacity measured over diameter of as-spun PEEK fibre

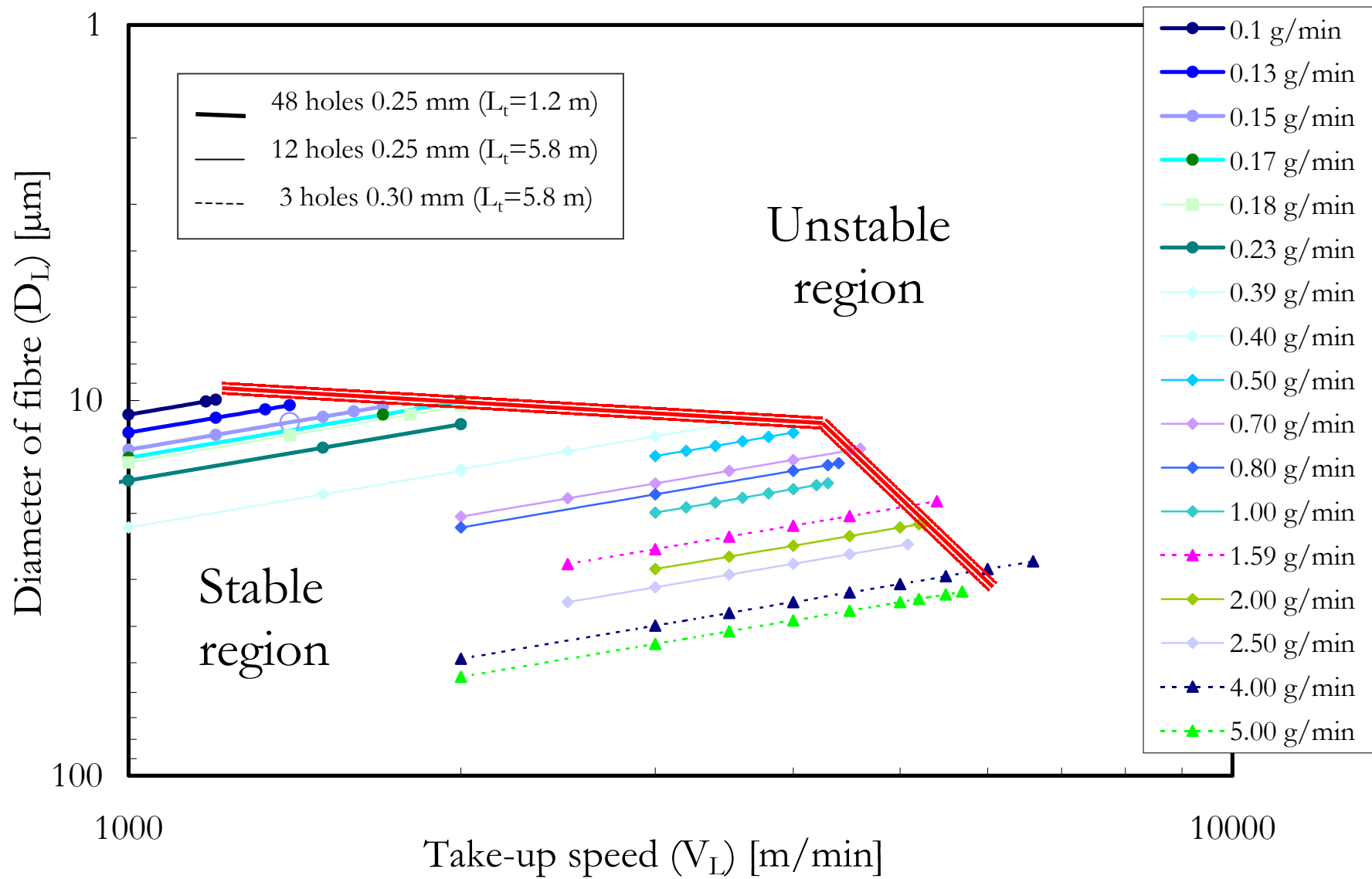


Figure A11 the fiber stability map for PEEK 151G Victrex under different spinning conditions, diameter over take-up speed

Lebenslauf

Persönliche Daten :

Name, Vorname: Golzar, Mohammad

Geburtsdatum/-ort: 24.04.1968 in Najaf

Ausbildung/ Abschluss als:

1980-1985 Abitur, Falsafi Gymnasium, Teheran

1985- 1990 BSc, Shiraz Univ. in Maschinenbau, Shiraz

1991- 1994 MSc, T.M. Teheran Univ. in Maschinenbau, Teheran

1999- 2001 Master Abschluss, Zusatzstudium an der TU Dresden

Berufserfahrung:

1989 Praktikum in Pars Khodro company-Kfz Hersteller, Teheran

1990 Dipl. Ing. im Forschungszentrum Amirkabir Uni., Teheran

1992-1994 Zusammenarbeit mit Azarab company, Teheran

1995-1997 Mitarbeiter in dem Schienenfahrzeug Entwicklung Zentrum,
Iran Railway, Teheran

1996-1999 Dipl. Ing. in Sharif Technologie Zentrum, Teheran.

2000-2004 wissenschaftliche Mitarbeiter im IPF Dresden e.V.
- DFG Projekt „Schmelzspinnen von PEEK-Garnen
mit feinartigen Filamenten“